Redox and Coordination Chemistry of Bis-Bidentate *Para*-Hydroquinones

by

Tyler Trefz
B.Sc., University of Calgary, 2004

A Thesis Submitted in Partial Fulfillment
of the Requirements for the Degree of

DOCTOR OF PHILOSOPHY

in the Department of Chemistry

Supervisory Committee

Redox and Coordination Chemistry of Bis-Bidentate *Para*-Hydroquinones

by

Tyler Trefz
BSc., University of Calgary, 2004

Supervisory Committee

Dr. Robin G. Hicks, (Department of Chemistry)
Supervisor

Dr. David J. Berg, (Department of Chemistry)
Departmental Member

Dr. Fraser A. Hof, (Department of Chemistry)
Departmental Member

Dr. Jay T. Cullen, (School of Earth and Ocean Sciences)
Outside Member

Abstract

Supervisory Committee

Dr. Robin G. Hicks, (Department of Chemistry)
Supervisor

Dr. David J. Berg, (Department of Chemistry)
Departmental Member

Dr. Fraser A. Hof, (Department of Chemistry)
Departmental Member

Dr. Jay T. Cullen, (School of Earth and Ocean Sciences)
Outside Member

The chemistry of a series of *para*-hydroquinones substituted in the 2,5-positions with a proton accepting amine group has been investigated. The *p*-hydroquinones are designed with bis-bidentate coordination pockets allowing for the bridging of two metals and extended multimetallic complexes. Several aspects of the hydroquinones chemistry was examined, including the redox behaviour and properties of the hydroquinones while in their free forms, complexed to palladium and complexed to boron.

The redox properties of *para*-hydroquinones which contain intramolecular hydrogen bonds as indicated by X-ray structural and spectroscopic data were examined. The cyclic voltammograms of some of these hydroquinones indicated they could be oxidized reversibly to give dicationic benzoquinones. The oxidized forms have been chemically isolated and characterized for the first time. Characterization data of the dicationic benzoquinones revealed the OH protons are transferred intramolecularly to the adjacent nitrogen bases. Spectroscopic solution data for the *p*-benzoquinone dications suggests

that the intramolecular hydrogen bonds in the redox related *p*-hydroquinone are no longer present. A correlation between the oxidation potential of the 2,5-substituted-*p*-hydroquinone and base strength of the nitrogen substituent was shown to exist.

The bis-bidentate *p*-hydroquinones were coordinated to palladium resulting in dinuclear complexes. The non-innocence of the ligand was preserved upon coordination but the complexes are oxidized at more positive potentials in comparison to the analogous *p*-benzoquinone species. Two of the palladium complexes were chemically oxidized resulting in the semiquinone radical redox state of the ligand. The EPR and UV-vis spectroscopy of the radical *p*-semiquinone palladium complexes indicates their properties are similar to *o*-semiquinone palladium complexes.

The bis-bidentate *p*-hydroquinones and some related ligands were also coordinated to the main group element, boron. Cyclic voltammetry of the boron complexes revealed the redox properties of the bridging *p*-hydroquinone were perturbed and redox processes occurred at even more positive potentials in comparison to the analogous palladium complexes. The dinuclear boron complexes were highly fluorescent with quantum yields calculated to be in the range of 0.36-0.52. These boron complexes incorporated an uncommon ancillary ligand, acetate. The acetate ligand was found to be advantageous for the solubility and fluorescence properties for one of the boron compounds in comparison to the analogous boron complex incorporating the more commonly used fluorine ancillary ligand.

Table of Contents

List of Tables

List of Figures

List of Numbered Compounds

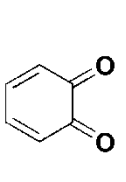
1.1

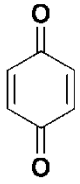
1.2

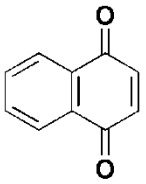
1.3

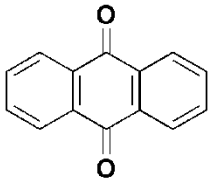
1.4

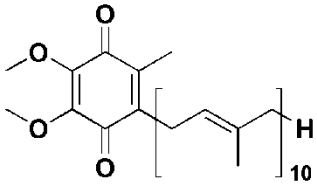
1.5

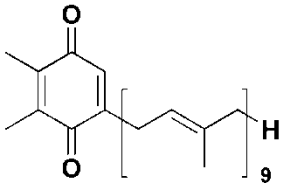
1.6

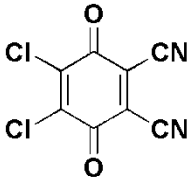
1.7

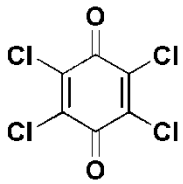
1.8


1.9

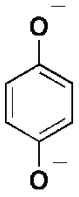
1.10

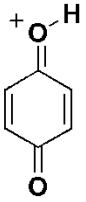
1.11


1.12

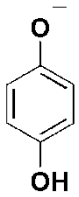
1.13

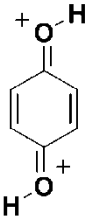
1.14

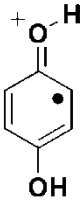
1.15

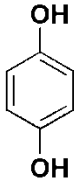
1.16

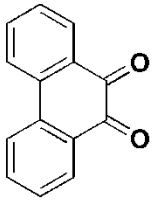
1.17

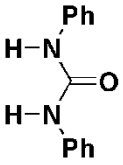
1.18

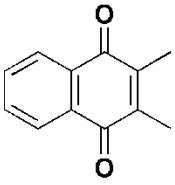
1.19

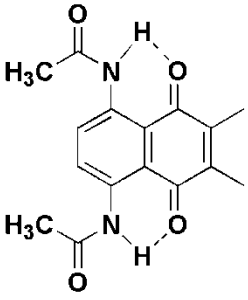
1.20

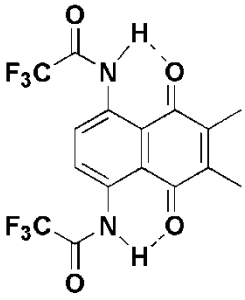
1.21

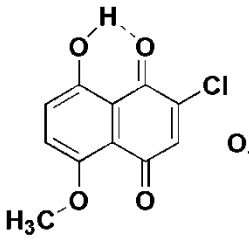
1.22

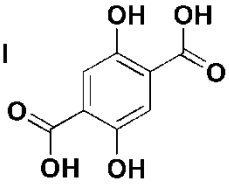
1.23

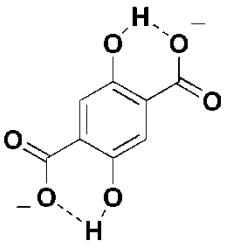
1.24

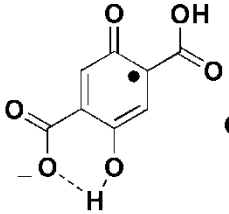
1.25

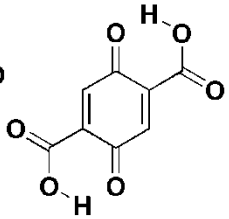
1.26

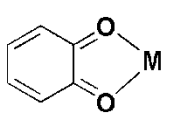

1.27

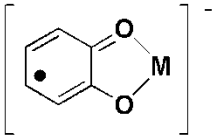

1.28

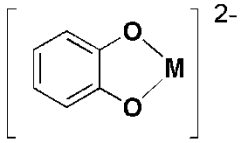

1.29

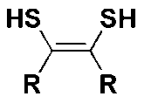

1.30

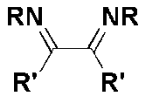

1.31

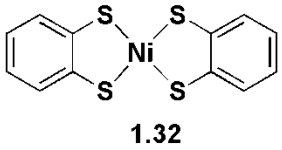

1.32

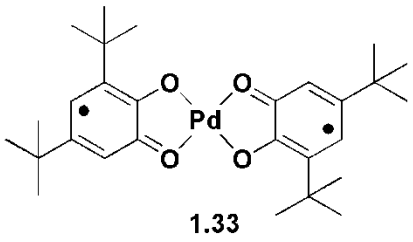

1.33

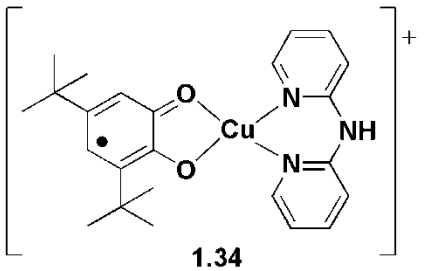

1.34

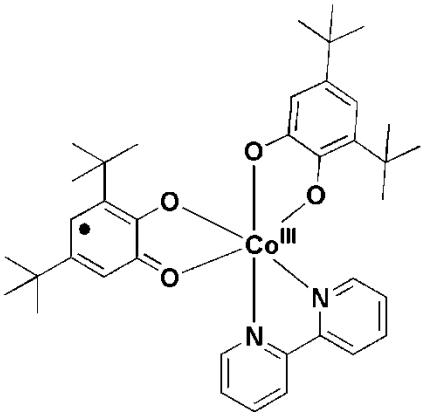

1.35

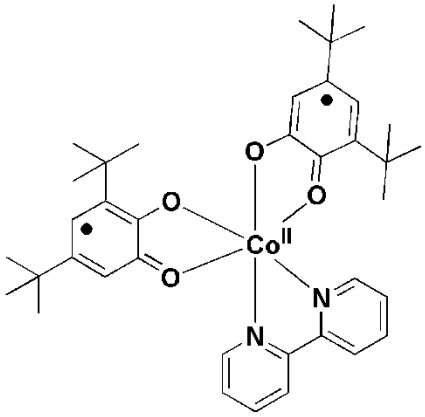

1.36

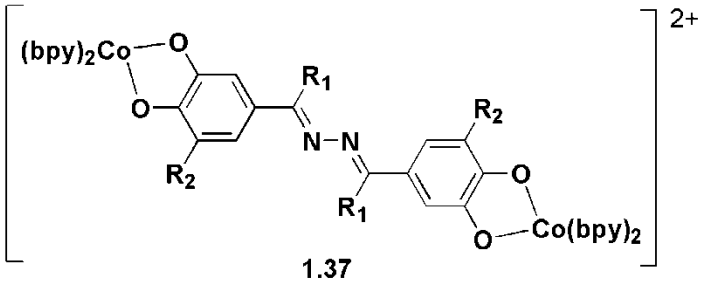

1.37

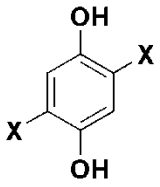

1.38

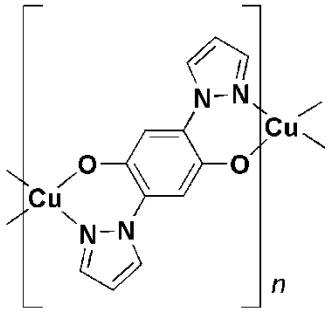

1.39

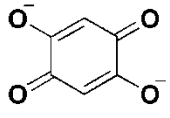

1.40

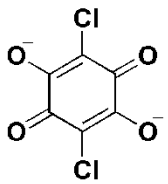

1.41

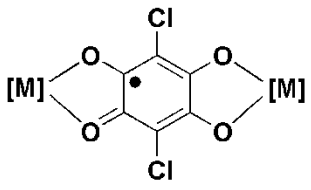

1.42

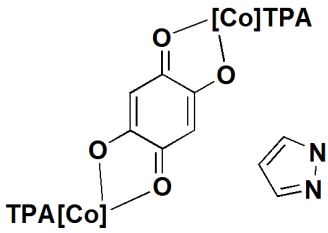

1.43

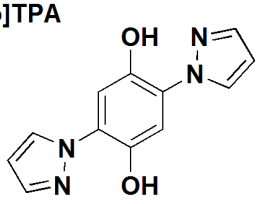

2.1

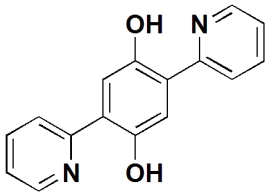

2.2

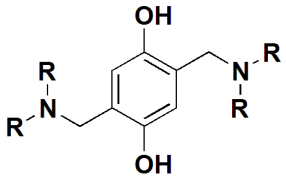

2.3

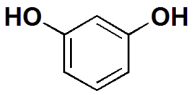

2.4

2.5

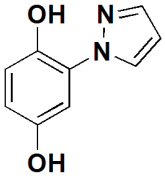

2.6

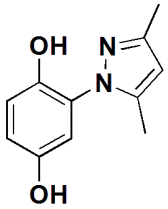

2.7

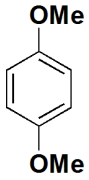

2.8

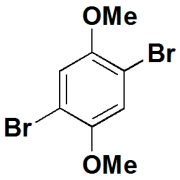

2.9

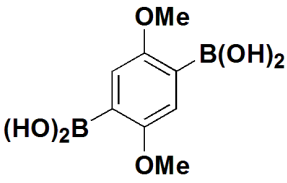

2.10

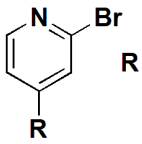

2.11 (R=H)
2.12 (R=*t*Bu)

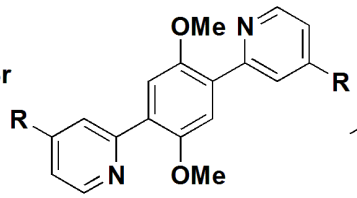

2.13 (R=H)
2.14 (R=*t*Bu)

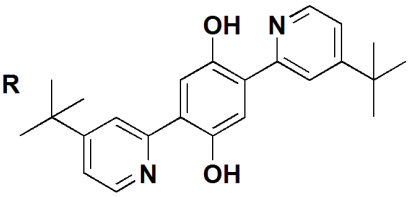

2.15

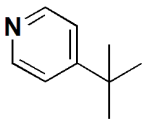

2.16

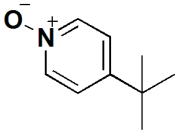

2.17

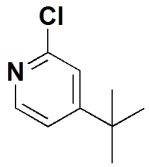

2.18

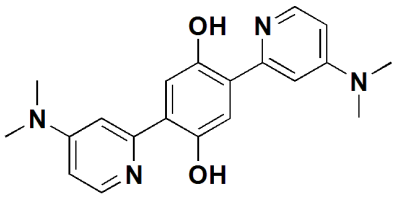

2.19

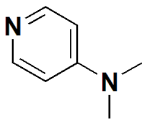

2.20

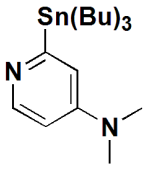

2.21

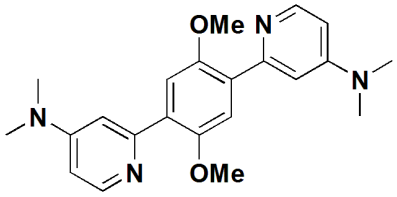

2.22

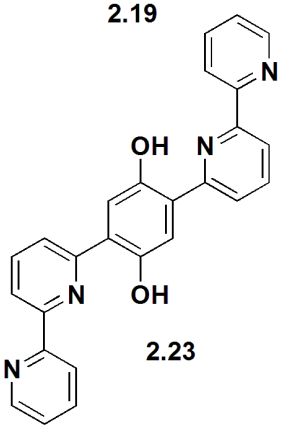

2.23

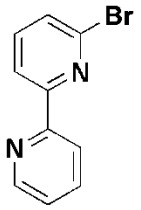

2.24

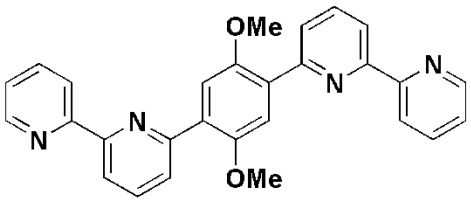

2.25

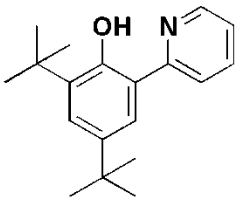

2.26

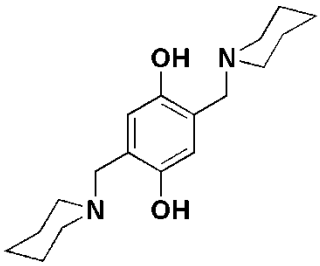

2.27

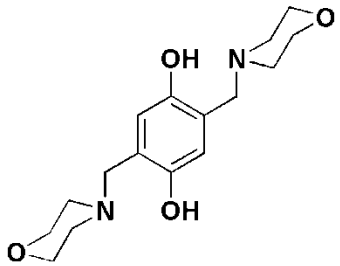

2.28

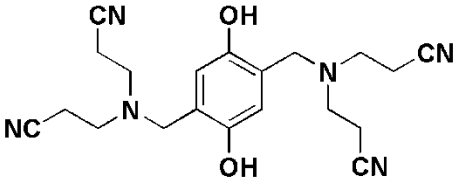

2.29

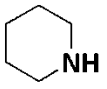

2.30

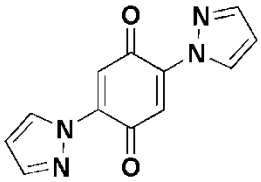

2.31

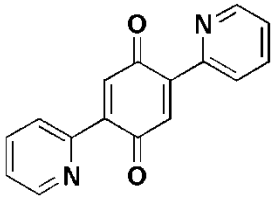

2.32

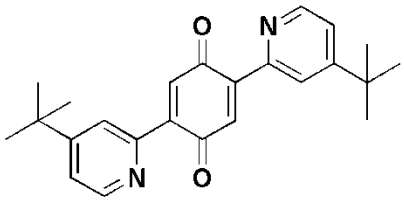

2.33

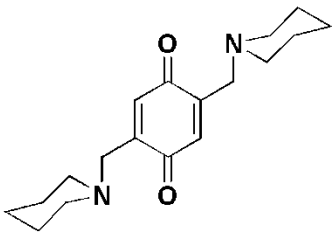

2.34

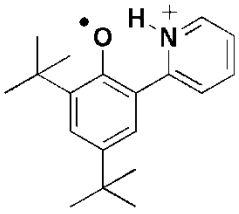

2.35

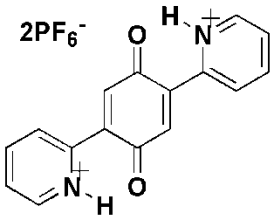

2.36

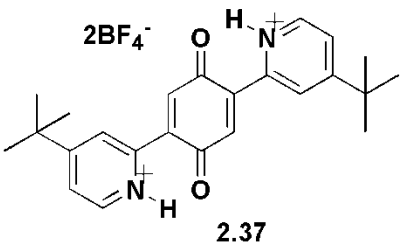

2.37

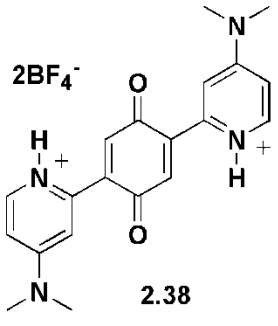

2.38

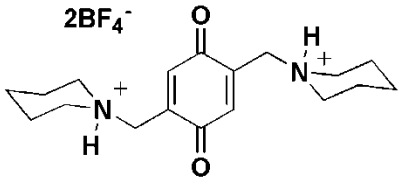

2.39

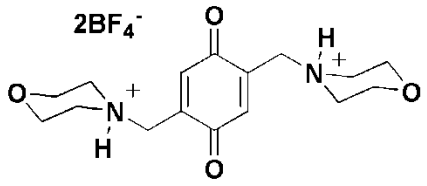

2.40

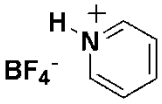

2.41

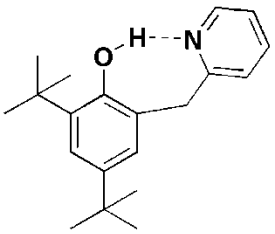

2.42

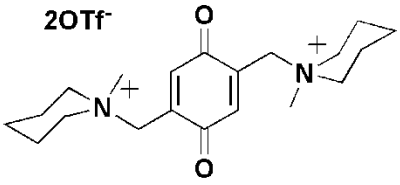

2.43

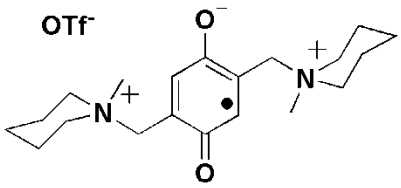

2.44

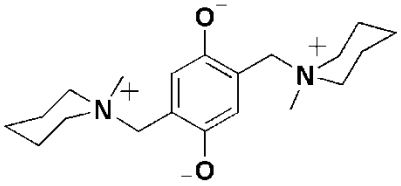

2.45

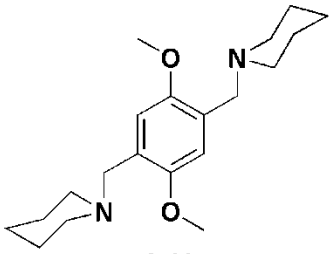

2.46

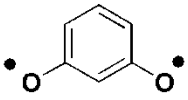

2.47

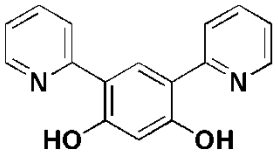

2.48

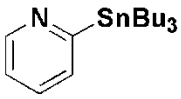

2.49

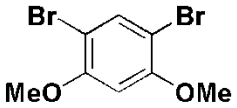

2.50

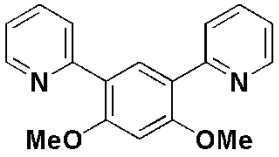

2.51

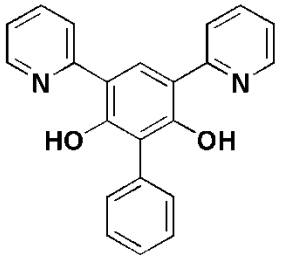

2.52

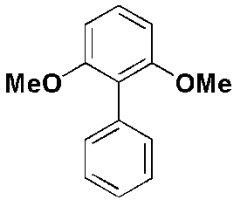

2.53

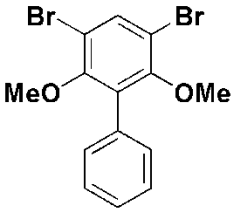

2.54

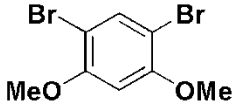

2.55

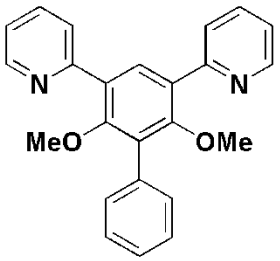

2.56

$V(CO)_6$

3.1

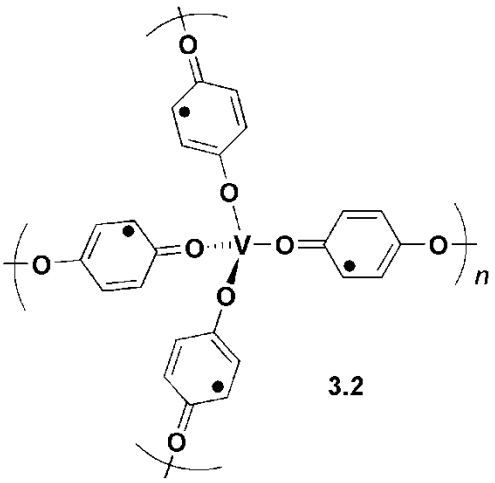

3.2

$[Ru(bipy)_2Cl_2] \cdot 2H_2O$

3.3

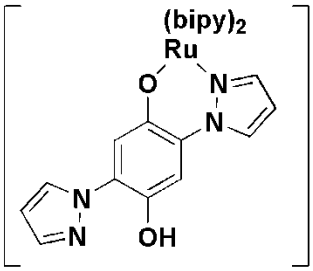

3.4

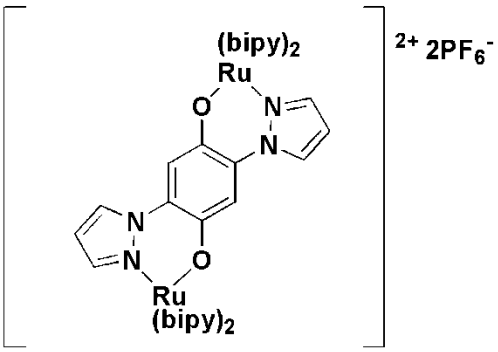

3.5

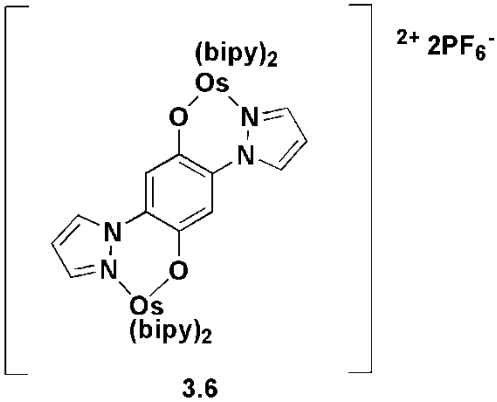

3.6

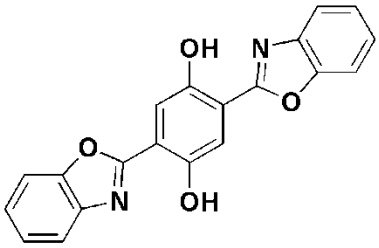

3.7

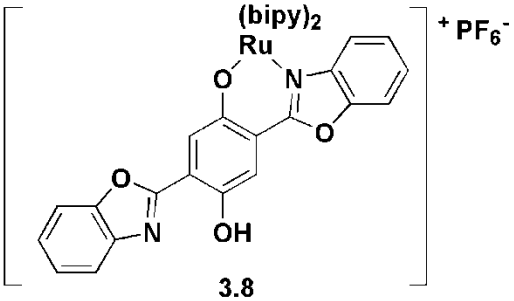

3.8

$[Os(bipy)_2Cl_2] \cdot 2H_2O$

3.9

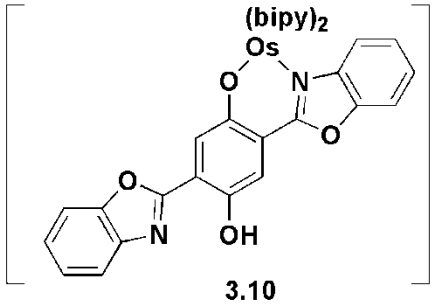

3.10

$CuBr_2$

3.11

$[Cu(PMDTA)(Me_2CO)Cl]PF_6$

3.12

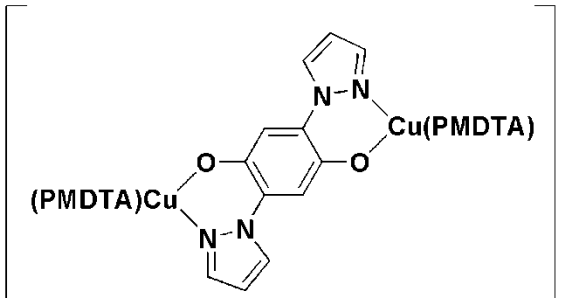

3.13

$PdCl_2$

3.14

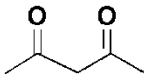

3.15

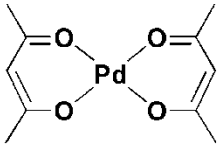

3.16

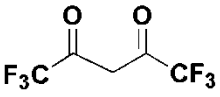

3.17

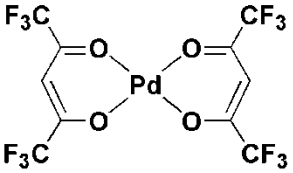

3.18

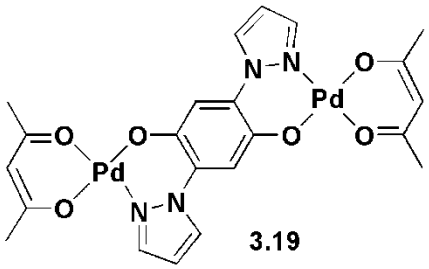

3.19

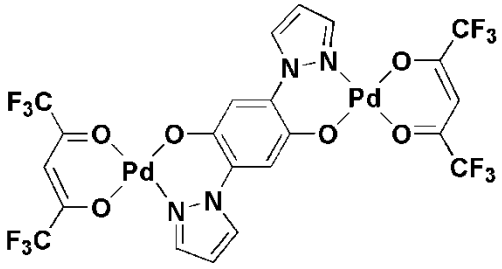

3.20

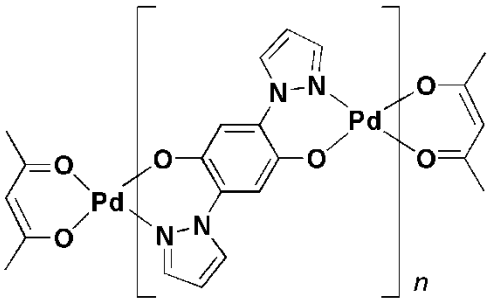

3.21

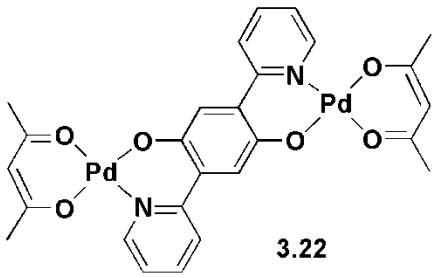

3.22

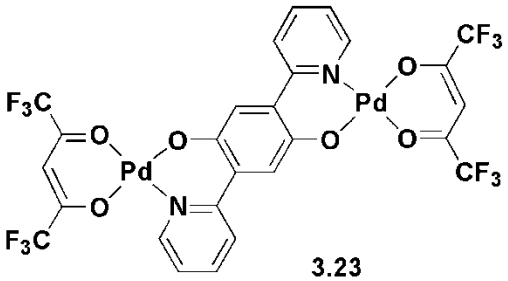

3.23

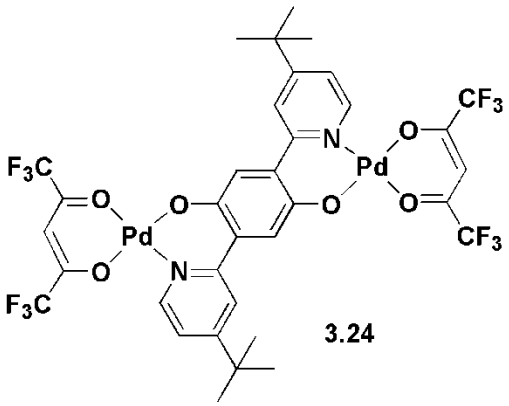

3.24

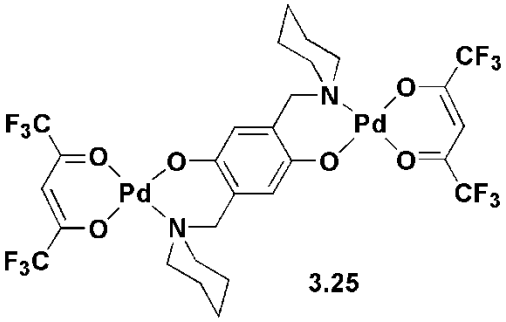

3.25

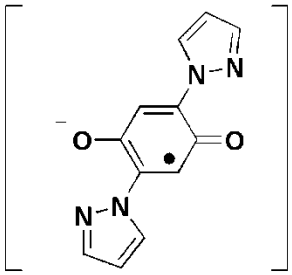

3.26

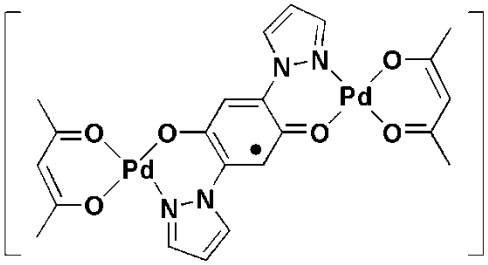

3.27

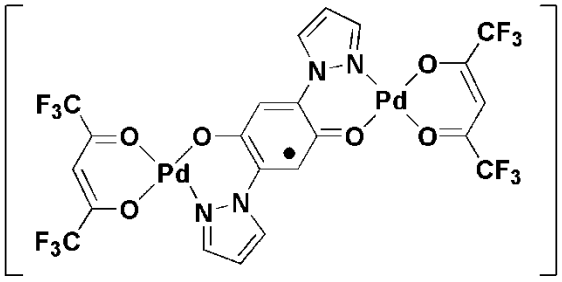

3.28

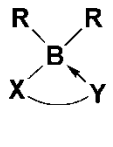

4.1

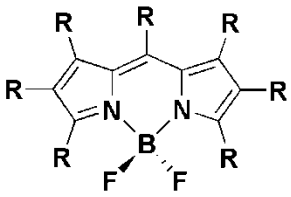

4.2

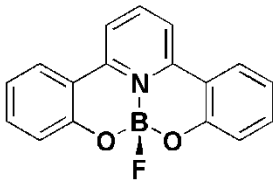

4.3

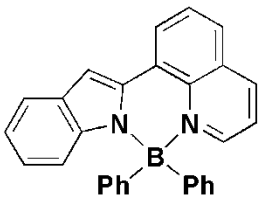

4.4

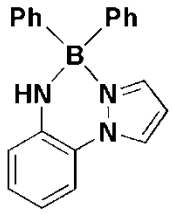

4.5

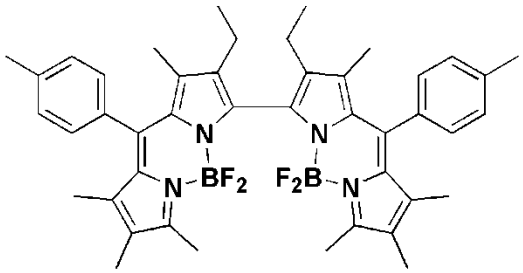

4.6

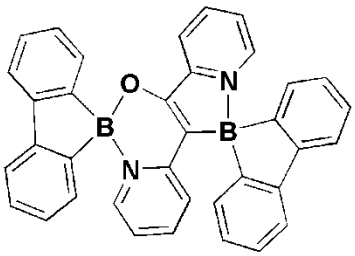

4.7

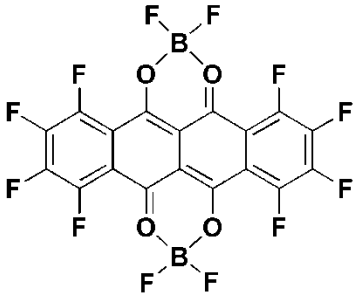

4.8

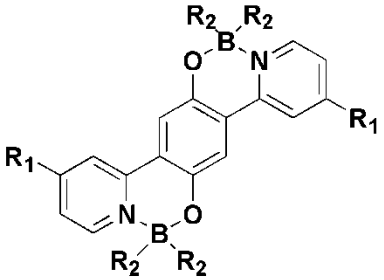

4.9 (R_1 = H, R_2 = Et)
4.10 (R_1 = CH_3, R_2 = Et)
4.11 (R_1 = H, R_2 = Ph)
4.12 (R_1 = CH_3, R_2 = Ph)

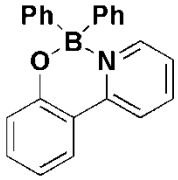

4.13

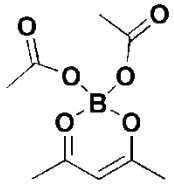

4.14

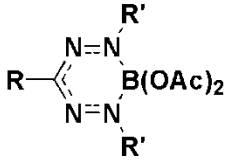

4.15

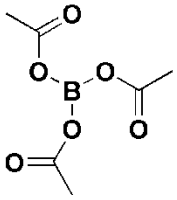

4.16

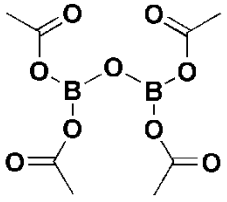

4.17

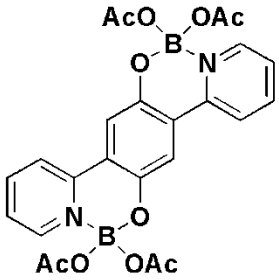

4.18

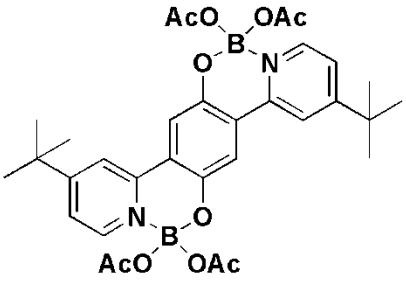

4.19

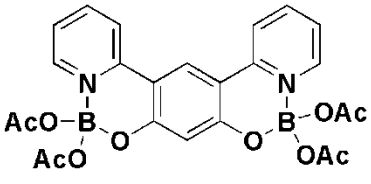

4.20

4.21

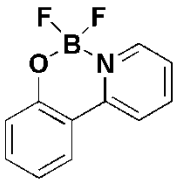

4.22

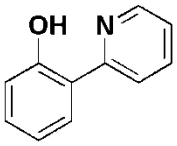

4.23

List of Abbreviations

α	hyperfine coupling constant
Å	angstrom
A	amperes
Ac	acetate
acac	acetylacetonate
AcOH	acetic acid
Ac_2O	acetic anhydride
ACN	acetonitrile
ATP	adenosine-5'-triphosphate
bipy	bipyridine
Bu	butyl
°C	degrees Celcius
ca	choranilate
calc	calculated
CPET	concerted proton electron transfer
cm	centimetre
cm^{-1}	wavenumber
CV	cylic voltammogram
d	doublet
DCM	dichloromethane
DDQ	2,3-dichloro-5,6-dicanobenzoquinone
dhbq	1,4-dihydroxybenzoquinone
DMF	dimethylformamide
DMSO	dimethyl sulfoxide
ε	extinction coefficient
E^o	standard electrode potential
E_{pa}	anodic peak potential
E_{pc}	cathodic peak potential
EPR	electron paramagnetic resonance
EtOH	ethanol
ET-PT	stepwise electron transfer and proton transfer

Fc	ferrocene
g	g-factor
g	gram
G	Gauss
h	hours
H-bond	hydrogen bond
hfac	1,1,1,5,5,5-hexafluoroacetylacetonato
HOMO	highest occupied molecular orbital
HQ	hydroquinone
Hz	hertz
I	current
IR	infrared
J	coupling constant (NMR) or magnetic exchange parameter
K	Kelvin
L	liters
LUMO	lowest unoccupied molecular orbital
µA	microamperes
m	multiplet
Me	methyl
min	minutes
mol	moles
mmol	millimoles
mL	millilitres
MS	mass spectrometry
mV	millivolts
m/z	mass per charge ratio
NADH	reduced form of nicotinamide adenine dinucleotide
n-BuLi	*n*-butyl lithium
NHE	coupled electron transfer
nm	nanometers
NMR	nuclear magnetic resonance
OAc	acetate
OMe	methoxy
OSWV	Osteryoung square wave voltammetry

p	para
Ph	phenyl
PMDTA	*N,N,N',N'',N''*-pentamethyldiethylenetriamine
PT-ET	stepwise proton transfer and electron transfer
pyz	pyrazine
Q	quinone
q	quartet
R	general functional group
R	agreement factor
RT	room temperature
s	seconds
S	spin quantum number
SCE	saturated calomel electrode
SQ	semiquinone
t	triplet
T	temperature
*t*Bu	*tert*-butyl
TCBQ	*p*-chloranil
TEAP	tetraethylammonium perchlorate
THF	tetrahydrofuran
TPA	tris(2-pyridylmethyl)amine
UV-vis	ultraviolet – visible
V	volts
λ_{max}	wavelength of maximum electronic absorption

Acknowledgments

I would first like to thank my supervisor, Robin, for his continuous guidance and encouragement over the last 5 years. His experience and knowledge in chemistry has been invaluable and will have a substantial impact on my future. In addition I am very grateful to the Hicks group members past (Joe, Raj, Sharon, Brian, Dan, Kabir, Peter and Simon) and present (Steve, Kevin, Bart, Graeme, Cooper and Kate) as they have made my time here more enjoyable and also contributed to my work in a variety of ways. I would like to thank the UVic Chemistry Department as a whole for making this a great place to work. In particular fellow grad students Mark, Danielle, Matt, Brynn, Michelle, Nick, Eric, Dean, Jakub, Shaun and Steve have all been great friends. I also am appreciative of the UVic support staff, particularly Chris Greenwood for her time and patience running countless NMR. As well thanks to Dr. Bohne and her group, who shared their lab space and equipment. Dr. Bohne also played a vital role in helping to design and interpret the fluorescence spectroscopy experiments while Effie Li made sure I was doing these experiments correctly in addition to performing the fluorescence lifetime measurements.

Dedication

For my parents Dale and Patsy, my brother Ryan and sister Tena. Thank you for always being there when I've needed you.

For Laura, my true source of happiness. You are my sunshine...

Chapter 1 Introduction and Background

1.1 General Introduction

Quinones are a class of organic compounds that possess two carbonyl groups *ortho* or *para* to each other (**1.1** and **1.2** respectively), conjugated with double bonds.[1] The structures of quinones are diverse as they can have many different substituents or additional fused aromatic groups (e.g. 1,4-naphthoquinone (**1.3**) and anthraquinone (**1.4**)).

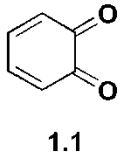

1.1

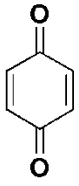

1.2

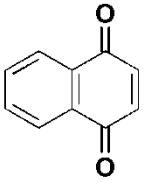

1.3

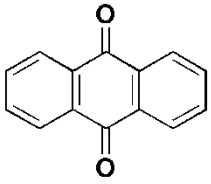

1.4

Due to quinones being redox-active and found extensively in nature, the quinone/hydroquinone redox couple is one of the most studied examples of a non-innocent ligand.[2,3] Quinones are best known for their roles in biological electron transport, mediating electron transfer between different electron-transfer chains while generating and releasing protons on differing sides of cell membranes.[4,5] For example, ubiquinone (**1.5**), is a component of aerobic respiration found in the mitochondria of most cells, mediating electron transfer between the reduced form of nicotinamide adenine dinucleotide (NADH) and succinate dehydrogenases as well as the cytochrome system, generating energy in the form of adenosine-5'-triphosphate (ATP).[6] In plants, plastoquinone (**1.6**), is involved in the energy transport chain of photosystem II.[7] Medicinal properties of some quinones include antibiotic, antimicrobial and anticancer

activity.[8] These examples represent only a small fraction of biologically important quinones.[9-21]

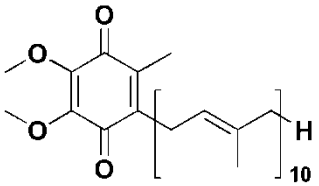

1.5

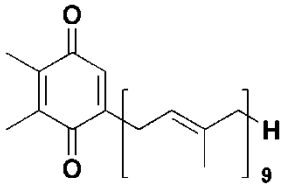

1.6

From a chemical perspective, quinones are best known for their use as redox agents. Industrially, basic solutions of hydroquinone are used as the reducing agent in developing photographic film.[22] In this process, silver bromide particles are activated by light and reduced to free silver, resulting in darkening of the film at these points. In the laboratory, quinones are most often utilized as oxidizing agents. For example, 2,3-dichloro-5,6-dicyanobenzoquinone (DDQ, **1.7**) is considered to be a strong organic oxidizing agent[23] and *p*-chloranil (**1.8**) is another, slightly weaker oxidizing agent. These oxidizing agents can also be used in oxidative coupling reactions, for example in the synthesis of benzothiazoles.[24]

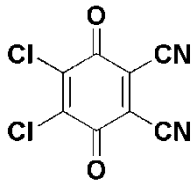

1.7

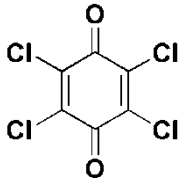

1.8

Quinones have received considerable attention in materials chemistry as redox active ligands. In this role the quinone ligand is considered to be non-innocent as its oxidation state is not always clear when bound to a metal.[25] Coordination compounds of quinones are particularly interesting due to their appeal from a theoretical standpoint and their

many potential technological applications. This chapter provides a general description of quinone redox properties, with emphasis on properties pertinent to this thesis.

1.2 Redox Chemistry of Quinones and Hydroquinones

The redox chemistry of the quinone/hydroquinone redox couple has been studied for over 70 years.[26] Simple quinones are reduced in aprotic solvents in two sequential, reversible one-electron processes to give initially the semiquinonate radical anion (**1.9**) and then the hydroquinonate dianion (**1.10**) as depicted by Scheme 1.1. The reduced species, **1.9** and **1.10**, both are long lived species in the absence of oxygen and water. Radical **1.9** is stabilized by delocalization of the unpaired electron.

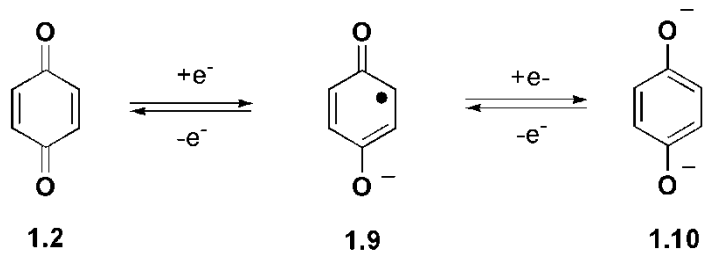

1.2 **1.9** **1.10**

Scheme 1.1 Reduction of quinone in aprotic solvents: *p*-benzoquinone (**1.2**), semiquinonate anion (**1.9**) and hydroquinonate dianion (**1.10**).

The reduction potentials of some simple quinones are given in Table 1.1. The reduction potentials are greatly influenced by the nature of the substituents. In the case of quinones fused to aromatic rings, such as **1.3** and **1.4**, the additional aromatic rings make the quinone species more difficult to reduce. On the other hand, electron withdrawing substituents such as halogens or cyano substituents, such as quinones **1.7** and **1.8**, make the quinones much easier to reduce which is why these quinones are favoured as oxidizing agents. In Table 1.1 only the first reduction potential has been reported for

each quinone since there are generally large discrepancies in the values reported for the second reduction potential. This discrepancy is thought to be due to the solvent containing trace amounts of water which can greatly affect the second reduction potential.[2]

Table 1.1. First reduction potential[27] of a few selected quinones.

Quinone #	$E_1^{o'}$ (V)	Quinone #	$E_1^{o'}$ (V)
1.1	-0.31	**1.4**	-0.94
1.2	-0.51	**1.7**	0.51
1.3	-0.71	**1.8**	0.01

(acetonitrile, reported potentials referenced vs a saturated calomel electrode (SCE), supporting electrolyte tetraethylammonium perchlorate (TEAP)).

The redox behaviour of quinones becomes more complex upon the addition of a proton source or performing the redox chemistry in protic solvents. When a proton source is available, electron and proton transfer steps are coupled to one another as depicted in Figure 1.1 and all 9 species have been proposed at one time or another by different authors under different conditions in aqueous solutions.[2] Depending on the relative acidity of the proton donor, different species may become protonated changing the redox behaviour of the quinone.[8] The following sections will outline the various ways in which protons can perturb the redox chemistry of quinones and hydroquinones.

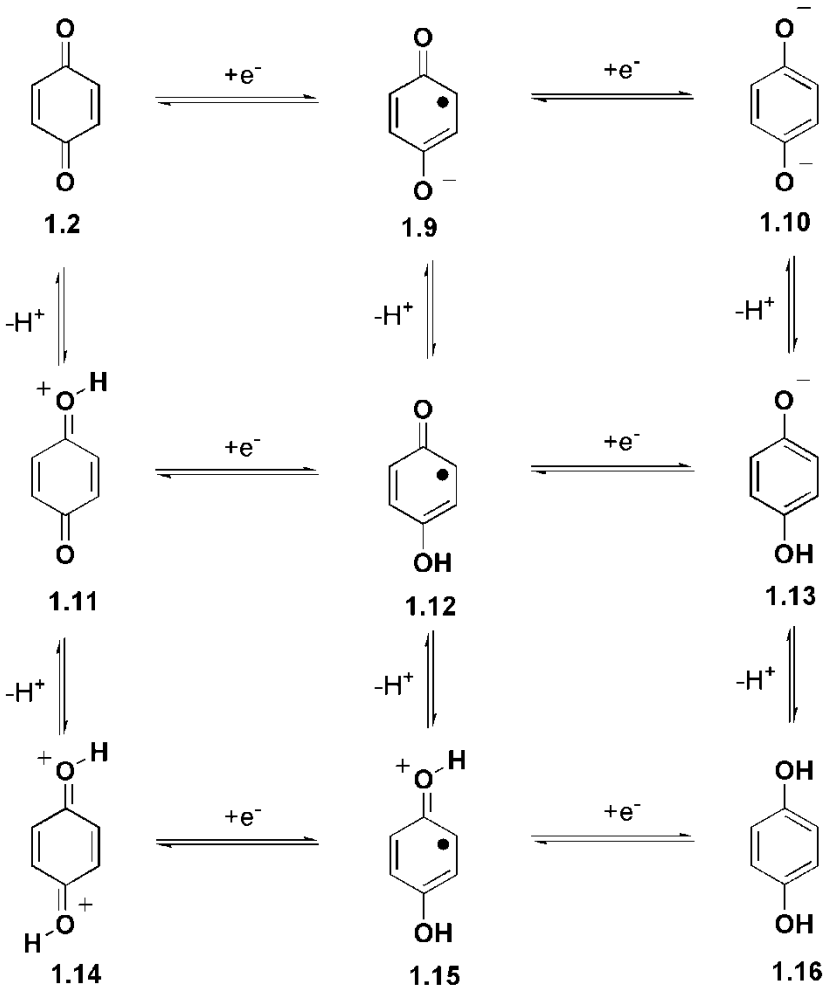

Figure 1.1. Different quinone/hydroquinone oxidation and protonation states.

1.2.1 Electrochemical studies of Quinones with Intermolecular Hydrogen Bonds

In aprotic solvents, the redox behaviour of quinones is influenced differently by the presence of various proton donors. For example, in benzonitrile *p*-chloranil (**1.8**) is reduced in two well separated reduction processes but if a weak acid such as ethanol is added, the second reduction wave moves closer to the first reduction wave and to more positive potentials due to weak hydrogen bonding interactions with the reduced species (Figure 1.2).[28]

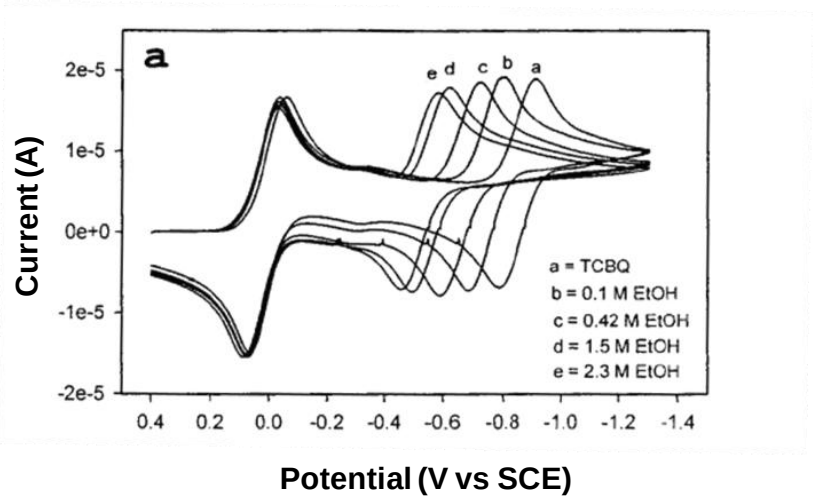

Figure 1.2. Cyclic voltammogram of *p*-chloranil (**1.8**) in benzonitrile with different concentrations of ethanol.[28]

Similarly, for anthraquinone (**1.4**) in dimethylformamide in the presence of a weak acid such as phenol, the second reduction wave moves to more positive potentials as a function of the concentration of the weak acid. In this case the dianion of **1.4** is thought to be protonated in addition to the weak hydrogen bonding interactions and if enough phenol is added the second reduction wave merges with the first reduction wave.[29] If a stronger acid such as benzoic acid is added, the first reduction wave increases in size as more acid is added while the second peak wanes.[29] This emphasizes the need for dry solvent when studying quinones electrochemical behaviour since even trace amounts of water can greatly affect the quinones redox behaviour.[30] Eventually once enough acid is added, the first reduction peak becomes a two electron process.[28,29,31] In the case of *p*-benzoquinone (**1.2**) in DMSO, the first reduction peak (Ia, Figure 1.3) changes from being reversible to irreversible upon addition of benzoic acid and if large amounts of the acid is added the wave shifts to slightly more positive potentials.[32]

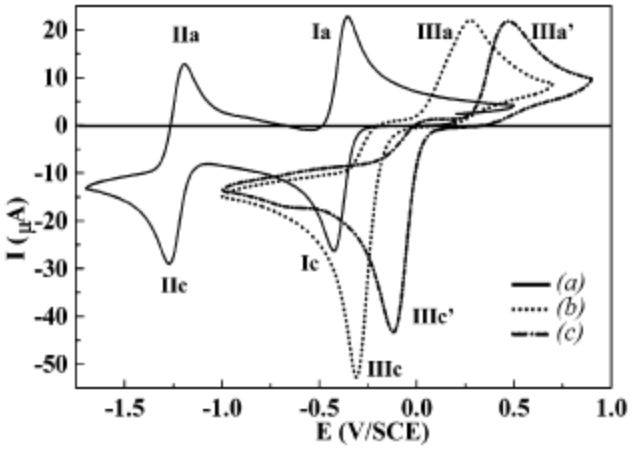

Figure 1.3. Cyclic voltammograms of *p*-benzoquinone (**1.2**) in DMSO with differing concentrations of benzoic acid (a) 0 M, (b) 0.03 M, (c) 1.0 M.[32]

Accordingly, a very strong acid such as perchloric acid, can doubly protonate a quinone to generate dication **1.14.** This results in two new quasi-reversible reduction peaks that are more positive than the original waves for quinone (**1.2**) as this is basically a series of two redox reactions between **1.14**/**1.15** and **1.15**/**1.16**.[33]

Weak proton sources that are available for hydrogen bonding have a similar effect as a weak acid as was previously described for *p*-chloranil since the second reduction wave shifts to more positive values.[34,35] With the appropriate proton source and quinone, the strength of the H-bond can be controlled depending on the quinones redox state. For example, 9,10-phenanthrenequinone (**1.17**) acts as a H-bond receptor for 1,3-diphenylurea (**1.18**) and forms a stronger H-bond when the quinone is in its fully reduced oxidation state.[36,37] The proton donor also causes the redox potentials of the quinone to shift more positive as shown by Figure 1.4.

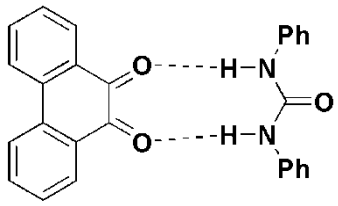

1.17 1.18

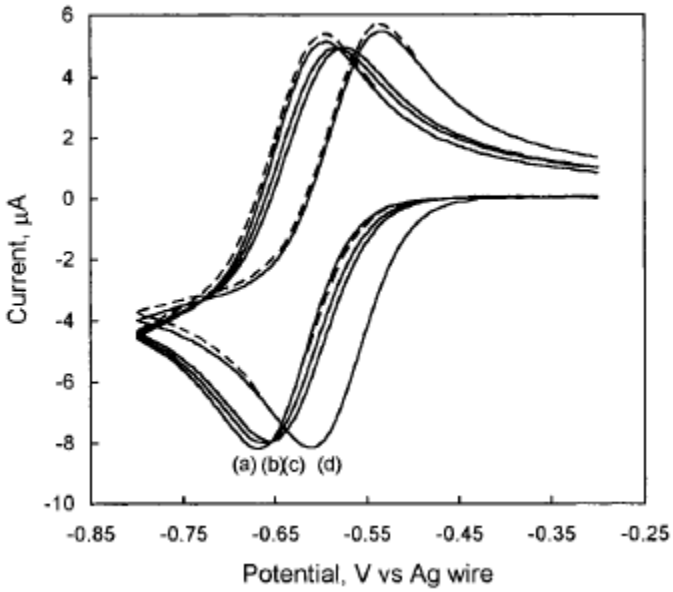

Figure 1.4. Cyclic voltammograms of 1mM of **1.17** in DMF with differing concentrations of proton donor **1.18** (a) 0 mM, (b) 0.5 mM, (c) 1 mM, (d) 10 mM.[36]

Similar results were obtained for ubiquinone with an appropriate amine such as a derivatized thiourea proton donor, demonstrating how specific recognition of quinones with H-bond donors can be utilized to control electron transfer processes.[38] In some cases H-bonding decreases the separation between the two reduction waves but the H-bonded semiquinone intermediate can still be observed by electron paramagnetic resonance (EPR) spectroscopy.[39]

In water the pH dominates the observed redox behaviour of the quinone.[40,41] In unbuffered acidic solutions or buffered solutions, the redox wave is irreversible and

appears similar to that observed for hydroquinone in aprotic solvents. If the solution is unbuffered with $[H^+] < [Q]$, the redox wave appears reversible and is a two electron process. In this case Scheme 1.2 is appropriate where the hydroquinonate dianion (**1.10**) is actually an equilibrium mixture of all three protonation states of the species (**1.10**, **1.13** and **1.16**). In unbuffered solutions, a further complication is that reduction of the quinone causes the pH near the electrode to increase since some protons are consumed. This is a problem since the quinones redox potential is pH dependent, for this reason electrochemical studies of quinones are usually carried out in buffered solutions.[40]

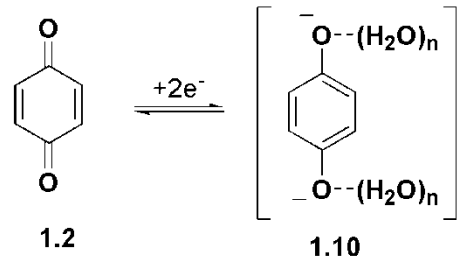

Scheme 1.2. Quinone reversible redox reaction in unbuffered H_2O where $[H^+] < [Q]$.

1.2.2 Electrochemical studies of Quinones with Intramolecular Hydrogen Bonds

Quinones with an internal H-bond behave similarly to quinones that have an external H-bond.[42] The strength of the H-bond has also been shown to correlate with the quinone reduction potential.[43] For example, 2,3-dimethylnaphthoquinone (**1.19**) is reduced at -623 mV (vs normal hydrogen electrode (NHE)), however with the addition of an intramolecular H- bond the reduction potential is shifted to -359 mV (vs NHE) for **1.20** and to -108 mV (vs NHE) for **1.21** which possesses a stronger intramolecular H-bond.

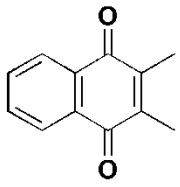

1.19

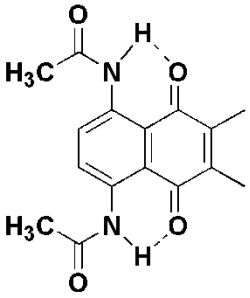

1.20

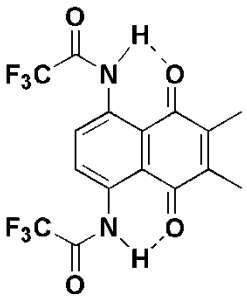

1.21

Depending on the nature of the intramolecular H-bond, self-protonation by means of an intramolecular proton transfer can also occur. In these systems the redox behaviour is more typical of the quinone in the presence of a medium strength acid such as benzoic acid or water.[44] For these quinones the semiquinone radical species can be observed by EPR.[45] For example, the electrochemical reduction of **1.22** produces a semiquinone whose EPR spectrum is shown in Figure 1.5. Analysis of this EPR spectrum indicates the upaired spin is delocalized throughout the quinone and also shows hyperfine splitting with the protons of the methoxy group.

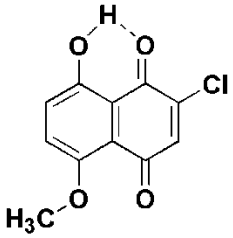

1.22

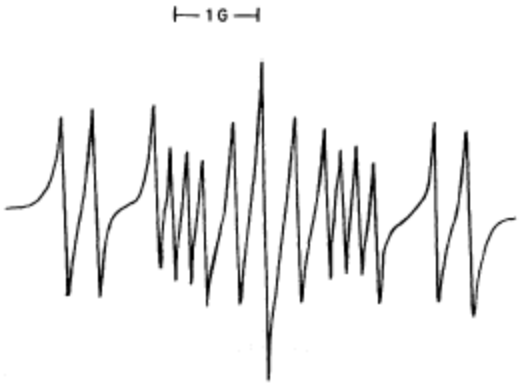

Figure 1.5 EPR spectrum of reduced quinone **1.22**.[45]

1.2.3 Electrochemical studies of Hydroquinones

Hydroquinone is oxidized in protic and aprotic solvents irreversibly in a two electron process (Scheme 1.3). In this process irreversibility arises from the proton loss upon oxidation. In the presence of strong acids such as triflic acid, the irreversible wave becomes reversible as the concentration of acid is increased, although the oxidation potential remains relatively unchanged (Figure 1.6).[46]

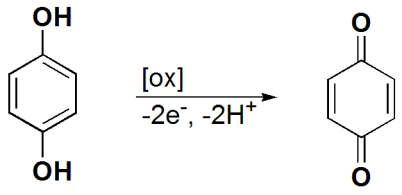

1.16 **1.2**

Scheme 1.3. Oxidation of hydroquinone.

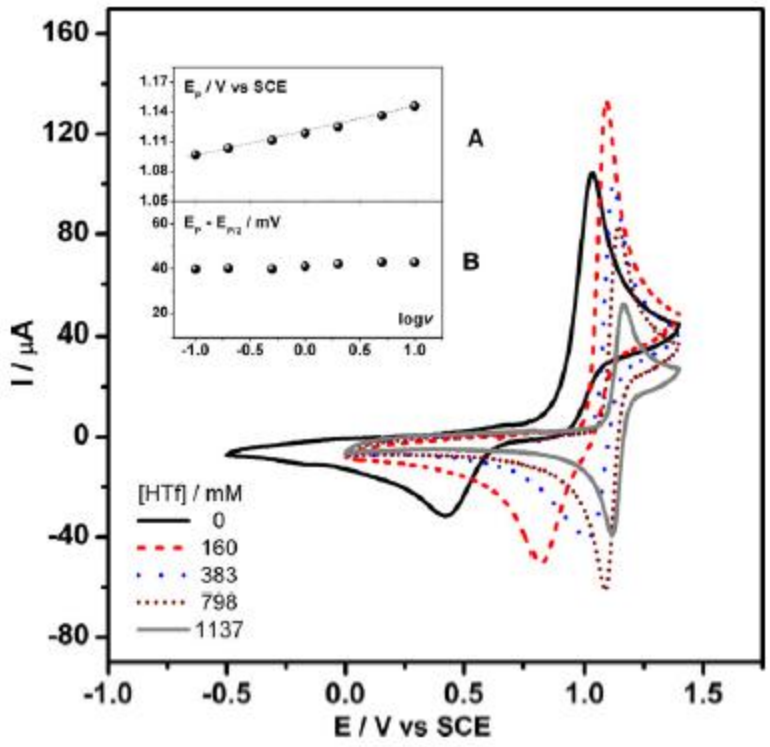

Figure 1.6. Cyclic voltammetry of 2 mM hydroquinone in acetonitrile with different concentrations of triflic acid.[46]

Amorati *et al*. have examined how the reactivity of 2,5-di-*tert*-amylhydroquinone with free radicals increases upon the addition of hydrogen bond acceptor solvents due to the difference in strength of hydrogen bonds formed in the parent hydroquinone and semiquinone radical.[47] Other than these studies there have been few investigations showing how hydrogen bonds and proton transfers perturb the reactivity and electrochemistry of hydroquinones.

Recently, Savéant *et al.* probed the effects of intramolecular H-bonds on the redox behaviour of a hydroquinone.[48] His work focused on a hydroquinone substituted with two carboxylic groups (**1.23**). Upon oxidation **1.23** shows an irreversible process typical of hydroquinone. If a strong base is added the dianion **1.24** is formed and the two

carboxylate groups can act as proton acceptors. Upon oxidation the dianionic hydroquinone, **1.24**, shows a quasi-reversible redox wave described as two closely spaced one electron waves depicted by the redox process in Scheme 1.4. The redox process shows a small deuterium isotope affect and as a result it was concluded that the oxidation mechanism is a concerted proton electron transfer (CPET).[48] A CPET process falls under the more general class known as proton coupled electron transfers (PCET), which until recently had been thought to be a stepwise electron and proton transfer (ET-PT) or stepwise proton and electron transfer (PT-ET).[49] This has been questioned and evidence shows that in some cases proton and electron transfer occurs synchronously, or in a CPET process. The CPET mechanism is particularly significant as higher energy intermediates are avoided by the coupled mechanism and may provide some insight in the efficiency of enzymatic and other biological systems. Similar results have been found for several phenols with intramolecular H-bonds. These systems, along with hydroquinone **1.23** will be discussed in more detail in Chapter 2.

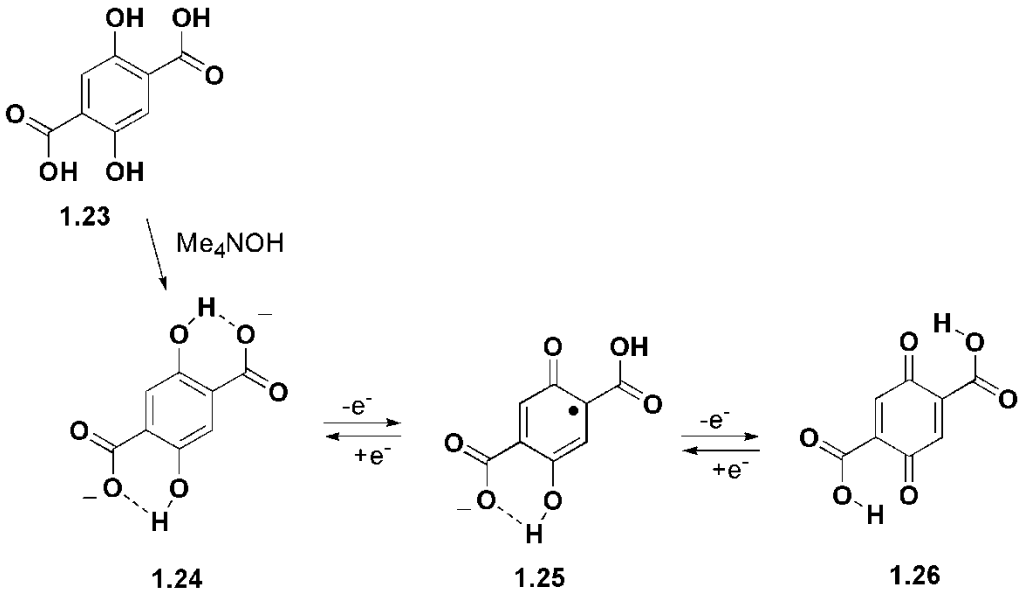

Scheme 1.4. Oxidation of hydroquinone dicarboxylate dianion **1.24** via CPET mechanism.[48]

1.3 Metal Complexes of Quinones

1.3.1 *Ortho*-Quinone Complexes

The development of the chemistry and physical properties of transition metal complexes of *ortho*-quinone (**1.1**) ligands began in earnest in the 1970s. The *o*-quinone ligands ability to chelate makes it an excellent ligand and when bound to a metal center its redox chemistry is preserved. In the last 30 years this subject has received a great deal of attention due to the biological relevance of some of these complexes.[50,51] Research has also focused on determining the electronic structure of these complexes to unequivocally establish the oxidation state of the non-innocent ligand.[52,53] In addition, some metal complexes of *o*-quinones display desirable physical properties such as magnetism.[54]

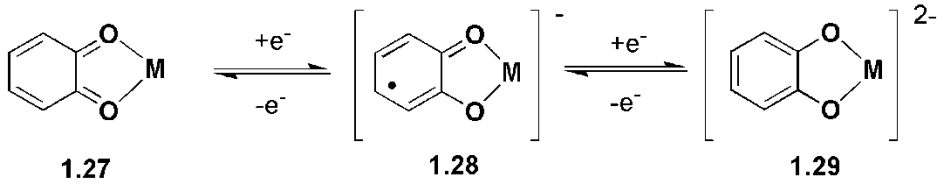

Scheme 1.5. Different oxidation states of the *o*-quinone ligand: benozoquinone (**1.27**), semiquinone (**1.28**) and catecholate (**1.29**).

Initially, most of the research on coordination complexes of *o*-quinone type ligands focused on their affinity for iron due to these complexes' biological relevance.[51] For example, siderophores are a class of low molecular weight iron chelating agents.[55] Of particular interest is enterochelin which is found in enteric bacteria using three catecholate groups to chelate ferric iron. Raymond *et al*. have estimated the formation constant of enterochelin with ferric iron to be very large (~10^{40}-10^{45}).[50] Since this time there have been many other papers studying biologically relevant coordination complexes

of *o*-quinones.[54] For example, very recently Solomon *et al*. have examined the reaction of a model complex of Tyrosinase with a phenolate to give a catecholate metal complex that ultimately results in a mixture of catechol and quinone products.[56]

Due to the redox nature of the *o*-quinone ligand, when coordinated to a transition metal the quinone ligand is described as being non-innocent since the origin of redox steps as being ligand- or metal-based can be ambiguous. The non-innocent ligand can coordinate to metal ions in distinctly different oxidation states resulting in discrepancies in the description of the electronic structures. Dithiolenes (**1.30**) and diimines (**1.31**), the sulphur and nitrogen analogues of quinones, are also redox active and considered to be non-innocent ligands. The electronic structure of transition metal complexes of **1.30** and **1.31** received considerable attention in the last century.[57-59] For example, two extremes were considered in the 1960s for the dithiolene complex of Ni^{II}, **1.32**. Gray contended that the dithiolene ligands of **1.32** should be viewed as two delocalized radicals[60] whereas Holm argued that **1.32** should be considered as a resonance structure where one dithiolene ligand was fully reduced and the other fully oxidized.[61] It is now widely accepted that the electronic structures for bis(1,2-dithiolene) complexes are best described as being delocalized.[58]

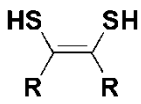

1.30

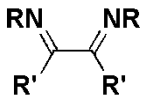

1.31

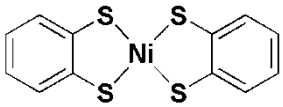

1.32

In contrast, the electronic structure of *o*-quinone complexes is generally best described as being charge localized, making it easier to identify the oxidation state of the quinone ligand.[53] Pierpont has studied periodic trends in charge distribution of *o*-quinone

complexes of a range of transition metal ions. He found that the energetic proximity of quinone and metal orbitals leads to distinctive ligand preferences for certain oxidation states based on which metal was used.[52,53,62] In particular, ruthenium and osmium *o*-quinone complexes were found to have metal and ligand orbitals close in energy as these complexes displayed evidence for increased ligand and metal orbital mixing.[52]

Particularly relevant to this work, Pierpont has also synthesized a semiquinone complex of palladium, **1.33**.[53] The two ligands in **1.33** were established by X-ray crystallography to be in the semiquinone redox state in agreement with EPR and UV-vis spectroscopic results. Despite the presence of two radical ligands, the complex was found to be diamagnetic by magnetic susceptibility measurements due to antiferromagnetic exchange between the two semiquinone ligands across the palladium metal. Examples of complexes containing non-innocent ligands exemplify that the physical oxidation state for such complexes should be a measured quantity by spectroscopic methods and crystal structure determination.[63,64]

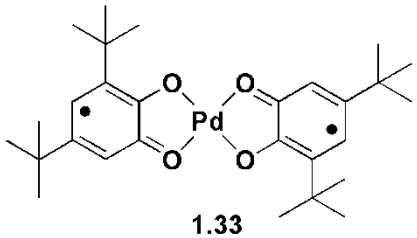

1.33

O-quinone complexes have more recently received considerable attention as building blocks for magnetic materials.[65] In particular, semiquinone ligands bound to a paramagnetic metal are of particular interest as the unpaired electrons of the metal and semiquinone have been shown to have strong magnetic exchange interactions.[51] For example, the copper-semiquinone complex **1.34**, exhibits strong metal-ligand ferromagnetic interactions ($J = 220 cm^{-1}$).[66]

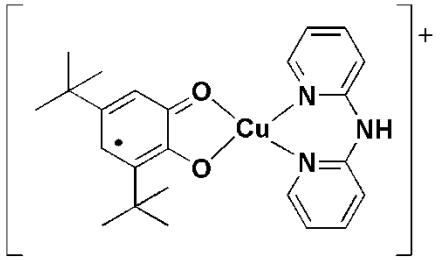

1.34

The redox activity of some *ortho*-quinone complexes leads to the phenomenon known as "valence tautomerism", defined as an intramolecular electron transfer between two redox-active centers resulting in the formation of two electronic isomers. Such electronically bistable molecules exhibit intramolecular electron transfers from a variety of external driving forces such as changes in pressure, temperature, pH and light.[67] One example is cobalt(2,2'-bipyridine)bis(3,5-di-*tert*-butyl-1,2-benzoquinone) (**1.35**) shown in Figure 1.7.[68] At room temperature, magnetic characterization indicates the compound has a magnetic moment corresponding to S = 1/2 but at high temperatures the magnetic moment corresponds to S = 5/2. Analysis of the crystal structures and other characterization data of the high and low temperature forms proved at low temperatures **1.35** dominates, in which cobalt has a low spin Co^{III} oxidation state and the unpaired spin arises from one semiquinone radical. At high temperatures **1.36** dominates, in which cobalt has a high spin Co^{II} oxidation state bound to two semiquinone radicals resulting in S = 5/2. The cobalt complex **1.35** was later shown to be reduced reversibly such that an array of 4 different states can be achieved.[69]

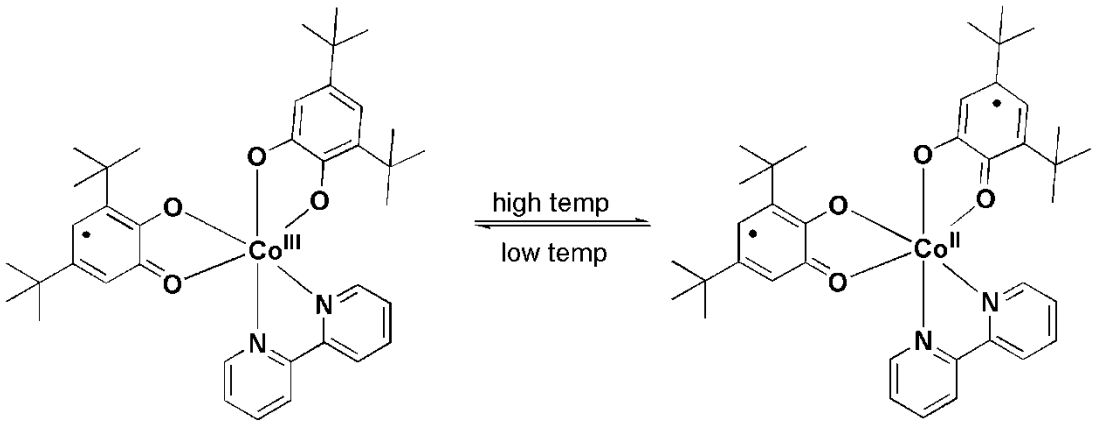

1.35 **1.36**

Figure 1.7. Valence tautomerism of **1.35** and **1.36** induced by a temperature change.

One limitation of *o*-quinone type ligands is their inability to chelate to more than one metal. The most desirable structure for bulk magnetism requires all of the individual spins to be covalently linked which requires a bridging ligand. For this reason two *o*-quinones tethered by a conjugated linker have been synthesized and used to make complexes with more than one metal.[65] One example of a dinuclear *o*-quinone complex is that of cobalt complexed by two semiquinone units tethered by a conjugated hydrazone bridge (**1.37**).[70] However, no extended examples of multimetallic complexes of *o*-quinones are known.

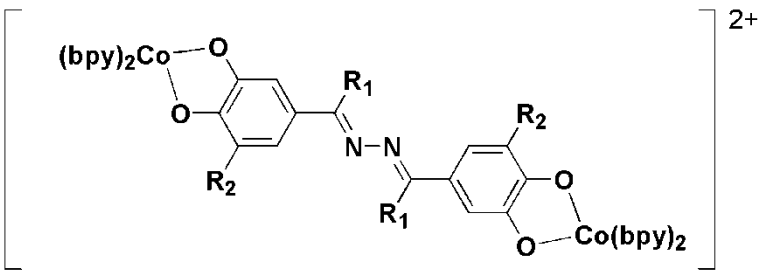

1.37

1.3.2 *Para*-Quinone Complexes

In comparison to their *ortho* counterparts, *para*-quinone complexes have been explored to a far lesser extent mainly due to the poor binding ability of most monodentate quinones. However, by installing adjacent chelating groups to the hydroxyl moieties (**1.38**), the ligand has been shown to complex transition metals and unlike the *o*-quinone ligand, can easily bind more than one metal.

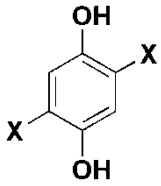

1.38

As a result, these types of chelating *p*-quinones are considered to be excellent candidates for molecular building blocks, where the possibility of designing metal-semiquinone based 2D chains and 3D networks may result in molecular magnets that display bulk magnetism.

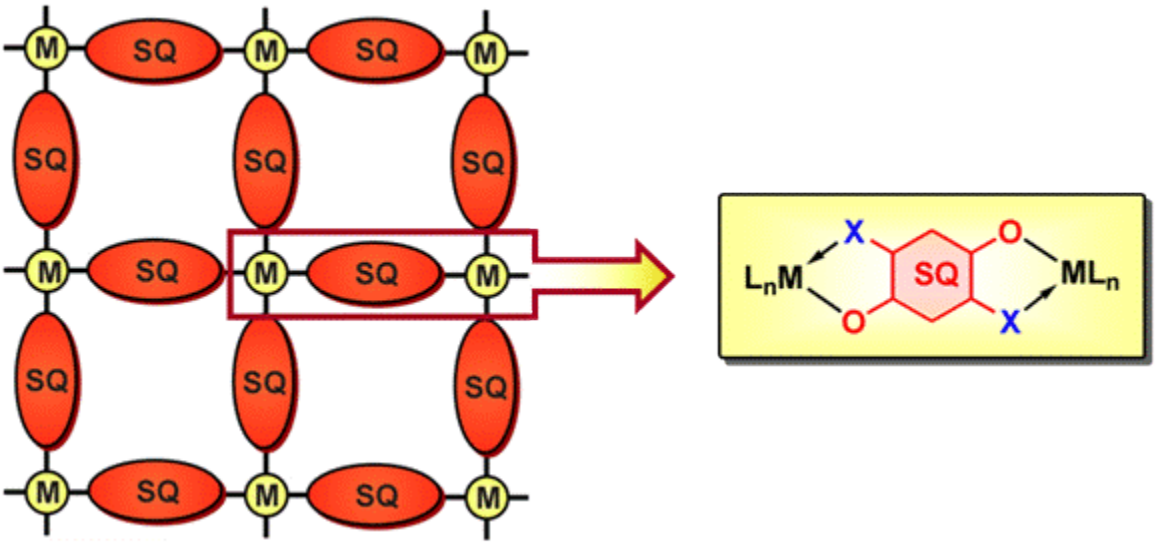

Figure 1.8 Example of a *p*-semiquinone-metal network and a binuclear model complex.

The first published example of a *p*-quinone complex was of duroquinone and nickel.[71] In this instance the quinone was bound to the metal as a π complex. Very few complexes of *p*-quinone ligands were found in the literature until the last 10 years. Keramidas *et al*. published the synthesis and structures of a hydroquinonate (**1.10**) and semiquinonate (**1.9**) type ligands bound to vanadium.[72] Miller recently expanded upon this work examining the magnetic properties of the vanadium complexes.[73] Keyes *et al*. has exploited poly-pyridyl hydroquinones to synthesize mono-nuclear ruthenium and osmium complexes examining primarily their optical properties.[74] Wagner *et al*. have synthesized chains (**1.39**) and smaller mono- and dinuclear complexes of Cu^{II} and 2,5-bis(pyrazol-1-yl)-1,4-hydroquinone.[75,76] Such compounds were found to have antiferromagnetic coupling between the two copper metals across the bridging hydroquinone. These examples of complexes of *p*-quinones will be discussed in more detail in Chapter 3.

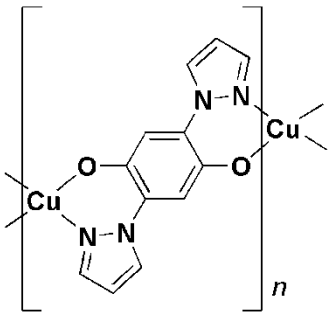

1.39

Tetraoxolene ligands (**1.40**) have also been used to make a variety of complexes including mono-, di-, and polynuclear metallic complexes.[77] Many different coordination polymers have been isolated including honeycomb and rectangular lattices, examples of which are given in Figure 1.9 and 1.10. However, the redox activity or paramagnetism of coordination polymers has not yet been demonstrated. Miller has recently published iron and cobalt complexes of chloranilate (**1.41**).[78-80] Dinuclear complexes (**1.42**) bridged by

the chloranilate radical trianion have much stronger intramolecular interactions (ie. spin coupling) than the analogous complexes bridged by the closed shell chloranilate dianion because the radical ligand can participate in direct spin exchange. In addition, related dinuclear tetraoxolene complexes of cobalt (**1.43**) have also been shown to display valence tautomerism.[81,82]

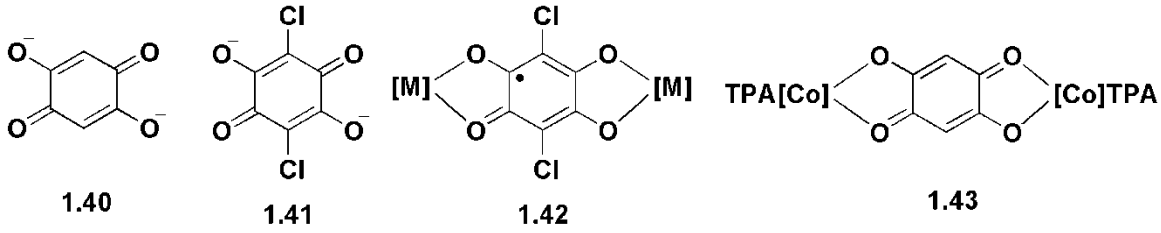

1.40 **1.41** **1.42** **1.43**

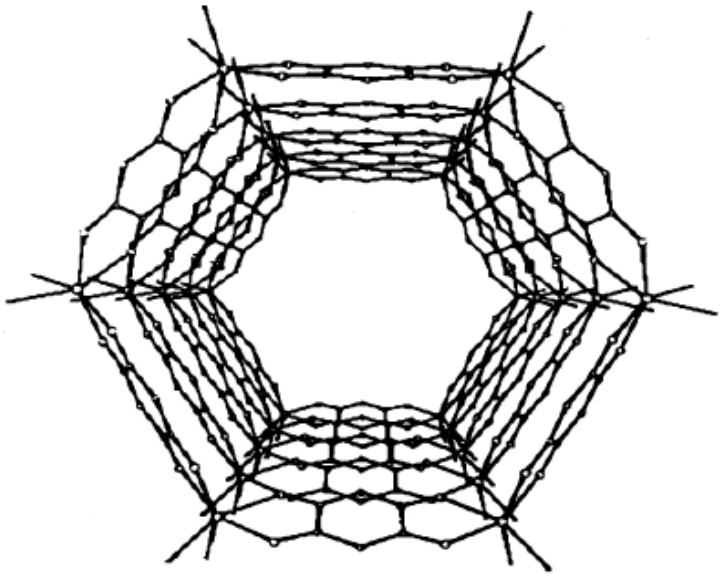

Figure 1.9. Example of stacked honeycomb layers of $[Na_2(H_2O)_{24}[Mn_2(dhbq)_3]]_n$ forming channels (where dhbq = **1.40**).[77]

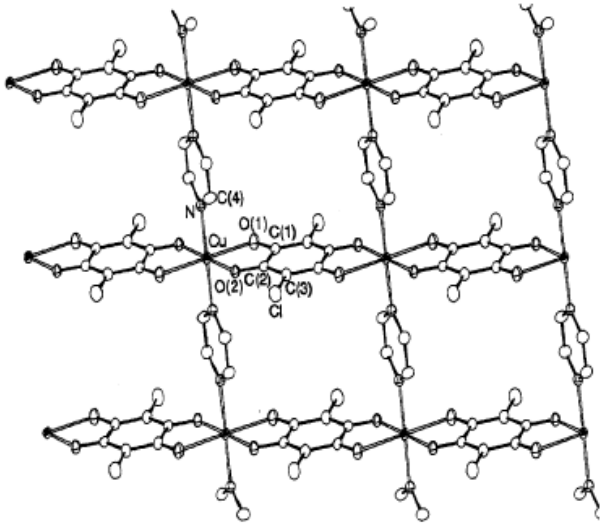

Figure 1.10. Example of a rectangular lattice of $[Cu(ca)(pyz)]_n$ (where ca = **1.41** and pyz = pyrazine).[83]

1.4 Thesis objectives

Complexes of paramagnetic metals and organic radicals have been shown to exhibit strong magnetic exchange. However bulk magnetic behaviour along with room temperature ordering is extremely rare.[84,85] There are many potential benefits of molecular magnets such as low density and solution based synthesis. Moreover, they may allow for the tailoring of the magnetic properties and provide other mechanical, electrical and/or optical properties that maybe useful.

Initially the goals of my research were to further develop the coordination chemistry of *p*-hydroquinones of the type exemplified by **1.38** where the electronic interaction across a quinone type bridge could be examined as depicted by the dinuclear complex in Figure 1.8. During the course of the synthesis and characterization of different *p*-hydroquinones

and their corresponding *p*-benzoquinone redox couples, some of the hydroquinones were discovered to possess unusual redox behaviour compared to conventional hydroquinones. These unexpected results prompted an in depth study of the redox properties of derivatized hydroquinones and the characterization of a new class of quinoidal dications. The synthesis, characterization and electrochemical behaviour of these compounds are presented in Chapter 2.

Transition metal complexes of *p*-quinones are primarily of interest due to the non-innocence of the ligand. The electronic structure of *o*-quinone complexes has been shown to be charge localized unlike dithiolenes and diimines. *P*-quinone complexes have been studied considerably less although copper, ruthenium and osmium complexes display similar features to their *o*-quinone analogues. To expand on the group of *p*-quinone complexes studied, dinuclear palladium complexes of the derivatized hydroquinones were synthesized. The electrochemical and characterization details of these complexes are presented in Chapter 3.

The final component of this thesis contains some studies on complexes of boron. There are very few examples of quinone coordination complexes of main group elements. We were interested to see if the coordination of a main group element perturbed the electrochemistry of the bridging ligand in a similar manner to palladium. To this end, derivatized hydroquinones were complexed with boron and found to be highly fluorescent. The synthesis, electrochemistry and characterization of these complexes are given in Chapter 4.

Chapter 2 Synthesis and Redox Properties of *Para*-Benzoquinones, *p*-Hydroquinones and Related Compounds

2.1 Introduction

As was described in Chapter 1, the initial focus of this thesis was to synthesize metal complexes of *para*-hydroquinones and to probe how the ligand's electrochemistry was perturbed. With this in mind *p*-hydroquinones derivatized with an adjacent nitrogen donor resulting in ligands with multiple chelating sites were targeted. In particular, the initial focus of this research was towards two literature hydroquinone compounds, *p*-hydroquinone substituted in the 2,5-positions with pyrazole (**2.1**)[86] or pyridine (**2.2**).[87] These hydroquinones have two bidentate coordination pockets which allows for the bridging of two metals. The corresponding quinone of **2.1** had not been published at the start of this research and the corresponding quinone or any coordination complexes of **2.2** were unknown. The synthesis of related hydroquinone/quinone redox couples of **2.2** were also pursued where the 4-position of pyridine was derivatized. During the course of the synthesis and characterization of **2.2** and related derivatives, the hydroquinones were found to possess very interesting electrochemical properties of their own. This prompted the synthesis of a second set of *p*-hydroquinones substituted in the 2,5-positions with non-conjugated amines separated by a methylene linker as depicted by **2.3**. This second set of non-conjugated hydroquinones help to probe the effects of conjugation (or lack thereof) on the redox chemistry of the hydroquinones. The syntheses and characterization, with a particular emphasis on the redox properties of these hydroquinones and their corresponding quinones, will be discussed in this chapter. The

redox properties of some related derivatives of resorcinol (**2.4**), the *meta* substituted analogue of *p*-hydroquinone, will also be examined.

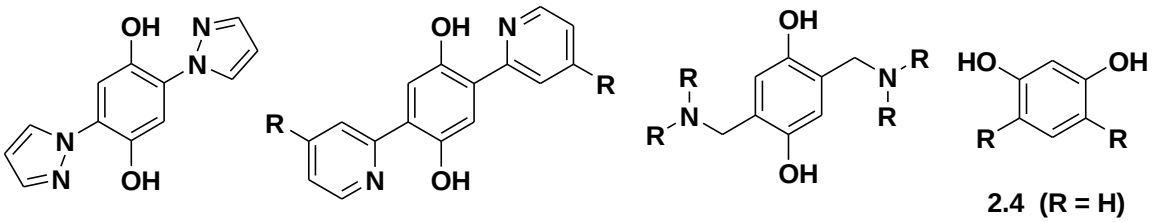

2.1 **2.2 (R = H)** **2.3** **2.4 (R = H)**

2.2 Synthesis and Characterization of Disubstituted *p*-Hydroquinones with Conjugated Substituents

2.2.1 2,5-Bis(pyrazol-1-yl)-1,4-hydroquinone

2,5-Bis(pyrazol-1-yl)-1,4-hydroquinone (**2.1**) can be synthesized by the direct reaction between pyrazole (**2.5**) and *p*-benzoquinone (**1.2**) (Scheme 2.1). In the original synthesis one equivalent of pyrazole is used, resulting in a 10% yield. In this reaction the pyrazole is actually in excess considering that 2/3 of the *p*-benzoquinone is used as an oxidizing agent.[88] We found that the yield of **2.1** could be doubled to 20% by using two equivalents of pyrazole for each equivalent of benzoquinone, changing the solvent to ethanol and increasing the reflux time to 16 hours. Attempts to increase the yield by adding an oxidizing agent such as cupric acetate monohydrate resulted in a mixture of products.

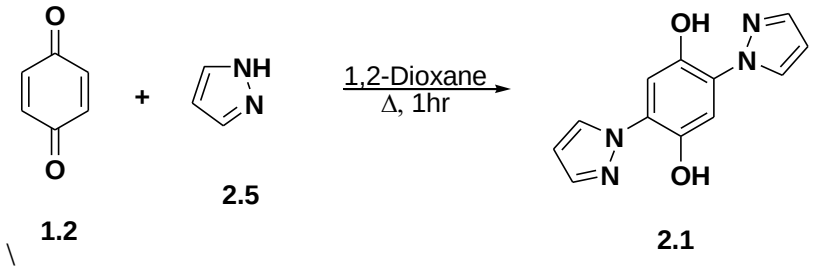

Scheme 2.1. Literature synthesis of **2.1**.[86]

The previously reported X-ray crystal structure of **2.1** shows the expected structural features for a hydroquinone, such as equal C-C bond lengths within the hydroquinone benzene ring.[86] The structure also has intramolecular hydrogen bonds between the phenolic protons and the adjacent pyrazoles with an O--N distance of 2.611 Å. The intramolecular hydrogen bonds are also evident in solution in the ^{1}H-NMR spectrum of **2.1** as the OH protons are found at 11.16 ppm in $CDCl_3$. In contrast, related compounds **2.6** and **2.7** have an additional phenolic proton that does not participate in an intramolecular hydrogen bond. The ^{1}H chemical shifts of the non-hydrogen bonded phenolic OH protons are at ~4 ppm in $CDCl_3$.[86] The solution infrared spectrum of **2.1** in CH_3CN was obtained and provides further evidence of the intramolecular hydrogen bond in solution: a broad absorption from ~3300-2600 cm^{-1} which is typical for a hydrogen bonded alcohol group.[89]

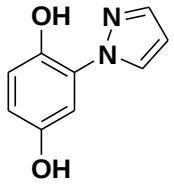

2.6

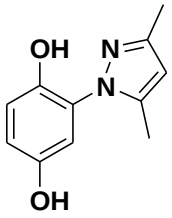

2.7

2.2.2 2,5-Bis(pyrid-2-yl)-1,4-hydroquinones

2,5-Bis(pyrid-2-yl)-1,4-hydroquinone (**2.2**) was first reported by Shu *et al.*[87] Their synthesis starts from 1,4-hydroquinone by protecting the OH groups with benzyl groups followed by the installation of the pyridine groups by a Suzuki-Miyaura coupling reaction. This general strategy was followed as shown in Scheme 2.2, except that methyl was used as the protecting group as the methoxy substituted compound, **2.8**, is commercially available.

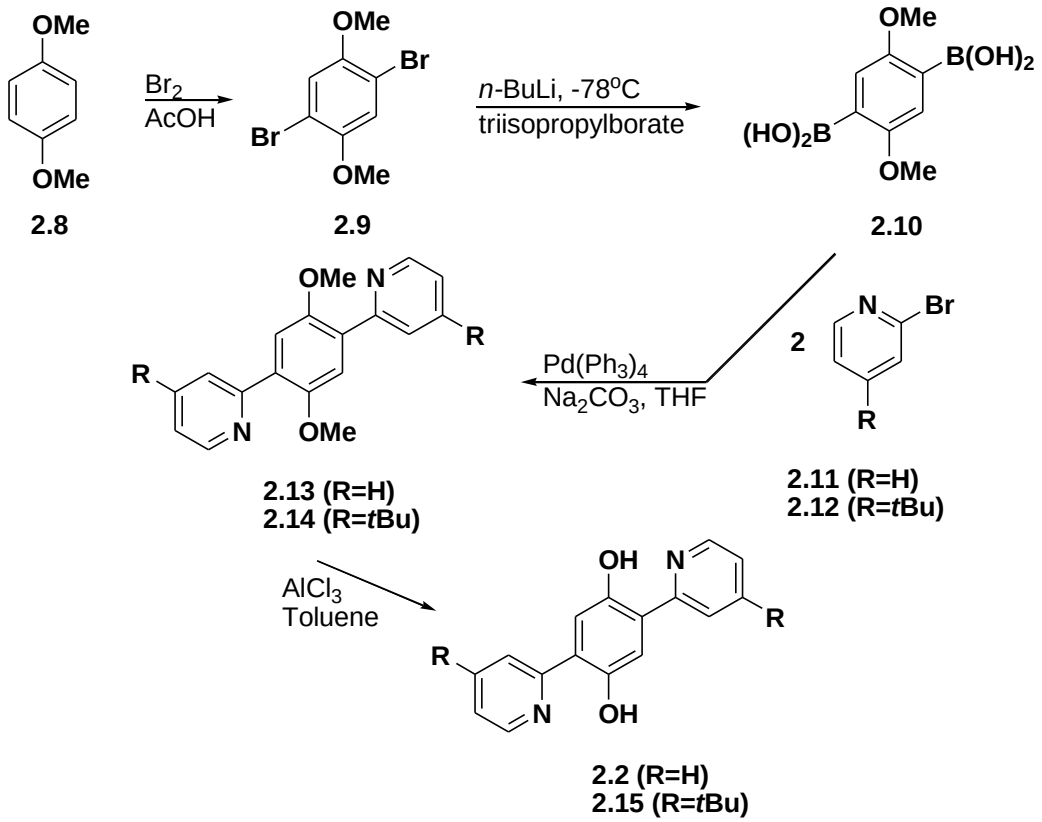

Scheme 2.2. Synthesis of **2.2** and the *tert*-butyl derivative **2.15**.

The first step in the synthesis of **2.2** was the bromination of 1,4-dimethoxybenzene in acetic acid as reported by Lopez-Alvarado *et al.*[90] This was then converted to the diboronic acid (**2.10**) which was then coupled with 2-bromopyridine in a Suzuki-Miyaura

coupling reaction, similarly to that reported by Monkman *et al.*[91] The methoxy groups of **2.13** were then deprotected with $AlCl_3$ to give **2.2**. The overall yield of the synthesis of **2.2** was 28%, an improvement over the original literature synthesis (7.8 % yield).[87]

Compound **2.2** is not very soluble in many solvents and this characteristic is even more pronounced for some of its coordination complexes discussed in Chapter 3 and 4. For this reason a derivative of **2.2** was synthesized with a bulky *tert*-butyl group in the 4-position of the pyridine group (**2.15**) to improve solubility properties. 2-Bromo-4-*tert*-butylpyridine (**2.12**) was synthesized in a similar manner reported by Barolo *et al.* as illustrated in Scheme 2.3.[92] 4-*Tert*-butylpyridine (**2.16**) was first converted to its *N*-oxide (**2.17**) by oxidation with *meta*-chloroperoxybenzoic acid (*m*CPBA). The *N*-oxide was then refluxed in an excess of $POCl_3$ converting it to 4-*tert*-butyl-2-chloropyridine (**2.18**). The chloride in **2.18** was then converted to bromide by treatment with HBr in acetic acid to give 2-bromo-4-*tert*-butylpyridine (**2.12**) in an overall yield of 57%. The 2-bromo-4-*tert*-butylpyridine was then used in a Suzuki-Miyaura coupling reaction to make 2,5-bis(4-*tert*-butyl-pyrid-2-yl)-1,4-dimethoxybenzene (**2.14**) and subsequently 2,5-bis(4-*tert*-butyl-pyrid-2-yl)-1,4-hydroquinone (**2.15**) (Scheme 2.2).

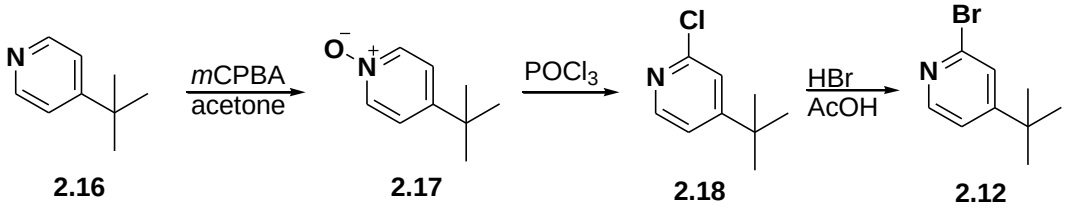

Scheme 2.3. Synthesis of *t*-butyl pyridine derivative **2.12.**

Another substituted derivative of **2.2** targeted was 2,5-bis(4-dimethylaminopyrid-2-yl)-1,4-hydroquinone (**2.19**). The Suzuki-Miyaura coupling strategy no longer worked with

the more electron-rich 2-bromo-4-dimethylaminopyridine under a variety of reaction conditions. Other coupling reactions (Stille, Kumada and Negishi) were attempted, however only Stille coupling of **2.9** with **2.21** yielded an appreciable amount of the methoxy precursor, **2.22** (Scheme 2.4). The tributyl stanyl precursor was prepared by direct C-2 lithiation of 4-dimethylaminopyridine (**2.20**) followed by treatment with $ClSnBu_3$, to give **2.21**.[93]

Although **2.22** could be isolated, yields of the Stille coupling were lower than desired. Electron rich compounds generally do not react as easily in Suzuki-Miyaura and Stille coupling reactions.[94,95] However, there are a few literature examples where derivatives of **2.20** were successfully coupled[96-98] and some of these examples were incorporated in attempts to increase the yield of the Stille coupling reaction. Examples include adding purified CuI, LiI, CsF or changing reaction conditions such as using higher boiling point solvents or incorporating longer reflux times, however, no major improvements in the yield were obtained. Limited success was achieved using a large amount of catalyst (~25%) and pumping on reagents overnight prior to use to remove any water or oxygen that may have been present. Given that the yield of the Stille coupling reaction approximately increased linearly with additional catalyst, the low yield was thought to be due to the product **2.22** binding irreversibly to the Pd catalyst. Despite the difficulties associated with this reaction, enough product was isolated to characterize **2.22** which was subsequently deprotected with $AlCl_3$ to give **2.19**.

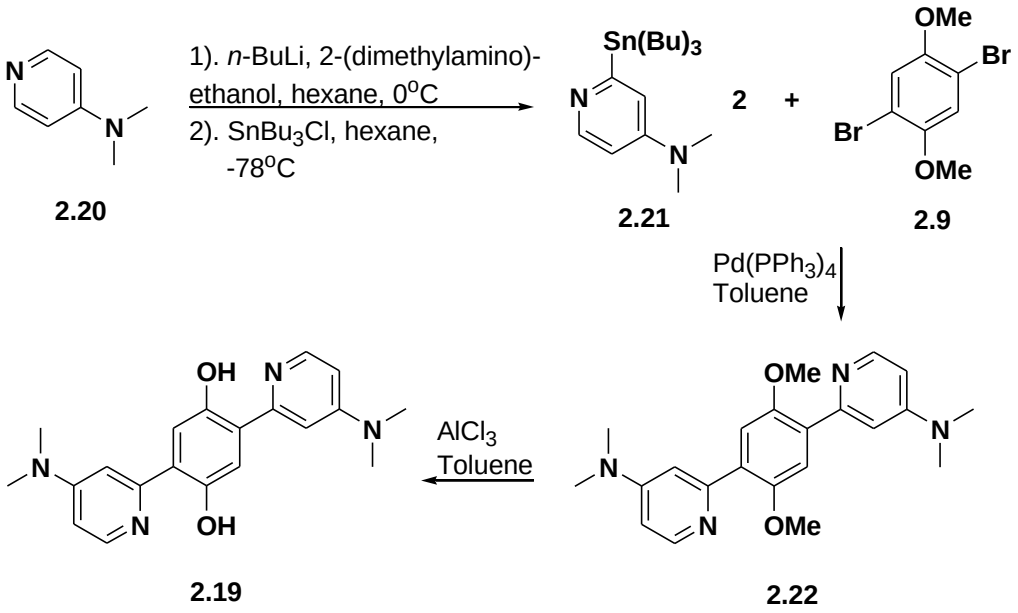

2.20 **2.21** **2.9** **2.19** **2.22**

Scheme 2.4. Synthesis of 2,5-bis(4-dimethylaminopyrid-2-yl)-1,4-hydroquinone **2.19.**

The last derivative of **2.2** targeted was 2,5-bis([2,2']-bipyrid-6-yl)-1,4-hydroquinone (**2.23**) whose synthesis is shown in Scheme 2.5. 6-Bromo-2,2-bipyridine[99] (**2.24**) was combined with **2.10** under Suzuki-Miyaura conditions to give **2.25** as a fluorescent blue compound which was subsequently deprotected, as was the case in the synthesis of **2.2**. All of the other conjugated methoxy precursors, **2.13**, **2.14** and **2.22** fluoresce blue under UV-irradiation but **2.25** was the only methoxy precursor whose fluorescence was visible under ambient conditions.

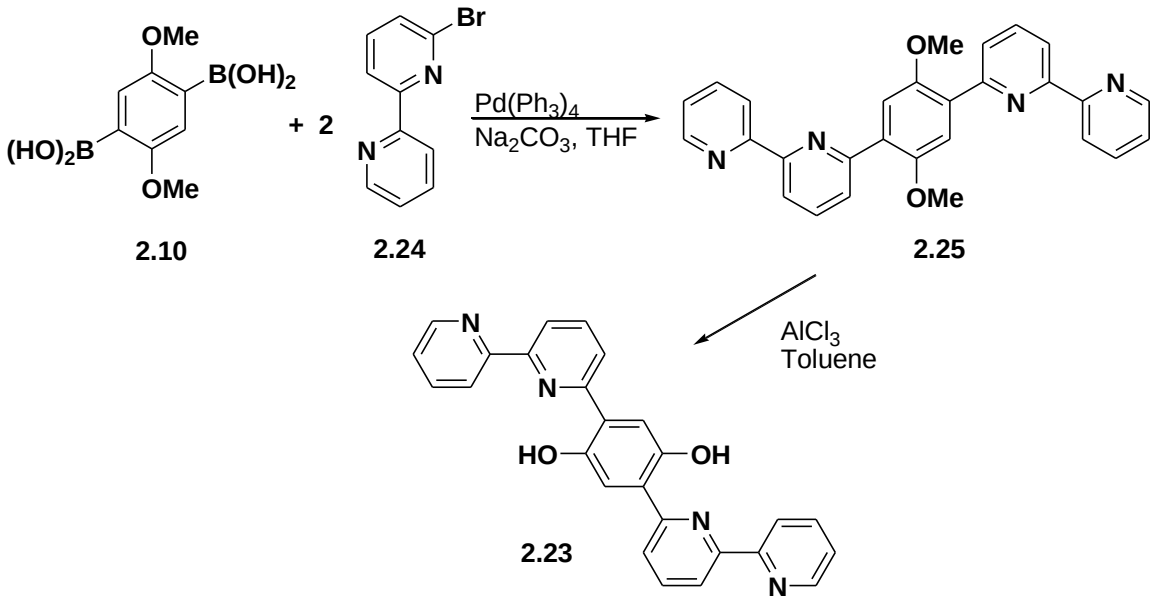

2.10 **2.24** **2.25** **2.23**

Scheme 2.5. Synthesis of **2.23.**

X-Ray quality crystals of **2.15** were obtained by slow evaporation from a methanol solution. The solid state structure of **2.15** is presented in Figure 2.1. The pyridyl rings are twisted from the plane of the hydroquinone ring by 20.17°. The structural features of the central ring are fully consistent with it being a 1,4-dihydroxybenzene (Table 2.1). The short O--N distance of 2.592 Å serves as evidence of intramolecular hydrogen bonds between the hydroxyl groups of the hydroquinone and nitrogens of the pyridine rings which is also supported by other characterization data discussed shortly. This O--N distance is analogous to the previously published structure of **2.2**, which has reported O--N distances of 2.558 Å.[87] The O--N distances for **2.15** and **2.2** are also comparable to the related pyridyl-phenol compound **2.26** (O--N 2.56-2.57 Å) reported by Mayer *et al.* which is discussed in more detail later in this chapter.[100]

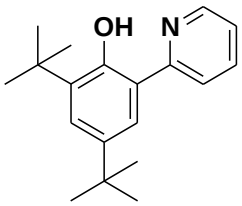

2.26

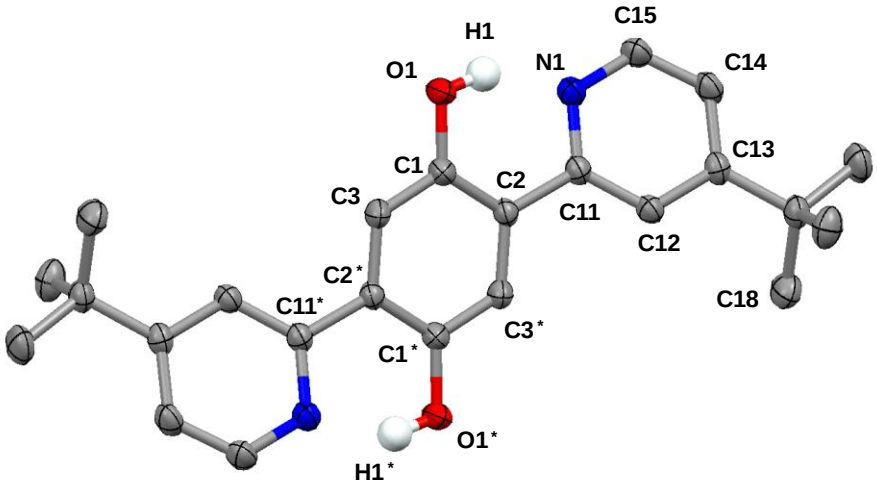

Figure 2.1. Molecular structure of **2.15** with thermal ellipsoids shown at 50% probability level. H atoms other than the phenolic OH have been omitted for clarity (OH protons located in a difference map and refined isotropically).

Table 2.1. Selected bond lengths (Å) and angles (º) for **2.15.**

Atoms	**2.15**	Atoms	**2.15**
Bond Lengths		C12-C13	1.3878(14)
C1-O1	1.3567(14)	C13-C14	1.3840(16)
C1-C3	1.3813(14)	C14-C15	1.3756(17)
C1-C2	1.4034(16)	*Bond Angles*	
C2-C3*	1.3856(16)	O1-C1-C3	117.60(10)
C11-N1	1.3457(15)	C1-C2-C11	121.38(10)
C11-C12	1.3851(15)	N1-C11-C2	116.68(10)

X-Ray quality crystals of **2.19** were obtained from dichloromethane and its structure is shown in Figure 2.2. Qualitatively the structure of **2.19** is similar to **2.15**; for instance structural data for **2.19** is consistent with the central ring being benzenoid in nature (Table 2.2). The two outer pyridine rings are nearly coplanar with the central benzene ring twisted slightly by angles of 2.75^{o} or 4.29^{o} for the pyridine rings containing N1 or N4 respectively. The O--N distances are 2.519 Å and 2.553 Å, again indicating there are intramolecular hydrogen bonds between the hydroxyl protons and pyridyl nitrogens.

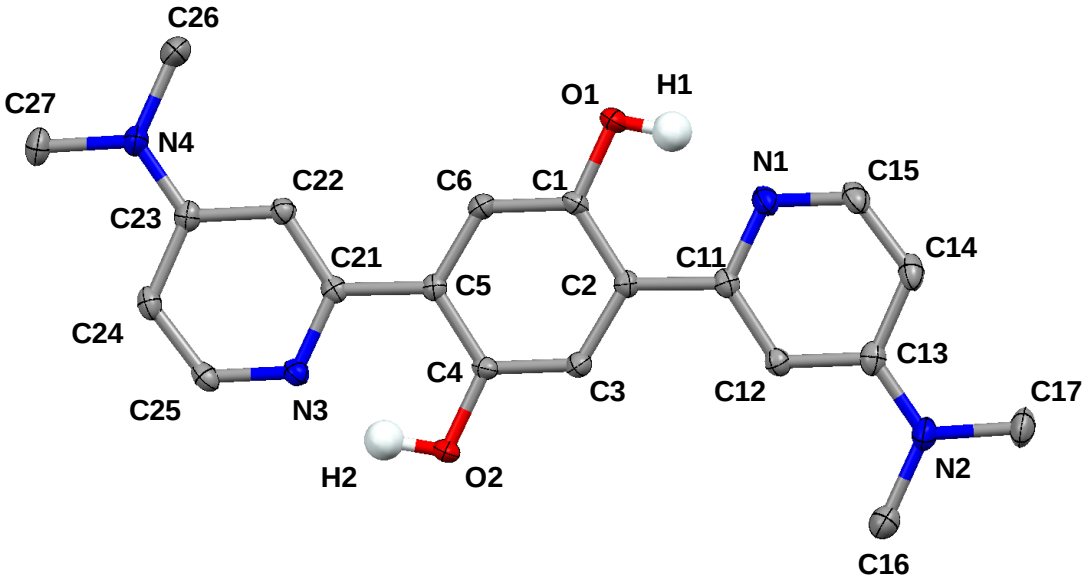

Figure 2.2. Molecular structure of **2.19** with thermal ellipsoids shown at 50% probability level. H atoms other than the phenolic OH have been omitted for clarity (OH protons located in a difference map and refined isotropically).

Table 2.2. Selected bond lengths (Å) and angles (º) for **2.19**.

Atoms	**2.19**	Atoms	**2.19**
Bond Lengths		N1-C15	1.344(2)
C1-O1	1.3669(17)	C13-N2	1.362(2)
C1-C2	1.4175(19)	*Bond Angles*	
C2-C3	1.394(2)	C6-C1-C2	120.25(13)
C3-C4	1.388(2)	O1-C1-C6	116.94(13)
C4-O2	1.3627(18)	C11-N1-C15	117.31(13)
C11-N1	1.359(2)	C16-N2-C7	120.39(14)

X-ray quality crystals of **2.23** were obtained from toluene and its structure is shown in Figure 2.3. As was the case for **2.15**, the structure of **2.23** shows the expected structural features for a hydroquinone (Table 2.3). The plane of the internal pyridyl rings containing N1 or N3 are twisted by 10.33^{o} or -2.99^{o} respectively with respect to the plane of the central hydroquinone ring. The outer pyridyl rings containing N2 or N4 both adopt an *anti* orientation with respect to the internal pyridyl rings. The outer pyridyl rings are twisted to the internal pyridine rings by 11.87^{o} or -28.82^{o} for pyridine rings containing N2 or N4 respectively. The N--O distances of 2.571 Å and 2.577 Å between the hydroxyl groups and internal pyridyl nitrogens N1 and N3 indicate that this compound also contains intramolecular hydrogen bonds.

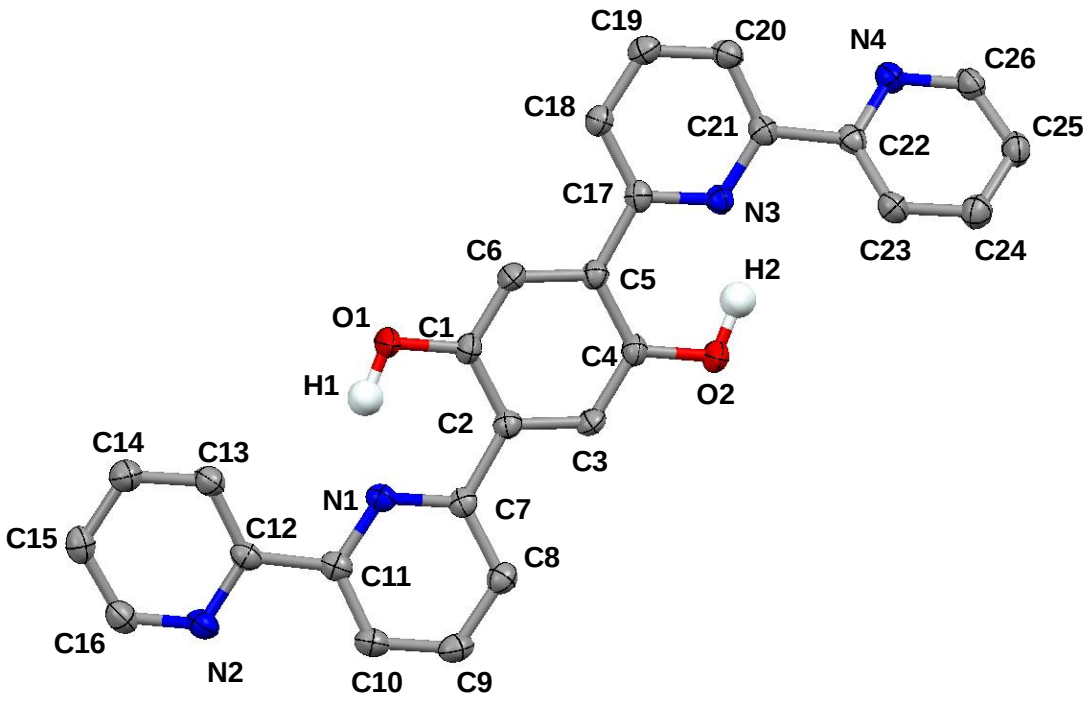

Figure 2.3. Molecular structure of **2.23** with thermal ellipsoids shown at 50% probability level. H atoms other than the phenolic OH have been omitted for clarity. (OH protons located in a difference map and refined isotropically).

Table 2.3. Selected bond lengths (Å) and angles (º) for **2.23**

Atoms	**2.23**	Atoms	**2.23**
Bond Lengths		*Bond Angles*	
C1-O1	1.360(2)	O1-C1-C2	122.49(16)
C1-C2	1.411(3)	C1-C2-C3	116.83(16)
C2-C3	1.394(2)	C1-C2-C7	122.05(16)
C3-C4	1.378(2)	N1-C7-C2	116.54(16)
C2-C7	1.478(2)	N1-C11-C12	117.03(16)

Broad absorptions found in the range between 3300-2100 cm^{-1} in the solid state IR are consistent with the structures for **2.2**, **2.15**, **2.19** and **2.23** containing intramolecular hydrogen bonds. Spectroscopic data for hydroquinones **2.2**, **2.15**, **2.19** and **2.23** suggests that the intramolecular hydrogen bonds are preserved in solution. For example, the chemical shifts of the OH protons for these hydroquinones are between 13-15 ppm in $CDCl_3$ or CD_3CN. In comparison, the OH protons in CD_3CN of 1,4-hydroquinone (**1.16**) are found at 6.42 ppm. Further evidence of the intramolecular hydrogen bond is also observed in the solution infrared spectra of **2.2**, **2.15**, **2.19** and **2.23**. Broad absorptions from ~3100-2600 cm^{-1} are observed which are typical for hydrogen bonded alcohol groups[89]. On the other hand 1,4-hydroquinone has a relatively strong and sharp absorption at 3418 cm^{-1} in acetonitrile.

2.2.3 2,5-Bis(aminomethyl)-1,4-hydroquinones

In an effort to probe how the nature of the hydrogen bond acceptor affects the redox properties of these compounds and their coordination complexes, hydroquinones with non-conjugated hydrogen bond accepting amines were targeted. To this end hydroquinones **2.27-2.29** containing aminoalkyl substituents were targeted.

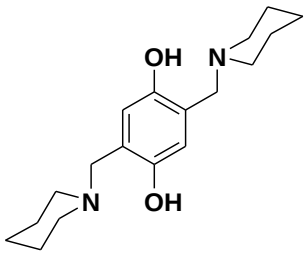

2.27

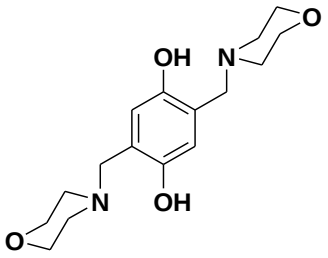

2.28

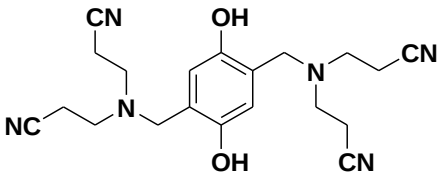

2.29

These non-conjugated hydroquinones were obtained by the Mannich reaction as shown in Scheme 2.6 for 2,5-bis(piperidin-1-ylmethyl)-1,4-hydroquinone (**2.27**) whose synthesis had previously been reported.[101] This synthetic method was employed to obtain the related compound, 2,5-bis(morpholin-4-ylmethyl)-1,4-hydroquinone (**2.28**), which also has been previously reported but not well characterized.[102] Comparable yields of 72% and 74% were obtained for **2.27** and **2.28** respectively. However, the synthesis of **2.28** required the reaction mixture being refluxed eight times longer in comparison to the synthesis of **2.27** due to the decreased nucleophilicity or basicity of morpholine. The third bis(aminomethyl)-hydroquinone targeted was 2,5-bis((bis(2-cyanoethyl)amino)methyl)-1,4-hydroquinone (**2.29**), which also has been reported but poorly characterized.[103] Using literature methods **2.29** was obtained but only with a 39% yield. The lower yield is again thought to be due to the lower nucleophilicity or basicity of bis(2-cyanoethyl)amine.

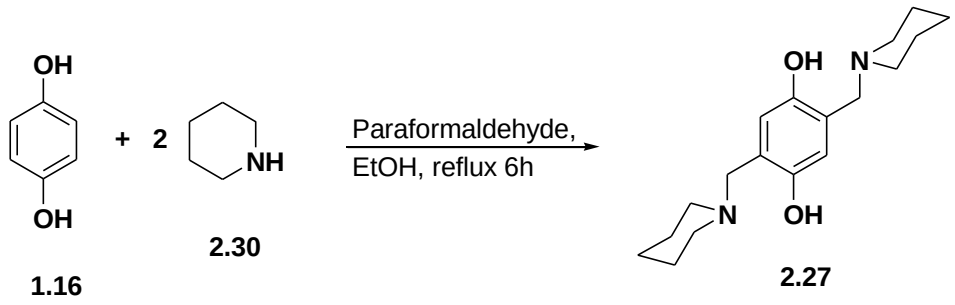

Scheme 2.6. Mannich reaction to produce **2.27**.[101]

The previously reported crystal structures of **2.27** and **2.28** both suggest the presence of intramolecular hydrogen bonds with O--N distances of 2.711 Å[101] and 2.688 Å[104] respectively. The crystal structure of **2.29** has not been reported; our attempts to obtain single crystals failed due in part to its poor solubility except in very polar solvents.

The spectroscopic data for **2.27** and **2.28** are consistent with the presence of intramolecular hydrogen bonds. The OH protons are found downfield at shifts of 10.81 ppm for **2.27** and 10.02 ppm for **2.28** in CD_3CN in their ^{1}H-NMR spectra. As expected, owing to their relative basicities, **2.27** has the most downfield shift relative to **2.28** which is a good indication that its hydrogen bond is stronger.[105] The intramolecular hydrogen bond is also confirmed by the solution infrared spectra of **2.27** and **2.28** in acetonitrile with broad absorptions from ~3400-2450 cm^{-1}. In contrast, the OH proton for **2.29** is found at 8.27 ppm in CD_3CN which is much closer to that observed for 1,4-hydroquinone (**1.16**) at 6.42ppm. Unfortunately, **2.29** is not soluble enough in acetonitrile to obtain a solution IR spectrum in this solvent. A solution IR spectrum could be obtained in dimethylformamide in which a broad absorption at 3275 cm^{-1} is found, more similar to the OH absorption in **1.16** than that observed for any of the intramolecularly hydrogen bonded hydroquinones. Thus, the ^{1}H-NMR and IR solution data indicates that there is no intramolecular hydrogen bond for **2.29**.

2.3 Synthesis and Characterization of 2,5-Disubstituted-1,4-Benzoquinones

2,5-Bis(pyrazol-1-yl)-1,4-hydroquinone (**2.1**) can be oxidized with DDQ (**1.7**) to give a near quantitative yield of 2,5-bis(pyrazol-1-yl)-1,4-quinone (**2.31**) as shown in Scheme 2.7. More recently the weaker oxidizing agent, 1,4-benzoquinone (**1.2**), was utilized to give lower yields (71%) of the quinone.[106] The crystal structure of **2.31** was also reported in this paper.

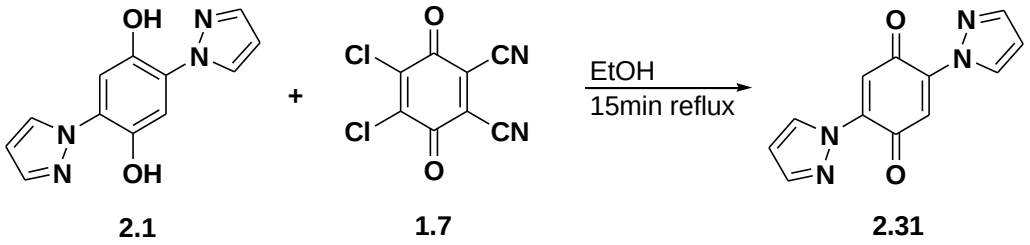

2.1 **1.7** **2.31**

Scheme 2.7. Chemical oxidation of **2.1** to give the corresponding quinone **2.31.**

The synthesis of the 2,5-bis(pyrid-2-yl)-1,4-quinone (**2.32**) was initially attempted using DDQ as the oxidant; colour changes indicated a reaction was taking place, but the desired compound could not be isolated. A variety of oxidants and conditions were attempted such as $FeCl_3$, CrO_3, $NaIO_4$ and $NOPF_6$ in some cases followed by treatment with strong base but all of these failed as well. However when lead tetraacetate was used, the desired quinone could be isolated in near quantitative yield (Scheme 2.8).

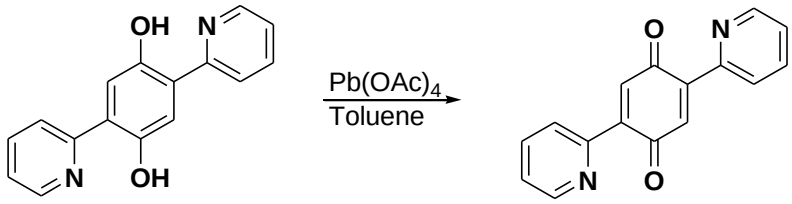

2.2 **2.32**

Scheme 2.8. Synthesis of quinone **2.32.**

The purification of **2.32** was quite challenging due to its limited stability in solution and water sensitivity. As a result the acetic acid by-product was difficult to remove. However, nearly analytically pure compound (established by elemental analysis) could be obtained by using a slight excess of $Pb(OAc)_4$ and putting the compound under vacuum for a few days. The identity of **2.32** was also confirmed by high resolution mass spectrometry.

$Pb(OAc)_4$ proved to be the oxidizing agent of choice for the synthesis of two other quinones, **2.33** and **2.34**. These quinones were also not stable in solution and their purification was sufficiently difficult such that their identities were also confirmed by high resolution mass spectrometry. The preliminary oxidation attempts using $Pb(OAc)_4$ with the other hydroquinones **2.19**, **2.23**, **2.28** and **2.29** suggested that the corresponding quinones could also be isolated but stability issues resulted in these quinones not being pursued.

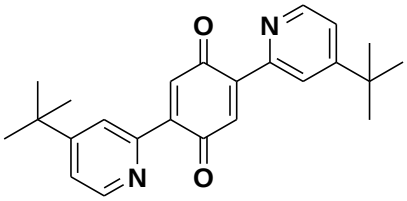

2.33

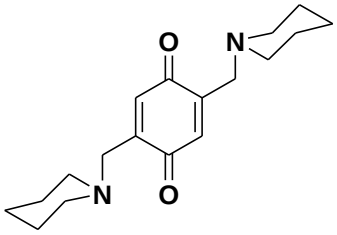

2.34

Characterization data for **2.31-2.34** confirms their formulation as *p*-benzoquinones. ^{13}C-NMR spectra for quinones **2.31-2.34** all possess carbonyl peaks in the range of 182-188 ppm in $CDCl_3$ and the carbonyl stretch in their infrared spectra was found in the range of 1640-1665 cm^{-1}. The electronic absorption spectra of the conjugated quinones **2.31-2.33** have weak absorptions at ~450 nm (468 nm, ε = 260 M^{-1}•cm^{-1} for **2.33**) in acetonitrile. This feature is typical of quinones and has been assigned to a forbidden n-π^* transition.[107] Benzoquinones with alkyl substituents are known to have n-π^* transitions blue shifted and this may result in the absorption not being observed for **2.34**.[1]

2.4 Electrochemical Studies of 2,5-Disubstituted-1,4-Benzoquinones

The redox properties of quinones **2.31-2.34** were investigated using electrochemical methods and the cyclic voltammograms of **2.32-2.34** are shown in Figure 2.4. All quinones show two reversible or quasi-reversible one-electron reduction processes which are qualitatively consistent with their formulation as benzoquinones.[2] The first reduction is assigned to the formation of semiquinone radical anion and the second reduction leads to the hydroquinonate dianion. In all of these cases the second reduction wave is shorter and wider than the first reduction peak, quasi-reversible and in most cases a small bump is observed in between the reduction waves. These features are reproducible, indicating that they are not a result of impurities and have been reported for other quinones. The smaller peak height of the second reduction has been proposed to be due to the quinone and the hydroquinonate dianion forming a complex.[49]

The reduction potentials for quinones **2.31-2.34** are summarized in Table 2.4. In acetonitrile there is ~0.70-0.75 V separation between the two reduction waves for all quinones. The conjugated quinones (**2.31-2.33**) are all slightly easier to reduce than 1,4-benzoquinone (**1.2**) due to the adjacent heterocyclic rings. In contrast, the non-conjugated quinone **2.34** is reduced as significantly lower potentials than **2.31-2.33** because the methyl-piperidinyl groups are electron donating.

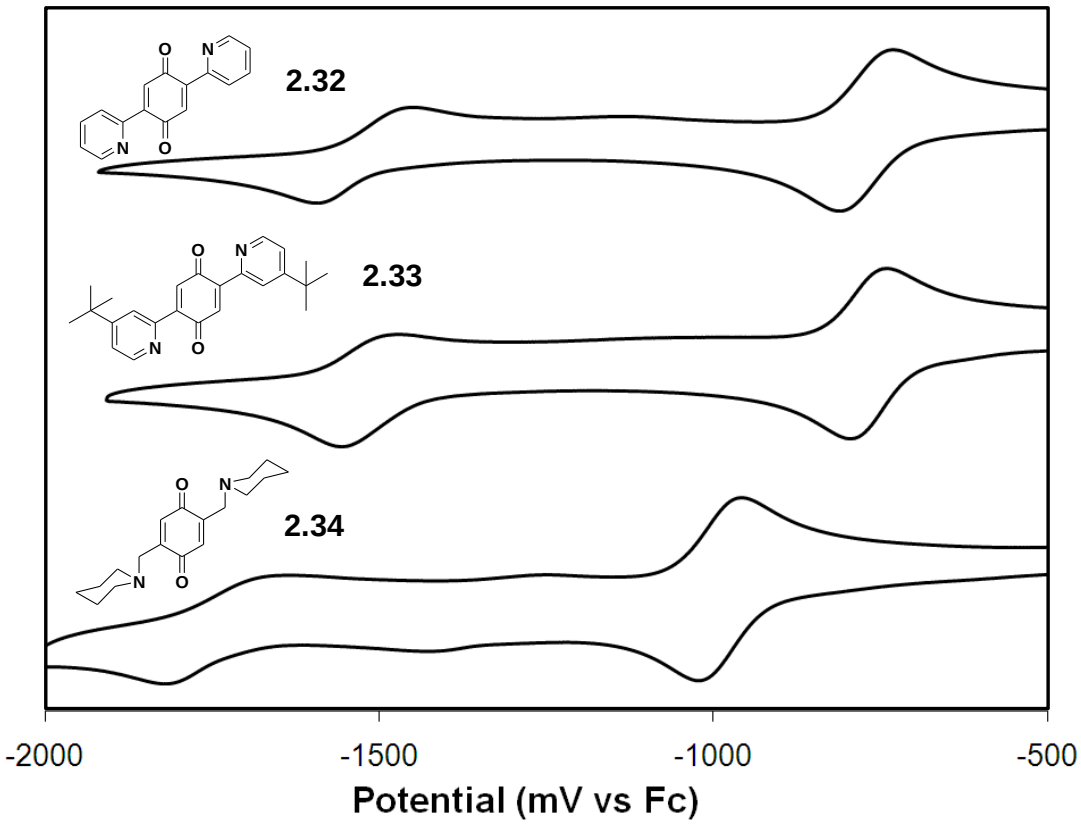

Figure 2.4. Cyclic voltammograms of **2.32**, **2.33** and **2.34** in acetonitrile (~1mM analyte with 0.1M Bu_4NBF_4 electrolyte).

The polarity of the solvent has a substantial effect on the redox values. For example, the reduction potential for **2.31** is more negative in dichloromethane than in more polar solvents because a less polar solvent does not help stabilize the negative charges that are produced upon reduction. Studies on the solvent effects on redox potentials have shown linear correlations based on different solvent parameters such as Gutman's donor number and acceptor number. Alternatively, the first redox potential of benzoquinone in different solvents has been shown to have a good correlation with Swain's A+B solvent polarity parameters,[108] which are best described as the anion and cation solvation terms derived from extensive data fitting.[109] Solvent dependence for the first reduction potential of **2.31**

follows the same trend reported for **1.2** in DCM, CH_3CN and DMF. The second reduction of **1.2** in different solvents has received less attention most likely due to the large variation of redox potentials reported for each solvent.[2] This disagreement is most likely due to small amounts of water being present which shifts the second reduction potential more than the first as discussed in the introduction of this chapter.

Table 2.4. Redox potentials (V vs Fc) for 2,5-disubstituted-1,4-quinones.

Quinone (#)	$E_1^{o'}$ Q/SQ^-	$E_2^{o'}$ SQ^-/HQ^{2-}	$\Delta E^{o'}$ $= \lvert E_1^o - E_2^o \rvert$
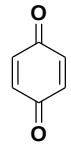 **(1.2)**	**-0.88** E_{1pa}= *-0.84* E_{1pc}= *-0.92*	**-1.59** E_{2pa}= *-1.45* E_{2pc}= *-1.74*	**0.71**
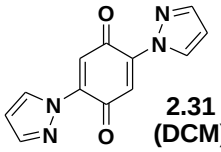 **2.31 (DCM)**	**-0.76** E_{1pa}= *-0.68* E_{1pc}= *-0.80*	**-1.37** E_{2pa}= *-1.30* E_{2pc}= *-1.44*	**0.61**
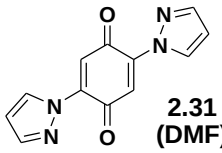 **2.31 (DMF)**	**-0.63** E_{1pa}= *-0.60* E_{1pc}= *-0.66*	**-1.50** E_{2pa}= *-1.47* E_{2pc}= *-1.53*	**0.87**
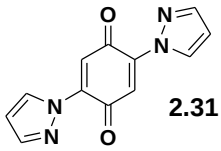 **2.31**	**-0.63** E_{1pa}= *-0.60* E_{1pc}= *-0.67*	**-1.34** E_{2pa}= *-1.30* E_{2pc}= *-1.37*	**0.71**
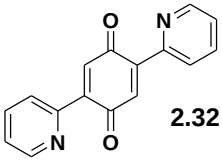 **2.32**	**-0.77** E_{1pa}= *-0.73* E_{1pc}= *-0.81*	**-1.53** E_{2pa}= *-1.46* E_{2pc}= *-1.60*	**0.76**
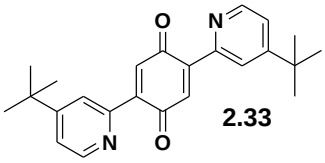 **2.33**	**-0.77** E_{1pa}= *-0.74* E_{1pc}= *-0.80*	**-1.52** E_{2pa}= *-1.47* E_{2pc}= *-1.57*	**0.75**
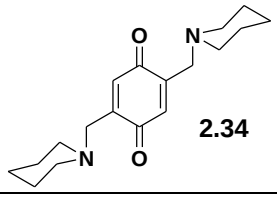 **2.34**	**-0.99** E_{1pa}= *-0.95* E_{1pc}= *-1.03*	**-1.73** E_{2pa}= *-1.63* E_{2pc}= *-1.83*	**0.74**

~1mM analyte in acetonitrile with 0.1M Bu_4NBF_4 electrolyte unless noted otherwise

Epa = Anodic peak potential (oxidation takes place), *Epc*= Cathodic peak potential (reduction takes place)

All cyclic voltammograms and their scan rates can be found in Appendix 1: Figure A-1 and Figure A-44 to A-49.

2.5 Electrochemical Studies of Hydroquinones

The redox properties of all of the 1,4-hydroquinones were also examined using electrochemical techniques. These studies were prompted due to the initial problems encountered in isolating quinone **2.32** as previously discussed. 1,4-Hydroquinone (**1.16**) is irreversibly oxidized at a potential of E_{pa} = +0.72 V vs Fc in CH_3CN due to the loss of its OH protons upon oxidation. The bis-pyrazole substituted hydroquinone, **2.1**, is also oxidized irreversibly (E_{pa} = +0.57 V).[106] Thus, when the cyclic voltammogram of the bis-pyridyl hydroquinone **2.2** was obtained we were surprised to find a reversible oxidation process at E^o = +0.25 V. The Osteryoung Square Wave Voltammogram (OSWV) of **2.2** showed that the peak area for the redox process at +0.25 V was about two times that of an equimolar quantity of octamethylferrocene standard, indicating that the oxidation process for **2.2** involves two electrons. Further inspection of the OSWV showed that the two electron process was actually two closely spaced one-electron oxidations, at potentials of +0.22 V and +0.28 V. Similar results have recently been published for **2.2** in dimethylformamide although in this solvent the oxidation peak of **2.2** is irreversible.[110]

The electrochemical data obtained for **2.2** qualitatively resembles results published by Saveant *et al.* although quantitative comparisons cannot not be made because the electrochemical studies were carried out in different solvents. By deprotonating 2,5-dicarboxy-1,4-hydroquinone (**1.23**) in DMF to give the dianion, **1.24**, the oxidation peak changed from a irreversible process typical of 1,4-hydroquinone to two closely spaced quasi-reversible one-electron oxidation process.[48] As outlined in Chapter 1, Saveant proposed that the phenolic hydrogens in **1.24** were transferred to the adjacent carboxylate group upon oxidation in a CPET mechamism. The similarities between the cyclic

voltammograms of **1.24** and **2.2** suggest that the oxidation of **2.2** also involved a CPET mechanism.

In a more general context, CPET has been firmly established in phenols containing intramolecular hydrogen bonds.[111-115] Phenols are generally oxidized irreversibly due to the loss of the proton of the corresponding radical cation. However, if the phenol has an *ortho*-substituent capable of hydrogen bonding to the phenolic OH, the oxidation becomes reversible and is accompanied by proton transfer to the adjacent proton acceptor. Mayer and others have examined the redox processes in intramolecular hydrogen bonded phenols and have found that their oxidation follows a CPET mechanism.[100,111,113] Although there are other examples of derivatized phenols that undergo a CPET mechanism upon oxidation, the pyridyl phenol **2.26** in particular is very similar to **2.2** in structure and was shown to undergo a CPET mechanism upon oxidation as shown in Scheme 2.9. This also suggests that the reversible oxidation of **2.2** proceeds by a CPET mechanism.

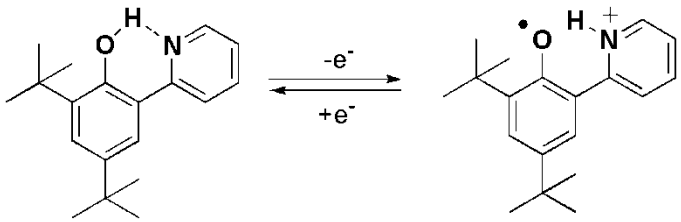

2.26 **2.35**

Scheme 2.9. Oxidation of **2.26** by a CPET mechanism to give phenoxyl radical **2.35.**

The unexpected electrochemical behaviour of **2.2** prompted us to examine the other hydroquinones synthesized. The redox potentials for all hydroquinones studied are summarized in Table 2.5; cyclic voltammograms of the conjugated hydroquinones **2.2**,

2.15 and **2.19** are presented in Figure 2.5 while cyclic voltammograms of the non-conjugated quinones **2.27-2.29** are found in Figure 2.6. All hydroquinones undergo reversible oxidation processes in acetonitrile except for the pyrazole- and cyanoethylamino- subsituted hydroquinones, **2.1** and **2.29** respectively. The cyclic voltammogram of **2.23** also includes a second irreversible oxidation process at +1.42 V and due to the poor solubility of **2.23** subsequent electrochemical experiments such as OSWV were not performed.

In addition to the oxidation processes, the voltammograms for the bis-pyridyl hydroquinones, **2.2** **2.15** and **2.19**, have two one-electron reduction processes at approximately -2.5 V. At slower scan rates these are irreversible but at very high scan rates they become quasi-reversible. These reductions are attributed to reduction of the pyridine groups.[116]

When weak bases (e.g. pyridine) are added to the electrochemical cell of **2.15** the reversible redox process becomes irreversible, but with very little change in the oxidation potential. Similar results are obtained when DMF is added. This is most likely due to the disruption of the proton transfer by these polar molecules, resulting in intermolecular H^+ transfer. This also explains why the oxidation of **2.2** has poor reversibility in DMF noted previously.

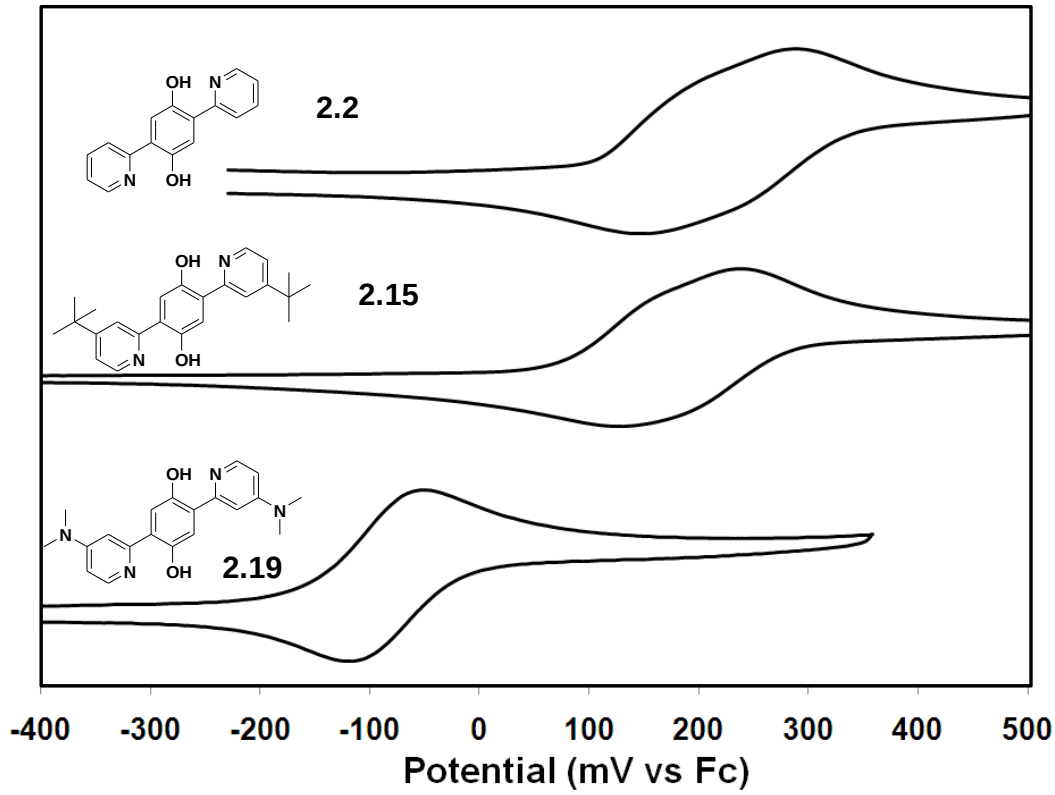

Figure 2.5. Cyclic voltammograms of conjugated hydroquinones **2.2**, **2.15** and **2.19**.

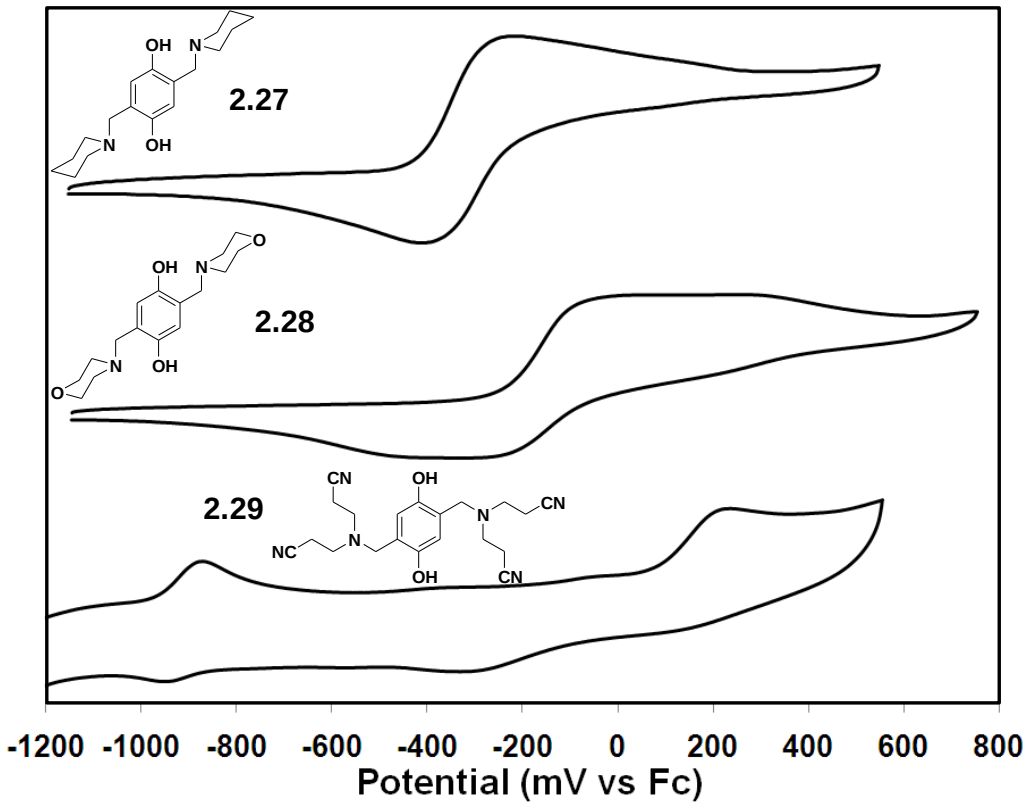

Figure 2.6. Cyclic voltammograms of non-conjugated hydroquinones **2.27**, **2.28** and **2.29**.

Table 2.5. Redox potentials (V vs Fc) for 2,5-disubstituted-1,4-hydroquinones.

Hydroquinone (#)	**$E_1^{o'}$ (V)** HQ/SQ^+	**$E_2^{o'}$ (V)** SQ^+/Q^{2+}	**$\Delta E^{o'}$ (V)** $= \lvert E_1^{o'} - E_2^{o'} \rvert$	**OSWV Peak Area**
(1.16)	$E_{pa} = +0.72^{**}$	-	n/a	n/a
(2.1)	$E_{pa} = +0.56^{**}$	-	n/a	n/a

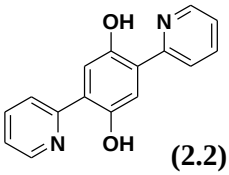 **(2.2)**	**+0.22** *E_{pc}= +0.18*	+**0.28** *E_{pa}= +0.31*	**0.06**	**2.0**
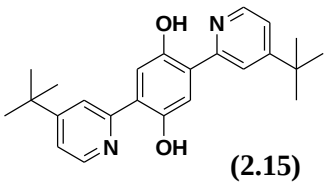 **(2.15)**	+**0.16** *E_{pc}= +0.13*	+**0.20** *E_{pa}= +0.24*	**0.04**	**1.7**
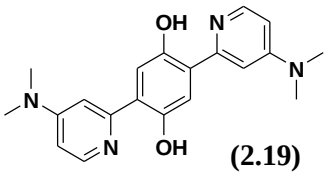 **(2.19)**	**-0.08** *E_{pc}= -0.12*	**-0.08** *E_{pa}= -0.04*	**~0**	**1.6**
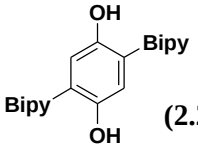 **(2.23)**	+**0.18*** *E_{pc}= +0.14*	+**0.18*** *E_{pa}= +0.22*	**~0**	n/a (poor solubility)
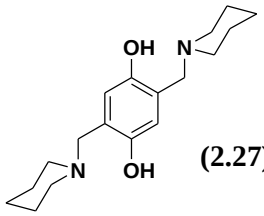 **(2.27)**	**-0.22*** *E_{pc}= -0.29*	**-0.22*** *E_{pa}= -0.15*	**~0**	**1.9*****
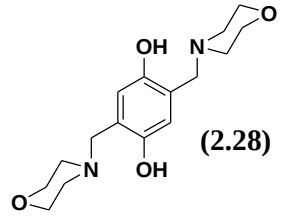 **(2.28)**	**-0.18*** *E_{1pa}= 0.04* *E_{1pc}= -0.40*	**-0.01*** *E_{2pa}= 0.26* *E_{2pc}= -0.28*	**0.17**	**1.2*****
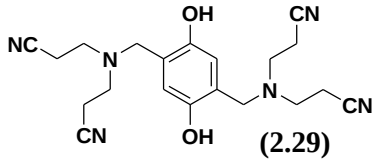 **(2.29)**	*E_{pc}= -1.35***	*E_{pa}= +0.23***	n/a	n/a

~1mM analyte in acetonitrile with 0.1M Bu_4NBF_4 electrolyte

* quasi-reversible peak , ** irreversible peak, *** includes tailing region at higher redox potential in OSWV

All cyclic voltammograms and their scan rates can be found in Appendix 1: Figure A-2 to A-43.

The last column of Table 2.5, denoted OSWV peak area, is the relative area under the oxidation peak in the Osteryoung square wave voltammogram of 1 equivalent of analyte compared to the peak corresponding to 1 equivalent of ferrocene (or a ferrocene derivative). This was done to explicitly show that there were two electrons transferred. However, for the non-conjugated hydroquinone **2.27** and **2.28** this is well below 2 unless the tailing region that occurs at higher potentials is taken into account, in particular for **2.28**. This is interpreted as being a result that not all of the hydroquinone is oxidized at this reversible redox potential, but some of the species is instead oxidized at higher potentials as supported by an irreversible oxidation peak that occurs at higher potentials (+1.20V vs Fc for **2.28**). Despite the irreversible oxidation process, no decomposition of the quasi-reversible peaks is observed when the cyclic voltammogram is scanned multiple times. This may be an indication that the CPET process for **2.27** and **2.28** is much slower and is discussed in further detail in Section 2.7.

The scan rate dependence of the peak potentials was probed to gain further insights into the electrochemical behaviour. The peak potentials of the hydroquinones studied are independent of scan rates at low scan rates, except for **2.28** whose anodic and cathodic peaks move slightly further apart as scan rate is raised, another sign of its quasi-reversibility. The scan rate dependence of **2.15** is shown in Figure 2.7 as an example. A plot of the square root of the scan rate against peak current (Figure 2.8 and 2.9) is linear, indicating that the mass transport of the hydroquinones to the electrode surface is diffusion controlled as noted by the Randle-Sevcik equation (equation **2.1**).[117,118] Where *I* is equal to the peak current, *n* is the number of electrons involved in the redox process,

A is the surface area of the electrode, C_o is the bulk concentration, D_o is the diffusion coefficient and v is the scan rate.

$$I = 2.69 \bullet 10^5 n^{3/2} A C_o D_o^{1/2} v^{1/2} \quad \textbf{(2.1)}$$

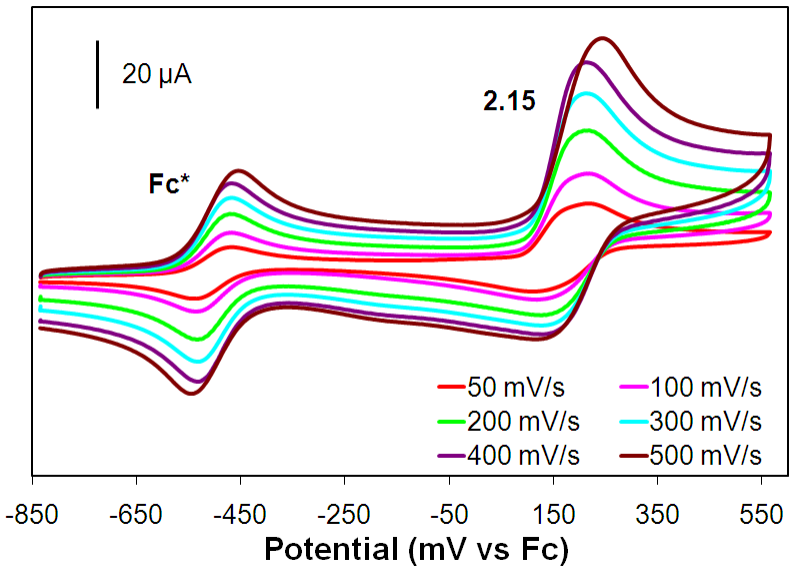

Figure 2.7. Cyclic voltammograms of **2.15** and decamethylferrocene (Fc^*) at different scan rates.

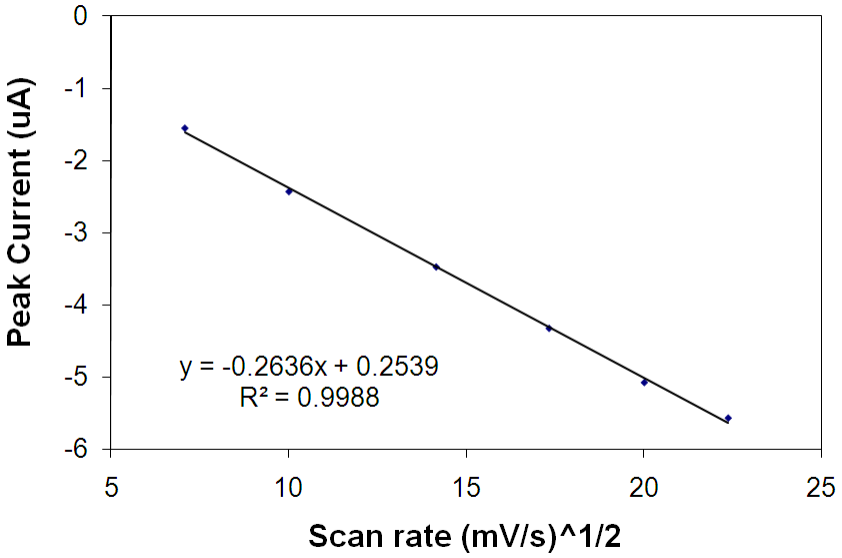

Figure 2.8. Scan rate$^{1/2}$ vs peak current for the oxidation peak (~ +240 mV vs Fc) of **2.15.**

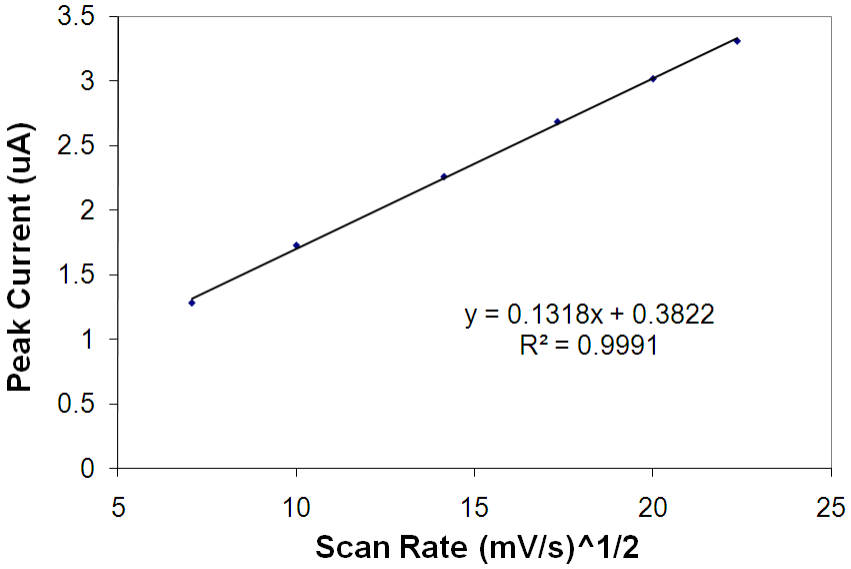

Figure 2.9. Scan rate$^{1/2}$ vs peak current for the reduction peak (~ +130 mV vs Fc) of **2.15.**

Diffusion coefficients (D_o) can be obtained from the slope of I vs $v^{1/2}$ if all other variables are known.[119] Although these other variables were unknown for our experiments, they are constant for each experiment so qualitative comparisons with

respect to the diffusion coefficients can be made for each individual experiment. For the decamethylferrocene standard the slope of the line which results from plotting I vs $v^{1/2}$ for the oxidation peak is close to the slope for the reduction peak. Thus for decamethylferrocene the diffusion coefficients for the oxidation and reduction processes are nearly equal. However, for the hydroquinone systems **2.2** and **2.15** the slope corresponding to the oxidation peak is much greater than that of the slope obtained for the reduction peak. This trend is also observed for the non-conjugated hydroquinones **2.27** and **2.28**, as well as the dimethylaminopyridine hydroquinone derivative **2.19** but to a much smaller extent. Because all other variables are kept constant in the Randle-Sevcik equation this means the diffusion coefficient is greater for the oxidation process in comparison to the reduction process. In the oxidation process of the hydroquinones, the species is neutral but in the corresponding reduction process the species is a dication. The diffusion coefficient of a charged species is known to be less than that of the original neutral complex assuming no major changes in the size or geometry of the complex occur because of increased interactions of the charged species with the solvent medium and electrolyte.[120,121] However, the difference in the diffusion coefficients is usually much smaller than is observed for **2.2** and **2.15.** The greater difference observed for these species is most likely since they possess twice the charge as typical complexes studied so a greater effect on the diffusion coefficients is observed. This trend may not be as pronounced for the non-conjugated species **2.27** and **2.28** because the nitrogen is tetrahedral in these compounds so the charge in their dications may not be as exposed or susceptible to interactions with the solvent or electrolyte, in comparison to the conjugated systems where the nitrogen is trigonal planar. Hence solvent/electrolyte molecules

interacts less with the positive charges of the piperidinium or morpholinium cations in comparison to the pyridinium cations and the diffusion constant is not affected as greatly for **2.27** and **2.28**. A similar argument can be made for **2.19** where in the oxidized form the charge is known to be delocalized on the dimethylamino group as is evident from its ^{1}H-NMR spectrum (Section 2.6). In this case, it is possible the delocalized charge interacts less with solvent or electrolyte molecules such that the change in the diffusion constants for the oxidation and reductions processes is not as pronounced. The comparison of the relative diffusion coefficients for the oxidation and reduction processes is further complicated because the redox process is two one-electron processes resulting in peaks that closely overlap such that caution must be taken when choosing the potential that the peak current is calculated from so that the same redox process is being compared.

As can be seen from the redox potentials summarized in Table 2.5 and even the cyclic voltammogram lineshape, which can be seen for each hydroquinone in the appendices, the nature of the hydrogen bond acceptor has a huge effect on the redox properties of the hydroquinones. The possible origins of the substituent effect are numerous but the relative basicity of the amine and conjugation or lack thereof with the hydroquinone appear to be two of the more important factors. These factors will be discussed in detail in Section 2.7 along with other aspects of the substituent which may be important.

2.6 Synthesis, Isolation and Properties of Quinone Dications

The intramolecular hydrogen-bonded phenols represented by **2.26** exhibit reversible electrochemistry, but their radical cations could only be characterized *in situ* as their gradual decomposition over minutes to hours did not permit their characterization (eg. $t_{1/2}$

~ 6hrs for **2.26** in DCM).[100] In the case of Saveants hydroquinone dianion, **1.24**, no attempt was reported to isolate or characterize the oxidized product **1.26**. The electrochemical reversibility of the hydroquinones presented here prompted us to explore the chemical stability of the quinone dications.

As previously mentioned, attempts to initially oxidize **2.2** to the corresponding quinone with $NOPF_6$ and other oxidizing agents resulted in a new compound with salt like properties. The ^{1}H-NMR of the isolated material was usually a mixture of two species whose ratios were variable and could not be separated, however during the many oxidation attempts a clean ^{1}H-NMR spectrum of each product was obtained. Unfortunately these results were not reproducible and pure samples could not be obtained. The infrared spectrum of this product mixture included a peak typical of a carbonyl group and once it was realized that the parent hydroquinones (**2.2**) cyclic voltammogram possessed a reversible 2e$^-$ oxidation, the dicationic salt **2.36** was proposed as one of the products in which the hydrogens had been transferred to the adjacent pyridine after oxidation (Scheme 2.10).

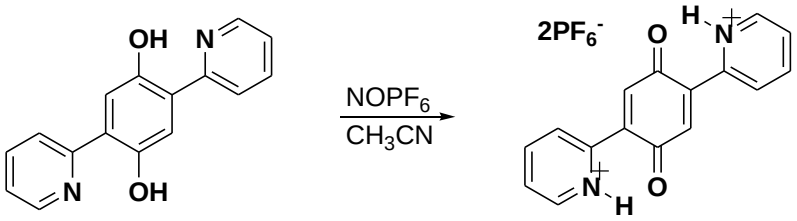

2.2 **2.36**

Scheme 2.10. Oxidation of **2.2** to give bis-pyridinium benzoquinone dication, **2.36**.

Fortunately the oxidation of **2.15** afforded a more stable dicationic quinone species. By dissolving **2.15** in acetonitrile and adding the oxidant $NOBF_4$, the oxidized product

2.37 could be precipitated as a pure product by adding diethyl ether under an argon atmosphere (Scheme 2.11). **2.37** was slightly unstable in solution, decomposing slowly overnight even if the solution was thoroughly deoxygenated and dried. However this compound was stable in the solid state such that it could be fully characterized by spectroscopic methods as well as elemental analysis. The CV of **2.37** is indistinguishable from that of **2.15**, indicating that **2.37** and **2.15** are part of the same redox couple.

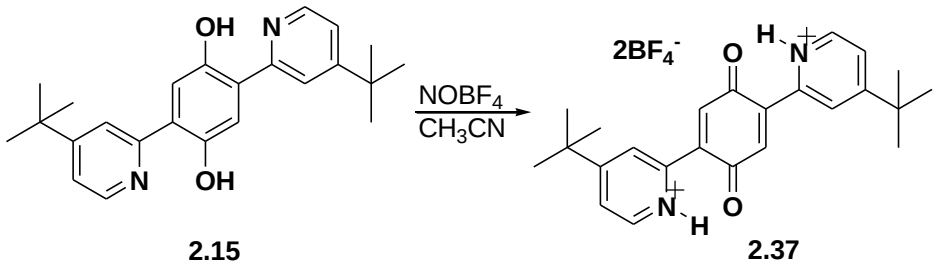

2.15 **2.37**

Scheme 2.11. Oxidation of **2.15** to give benzoquinone dicationic salt, **2.37**.

The method used to synthesize **2.37** was applied to some of the other hydroquinones to give new compounds **2.38**, **2.39** and **2.40**. Dicationic quinone **2.38** had similar stability traits as **2.37** whereas the non-conjugated examples **2.39** and **2.40** were found to be more stable, even in solution. Characterization data for these oxidized species established their structure as quinones: their solution infrared spectra possess carbonyl stretches in CH_3CN at ~1670cm^{-1} and their ^{13}C NMR spectra have resonances attributed to carbonyls at ~185ppm. Electronic spectra of the conjugated dications have weak absorptions at ~450nm typical of quinones as discussed in Section 2.3.

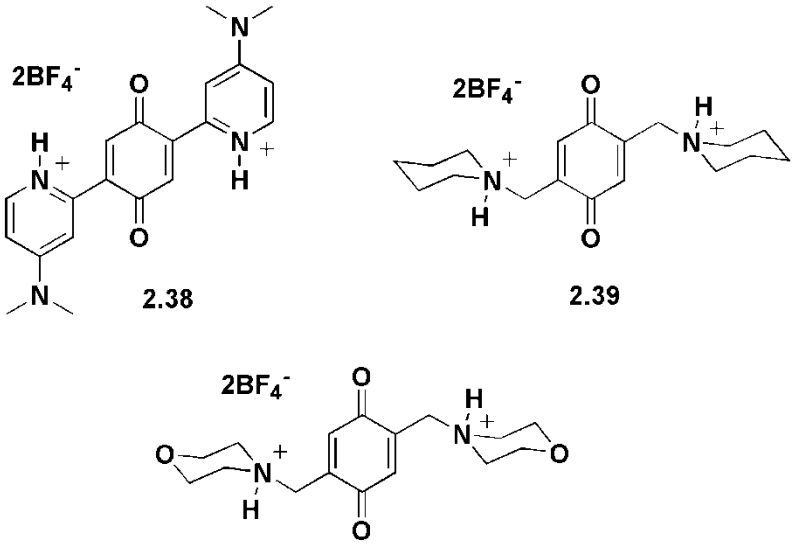

The increased stability of the non-conjugated compounds **2.39** and **2.40** allowed for the growth of X-ray quality crystals from acetonitrile and diethyl ether mixtures. The structures of **2.39** and **2.40** are shown in Figures 2.10 and 2.11 respectively. The CO and CC bond lengths associated with the central ring are fully consistent with their characterization as being quinoidal (Tables 2.6 and 2.7).

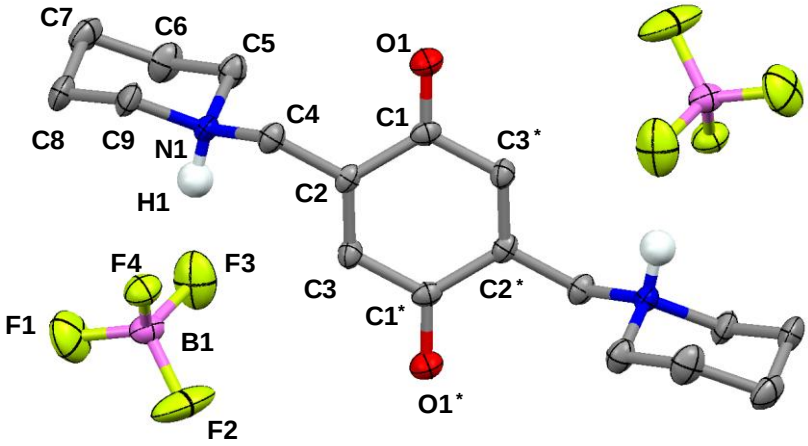

Figure 2.10. Molecular structure of **2.39** with thermal ellipsoids shown at 50% probability level. H atoms other than the piperidinium NH have been omitted for clarity (NH protons located in a difference map and refined isotropically).

Table 2.6. Selected bond lengths (Å) and angles (°) for **2.39.**

Atoms	**2.39**	Atoms	**2.39**
Bond lengths		*Bond Angles*	
C1-O1	1.2245(18)	O1-C1-C2	121.12(14)
C1-C3*	1.472(2)	C1-C2-C4	117.26(14)
C1-C2	1.4848(19)	C5-N1-C9	110.92(13)
C2-C3	1.334(2)	N1-C4-C2	113.88(12)
C2-C4	1.505(2)	C3-C2-C4-N1	59.4(2)

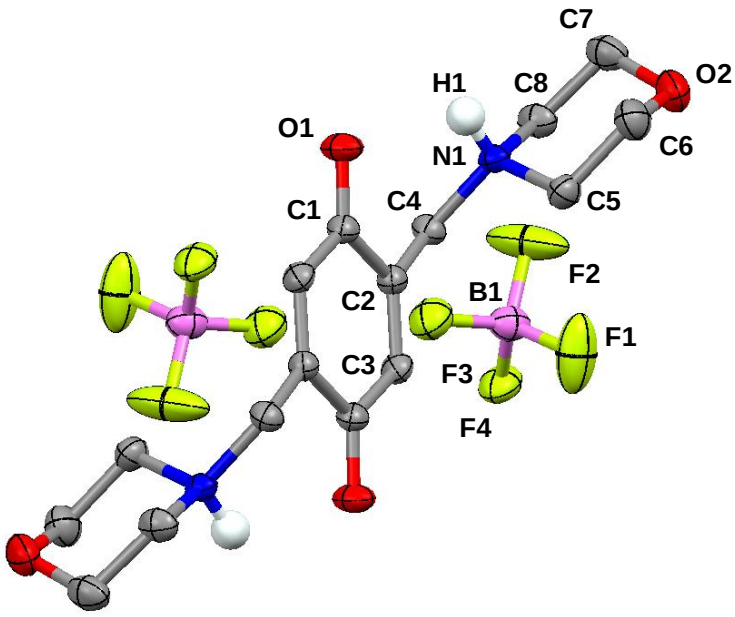

Figure 2.11. Molecular structure of **2.40** with thermal ellipsoids shown at 50% probability level. H atoms other than the morpholinium NH have been omitted for clarity (NH protons located in a difference map and refined isotropically).

Table 2.7. Selected bond lengths (Å) and angles (°) for **2.40.**

Atoms	**2.40**	Atoms	**2.40**
Bond lengths		*Bond Angles*	
C1-O1	1.224(2)	O1-C1-C2	120.01(17)
C1-C3*	1.471(3)	C3*-C1-C2	120.06(16)
C1-C2	1.483(3)	C1-C2-C4	117.57(14)
C2-C3	1.333(2)	C5-N1-C8	109.99(15)
C2-C4	1.499(2)	C2-C4-N1	113.54(15)
C6-O2	1.418(3)	C3-C2-C4-N1	124.78(18)

The crystal structures of **2.39** and **2.40** reveal that after oxidation, there was a different outcome with respect to the fate of the transferred proton. The crystal structure of **2.39** does not contain intramolecular hydrogen bonds, as the piperidinium NH proton bond is oriented away from the carbonyl group of the quinone. Instead the NH protons interact weakly with nearby tetrafluoroborate anions, forming a close contact of 2.848 Å between N1 of the piperidinium ring and F4 of the BF_4^- anion. In the case of **2.40**, the morpholinium ring is situated differently and has a substantially different dihedral angle for N1-C4-C2-C3 of 124.79° in comparison to the analogous atoms of **2.39** whose dihedral angle is 59.44°. As a result, **2.40** has a much closer N--O distance of 2.898 Å which is comparable to the corresponding hydroquinone, **2.28**, indicating **2.40** does posses an intramolecular hydrogen bond. However, the solid state IR has a sharp peak at 3156 cm^{-1} which is more typical of a non-hydrogen bonded aminium proton. This result

suggests that the intramolecular hydrogen bond observed in the crystal structure of **2.40** is very weak.

The solution ^{1}H-NMR and IR data obtained in acetonitrile for the oxidized hydroquinones **2.37**-**2.40** suggests that these species contain no hydrogen bond in solution. The H-NMR chemical shifts of the pyridinium protons for **2.37** are 13.34 ppm, comparable to the NH shift in the model compound pyridinium tetrafluoroborate[122] (**2.41**) (13.13 ppm).

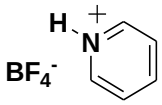

2.41

The NH chemical shift of **2.38** is found significantly upfield at 11.31 ppm suggesting this is also non-hydrogen bonded in solution, but cannot be confirmed conclusively without a better model compound. The non-conjugated dicationic salts, **2.39** and **2.40**, have NH chemical shifts of ~7 ppm which is consistent with non-hydrogen bonded trialkylammonium salts.[123,124] The solution IR of the dications show fairly sharp NH absorptions at frequencies well above 3000 cm^{-1} which is also a good indication that the intramolecular hydrogen bond is no longer present.[89] Hydrogen bonds would result in red shifting of the NH absorption, having stretching frequencies near 3200 cm^{-1} for non-hydrogen bonded pyridinium salts and near 2800 cm^{-1} in hydrogen bonded pyridinium salts,[122] also peak broadening would be expected similar to what is observed for hydrogen bonded OH peaks. When comparing the solution IR to the solid state IR of the same compound, some peak broadening of the NH absorptions is observed. This could be an indication of intramolecular hydrogen bonding but is more likely due to intermolecular

hydrogen bonding with acetonitrile solvent molecules. This is particularly true for the solution IR of **2.40** which possesses a sharp peak at 3153 cm^{-1} but also a broadened peak from 3150-3000 cm^{-1} which is not observed in its solid state IR spectrum. Although not conclusive, the ^{1}H-NMR and solution IR spectra indicate the intramolecular hydrogen bonds are not retained in the quinone dications in solution.

The ^{1}H-NMR and ^{13}C-NMR spectra of **2.38** reveal an interesting structural feature resulting from the 4-dimethylamino group. Both spectra have two distinct methyl resonances indicating that rotation of the dimethylamino group is restricted. This indicates that the resonance structure depicted in the right-hand side of Figure 2.12, where the dimethylamino nitrogen has donated its lone pair forming a double bond with the adjacent carbon of the pyridine ring which in turn pushes an electron pair onto the pyridinium nitrogen neutralizing its positive charge, is a significant contributor to the true structure of **2.38**.

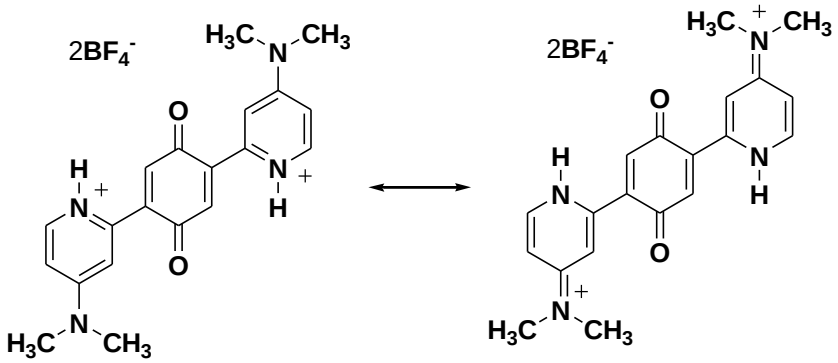

Figure 2.12. Resonance structures of **2.38**.

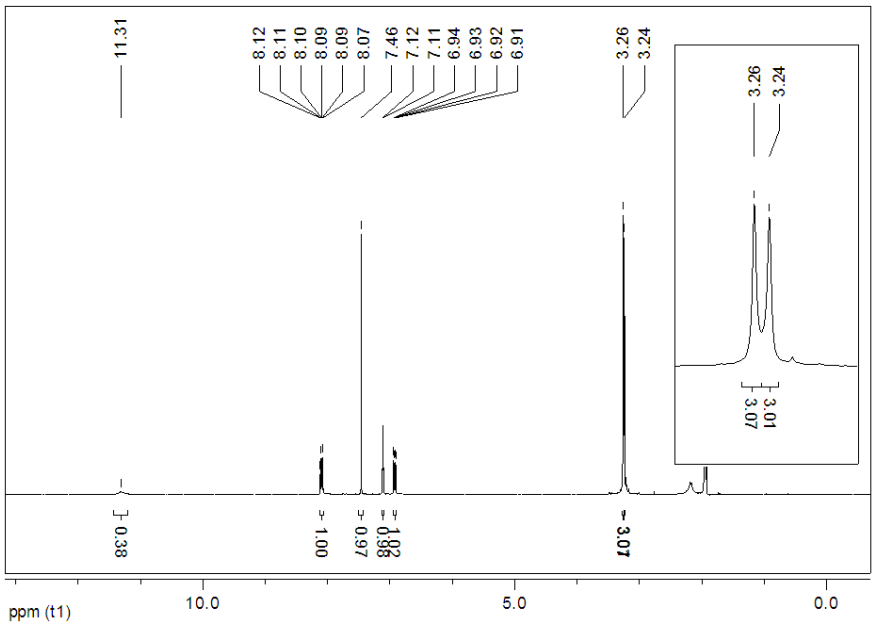

Figure 2.13. ^{1}H-NMR spectrum of **2.38** in CD_3CN.

2.7 Discussion of Redox Properties of Hydroquinones

Hydroquinones derivatized with adjacent hydrogen bond acceptors have been shown to be reversibly oxidized in some cases. Their electrochemical behaviour is dependent on the nature of the hydrogen accepting substituents. In this section the changes in the electrochemical behaviour of the derivatized hydroquinones are rationalized. To help with this analysis the derivatized hydroquinones studied are grouped into two categories: those based on conjugated systems (pyridyl substituents) and those based on non-conjugated systems (aminoalkyl substituents). As can be seen from Figures 2.6 and 2.7, the line shape of the cyclic voltammograms of the non-conjugated hydroquinones differ greatly from those of the conjugated hydroquinones and this difference is also discussed.

2.7.1 Conjugated vs Non-conjugated Pendant Bases

Mayer has studied the effect of conjugation between the hydrogen bond acceptor substituent and the phenol on their redox properties. Specifically he synthesized **2.42** to be a non-conjugated analogue of **2.26** by introducing a methylene linker between the phenol and pyridyl groups.[125]

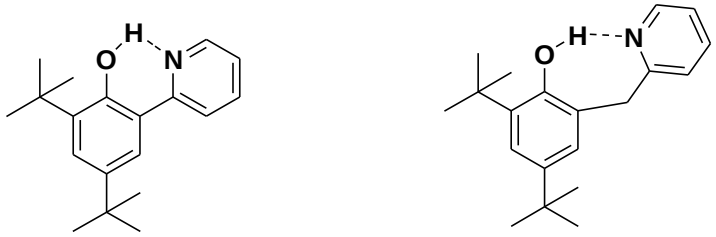

2.26 **2.42**

The chemical shift of the phenolic proton in the non-conjugated phenol **2.42** is lower (11.15 ppm) compared to **2.26** (14.83 ppm). The CCl_4 solution IR spectrum of **2.42** also showed that the phenolic proton is shifted to higher wavenumbers in comparison to **2.26** ($\nu_{(OH)}$ = 3400-2400 cm^{-1} **2.42** vs $\nu_{(OH)}$ = 3100-2200 cm^{-1} **2.26**). These results suggest that conjugation produces stronger intramolecular hydrogen bonds, a phenomena coined as resonance-assisted hydrogen bonds (RAHBs).[105] The RAHB in these phenol systems can be depicted by the resonance structures shown in Figure 2.15. Mayer found that phenols containing RAHBs were oxidized at a rate much faster than those that were not conjugated.

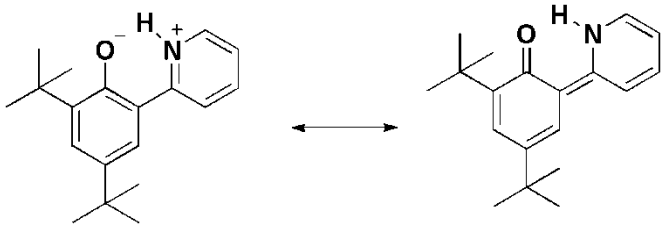

Figure 2.14. Resonance structure of zwitterionic structure of **2.26.**[105]

The hydrogen bonded OH resonance of the conjugated hydroquinones **2.2**, **2.15**, **2.19** and **2.23** come in the range between 13.67-15.52 ppm in comparison to the OH resonance of the non-conjugated hydroquinones **2.27** and **2.28** found in the range of 10.02-10.81 ppm. In addition, the solution OH absorptions are generally shifted to higher wavenumbers for the non-conjugated compounds. By analogy to the phenolic systems, this suggests that the intramolecular hydrogen bond is stronger in the conjugated systems. Thus, the weaker hydrogen bond formed for the non-conjugated systems would also be expected to result in a slower rate of CPET. Examining the redox processes for the conjugated (Figure 2.5) and non-conjugated hydroquinones (Figure 2.6), one major difference within the CVs is the line shape of the redox processes. It is proposed that the slower rate of CPET is manifested in the cyclic voltammetry of the non-conjugated systems as larger peak separations between the cathodic and anodic peaks as well as the abnormal shapes observed for the redox process. However, the mechanistic details of the redox processes are beyond the scope of this work.

2.7.2 Basicity of the Hydrogen Bond Acceptor

There appears to be a correlation between the oxidation potential of a given hydroquinone and the basicity of the hydrogen acceptor. Unfortunately the quinones and the quinone dications studied are not water soluble or stable enough in aprotic solvents so pKa assessment of the hydrogen bond acceptors for these systems is not viable. For this reason, basicity trends were assessed based on model compounds of the pendant substituents as shown in Table 2.8. For example, the basicity of the pyrazole substituents

of hydroquinone **2.1** was modeled from pyrazole with a pKa of 2.5. These model systems should be used with caution since all of the reported pKa data are based in water whereas our work was performed in acetonitrile. A second assumption is that the pKa data for the model bases will change by approximately the same amount when substituted to hydroquinone. This systematic change should have a comparable affect on each pKa such that the relative basicities are expected to be qualitatively of the same order although such an assertion cannot be made quantitatively. The pKa of the amines of the conjugated systems are likely affected more by the presence of the hydroquinone than the non-conjugated systems so direct comparisons have not been made between the conjugated and non-conjugated systems.

Table 2.8. Literature pKa value of amines conjugate acid and hydroquinones redox potential.

Hydroquinone and Model Amine	pKa of Conjugate acid of Hydrogen Bond Acceptor Substituent	Hydroquinone Redox Potential (V vs Fc)
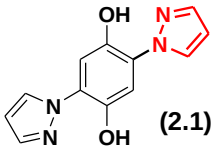 (2.1)	2.5[126] pyrazole	E_{pa} +0.56**
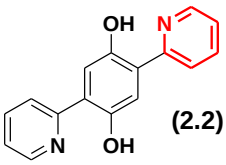 (2.2)	5.17[127] pyridine	+0.22, +0.28
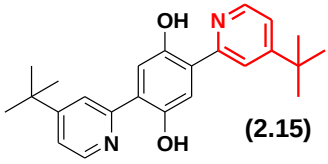 (2.15)	5.99[127] 4-*tert*-butylpyridine	+0.16, +0.20
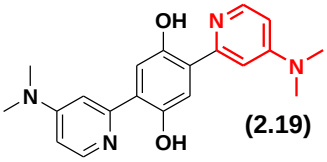 (2.19)	9.59[128] 4-dimethylaminopyridine	-0.08
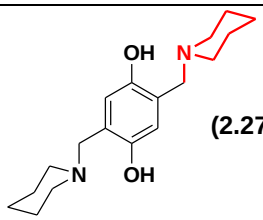 (2.27)	10.13[129] *N*-methylpiperidine	-0.22*
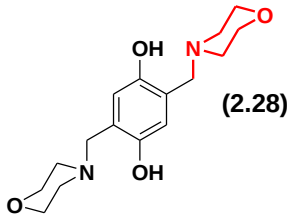 (2.28)	7.41[129] *N*-methylmorpholine	-0.18*, -0.01*
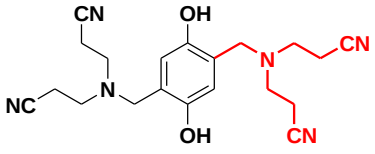 (2.29)	4.55[130] 3-[(2-Cyano-ethyl)-ethyl-amino]-propionitrile	E_{pa} +0.23**

* partially irreversible peak, ** irreversible peak

The more basic amines correlate with lower oxidation potentials of the corresponding hydroquinone. This can be rationalized since a stronger hydrogen bond acceptor would pull the hydroxyl proton away from the oxygen resulting in the oxygen having more of a partial negative charge associated with it. As a result, the oxidation of the hydroquinone moiety would be easier and thus occur at more negative potentials. Another way of putting this is that the hydroquinone with a very strong intramolecular hydrogen bond would be more similar to the hydroquinonate dianion which is oxidized very easily at very negative potentials. Also of note is that as the relative basicity is increased the separation between the two redox processes disappears. In Mayer's work the nature of the base is said not to be critical with respect to the rate of the CPET process,[125] nevertheless this data shows that the nature of the base is an important contributing factor to the redox potential of the oxidation process.

The apparent base strengths and potential correlation helps to explain why **2.1** is irreversibly oxidized since the pyrazole is not a strong enough base to hold onto the protons once the hydroquinone is oxidized. A similar argument could be made for **2.29**. However, another possible reason for the irreversibility may be the lack of the intramolecular hydrogen bond.[125] The hydrogen bond may be absent in **2.29** due to the weak basicity of the 3-[(2-cyano-ethyl)-ethyl-amino]-propionitrile substituent but other factors such as the greater degree of conformational flexibility of the amino substituent may favour conformations with no hydrogen bond.

Some of the other factors that may be of importance are interdependent and hard to separate from one another. For example, a conjugated pendant base influences the oxidation potential through both electron donating and basicity effects. The flexibility of

the pendant base could also affect the electrochemical behaviour. The non-conjugated amines are separated by a methylene linker which allows the amine more degrees of freedom. Therefore, once the non-conjugated hydroquinone is oxidized and no longer locked by the intramolecular hydrogen bond it would be able to move further away from the oxygen anion impacting the ease of its reduction. This may in part explain why the non-conjugated hydroquinones are less reversible as suggested by the OSWV data and the odd line shapes of these redox processes.

2.8 Synthesis and Electrochemical Studies of *N*-methylated 2,5-Bis(1-piperidinylmethyl)-1,4-benzoquinone

2.8.1 Synthesis and characterization

Characterization of the dicationic salts obtained by chemical oxidation of the corresponding hydroquinone established their structures as quinoidal but their redox properties are very different from a typical quinone. Clearly the proton transfer effects their redox behaviour, but presence of the positive charge is also expected to alter the redox behaviour. To probe how positive charge affects the redox potentials of a quinone, the dimethylated quinone 2,5-bis(N,N`-dimethyl-piperidinium)-1,4-benzoquinone bistriflate (**2.43**) was prepared by alkylation with methyl triflate (Scheme 2.12). Attempts to prepare analogous methylated quinones was unsuccessful as products proved to be unstable.

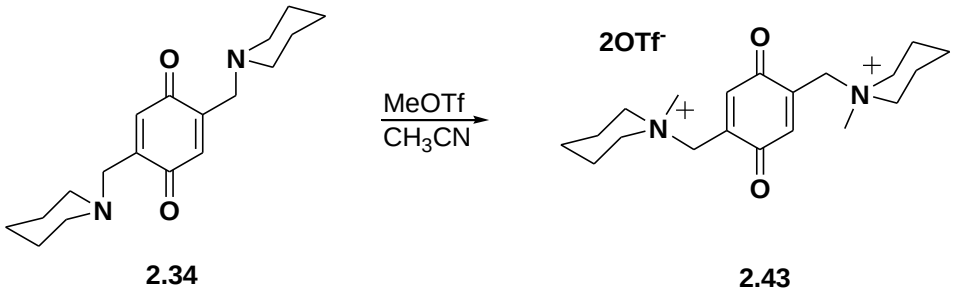

2.34 **2.43**

Scheme 2.12. Synthesis of **2.43.**

2.43 was less stable in solution than the protonated piperidinium quinone salt, **2.39**, and also decomposed slowly in the solid state if exposed to air, making it difficult to obtain an analytically pure sample. However it was possible to isolate a sample whose element analysis was very close to the theoretical value (analysis calculated for $C_{22}H_{32}F_6N_2O_8S_2$: C, 41.90; H, 5.11; N, 4.44. Found: C, 41.46; H, 4.92; N, 4.40) and all other data acquired is consistent with the proposed structure. For example, the solution IR spectrum of **2.43** in acetonitrile shows a carbonyl peak at 1669 cm^{-1}, very similar to **2.39** at 1666 cm^{-1}. There are no IR absorptions that could be assigned to hydroxyl or amine protons. The carbonyl carbons have a ^{13}C chemical shift of 186 ppm while the N-methyl groups are found at 2.99 ppm in the ^{1}H- NMR.

2.8.2 Electrochemical studies of 2.43

The cyclic voltammogram of **2.43** is shown in Figure 2.16. A one-electron reversible reduction is observed at a potential of -0.45 V (vs Fc). This redox peak is established as a one-electron process by comparing the peak area with the oxidation peak of an equimolar concentration of ferrocene. The reduction peak of **2.43** shows no degradation if scanned multiple times between 0V to -0.80 V. This first reduction peak is 0.54 V more positive

than the corresponding quinone **2.34** (E_1^o = -0.99 V vs Fc). This can be attributed to the dicationic charges of **2.43** which should increase the reduction potential to more positive potentials relative to the neutral quinone. However, the first reduction of **2.43** is still much lower than the potential observed for the two electron reduction of the protonated piperidine quinone salt **2.39** (E_1^o = -0.22 V vs Fc) which again implicates the importance of the proton transfer accompanying the reduction of the protonated quinone dications. The higher potential of **2.27**/**2.39** redox couple cannot be due to the positive charge alone and is also thought to be a result of the intramolecular hydrogen bonds when present and resulting proton transfer. Computational studies and experimental data for the oxidation of related phenols with a pendant base have shown that the mere existence of a hydrogen bond (ie. with no proton transfer) has a minimal effect on the redox potentials and the significantly lower redox potentials must be due to the proton transfer.[100,112,131]

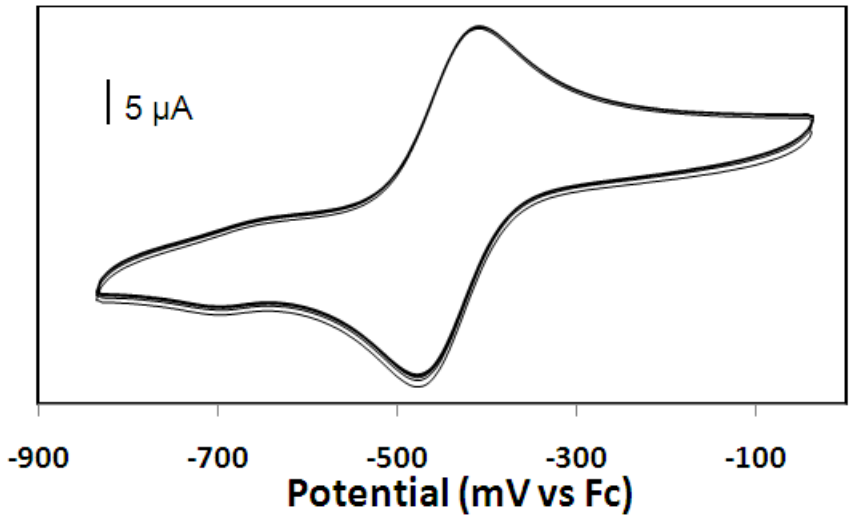

Figure 2.15. Cyclic voltammogram of **2.43** with multiple cycles in acetonitrile.

Upon scanning to even more negative potentials a second irreversible reduction process is observed at -1.30V. Multiple cycling past the second reduction peak causes the active species to slowly disappear until no redox processes are observed (Figure 2.15). This behaviour is speculated to arise from the transfer of the methyl group from the piperidinium groups to the reduced hydroquinonate dianion resulting in **2.46** as depicted by Scheme 2.13 but further experiments would be needed to confirm this proposition. **2.46** is expected to be redox inactive, given that 2,5-bis(4-*tert*-butyl-pyrid-2-yl)-1,4-dimethoxybenzene (**2.14**) has been shown to be redox inactive except for the reduction of the pyridine groups observed at very negative potentials.

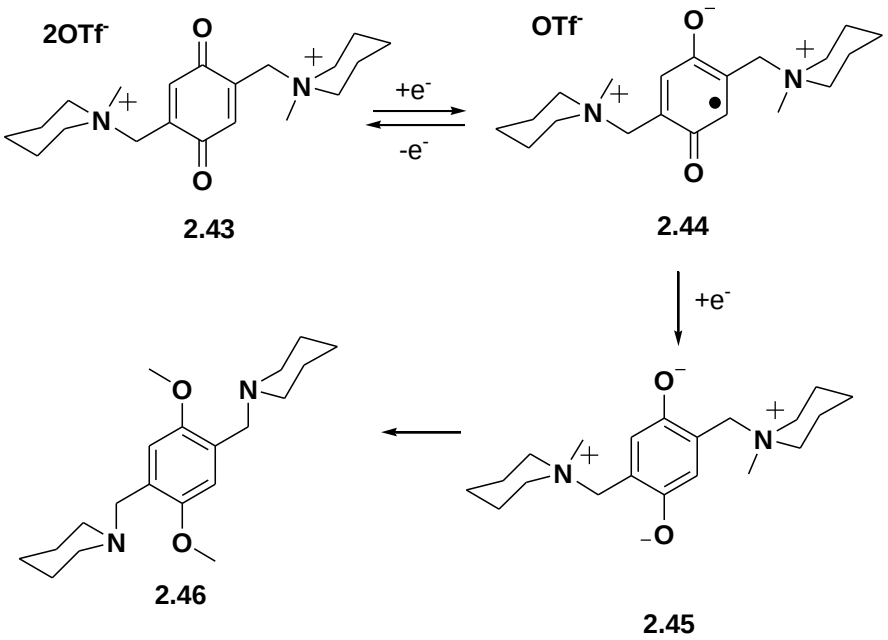

Scheme 2.13. Hypothesized redox behaviour of **2.43**.

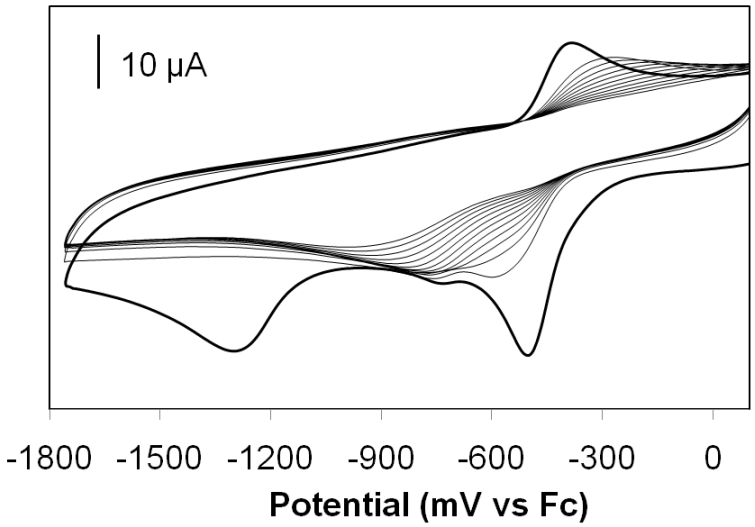

Figure 2.16. Cyclic voltammetry of **2.43**: multiple cycling past 2nd reduction peak.

As was observed for the hydroquinones in Section 2.5, a plot of scan rate$^{1/2}$ vs peak current is linear for the first redox process showing that the mass transport of **2.43** to the electrode surface is diffusion controlled. However in this case the slope obtained from a plot of scan rate$^{1/2}$ vs peak current for the reduction peak is greater than that of the corresponding oxidation peak. In this case reduction may result in a species which has more charge associated with it then **2.43** resulting in the corresponding oxidation diffusion coefficient being lower than that of the reduction process.

2.9 Synthesis and Electrochemistry of Hydrogen Bonded Resorcinols

Resorcinol (**2.4**), or "*meta* hydroquinone" is fundamentally different from the *ortho* and *para* forms. If deprotonated and oxidized by two electrons, a diradical form is generated (Scheme 2.13) rather than the quinoidal species which is typical for the

oxidized forms of *ortho* and *para*-hydroquinones. This is because substitution in the 1,3-positions of benzene result in cross-conjugation, with molecules whose singly occupied molecular orbitals (SOMOs) are said to be nondisjoint.[132,65]

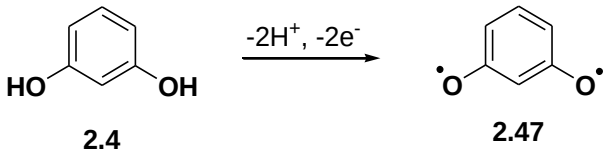

2.4 **2.47**

Scheme 2.14. Theoretical diradical form (**2.47**) of resorcinol.

If a hydrogen acceptor such as pyridine is installed adjacent to the hydroxyl groups, it was hoped that oxidation by two electrons would be electrochemically reversible (analogous to the hydroquinones discussed earlier) and lead to an intramolecular proton transfer resulting in a new diradical, dicationic species. With this in mind, two pyridine substituted resorcinol derivatives were synthesized (Scheme 2.15). The attempted Suzuki-Miyaura coupling of 1,3-dimethoxy-4,6-benzenediboronic acid with 2-bromopyridine failed, so 2-tributylstannanyl-pyridine (**2.49**)[133] was prepared and coupled to 4,6-dibromo-1,3-dimethoxybenzene (**2.50**)[134] via a Stille coupling reaction. The removal of the methyl protecting groups from **2.51** was achieved in a similar manner as was described for the *p*-hydroquinones with the aid of $AlCl_3$ to give **2.48**. A second derivative, **2.52**, with a phenyl group in the 2-position separating the hydroxyl groups was also synthesized with the hope that the oxidized diradical may be stabilized. This was achieved by first synthesizing 2,6-dimethoxybiphenyl (**2.53**)[135] and then following a similar route as that described for **2.48**.

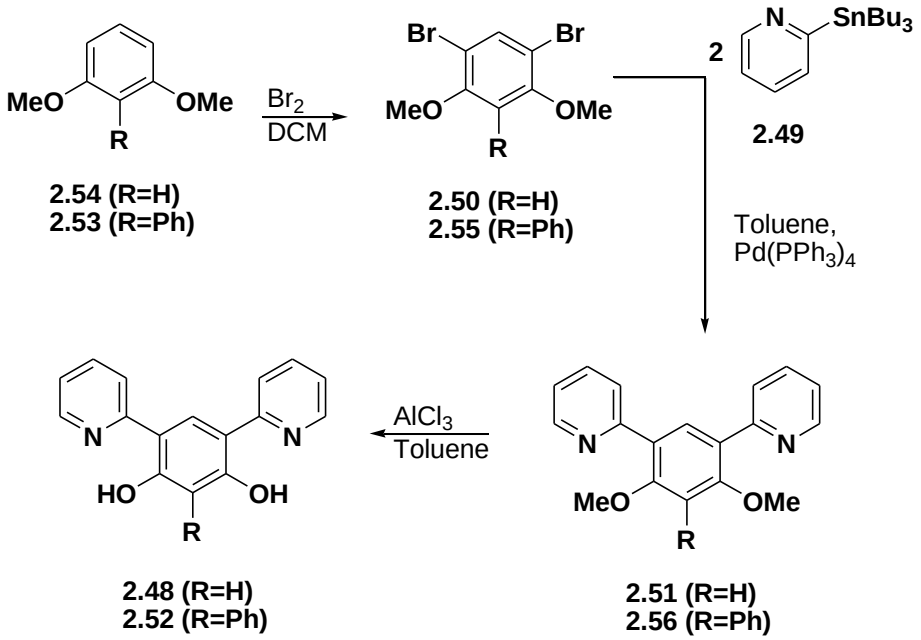

Scheme 2.15. Synthesis of **2.48** and **2.52**.

The characterization data for the two derivatives of resorcinol shows some similarities to their *para* counterparts. The OH protons have very high chemical shifts typical of hydrogen bonded hydroxyl protons (**2.48** $\delta_{(OH)}$ = 14.81 ppm and **2.52** $\delta_{(OH)}$ = 15.36 ppm). Their solution infrared spectra contain weak broad absorptions at ~2950-2400cm^{-1} also typical of hydrogen bonded phenols. Single crystals of **2.48** and **2.52** suitable for X-ray crystallography were obtained from toluene (Figures 2.18 and 2.19 respectively). The structure of **2.48** is planar: the plane defined by the pyridine ring containing N1 is twisted by 1.8^{o} with respect to the central benzene ring. Similarly, for **2.52**, the planes defined by the central benzene ring and pyridine ring containing N1 are slightly twisted by 1.4^{o}. The phenyl substituent of **2.52** is twisted by 56.8^{o} with respect to the central benzene ring. The structures of **2.48** and **2.52** have carbon-carbon and oxygen-carbon bond lengths similar to the derivatized 1,4-hydroquinones (Tables 2.9 and 2.10 respectively). The

structures of **2.48** and **2.52** possess N--O bond distances of ~2.52 Å in agreement with the solution data that the hydroxyl protons are hydrogen bound.

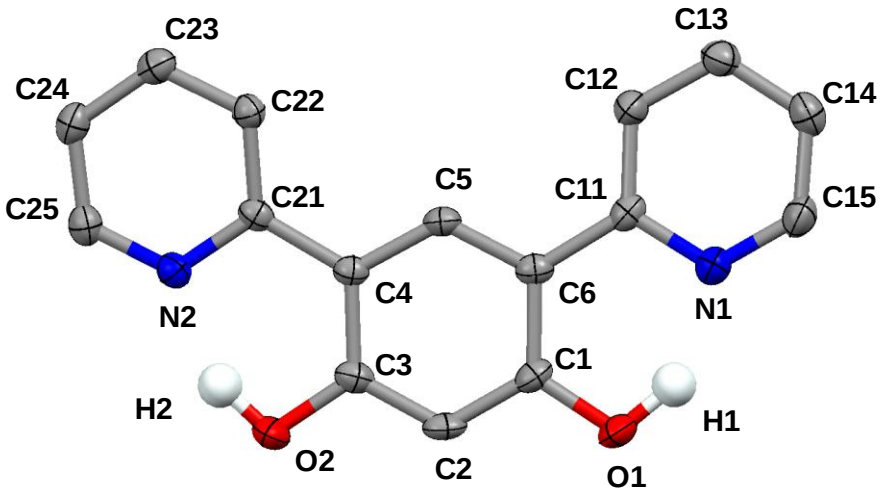

Figure 2.17. Molecular structure of **2.48** with thermal ellipsoids shown at 50% probability level. H atoms other than the phenolic OH have been omitted for clarity (OH protons located in a difference map and refined isotropically).

Table 2.9. Selected bond lengths (Å) and angles (°) for **2.48**.

Atoms	**2.48**	Atoms	**2.48**
Bond Lengths		C4-C5	1.384(3)
C1-O1	1.339(3)	C5-C6	1.386(3)
C3-O2	1.342(3)	C1-C6	1.413(3)
C1-C2	1.371(3)	C4-C21	1.465(3)
C2-C3	1.369(3)	*Bond Angle*	
C3-C4	1.412(3)	O1-C1-C2	117.4(2)

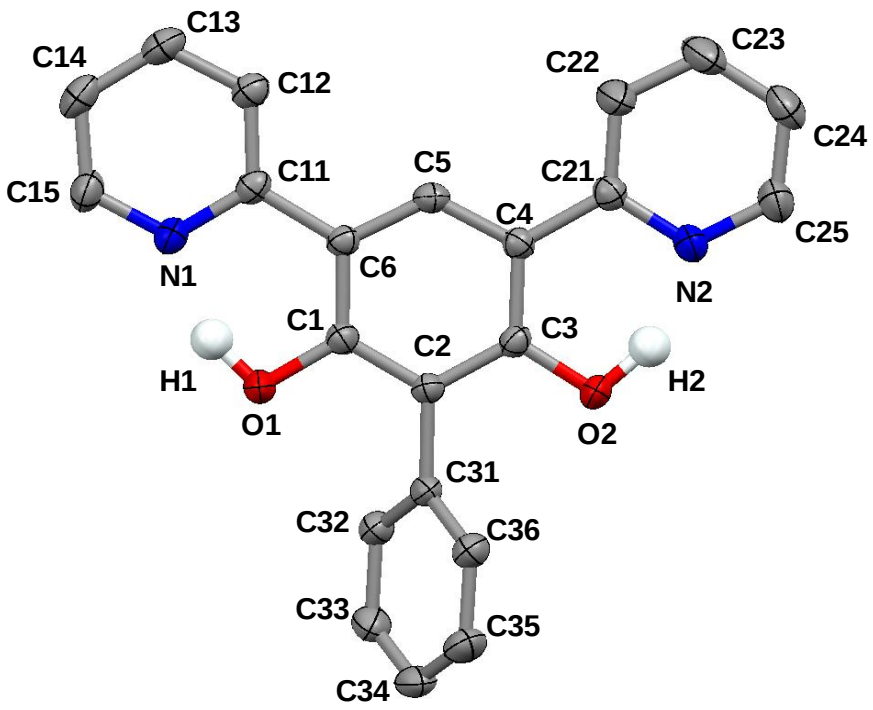

Figure 2.18. Molecular structure of **2.52** with thermal ellipsoids shown at 50% probability level. H atoms other than the phenolic OH have been omitted for clarity (OH protons located in a difference map and refined isotropically).

Table 2.10. Selected bond lengths (Å) and angles (º) for **2.52**.

Atoms	**2.52**	Atoms	**2.52**
Bond Lengths		C5-C6	1.381(2)
C1-O1	1.3460(2)	C1-C6	1.414(2)
C3-O2	1.3444(2)	C2-C31	1.4872(2)
C1-C2	1.398(2)	C1-C11	1.477(2)
C2-C3	1.395(2)	*Bond Angles*	
C3-C4	1.418(2)	O1-C1-C2	117.72(13)
C4-C5	1.383(2)	C5-C4-C3	116.87(14)

The cyclic voltammograms of the resorcinol derivatives shows that both are irreversibly oxidized at quite high potentials. The cyclic voltammogram of **2.48** is shown in Figure 2.20 and the potentials of the oxidations of **2.48** and **2.52** are summarized in Table 2.11. The phenylated derivative, **2.52**, is oxidized at a slightly lower potential than **2.48** which is consistent with the phenyl group being electron donating. The exact reason for the irreversibility is unknown but it is possible that the diradical that would be produced is not stable and decomposes or dimerizes rapidly. Scanning the cyclic voltammetries at high scan rates did not improve the reversibility of the oxidations.

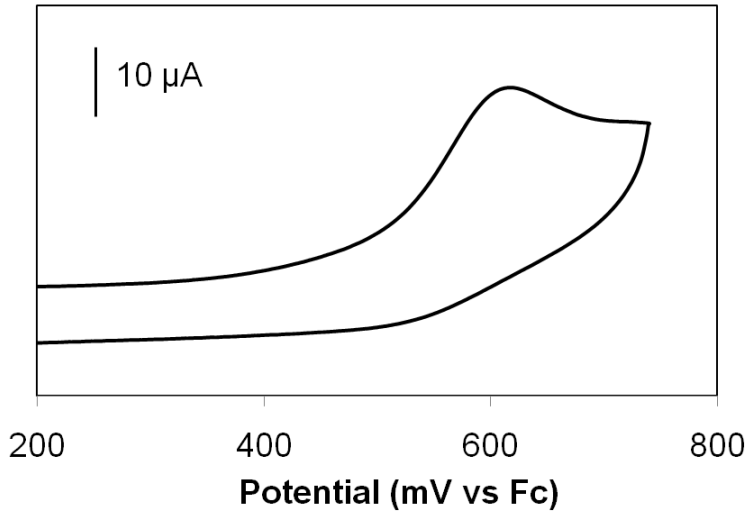

Figure 2.19. Cyclic voltammogram of **2.48.**

Table 2.11. Redox potentials (V vs Fc) for **2.48** and **2.52**.

Compound #	$E_1^{o'}$ (V)
2.48	E_{pa} = +0.63*
2.52	E_{pa} = +0.61*

* denotes irreversible peaks

All cyclic voltammograms and their scan rates can be found in Appendix 1: Figure A-59 and Figure A-60.

2.10 Summary

The synthesis of literature hydroquinones **2.1** and **2.2** were optimized. By derivatizing the pyridine groups of **2.2**, three novel hydroquinones **2.15**, **2.19** and **2.23** were also prepared. A second set of literature hydroquinones **2.27**, **2.28** and **2.29**, incorporating an amine non-conjugated with the central benzene ring were also prepared. For all hydroquinones prepared except for **2.29**, an intramolecular hydrogen bond was shown to exist in solution between the hydroxyl groups and adjacent amine. The chemical shifts of the hydroxyl protons of the conjugated hydroquinones other than **2.1** are between 13-15 ppm indicating they possess strong intramolecular hydrogen bonds. The non-conjugated hydroquinones **2.27** and **2.28** also posses intramolecular hydrogen bonds which are thought to be weaker as indicated by their OH chemical shifts. On the other hand, **2.29** does not have an intramolecular hydrogen bond perhaps due to the low basicity or increased flexibility of the pendant base. The quinone forms of some of these hydroquinones were also prepared.

All derivatized hydroquinones, except for **2.1** and **2.29** can be reversibly oxidized by cyclic voltammetry. This oxidation process is thought to be by means of a CPET process by analogy to work done by Saveant[48], Mayer[114,125] and others. The hydroquinone oxidation potential correlates with the basicity of the amine hydrogen acceptor. Hydroquinones with the most basic amines are oxidized more easily than hydroquinones with less basic amines. In the case of **2.1**, the low basicity of the pyrazole group is thought to be responsible for the irreversibility of its oxidation.

Hydroquinones which were reversibly oxidized electrochemically were subsequently chemically oxidized with $NOBF_4$ and a new set of quinone dications, where the hydrogen

atoms of the corresponding hydroquinone had been transferred intramolecularly to the adjacent amine groups, were isolated and characterized for the first time. Solution data of the quinone dications isolated indicate the intramolecular hydrogen bond normally no longer exists. A methylated bis-piperidinyl quinone dication, **2.43** was also prepared as a model compound. The electrochemical behaviour of **2.43** suggests that the corresponding hydroquinone **2.27** is oxidized at much higher potentials than its quinone form **2.34** due to the positive charges in addition to the intramolecular hydrogen bonds and proton transfer that occurs upon oxidation.

Resorcinol derivatives **2.48** and **2.52** incorporating an adjacent hydrogen accepting pyridine group were synthesized and characterized. These compounds shared some similarities with their *para* counterparts such as strong intramolecular hydrogen bonds. However, unlike their *para* counterparts, the cyclic voltammetries of **2.48** and **2.52** showed that these compounds were irreversibly oxidized at high positive potentials.

2.11 Experimental

2.11.1 General

Unless noted otherwise, reagents used were purchased commercially and used as received. In the case of water sensitive reactions, all solvents were dried/distilled prior to use with CaH_2 for dichloromethane or acetonitrile and sodium/benzophenone for tetrahydrofuran, diethyl ether or toluene. Solvents used for air sensitive compounds were bubbled with argon for ~20 minutes prior to use. ^{1}H-NMR were run on a Bruker AMX 300 MHz instrument (^{13}C-NMR 125 MHz). IR samples were run on a Perkin Elmer

Spectrum One FT-IR spectrometer and solution IR samples were run in a quartz cell. UV-vis spectra were obtained using a Cary 50 instrument.

The following compounds have been reported in literature before, however synthetic details are included here because either the procedure has been modified or additional characterization data has been included: (**2.1**)[86], (**2.2**)[87], (**2.17**)[92], (**2.27**)[101], (**2.28**)[102], (**2.29**)[103] and (**2.31**)[106]. The following compounds have been reported in literature with no major modifications and have not been included in the experimental: (**2.9**)[90], (**2.10**)[91], (**2.11**)[91], (**2.12**)[92], (**2.18**)[92], (**2.21**)[93], (**2.24**)[99], (**2.49**)[133], (**2.50**)[134] and (**2.53**)[135].

2.11.2 Electrochemistry

Cyclic voltammetry experiments were run on a Bioanalytical Systems CV50 voltammetric analyzer using an electrochemical cell containing the analyte (1 mM), $Bu_4N^+BF_4^-$ (0.1 M) electrolyte, a silver wire as the reference electrode, a glassy carbon electrode as the working electrode, a platinum wire as the counter electrode and ferrocene (1 mM) as the internal standard. Solvents used (DCM, CH_3CN and DMF) were dried with CaH_2, distilled and bubbled with argon for ~20 minutes prior to use.

Redox processes were established to be reversible (or quasi-reversible) based on their anodic and cathodic peak currents being the same and the peak separations being close to that of the internal standard, usually ferrocene. Peak separation ideally should be 59 mV however small deviations may be caused from a variety of reasons, for example in dichloromethane, anodic and cathodic peak separations are generally higher due to its poor conductivity. However by comparing with an internal standard that is known to be well behaved and reversible, one can differentiate whether the analyte is indeed

reversible or if deviations are caused by the solvent or other factors. In the case of the reversible oxidation processes of the hydroquinones summarized in Table 2.4, the redox processes are best described as being quasi-reversible since the peak separation is greater than the ideal value. However the deviation is small for most except for **2.28** whose large peak separation is one indication of its poor reversibility.

2.11.3 Synthesis

2,5-Bis(pyrazol-1-yl)-1,4-hydroquinone (2.1). Absolute ethanol (100 mL) was mixed

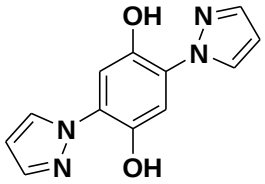

with *p*-benzoquinone (5.00 g, 46 mmol) and pyrazole (6.30 g, 92.5 mmol) then thoroughly deoxygenated. The mixture was refluxed for 16 hours then allowed to cool to room temperature. A fluffy, white precipitate was filtered and the crude product was purified by column chromatography on silica gel using chloroform as the eluent. The 2,5-bis(pyrazol-1-yl)-1,4-hydroquinone can be further purified by recrystallization from hot methanol resulting in a total yield of 2.31 g (21%) of **2.1** as an off-white powder. ^{1}H NMR ($CDCl_3$): δ 11.14 (s, 2H), 7.98 (d, 2H), 7.74 (d, 2H), 7.14 (s, 2H), 6.53 (t, 2H). FT-IR (CH_3CN solution): 3300-2600 (br. w, O-H) cm^{-1}. FT-IR (nujol mull): 3170-2400 (br. w, O-H) cm^{-1}.

2,5-Bis(pyrid-2-yl)-1,4-hydroquinone (2.2). 2,5-Bis(pyrid-2-yl)-1,4-dimethoxybenzene (2.2 g, 7.5 mmol) was dissolved in toluene (150 mL) and stirred with $AlCl_3$ (4.0 g, 30 mmol). The solution was purged with argon and then the yellow slurry was refluxed for 5 hours. After cooling the reaction mixture was quenched by adding water and then

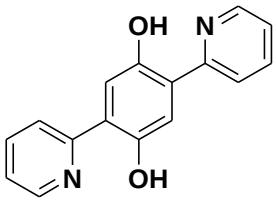

extracted with dichloromethane. The organic layer was separated, dried over $MgSO_4$ and filtered. Solvent was removed under reduced pressure. Column chromatography of the residue on silica gel using chloroform as the eluent yielded 1.28 g (65%) of compound **2.2** as a yellow powder. Crystals were obtained by slow evaporation of the compound in ethanol. ^{1}H NMR ($CDCl_3$): δ 13.67 (s, 2H), 8.55 (d, 2H), 7.95 (d, 2H), 7.87 (ddd, 2H), 7.48 (s, 2H), 7.30 (m, 2H). FT-IR (CH_3CN solution): 3100-2400 (br. w, O-H) cm^{-1}. FT-IR (nujol mull): 3300-2100 (br. w, O-H) cm^{-1}. HR-MS calcd for $C_{24}H_{26}N_2O_2$ (M+) 262.0742, found 262.0742.

2,5-Bis(4-*tert*-butyl-pyrid-2-yl)-1,4-dimethoxybenzene (2.14) In anhydrous

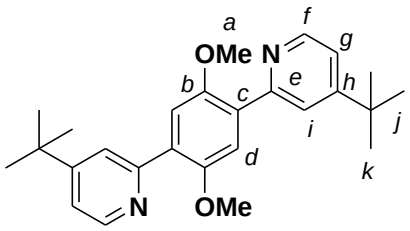

tetrahydrofuran (150 mL) there was added 2-bromo-4-*tert*-butylpyridine (4.0 g, 0.019 mol), 1,4-benzenediboronic acid (1.384 g, 0.0061 mol) and $Na_2CO_{3(aq)}$ (1 M, 20 mL). The solution was deaerated with argon and then tetrakistriphenylphosphine palladium (460 mg, 0.0004 mol) was added. The yellow solution was refluxed for 48 hours. The resulting solution was washed with brine. The aqueous phase was then extracted with dichloromethane (2 * 30 mL). The combined organic extracts were dried with $MgSO_4$, filtered and then the solvent was removed under reduced pressure. The crude product was purified by column chromatography on silica gel with diethyl ether to yield 1.99 g (80.5%) of **2.14** as an off-white solid. δ ^{1}H NMR ($CDCl_3$): δ 8.63 (d, 2H*f*, *J* = 5.4 Hz), 7.96 (d, 2H*i*, *J* = 1.8 Hz), 7.55 (s, 2H*d*), 7.22 (dd, 2H*g*, *J* = 5.4, 1.8 Hz), 3.91 (s, 6H*a*), 1.37 (s, 18H*k*) ppm. ^{13}C

NMR ($CDCl_3$): δ 159.5 (*h*), 155.3 (*e*), 151.3 (*b*), 149.3 (*f*), 130.2 (*c*), 122.5 (*i*), 119.0 (*g*), 114.8 (*d*), 56.4 (*a*), 34.8 (*j*), 30.6 (*k*) ppm. Anal. Calcld for $C_{26}H_{32}N_2O_2$: C, 77.19; H, 7.97; N, 6.92. Found: C, 77.03; H, 7.99; N, 6.90**.**

2,5-Bis(4-*tert*-butyl-pyrid-2-yl)-1,4-hydroquinone (2.15). 2,5-Bis(4-*tert*-butyl-pyrid-2-yl)-1,4-dimethoxybenzene (2.2 g, 0.0054 mol) was dissolved in toluene (150 mL) and stirred with $AlCl_3$ (7.0 g, 0.052 mol). The solution was purged with argon and then the yellow slurry was refluxed for 4 hours. After cooling the reaction mixture was quenched by adding water and then extracted with dichloromethane. The organic layer was separated, dried over $MgSO_4$ and filtered. Solvent was removed under reduced pressure. Column chromatography of the residue on silica gel with chloroform yielded 1.22 g (60%) of the target hydroquinone as a yellow powder. Single crystals were obtained by slow evaporation of the compound in ethanol. ^{1}H NMR ($CDCl_3$): δ 13.85 (s, 2H, *a*), 8.45 (d, 2H*f*, *J* = 5.4Hz), 7.95 (s, 2H*i*), 7.51 (s, 2H*d*), 7.28 (dd, 2H*g*, *J* = 5.4, 1.7 Hz), 1.39 (s, 18H*k*) ppm. ^{1}H NMR (CD_3CN): δ 13.57 (s, 2H*a*), 8.50 (d, 2H*f*, *J* = 5.4Hz), 8.06 (d, 2H*i*, *J* = 1.2 Hz), 7.59 (s, 2H*d*), 7.50 (dd, 2H*g*, *J* = 5.7, 1.8 Hz), 1.40 (s, 18H*k*) ppm. ^{13}C NMR ($CDCl_3$): δ 162.0 (*h*), 156.8 (*e*), 151.9 (*b*), 145.9 (*f*), 121.9 (*c*), 119.4 (*i*), 116.6 (*g*), 114.6 (*d*), 35.2 (*j*), 30.5 (*k*) ppm. FT-IR (CH_3CN solution): 3300-2400 (br. w, O-H) cm^{-1}. FT-IR (nujol mull): 3300-2040 (br. w, O-H) cm^{-1}. UV-Vis (CH_3CN): λ_{max} 286 (ε = 24000 M^{-1}•cm^{-1}), 390 (ε = 14000 M^{-1}•cm^{-1}) nm. Anal. Calcld for $C_{24}H_{28}N_2O_2$: C, 76.56; H, 7.50; N, 7.44. Found: C, 76.70; H, 7.60; N, 7.28.

4-*Tert*-butylpyridine-1-oxide (2.17). In acetone (100 mL) there was added 4-*tert*-butylpyridine (5.0 g, 0.037 mol). 3-Chloroperoxybenzoic acid (<77%, 11 g, 0.064 mol) was added and the solution was stirred for 1 hour. The solvent was removed under reduced pressure to give a fluffy solid which was dissolved in dichloromethane (60 mL) and washed with an aqueous solution of NaOH (1M, 3x 30 mL). The organic extracts were dried and solvent removed under reduced pressure. If necessary the crude product can be purified by column chromatography (silica, diethyl ether/methanol 3:1). Yield of **2.17** is 5.0 g (89%) isolated as an off-white solid. ^{1}H NMR ($CDCl_3$): δ 8.14 (d, 2H), 7.25 (d, 2H), 1.31 (s, 9H) ppm.

2,5-Bis-(4-dimethylamino-pyrid-2-yl)-1,4-hydroquinone (2.19).

2,5-Bis-(4-dimethylamino-pyrid-2-yl)-1,4-dimethoxybenzene (0.45 g, 1.2 mmol) was dissolved in toluene (150 mL) and stirred with $AlCl_3$ (1.6 g, 12 mmol). The slurry was purged with argon and then refluxed for 1 hour. After cooling the reaction mixture was quenched by adding water, made basic and then extracted with diethyl ether (1 * 50 mL) and then dichloromethane (3 * 100 mL). The organic layers were combined then washed with $NaHCO_3$ followed by brine, dried over $MgSO_4$ and filtered. Solvent was removed under reduced pressure to give a yellow powder. Column chromatography of the residue on alumina gel using a solution of chloroform/1% methanol as the eluent yielded 162 mg (39%) of the target compound as a yellow powder. Single crystals were obtained by slow evaporation of the compound from dichloromethane. ^{1}H NMR (CD_2Cl_2): δ 13.80 (s, 2H*a*), 8.13 (d, 2H*f*, *J* =

6.2 Hz), 7.38 (s, 2H*d*), 7.08 (d, 2H*i*, *J* = 2.5 Hz) 6.53 (dd, 2H*g*, *J* = 6.2, 2.5 Hz), 3.10 (s, 12H*j*) ppm. ^{1}H NMR ($CDCl_3$): δ 14.52 (s, 2H*a*), 8.14 (d, 2H*f*, *J* = 6.2 Hz), 7.41 (s, 2H*d*), 7.07 (d, 2H*i*, *J* = 2.5 Hz) 6.48 (dd, 2H*g*, *J* = 6.1, 2.5 Hz), 3.10 (s, 12H*j*) ppm. ^{13}C NMR (CD_2Cl_2): δ 157.3 (*h*), 155.7 (*e*), 152.5 (*f*), 146.1 (*b*), 122.2 (*c*), 114.5 (*d*), 105.7 (*i*), 101.5 (*g*), 39.6 (*j*) ppm. FT-IR (DCM solution): 3250-2100 (w, O-H) cm^{-1}. FT-IR (nujol mull): 3400-2460 (br. w, O-H) cm^{-1}. Anal. Calcld for $C_{20}H_{22}N_4O_2$: C, 68.55; H, 6.33; N, 15.99. Found: C, 68.27; H, 6.33; N, 15.71.

2,5-Bis-(4-dimethylamino-pyrid-2-yl)-1,4-dimethoxybenzene (2.22). In anhydrous

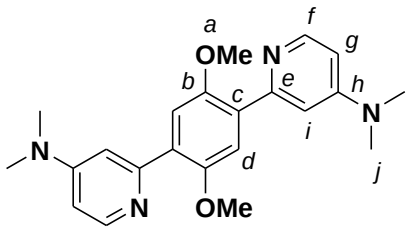

toluene (125 mL) dimethyl-(2-tributylstannanyl-pyrid-4-yl)-amine (3.38 g, 8.23 mmol) and 1,4-dibromo-2,5-dimethoxybenzene (0.66 g, 2.2 mmol) were added. The solution was deaerated with argon and then (tetrakistriphenylphosphine)palladium (600 mg, 0.52 mmol) was added. The yellow solution was refluxed for 48 hours then allowed to cool to room temperature. Celite was then added and the mixture was filtered. The solvent was removed from the filtrate under reduced pressure yielding an off white powder. The crude product was purified by column chromatography on alumina gel using ethyl acetate with up to 5% methanol as the eluent to yield 207 mg (25%) of the target compound as an off-white solid. ^{1}H NMR ($CDCl_3$): δ 8.36 (d, 2H*f*, *J* = 6.2 Hz), 7.50 (s, 2H*d*), 7.18 (d, 2H*i*, *J* = 2.6), 6.49 (dd, 2H*g*, *J* = 6.0, 2.7 Hz), 3.88 (s, 6H*a*), 3.04 (s, 12H*j*) ppm. ^{13}C NMR ($CDCl_3$): δ 155.6 (*h*), 154.3 (*e*), 151.2 (*f*), 149.5 (*b*), 130.6 (*c*), 114.9 (*d*), 108.2 (*i*), 105.3 (*g*), 56.5 (*a*), 39.2 (*j*) ppm.

Anal. Calcld for $C_{22}H_{26}N_4O_2$: C, 69.82; H, 6.92; N, 14.80. Found: C, 69.32; H, 6.86; N, 14.47.

2,5-Bis([2,2']-bipyrid-6-yl)-1,4-hydroquinone (2.23). 2,5-Bis([2,2']-bipyrid-6-yl)-1,4-dimethoxybenzene (0.60 g, 1.3 mmol) was dissolved in anhydrous toluene (120 mL) and stirred with $AlCl_3$ (1.8 g, 13 mmol). The solution was purged with argon and then the yellow slurry was refluxed for 3 hours. After cooling, the reaction mixture was quenched by adding water and then extracted with dichloromethane. The aqueous phase was made basic and extracted with DCM (3 * 30 mL). The organic layer was separated, dried over $MgSO_4$ and filtered. Solvent was removed under reduced pressure to give a yellow oil. Column chromatography of the residue on alumina gel using chloroform with up to 1% MeOH as the eluent yielded 212 mg (38%) of the target hydroquinone as a yellow powder. Single crystals were obtained by slow evaporation of the compound in toluene. ^{1}H NMR ($CDCl_3$): δ 13.90 (s, 2H*a*), 8.76 (ddd, 2H*k*, *J* = 4.7, 1.7, 0.9 Hz), 8.38 (dd, 2H*h*, *J* = 7.2, 1.6 Hz), 8.23 (ddd, 2H*n*, *J* = 8.0, 0.9, 0.9 Hz), 8.1-7.97 (m, 4H*f*,*g*), 7.90 (ddd, 2H*m*, , *J* = 7.7, 7.7, 1.8 Hz), 7.57 (s, 2H*c*), 7.39 (ddd, 2H*l*, , *J* = 7.6, 4.7, 1.1 Hz) ppm. ^{13}C NMR ($CDCl_3$): δ 156.5 (*i*), 154.6 (*j*), 153.6 (*e*), 151.9 (*k*), 149.7 (*b*), 139.0 (*g*), 137.3 (*m*), 124.2 (*n*), 122.0 (*d*), 120.8 (*l*), 120.0 (*f*), 120.0 (*h*), 115.0 (*c*) ppm. FT-IR (DCM solution): 3350-2300 (br. w, O-H) cm^{-1}. Anal. Calcld for $C_{26}H_{18}N_4O_2$: C, 74.63; H, 4.34; N, 13.39. Found: C, 74.47; H, 4.40; N, 13.26**.**

2,5-Bis([2,2']-bipyrid-6-yl)-1,4-dimethoxybenzene (2.25).

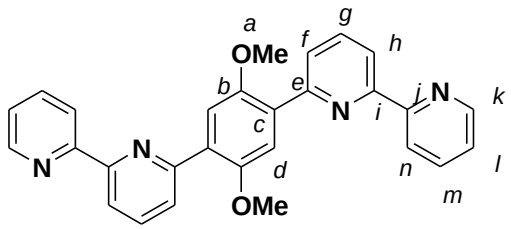

In anhydrous tetrahydrofuran (250 mL) there was added 2-bromo-[2,2']-bipyridine (1.44 g, 6.1 mmol), 2,5-dimethoxy-1,4-benzenediboronic acid (0.552, 2.4 mmol) and $Na_2CO_{3(aq)}$ (1 M, 8 mL). The solution was deaerated with argon and then tetrakistriphenylphosphine palladium (160 mg, 0.14 mmol) was added. The yellow solution was refluxed for 72 hours and then after cooling was washed with brine. The aqueous phase was extracted with dichloromethane (2*30 mL). The organic extracts were dried with $MgSO_4$, filtered and then the solvent was removed under reduced pressure. The crude product was purified by column chromatography on alumina gel using a hexanes/ethyl acetate gradient to yield 0.72 g (72%) of the target compound as a white solid. ^{1}H NMR ($CDCl_3$): δ 8.72 (ddd, 2H*k*, *J* = 4.7, 1.8, 0.9 Hz), 8.60 (ddd, 2H*n*, *J* = 8.0, 1.0, 1.0 Hz), 8.39 (dd, 2H*h*, *J* = 7.8, 1.0 Hz), 8.08 (dd, 2H*f*, *J* = 7.9, 1.0 Hz), 7.90-7.81 (m, 4H*g*,*m*), 7.83(s, 4H*d*), 7.33 (ddd, 2H*l*, *J* = 7.5, 4.9, 1.2 Hz), 3.98 (s, 6H*a*) ppm. ^{13}C NMR ($CDCl_3$): δ 156.5 (*j*), 155.6 (*i*), 154.4 (*e*), 151.8 (*b*), 149.1 (*k*), 136.8 (*g*), 136.7 (*m*), 130.0 (*n*), 125.3 (*c*), 123.6 (*l*), 121.1 (*h*), 119.2 (*f*), 115.1 (*d*), 56.5 (*a*) ppm. Anal. Calcld for $C_{28}H_{22}N_4O_2$: C, 75.32; H, 4.97; N, 12.55. Found: C, 74.53; H, 4.97; N, 12.26.

2,5-Bis(piperidin-1-ylmethyl)-1,4-hydroquinone (2.27). *P*-formaldehyde (5.4 g, 178 mmol) and *p*-hydroquinone (1.08 g, 9.7 mmol) were suspended in ethanol (100 mL). Piperidine (1.67 g, 19.4 mmol) was added and the cloudy solution was refluxed for 6 hours, turning completely clear in the first hour. Solvent was removed to give the crude

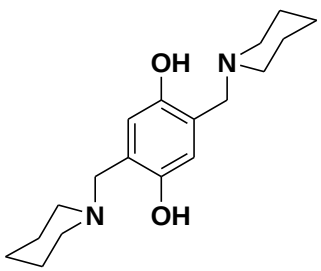

target compound as a white solid. This was recrystallized from ethanol to give pure 2,5-bis(piperidin-1-ylmethyl)-1,4-hydroquinone with an overall yield of 2.12 g (72%). ^{1}H NMR ($CDCl_3$): δ 10.81 (s, 2H), 6.45 (s, 2H), 3.58 (s, 4H), 2.49 (m, 8H), 1.65-1.45 (m, 12H) ppm. ^{1}H NMR (CD_3CN): δ 10.58 (s, 2H), 6.37 (s, 2H), 3.56 (s, 4H), 2.45 (m, 8H), 1.60-1.40 (m, 12H) ppm. ^{13}C NMR ($CDCl_3$): δ 150.07, 121.18, 115.57, 61.88, 53.82, 25.81, 23.96 ppm. FT-IR (CH_3CN solution) 3300-2500 (br. w, O-H) cm^{-1}. FT-IR (thin film): 3400-2400 (br. w, O-H) cm^{-1}. UV-Vis (CH_3CN): λ_{max} 303 (ε = 5000 M^{-1}•cm^{-1}) nm.

2,5-Bis(morpholin-4-ylmethyl)-1,4-hydroquinone (2.28). *P*-formaldehyde (5.4 g, 178

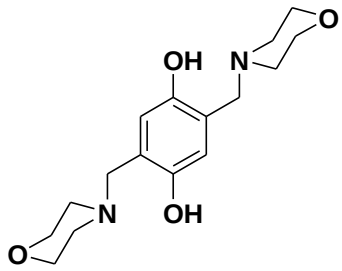

mmol) and *p*-hydroquinone (1.08 g, 9.7 mmol) were suspended in ethanol (100 mL). Morpholine (1.69 g, 19.4 mmol) was added and the cloudy solution was refluxed for 48 hours, turning completely clear in the first few hours. Solvent was removed to give the crude target compound as a white solid. This can be recrystallized from ethanol to give pure 2,5-bis(morpholin-4-ylmethyl)-1,4-hydroquinone with an overall yield of 2.21 g (74%). ^{1}H NMR ($CDCl_3$): δ 10.02 (s, 2H), 6.49 (s, 2H), 3.73 (t, 8H, *J* = 4.4 Hz), 3.63 (s, 4H), 2.55 (s, 8H) ppm. ^{13}C NMR ($CDCl_3$): δ 149.9, 120.8, 116.1, 66.8, 61.6, 52.9 ppm. ^{1}H NMR (CD_3CN): δ 9.94 (br. s, 2H), 6.44 (s, 2H), 3.65 (t, 8H, *J* = 4.7Hz), 3.60 (s, 4H), 2.47 (t, 8H, *J* = 4.4Hz) ppm. FT-IR (CH_3CN solution) 3300-2450 (br. w., O-H) cm^{-1}. FT-IR (thin film): 3450-2300 (br. w, O-H) cm^{-1}.

2,5-Bis((bis(2-cyanoethyl)amino)methyl)-1,4-hydroquinone (2.29). *P*-formaldehyde (0.61 g, 19.8 mmol) and *p*-hydroquinone (1.08 g, 9.7 mmol) were suspended in ethanol (100 mL) and water (20 mL). Bis(2-cyanoethyl)amine (90%, 2.73 g, 20.0 mmol) was added and the cloudy solution was refluxed for 24 hours, turning completely clear in the first couple hours. Solvent was removed to give a white precipitate in the remaining water which was isolated by filtration. This was recrystallized from hot dimethylformamide and methanol to give pure 2,5-bis((bis(2-cyanoethyl)amino)methyl)-1,4-hydroquinone with an overall yield of 1.44 g (39%). ^{1}H NMR (DMSO): δ 8.74 (s, 2H), 6.68 (s, 2H), 3.60 (s, 4H), 2.78 (t, 8H, *J* = 6.5 Hz), 2.66 (t, 8H, *J* = 6.5 Hz) ppm. ^{1}H NMR (CD_3CN): δ 8.27 (s, 2H), 6.58 (s, 2H), 3.76 (s, 4H), 2.88 (t, 8H, *J* = 6.8 Hz), 2.60 (t, 8H, *J* = 6.8 Hz) ppm. ^{13}C NMR (DMSO): δ 148.1, 122.8, 119.7, 116.7, 50.8, 48.0, 14.9 ppm. FT-IR (DMF solution) 3400-3000 (br. s., O-H), 2245 (s, CN) cm^{-1}. FT-IR (KBr Pellet) 3237 (br. s., O-H), 2248 (s, CN) cm^{-1}.

2,5-Bis(pyrazol-1-yl)-1,4-quinone (2.31). 2,5-Bis(pyrazol-1-yl)-1,4-hydroquinone (120 mg, 0.495 mmol) was dissolved in ethanol (100%, 50 mL). This solution was purged with argon and DDQ (114 mg, 0.502 mmol) was added. This was refluxed for 30 min resulting in an orange solution. Solvent was removed from the filtrate under reduced pressure to give 112 mg (94%) of the target quinone as an orange powder. ^{1}H NMR ($CDCl_3$): δ 8.64 (d, 2H), 7.80 (d, 2H), 7.39 (s, 2H), 6.53 (dd, 2H) ppm. ^{13}C NMR ($CDCl_3$): δ182.1, 143.7, 139.6,

133.1, 119.3, 110.2 ppm. FT-IR (nujoll mull) 1666 (s, C=O) cm^{-1}. UV-Vis (CH_3CN): λ_{max} 255 (ε = 23000 M^{-1}•cm^{-1}), 335 (ε = 17000 M^{-1}•cm^{-1}), 432 (ε = 1600 M^{-1}•cm^{-1}), 486 (ε = 1000 M^{-1}•cm^{-1}) nm.

2,5-Bis(pyrid-2-yl)-1,4-benzoquinone (2.32). 2,5-Bis(pyridin-2-yl)-1,4-hydroquinone

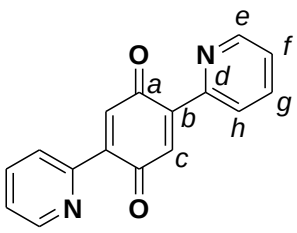

(50 mg, 0.19 mmol) was dissolved in toluene (50 mL). This solution was purged with argon and $Pd(OAc)_2$ (111 mg, 0.18 mmol) was added. This was stirred for 30 min and then filtered. Solvent was removed from the filtrate under reduced pressure to give 44 mg (89%) of the target compound as a light yellow powder. ^1H NMR ($CDCl_3$): δ 8.72 (d, 2H*e*, *J* = 4.2Hz), 7.99 (d, 2H*h*, *J* = 8.1Hz), 7.80 (ddd, 2H*g*, *J* = 8.1, 8.1, 2.1Hz), 7.59 (s, 2H*c*), 8.72 (m, 2H*f*) ppm. ^{13}C NMR ($CDCl_3$): δ187.3 (*a*), 150.1 (*b*), 149.9 (*d*), 142.7 (*e*), 136.3 (*c*), 135.3 (*g*), 126.0 (*f*), 124.7 (*h*) ppm. FT-IR (nujoll mull): 1647 (s, C=O) cm^{-1}. UV-Vis (CH_3CN): λ_{max} 287 (ε = 22000 M^{-1}•cm^{-1}), 314 (ε = 24000 M^{-1}•cm^{-1}), 390 (ε = 11000 M^{-1}•cm^{-1}), 485 (ε = 300 M^{-1}•cm^{-1}) nm. This quinone species was not stable enough to be sent for elemental analysis. Therefore high resolution electrospray ionization mass spectrometry was used to confirm the identity of this compound. HR-MS calcd for $C_{16}H_{10}N_2O_2$ (M+) 262.0742, found 262.0742.

2,5-Bis(4-*tert*-butyl-pyrid-2-yl)-1,4-benzoquinone (2.33). 2,5-Bis(4-*tert*-butyl-pyrid-2-yl)-1,4-hydroquinone (50 mg, 0.13 mmol) was dissolved in toluene (50 mL). This solution was purged with argon and $Pd(OAc)_2$ (79 mg, 0.18 mmol) was added. This was stirred for 30 min and then filtered. Solvent was removed from the filtrate under reduced

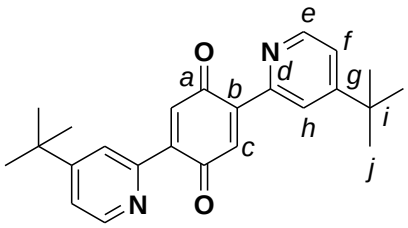

pressure to give 45 mg (92%) of the target compound as a light yellow powder. ^{1}H NMR ($CDCl_3$): δ 8.61 (d, 2H*e*, *J* = 5.1Hz), 7.95 (d, 2H*h*, *J* = 1.5Hz), 7.54 (s, 2H*c*), 7.36 (dd, 2H*f*, *J* = 5.2, 2.0 Hz), 1.37 (s, 18H*j*) ppm. ^{1}H NMR (CD_3CN): δ 8.60 (d, 2H*e*, *J* = 5.1Hz), 7.94 (d, 2H*h*, *J* = 1.5Hz), 7.47 (dd, 2H*f*, *J* = 5.4, 2.1 Hz), 7.40 (s, 2H*c*), 1.35 (s, 18H) ppm. ^{13}C NMR ($CDCl_3$): δ 187.4 (*a*), 160.5 (*b*), 149.9 (*g*), 149.0 (*d*), 143.2 (*e*), 135.2 (*c*), 123.3 (*f*), 121.7 (*h*), 35.0 (*i*), 30.5 (*j)* ppm. FT-IR (nujoll mull): 1643 (s, C=O) cm^{-1}. UV-Vis (CH_3CN): λ_{max} 323 (ε = 12000 M^{-1}•cm^{-1}), 468 (ε = 260 M^{-1}•cm^{-1}) nm. Anal. Calcld for $C_{24}H_{26}N_2O_2$: C, 76.98; H, 7.00; N, 7.48. Found: C, 76.21; H, 7.06; N, 6.06. This quinone species was not stable enough to obtain satisfactory elemental analysis results. Therefore high resolution electrospray ionization mass spectrometry was used to confirm the identity of this compound. HR-MS calcd for $C_{24}H_{26}N_2O_2$ (M+) 374.1994, found 374.1993.

2,5-bis(piperidin-1-ylmethyl)-1,4-benzoquinone (2.34). 2,5-Bis(piperidin-1-ylmethyl)-

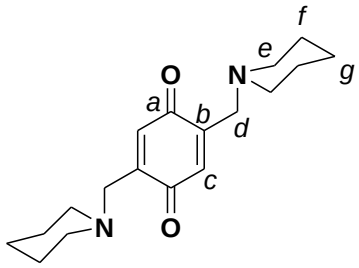

1,4-hydroquinone (50 mg, 0.16 mmol) was dissolved in toluene (50 mL). This solution was purged with argon and $Pd(OAc)_4$ (88 mg, 0.19 mmol) was added. This was stirred for 30 min and then filtered. Solvent was removed from the filtrate under reduced pressure to give 43 mg (87%) of the target compound as a pale light yellow powder. ^{1}H NMR ($CDCl_3$): δ 6.78 (t, 2H*c*, *J* = 1.9 Hz), 3.30 (d, 4H*d*, *J* = 2.0 Hz), 2.41 (t, 8H*e*, *J* = 5.0 Hz), 1.58 (p, 8H*f*, *J* = 5.5 Hz), 1.46 (m, 4H*g*) ppm. ^{13}C NMR ($CDCl_3$): δ 188.5 (*a*), 145.5 (*b*), 133.2 (*c*), 55.5 (*d*), 54.9 (*e*), 26.0 (*f*), 24.1 (*g*) ppm.

FT-IR (nujol mull): 1652 (s, C=O) cm^{-1}. UV-Vis (CH_3CN): λ_{max} 264 nm (ε = 19000 $L \bullet mol^{-1} \bullet cm^{-1}$) 305 nm ($\varepsilon$ = 1600 $L \bullet mol^{-1} \bullet cm^{-1}$), 362 nm ($\varepsilon$ = 1000 $L \bullet mol^{-1} \bullet cm^{-1}$). This quinone species was not stable enough to be sent for elemental analysis. Therefore high resolution electrospray ionization mass spectrometry was used to confirm the identity of this compound. HR-MS calcd for $C_{18}H_{26}N_2O_2$ (M+) 303.2072, found 303.2072.

2,5-Bis(4-*tert*-butyl-2-pyridinium)-1,4-benzoquinone bis(tetrafluoroborate) (2.37).

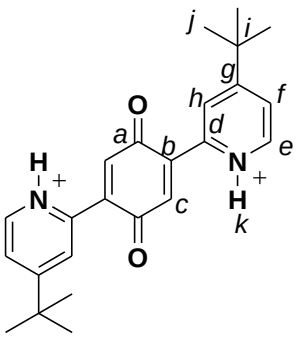

2,5-Bis(4-*tert*-butyl-pyrid-2-yl)-1,4-hydroquinone (60 mg, 0.16 mmol) was dissolved in acetonitrile (50 mL). This solution was purged with Ar and then $NOBF_4$ (40 mg, 0.34 mmol) was added. The reaction mixture was stirred for 1 hour and then solvent was reduced to ~5 mL under reduced pressure. Diethyl ether (50mL) was then added resulting in a light yellow precipitate that was recovered by filtration yielding 82 mg (94%) of the target salt. ^1H NMR (CD_3CN): δ 13.34 (s, 2H*k*) 8.78 (d, 2H*e*, *J* = 6.3Hz), 8.31 (d, 2H*h*, *J* = 1.7Hz), 8.16 (dd, 2H*f*, *J* = 6.5, 2.0 Hz), 7.69 (s, 2H*c*), 1.46 (s, 18H*j*) ppm. ^{13}C NMR (CD_3CN): δ 185.1 (*a*), 174.7 (*b*), 144.1 (*g*), 142.7 (*d*), 138.7 (*e*), 136.5 (*c*), 126.8 (*f*), 126.5 (*h*), 38.0 (*i*), 29.9 (*j*) ppm. FT-IR (nujol mull): 3286 (w, N-H), 3179 (w, N-H), 1664 (s, C=O) cm^{-1}. FT-IR (CH_3CN solution): 3253 (w, N-H), 1672 (s, C=O) cm^{-1}. UV-Vis (CH_3CN): λ_{max} 288 (ε = 16000 $M^{-1} \bullet cm^{-1}$), 368 (shoulder, ε = 1200 $M^{-1} \bullet cm^{-1}$) nm. Anal. Calcld for $C_{24}H_{28}B_2F_8N_2O_2$: C, 52.40; H, 5.13; N, 5.09. Found: C, 52.14; H, 5.08; N, 4.78.

2,5-Bis-(4-dimethylamino-2-pyridinium)-1,4-benzoquinone bis(tetrafluoroborate) (2.38).

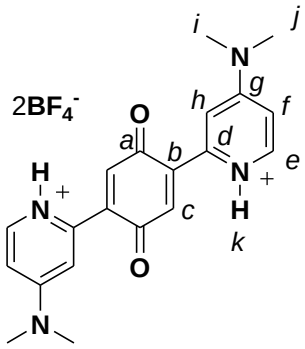

2,5-Bis-(4-dimethylamino-pyrid-2-yl)-1,4-hydroquinone (20 mg, 0.057 mmol) was dissolved in acetonitrile (50 mL). This solution was purged with argon and then $NOBF_4$ (13 mg, 0.14 mmol) was added. The reaction mixture was stirred for 15 minutes and then solvent was reduced to ~10 mL under reduced pressure. Diethyl ether (50 mL) was then added resulting in an orange precipitate that was recovered by filtration yielding 25 mg (83%) of the target salt. ^{1}H NMR (CD_3CN): δ 11.31 (s, 2H*k*), 8.11 (dd, 2H*e*, *J* = 7.5, 3.5 Hz), 7.46 (s, 2H*c*), 7.12 (d, 2H*h*, *J* = 2.9 Hz) 6.93 (dd, 2H*f*, *J* = 7.4, 2.9 Hz), 3.26 (s, 6H*i*), 3.24 (s, 6H*j*), ppm. ^{13}C NMR (CD_3CN): δ 185.4 (*a*), 158.5 (*b*), 142.5 (*g*), 140.0 (*d*), 139.9 (*e*), 137.8 (*c*), 109.3 (*h*), 108.0 (*f*), 41.0 (*i*), 40.9 (*j*) ppm. FT-IR (nujol mull): 3269 (w, N-H), 1661 (s, C=O) cm^{-1}. FT-IR (CH_3CN solution): 3279 (w, N-H), 1669 (s, C=O) cm^{-1}. UV-Vis (CH_3CN): λ_{max} 233 (ε = 43000 M^{-1}•cm^{-1}), 283 (ε = 53000 M^{-1}•cm^{-1}), 361 (shoulder, ε = 7300 M^{-1}•cm^{-1}) nm. Anal. Calcld for $C_{20}H_{22}B_2F_8N_4O_2$: C, 45.84; H, 4.23; N, 10.69. Found: C, 45.47; H, 4.20; N, 10.52.

2,5-Bis(1-methylpiperidinium)-1,4-hydroquinone bis(tetrafluoroborate) (2.39).

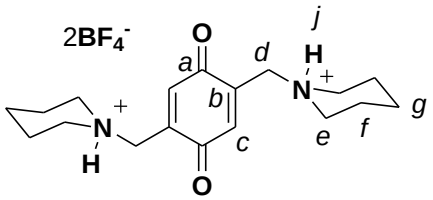

2,5-Bis(piperidin-1-ylmethyl)-1,4-hydroquinone (55 mg, 0.18 mmol) was dissolved in acetonitrile (50 mL). This solution was purged with argon and then $NOBF_4$ (50 mg, 0.43 mmol) was added. The reaction mixture was stirred for 1 hour and

then solvent was reduced to ~5 mL under reduced pressure. Diethyl ether (50 mL) was then added resulting in a light yellow precipitate that was recovered by filtration yielding 83 mg (96%) of the target salt. ^{1}H NMR (CD_3CN): δ 7.12 (s, 2H*c*) 6.89 (br. s, 2H*j*), 4.07 (d, 4H*d*, *J* = 4.6Hz), 3.49 (d, 4H$e_{(ax)}$, *J* = 11.8 Hz), 2.98 (q, 4H$e_{(eq)}$, *J* = 11.3 Hz), 1.90-1.70 (m, 10H*f*, $g_{(ax)}$), 1.49 (m, 2H$g_{(eq)}$) ppm. ^{13}C NMR (CD_3CN): δ 186.7 (*a*), 140.5 (*b*), 138.1 (*c*), 55.4 (*d*), 54.4 (*e*), 23.6 (*f*), 21.8 (*g*) ppm. FT-IR (nujol mull): 3155 (w, N-H), 1663 (s, C=O) cm^{-1}. FT-IR (CH_3CN solution): 3093 (w, N-H), 1666 (s, C=O) cm^{-1}. UV-Vis (CH_3CN): λ_{max} 249 (ε = 17000 M^{-1}•cm^{-1}), 308 (ε = 1100 M^{-1}•cm^{-1}) nm. Anal. Calcld for $C_{18}H_{28}B_2F_8N_2O_2$: C, 45.23; H, 5.90; N, 5.86. Found: C, 45.26; H, 5.74; N, 5.88.

2,5-Bis(4-methyl-morpholin-4-ium)-1,4-benzoquinone bis(tetrafluoroborate) (2.40).

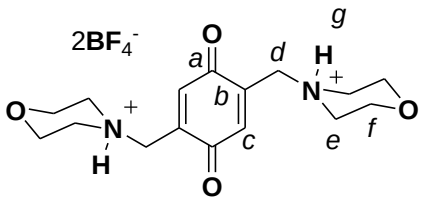

2,5-Bis(morpholin-4-ylmethyl)-1,4-hydroquinone (60 mg, 0.23 mmol) was dissolved in acetonitrile (50 mL). This solution was purged with argon and then $NOBF_4$ (60 mg, 0.51 mmol) was added. The reaction mixture was stirred for 15 minutes and then solvent was reduced to ~10 mL under reduced pressure. Diethyl ether (50 mL) was then added resulting in a light yellow precipitate that was recovered by filtration yielding 99 mg (91%) of the target salt. ^{1}H NMR (CD_3CN): δ 7.37 (br. s, 2H), 7.16 (s, 2H), 4.16 (d, 4H, *J* = 5.4 Hz) 4.02 (d, 4H, *J* = 13.1 Hz), 3.77 (t, 4H, *J* = 13.5 Hz), 3.47 (d, 4H, *J* = 12.6 Hz), 3.19 (q, 4H, 13.0 Hz) ppm. ^{13}C NMR (CD_3CN): δ 186.3, 140.7, 137.4, 64.3, 54.6, 53.9 ppm. FT-IR (nujol mull): 3156 (w, N-H), 1654 (s, C=O) cm^{-1}. FT-IR (CH_3CN solution): 3153 (w, N-H), 3150-3000 (br. w, N-H), 1665 (s, C=O) cm^{-1}. UV-Vis

(CH_3CN): λ_{max} 248 (ε = 22000 M^{-1}•cm^{-1}), 295 (shoulder, ε = 600 M^{-1}•cm^{-1}). Anal. Calcld for $C_{16}H_{24}B_2F_8N_2O_4$: C, 39.87; H, 5.02; N, 5.81. Found: C, 39.60; H, 5.06; N, 5.79.

2,5-Bis(1,1'-dimethyl-piperidinium)-1,4-benzoquinone bis(triflate) (2.43).

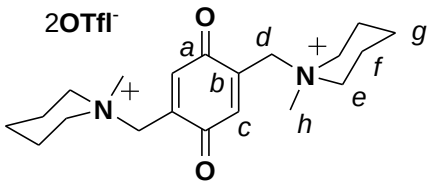

2,5-Bis(1-piperidinylmethyl)-1,4-benzoquinone (50 mg, 0.16 mmol) was dissolved in acetonitrile (50 mL). This solution was purged with argon and then an excess of methyl triflate (85 mg, 0.52 mmol) was added under an argon atmosphere. The reaction mixture was stirred for 10 minutes and then solvent was reduced to ~5mL under reduced pressure. Diethyl ether (50mL) was then added resulting in a light yellow precipitate recovered by filtration under argon yielding 82 mg (78%) of the methylated piperdinium salt. ^{1}H NMR (CD_3CN): δ 7.22 (s, 2H*c*), 4.27 (s, 4H*d*), 3.34 (t, 8H*e*, *J* = 5.6 Hz) 2.99 (s, 6H*h*), 1.91-1.53 (m, 12H*f*, *g*) ppm. ^{13}C NMR (CD_3CN): δ 186.0 (*a*), 144.1 (*b*), 136.3 (*c*), 62.9 (*e*), 60.8 (*d*), 48.0 (*j*), 21.3 (*f*), 20.6 (*g*) ppm. FT-IR (nujol mull): 1662 (s, C=O) cm^{-1}. FT-IR (CH_3CN solution): 1669 (s, C=O) cm^{-1}. Anal. Calcld for $C_{22}H_{32}F_6N_2O_8S_2$: C, 41.90; H, 5.11; N, 4.44. Found: C, 41.46; H, 4.92; N, 4.40. HR-MS calcd for $C_{21}H_{32}F_3N_2O_5S$ (M+) 481.1984, found 481.1984.

4,6-Bis(pyrid-2-yl)-resorcinol (2.48). In anhydrous toluene (100 mL) 4,6-bis(pyrid-2-yl)-1,3-dimethoxy-benzene (320 mg, 1.1 mmol) was dissolved. Under an argon atmosphere $AlCl_3$ (1.45 g, 11 mmol) was added and then the slurry was refluxed for 4 hours turning dark red. After cooling the reaction the excess $AlCl_3$ was consumed by adding water and then this was extracted with dichloromethane (3*30 mL).

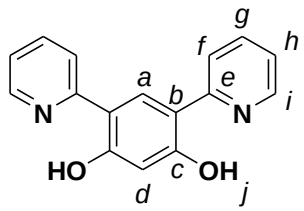

The organic layers were combined, dried over $MgSO_4$ and filtered. Solvent was removed under reduced pressure. Column chromatography of the crude material on silica gel using chloroform with up to 1% methanol as the eluent yielded pure compound as a yellow powder with a yield of 240 mg (75%) Single crystals suitable for X-Ray analysis were obtained by recrystallization from toluene. ^{1}H NMR ($CDCl_3$): δ 14.81 (s, 2H*j*), 8.44 (ddd, 2H*i*, *J* = 5.0, 1.8, 0.9 Hz), 8.24 (s, 1H*a*), 7.91-7.75 (m, 4H*f*, *g*), 7.19 (ddd, 2H*h*, *J* = 7.1, 5.1, 1.3 Hz), 6.62 (s, 1H*d*), ^{13}C NMR ($CDCl_3$): δ 163.5 (*c*), 157.8 (*e*), 145.7 (*i*), 137.7 (*c*), 124.5 (*a*), 120.6 (*f*), 118.0 (*h*), 111.6 (*b*), 106.1 (*d*) ppm. FT-IR (CH_3CN solution): 3950-2400 (br. w, O-H) cm^{-1}. Calcld for $C_{16}H_{12}N_2O_2$: C, 72.72; H, 4.58; N, 10.60. Found: C, 72.81; H, 4.39; N, 10.56**.**

4,6-Bis(pyrid-2-yl)-1,3-dimethoxybenzene (2.50). In anhydrous toluene (150 mL), 4,6-dibromo-1,3-dimethoxybenzene (0.72 g, 2.4mmol) and 2-tributylstannanyl-pyridine (1.8 g, 4.9 mmol) was dissolved. This solution was thoroughly deaerated by bubbling argon gas through it. To this solution was added (tetrakistriphenylphosphine)palladium (250 mg, 0.22 mmol) under an argon atmosphere and then refluxed for 40 hours turning a dark brown. Solvent was removed and the crude product was purified by flash chromatography on silica using a hexanes/ethyl acetate gradient from (1:20) up to (1:1). The purified product obtained was a yellow powder with a total yield of 0.297 g (42% yield). ^{1}H NMR ($CDCl_3$): δ 8.66 (ddd, 2H*i*, *J* = 4.8, 1.8, 1.0 Hz), 8.23 (s, 1H*a*), 7.78 (ddd, 2H*f*, *J* = 8.0, 1.1, 1.1 Hz), 7.65 (ddd, 2H*g*, *J* = 7.9, 7.9, 1.9 Hz), 7.14 (ddd, 2H*h*, *J* = 7.4, 4.9, 1.2 Hz), 6.63 (s, 1H*d*) 3.92 (s, 6H*j*) ppm. ^{13}C

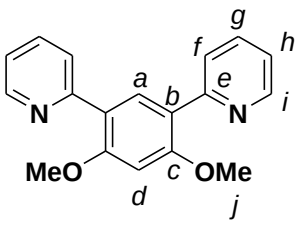

NMR ($CDCl_3$): δ 158.4 (*c*), 155.8 (*e*), 149.3 (*i*), 135.5 (*g*), 134.0 (*a*), 124.6 (*f*), 122.2 (*b*), 121.1 (*h*), 95.6 (*d*), 55.8 (*j*) ppm. Calcld for $C_{18}H_{16}N_2O_2$: C, 73.95; H, 5.52; N, 9.58. Found: C, 73.49; H, 5.45; N, 9.37**.**

4,6-Bis(pyrid-2-yl)-2-phenyl-resorcinol (2.52). 3,5-Bis(pyrid-2-yl)-2,6-dimethoxybiphenyl (520 mg, 1.4 mmol) was dissolved in anhydrous toluene (60 mL). Under an argon atmosphere $AlCl_3$ (1.9 g, 14 mmol) was added and then the slurry was refluxed for 4 hours turning dark red. After cooling the reaction mixture was quenched by carefully adding water and then extracted with dichloromethane. The organic layer was separated, dried over $MgSO_4$ and filtered. Solvent was removed under reduced pressure. Column chromatography of the crude material on silica gel using chloroform with up to 1% methanol as the eluent yielded 360 mg (76%) of the target compound as a golden yellow powder. Single crystals were obtained by recrystallization from toluene. ^{1}H NMR ($CDCl_3$): δ 15.36 (s, 2H*n*), 8.38 (ddd, 2H*i*, *J* = 5.0, 1.8, 0.9 Hz), 8.31 (s, 1H*a*), 7.88 (d, 2H*f*, *J* = 8.5 Hz), 7.83 (ddd, 2H*g*, *J* = 7.4, 7.4, 1.9 Hz), 7.54-7.45 (m, 4H*k*, *l*), 7.37-7.31 (m, 1H*m*), 7.21 (ddd, 2H*h*, *J* = 7.3, 5.0, 1.1 Hz) ppm. ^{13}C NMR ($CDCl_3$): δ 160.8 (*c*), 157.9 (*e*), 145.3 (*i*), 137.7 (*g*), 134.3 (*j*), 130.8 (*l*), 128.0 (*k*), 126.9 (*m*), 123.6 (*a*), 120.6 (*f*), 118.9 (*b*), 118.2 (*h*), 111.1 (*d*) ppm. FT-IR (CH_3CN solution): 3000-2400 (br. w, O-H) cm^{-1}. Calcld for $C_{22}H_{16}N_2O_2$: C, 77.63; H, 4.74; N, 8.23. Found: C, 77.50; H, 4.75; N, 8.23**.**

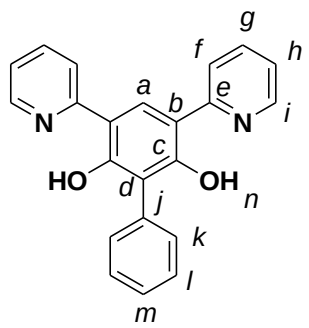

3,5-Dibromo-2,6-dimethoxybiphenyl (2.55). 2,6-Dimethoxybiphenyl (2.0 g, 9.3 mmol) was dissolved in dichloromethane (30mL),. An excess of Br_2 (1 mL, 19.4 mmol) was then added dropwise. This mixture was then allowed to stir at room temperature overnight allowing the solvent and excess Br_2 to evaporate leaving an orange crystalline solid. This was purified by column chromatography on silica gel using hexanes/diethyl ether (1:1) as the eluent to give 3.37 g (97% yield) of a white solid. ^{1}H NMR ($CDCl_3$): δ 7.76 (s, 1H*a*), 7.45-7.36 (m, 5H*f*-*h*), 3.37 (s, 6H*i*) ppm. ^{13}C NMR ($CDCl_3$): δ 154.9 (*c*), 134.9 (*e*), 132.7 (*a*), 132.3 (*d*), 130.1 (*g*), 128.1 (*f*), 127.9 (*h*), 113.1 (*b*), 60.5 (*i*) ppm. Calcld for $C_{14}H_{12}Br_2O_2$: C, 45.20; H, 3.25. Found: C, 45.31; H, 3.30**.**

3,5-Bis(pyrid-2-yl)-2,6-dimethoxybiphenyl (2.56). (125 mL) 3,5-Dibromo-2,6-dimethoxybiphenyl (1.5 g, 4.4 mmol) and 2-tributylstannanyl-pyridine (3.25 g, 8.8 mmol) was dissolved in anhydrous toluene. This solution was thoroughly deaerated by bubbling argon gas through it. The catalyst, (tetrakistriphenylphosphine)palladium (508 mg, 0.44 mmol), was then added under an argon atmosphere. The yellow solution was refluxed for 40 hours turning a dark brown. Solvent was removed and the crude product was purified by flash chromatography on silica gel using a hexanes/ethyl acetate gradient from (1:20) up to (1:1). The purified product was obtained as a light yellow powder with a final yield of 0.637 g (39% yield). ^{1}H NMR ($CDCl_3$): δ 8.70 (ddd, 2H*i*, *J* = 4.8, 1.8, 0.9 Hz), 8.14 (s,

1H*a*), 7.88 (ddd, 2H*f*, *J* = 8.0, 1.0, 1.0 Hz), 7.71 (ddd, 2H*g*, *J* = 7.7, 7.7 1.9 Hz), 7.48-7.34 (m, 5H*k*-*m*), 7.21 (ddd, 2H*h*, *J* = 7.4, 4.8, 1.2 Hz), 3.19 (s, 6H*n*) ppm. ^{13}C NMR ($CDCl_3$): δ 156.7 (*c*), 156.1 (*e*), 149.5 (*i*), 135.9 (*f*), 134.2 (*g*), 132.9 (*j*), 130.6 (*l*), 130.3 (*a*), 127.9 (*k*), 127.7 (*m*), 127.2 (*h*), 124.5 (*b*), 121.8 (*d*), 60.9 (*n*) ppm. Calcld for $C_{24}H_{20}N_2O_2$: C, 78.24; H, 5.47; N, 7.60. Found: C, 78.51; H, 5.29; N, 7.62**.**

Chapter 3 Dinuclear Palladium Complexes of *p*-Hydroquinones

3.1 Introduction

As outlined in Chapter 1, one approach to designing molecular magnets is to assemble paramagnetic metal ions and organic bridging radical ligands. The derivatized *para*-hydroquinones presented in the previous chapter were targeted with this goal in mind. When the semiquinone radical anion is complexed to a paramagnetic metal species, strong spin coupling is expected as is observed for some of the *ortho*-semiquinone and tetraoxolene complexes introduced in Chapter 1. In addition, the rich redox chemistry or non-innocence of the hydroquinone ligand is preserved upon coordination such that the semiquinone redox state can be accessed. However, due to the hydroquinone ligand being non-innocent, the formal redox state of the ligand can be ambiguous especially when complexed to a redox-active metal. Consequently the charge distribution of *p*-hydroquinone complexes is also of interest. The charge distribution is particularly important to designing molecular magnets with *p*-hydroquinone since the semiquinone redox state is desired. However, accessing the semiquinone redox state can be complicated in the presence of redox-active metal ions and accordingly being able to identify the ligand when it is in the semiquinone redox state is of importance.

Despite the *p*-hydroquinone ligand's potential as a building block for molecular magnets, or as a redox-active ligand with the potential to make bistable complexes, the coordination chemistry of *p*-hydroquinones remains relatively undeveloped. Most of the work in this area has focused on complexes of tetraoxolene and chloranilate ligands as discussed in Chapter 1. Keramidas and coworkers first reported the reaction of a *p*-

hydroquinone derivative with a source of vanadium to give two new metal complexes, that of V^{V} with a *p*-hydroquinonate and V^{IV} with *p*-semiquinonate bridging ligand.[72] In addition to his work with the chloranilate dianion ligand, Miller has also examined the coordination of simple quinones, including 1,4-benzoquinone (**1.2**), with vanadium.[73] By reacting hexacarbonylvanadium(0) with **1.2** (Scheme 3.1), an amorphous powder was obtained that was found to contain V^{II} ions bound to semiquinone radical ions based partly on elemental analysis and IR spectroscopy. In this reaction it was proposed that the quinone first complexes with vanadium resulting in the release of CO followed by electron transfer where the vanadium is oxidized by two electrons and two of the quinones are reduced to give semiquinone radical anions. It was found that the V^{II} (S = 3/2) couples antiferromagnetically with the semiquinone radicals (S = 1/2) but do not magnetically order above 5 K. The products geometry was unknown but the vanadium is most likely tetrahedral as shown for **3.2** or octahedral.

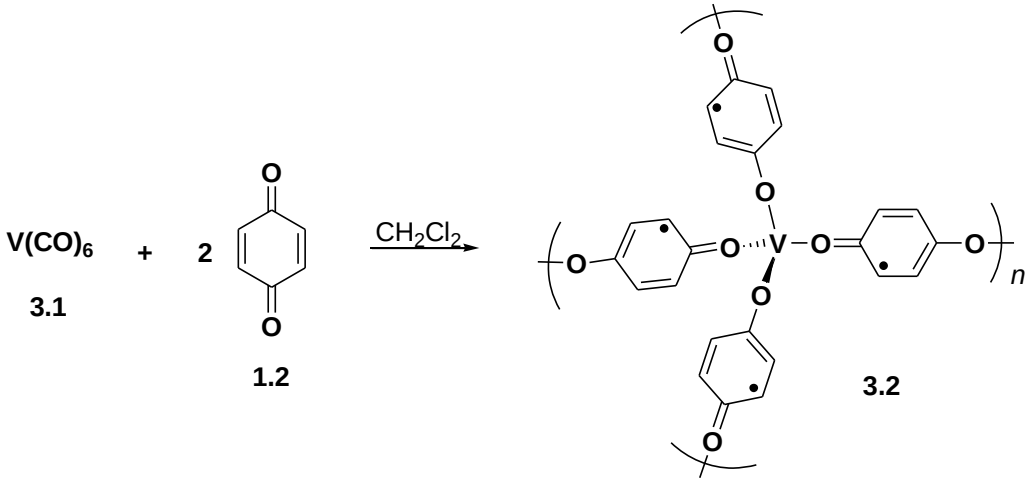

Scheme 3.1. Synthesis of **3.2** from benzoquinone.

Ruthenium complexes of 2,5-bis(pyrazol-1-yl)-1,4-hydroquinone (**2.1**) have been investigated by Vos *et al.* By first deprotonating **2.1** and then adding a ruthenium

bipyridine complex (**3.3**) the mononuclear ruthenium complex **3.4** was synthesized as depicted in Scheme 3.2.[136] The resonance-Raman spectrum of **3.4** provided evidence of a low energy charge transfer from the hydroquinone to the bipyridine moieties. The two-electron oxidized product was described as being a Ru^{II}-quinone complex and the absorption spectrum possessed bands far into the visible region with the presence of metal to ligand charge transfer bands assigned to be due to a Ru^{II} to quinone charge transfer.

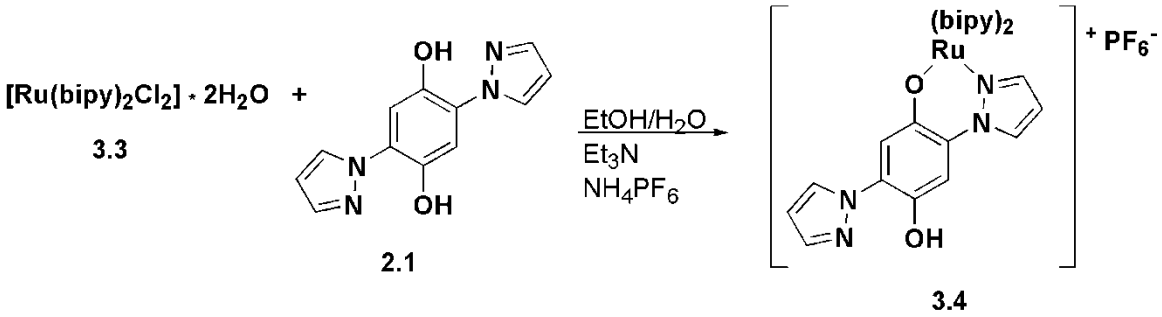

Scheme 3.2. Synthesis of the mononuclear ruthenium complex **3.4**.

Dinuclear ruthenium and osmium complexes of **2.1** were subsequently reported and were prepared in a similar manner as depicted in Scheme 3.2.[137] These two dinuclear complexes, **3.5** and **3.6**, posses four reversible one-electron oxidation processes in which the first two oxidation**s** were assigned to the hydroquinone. The mixed valence $M^{II}M^{III}$ complexes of the quinone were also observed electrochemically with little metal-metal communication across the bridging quinone. Each oxidation state of the complex was characterized by UV-vis spectroelectrochemistry with the greatest degree of metal-ligand orbital mixing occurring when the ligand was in the hydroquinonate redox state and least metal-ligand communication occurring for the bridging ligand in the quinone redox state. In addition ruthenium provided better metal-ligand orbital mixing than osmium. This

work showed how the different oxidation states of the ligand and metals, in addition to the identity of the metal, can allow for the control of the amount of communication between the metal and bridging ligands.

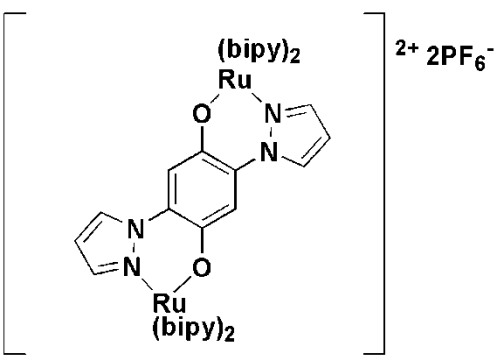

3.5

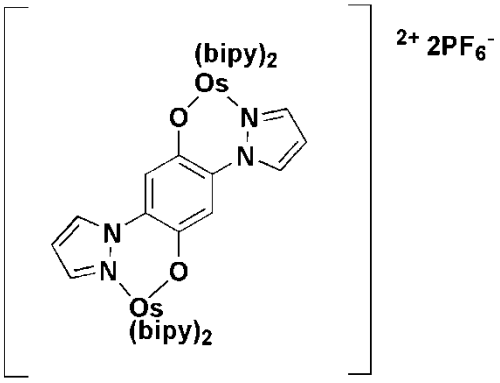

3.6

In related work, Keyes and Leane used **3.7** to make mononuclear complexes as depicted in Scheme 3.3.[74] The mononuclear complexes **3.8** and **3.10** were shown to be redox-active, with the ligand being oxidized more easily than the metal. The optical properties of the neutral and oxidized species were also examined and shown to differ such that the absorption wavelengths can be controlled by altering the redox state. The semiquinone complexes of **3.8** and **3.10** were generated by oxidation electrochemically and were very stable to disproportionation with the osmium complex being the most stable. Metal and ligand orbital mixing along with the π-accepting ability of the metal are thought to be the key factors with respect to the stability of the osmium complex.

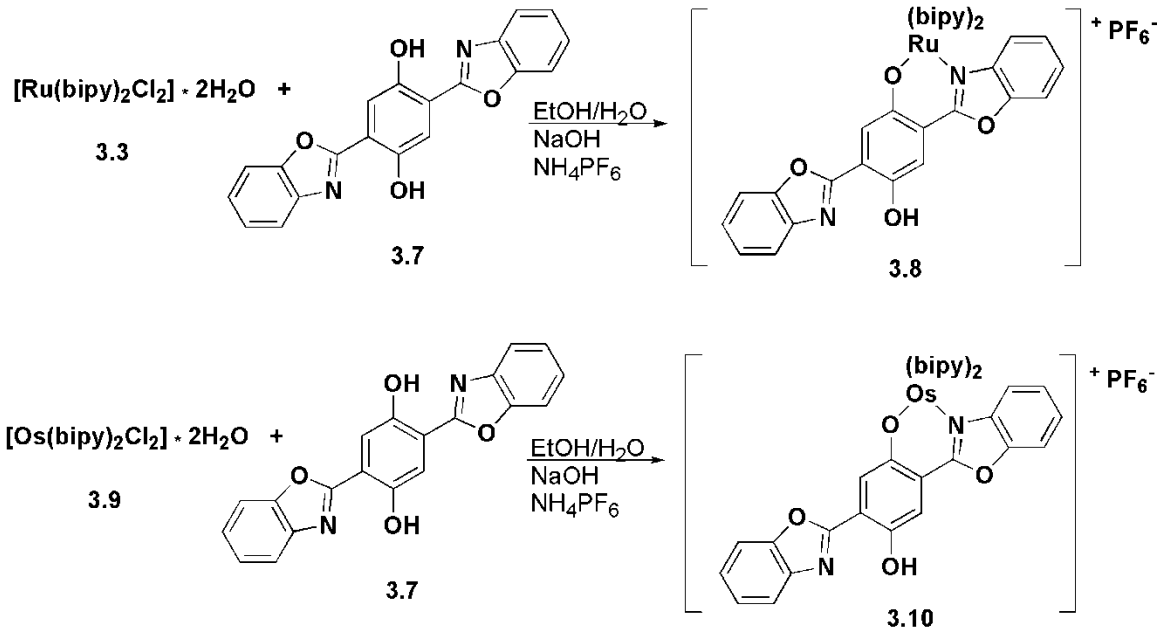

Scheme 3.3. Synthesis of mononuclear complexes **3.8** and **3.10**.

Wagner *et al*. also used the strategy of deprotonating **2.1** and complexing the resulting hydroquinonate dianion with copper (II) to give the polymeric complex **1.39 (**Scheme 3.4). The structure of **1.39** consists of Cu^{II} ions coordinated in a square planar geometry bridged by **2.1**. Due to the poor solubility of **1.39** the redox chemistry was not explored. Neighbouring Cu sites in **1.39** coupled antiferromagnetically across the bridging ligand.[75]

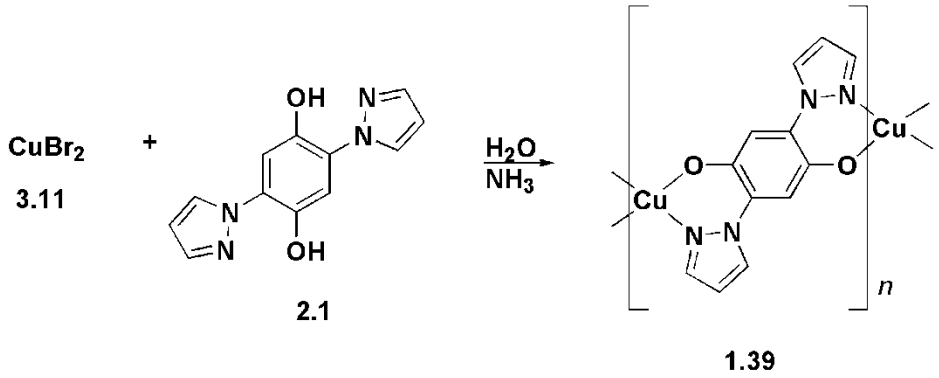

Scheme 3.4. Synthesis of copper-hydroquinone polymer **1.39**.

Bimetallic model copper complexes such as **3.13** were prepared as shown in Scheme 3.5.[76] The dinuclear complex presented some synthetic challenges since using typical bases for deprotonation resulted in polymeric material similar to **1.39**. This was thought to be due to the insoluble nature of the polymeric material. By using thallium ethoxide as the base, reasonable yields of the dinuclear complex **3.13** were obtained. This synthesis of the dinuclear copper complex highlights one of the major challenges with respect to the use of bidentate hydroquinonate dianions as bridging ligands, in that the ligand can readily displace other ligands favouring the formation of polymeric complexes.

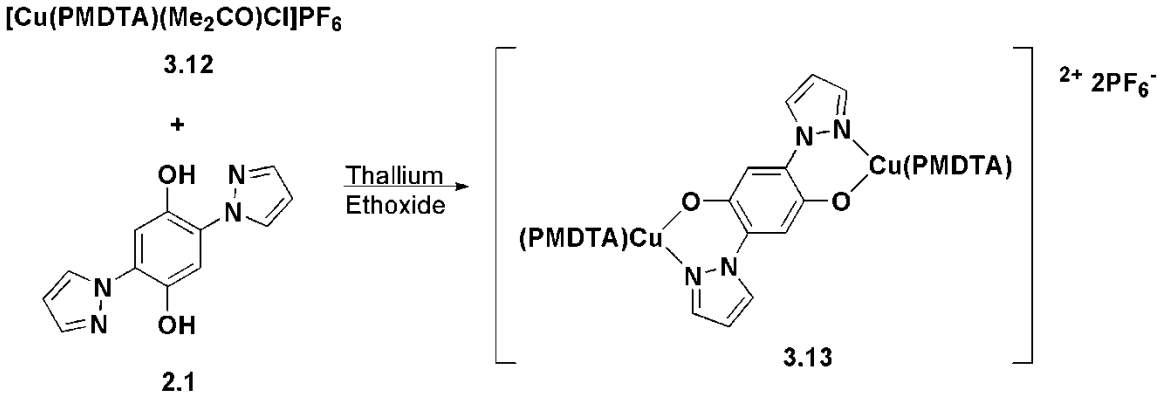

Scheme 3.5. Synthesis of dinuclear copper complex **3.13** (PMDTA = *N,N,N',N'',N''*-pentamethyldiethylenetriamine).

The complexes previously discussed represent the few examples where a *p*-hydroquinone has been used as a bridging ligand between metals. Discrete bimetallic complexes of *p*-hydroquinones allow for the study of how the coordination of metals perturbs the redox chemistry of the hydroquinone ligand as well as probing the metals electronic communication across the conjugated bridge. If the semiquinone redox state is

accessed, spectroscopic methods such as EPR and UV-vis provide valuable information with respect to the electronic structure of the complexes.

To this end, bimetallic complexes of 2,5-bis(pyrazol-1-yl)-1,4-hydroquinone (**2.1**) were initially pursued. To simplify the study of ligand based electron transfer processes in these complexes, redox inactive metals bridged by **2.1** were targeted. The characterization of these complexes will provide the basis for future studies on complex paramagnetic metal systems. Bimetallic palladium(II) complexes of **2.1** were targeted because Pd(II) is not easily oxidized or reduced. The synthesis and characterization of these dinuclear complexes should facilitate a better understanding of how multiple metals perturb the redox chemistry of the hydroquinone ligand in addition to providing the framework for synthesizing and identifying complexes of paramagnetic and redox-active metals such as copper, nickel, cobalt or manganese.

There are many examples of simple Pd (II) complexes that could be potential starting materials for bimetallic hydroquinone complexes. The palladium complex of acetylacetonate (acac) is easy to synthesize to give $Pd(acac)_2$ as shown in Scheme 3.6.[138] Similar to the acac ligand is 1,1,1,5,5,5-hexafluoroacetylacetonate (hfac) which can also be used to synthesize $Pd(hfac)_2$.[139] Relative to acac, the hfac ligand is strongly electron withdrawing causing the metal to be more electron deficient. These palladium complexes were used to synthesize two new bimetallic complexes of **2.1** where the effects of varying the Lewis acidity of the palladium ions could be probed. The electrochemistry and characterization data of these complexes are presented. These two complexes were also oxidized and the *in situ* characterization data of these semiquinone based ligands are shown later in this chapter with comparisons to the uncomplexed **2.1** semiquinone radical

also synthesized and characterized *in situ*. Other hydroquinones, **2.2**, **2.15** and **2.27** presented in Chapter 2 were also reacted with $Pd(hfac)_2$ and the characterization data of the resulting complexes is discussed with comparisons to the palladium complexes of **2.1**.

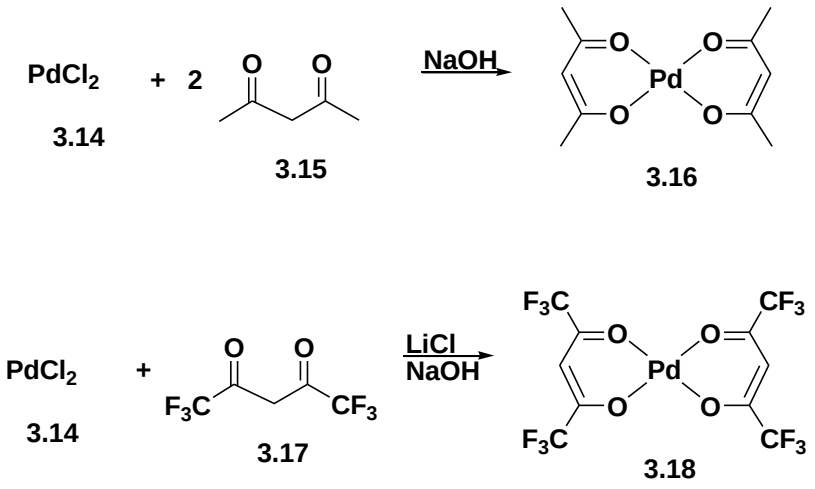

Scheme 3.6. Synthesis of palladium starting materials, **3.16** and **3.18**.

3.2 Synthesis and Characterization of Palladium Complexes

3.2.1 Synthesis and Characterization

The reaction of 2,5-bis(pyrazol-1-yl)-1,4-hydroquinone (**2.1**) with $Pd(acac)_2$ (**3.16)** and $Pd(hfac)_2$ (**3.18**) gave two new dinuclear palladium complexes **3.19** and **3.20** respectively (Scheme 3.7).

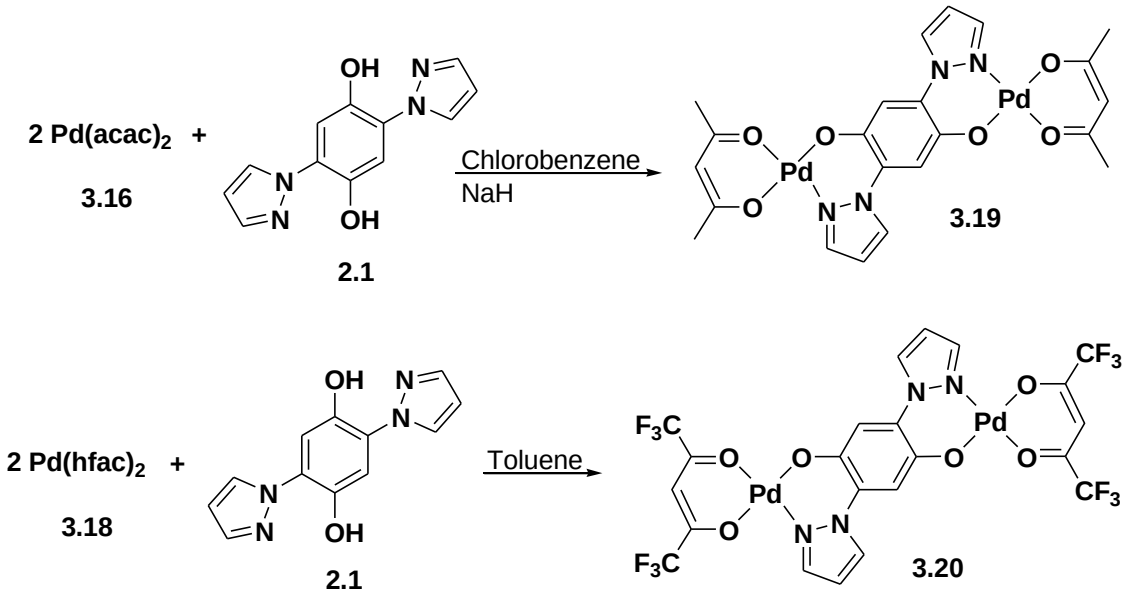

Scheme 3.7. Synthesis of dinuclear palladium complexes, **3.19** and **3.20**.

The reaction of **2.1** with **3.16** required the use of a base. It appears this reaction also produced oligomeric or polymeric palladium complexes (**3.21**) as an insoluble red precipitate. By adding a solution of deprotonated **2.1** dropwise to an excess of the $Pd(acac)_2$ this insoluble by-product could be minimized. The reaction of **2.1** with $Pd(hfac)_2$ does not require base and no insoluble by-product was observed. The purification of **3.19** proved to be more difficult than for **3.20** because **3.19** is less soluble and the use of coordinating solvents in the synthesis or purification of **3.19** resulted in by-products.

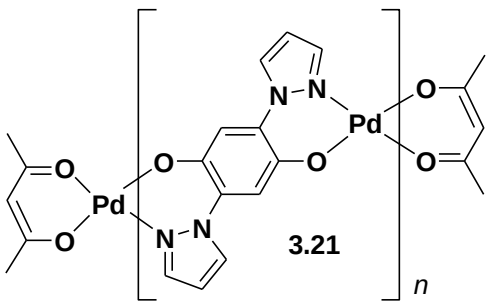

The reaction of **2.2** with $Pd(acac)_2$ also resulted in a dinuclear species **3.22** in addition to an insoluble product thought to be composed of oligomeric palladium complexes of **2.2**. Purification of **3.22** also proved to be difficult for the same reasons as **3.19** and no analytically pure compound was isolated. For this reason, other metal complexes of hydroquinone ligands were limited to reactions with $Pd(hfac)_2$ in a similar manner as that described for **3.20** in Scheme 3.7 to give complexes **3.23**, **3.24** and **3.25**.

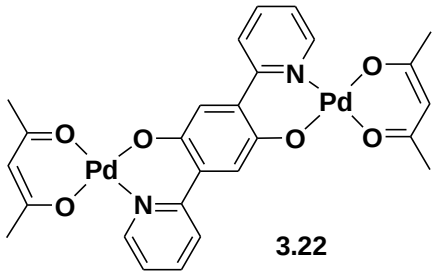

3.22

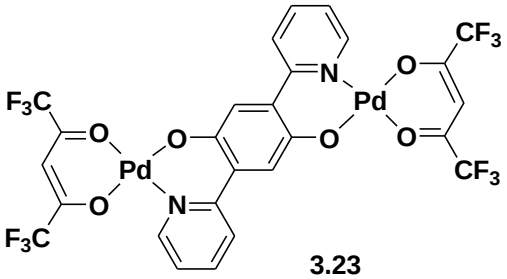

3.23

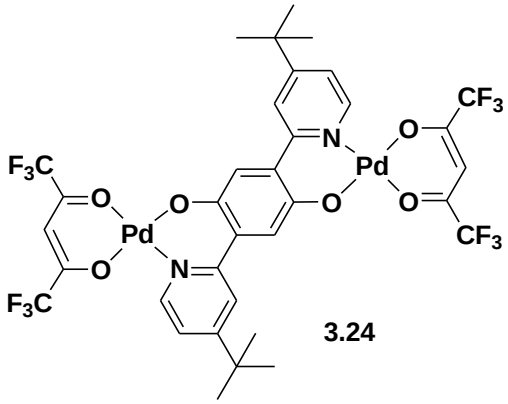

3.24

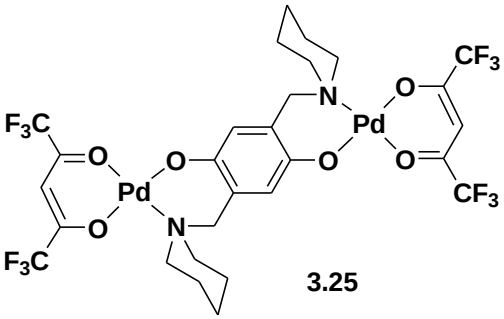

3.25

The characterization data for each of the dinuclear palladium(II) complexes is consistent with their proposed structures. In the case of **3.19**, the ^{1}H-NMR spectrum possesses a singlet at 5.41 ppm and two singlets at 2.10 and 2.01 ppm which is consistent with other palladium acetylacetonate complexes in which the acetylacetonate ligand is not symmetrical. All palladium hexafluoroacetylacetonate complexes, **3.20** and **3.23-**

3.25, have singlets at ~6.2 ppm in their ^{1}H-NMR spectra as well as two singlets at approximately -74 ppm in their ^{19}F-NMR spectra. The fluorines also couple to the adjacent carbons resulting in two quartets at ~116 ppm in the ^{13}C-NMR spectra with typical *J* values of ~284 Hz. Fluorine coupling is also seen for the CO carbons of the hfac ligand resulting in quartets at ~175 ppm with ^{2}J values of ~36Hz in their ^{13}C-NMR spectra, consistent with previously published copper complexes of hfac.[140]

The absorption spectra of the palladium hfac complexes, **3.20** and **3.23-3.25**, all have weak absorptions above 560 nm and as a result appear as different shades of purple in solution and the solid state. For example, **3.20** has a weak absorbance with a maxima at 522 nm that extends up to 680 nm and appears as a purple compound. In contrast, the palladium acac complex **3.19** has no absorbances over 500 nm and appears orange in solution and the solid state. This compound also had the strongest molar absorptivities although the reason for this is unknown. The non-conjugating bridged complex, **3.25**, has the weakest absorptions most likely due to it being less conjugated than the other complexes studied.

3.2.2 Crystal Structures

Complexes **3.19** and **3.20** suffer from poor solubility, hampering crystallization attempts. However, palladium hfac derivatives **3.23** and **3.24** crystallized from solutions of toluene resulting in X-ray quality crystals. The structure of **3.23** is shown in Figure 3.1. The palladium ions are in distorted square planar geometries with bond angles at Pd deviating slightly from 90^{o} and the carbon-oxygen bond lengths of the hydroquinone moiety are typical for a CO single bond (Table 3.1). The pyridine rings are twisted in

opposite directions with respect to the central hydroquinone such that the nitrogens point above the plane of ring for N2 and below for N1 resulting in a "step" type structure overall. The pyridine ring containing N1 is twisted by 32.78° and the pyridine ring containing N2 is twisted by 26.68° with respect to the central ring. The planes containing the palladium ions are twisted further from the plane of the central ring by 53.27° for the plane containing Pd1 and by 41.71° for the plane containing Pd2.

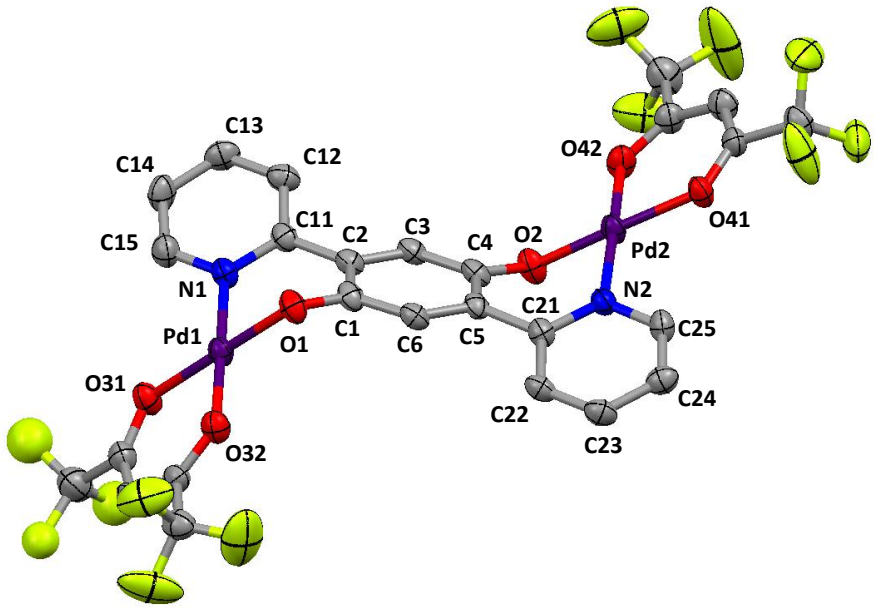

Figure 3.1 Molecular structure of **3.23** with thermal ellipsoids shown at 50% probability level. H atoms have been omitted for clarity.

Table 3.1 Selected bond lengths (Å) and angles (°) for **3.23**.

Atoms	**3.23**	Atoms	**3.23**
Bond lengths		Pd1-O31	2.027(4)
C1-O1	1.340(7)	Pd1-O32	2.028(4)
C1-C2	1.431(9)	O31-C32	1.256(8)

C2-C3	1.396(9)	O32-C34	1.258(8)
C3-C4	1.387(9)	*Bond Angles*	
Pd1-O1	1.950(4)	O1-Pd1-N1	88.9(2)
Pd1-N1	2.001(6)	O31-Pd1-O32	92.24(19)

The crystal structure of **3.24** contains two independent molecules, denoted **A** and **B** (Figure 3.2). Both conformers **A** and **B** share many similarities with **3.23** such as the palladium ions being pseudo-square planar and the carbon-oxygen bond lengths of the hydroquinone being characteristic of a CO single bond (Table 3.2). However, the two molecules have very different conformations. Conformer **3.24 A** has a comparable geometry to **3.23**. The outer pyridine rings for **A** are twisted in opposite directions by 27.47^{o} with respect to the central ring with one nitrogen pointing above and the second nitrogen pointing below the plane of the hydroquinone ring resulting in the same "step" type structure as **3.23**. In contrast the outer pyridine rings of **3.24 B** are twisted in such a way that both nitrogens point above the plane of the central hydroquinone ring resulting in a "butterfly" type structure. For conformer **B** the pyridine ring containing N1 is twisted by 31.83^{o} and the pyridine ring containing N2 is twisted by 28.18^{o} with respect to the central ring.

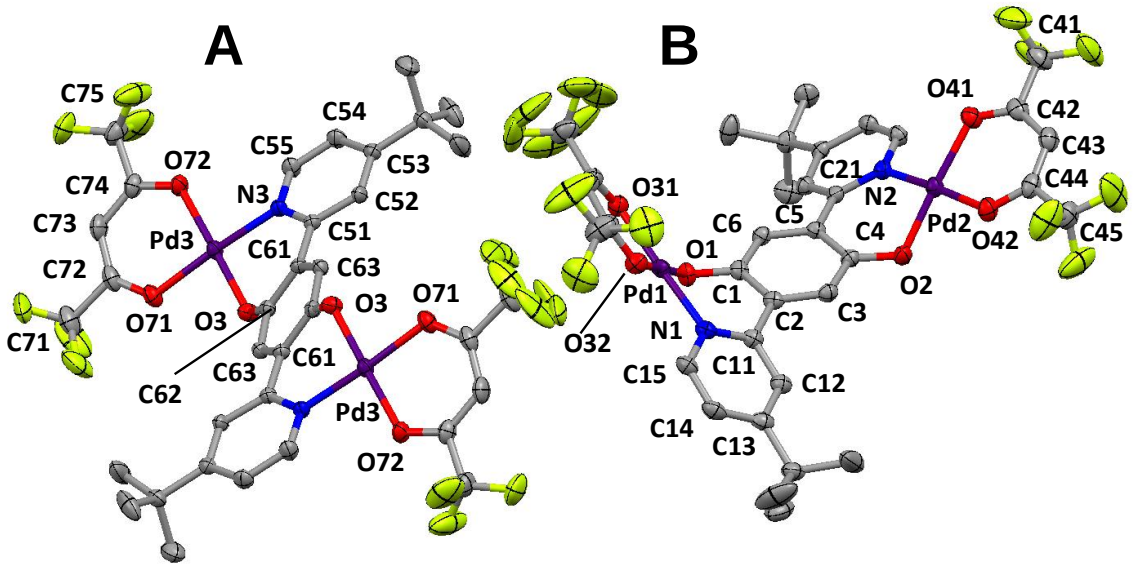

Figure 3.2 Molecular structure of **3.24** showing conformers **A** and **B** with thermal ellipsoids shown at 50% probability level. H atoms have been omitted for clarity.

Table 3.2 Selected bond lengths (Å) and angles (º) for **3.24 A**.

Atoms	**3.24 A**	Atoms	**3.24 A**
Bond lengths		Pd3-O72	1.9878(15)
C62-O3	1.312(2)	O71- C72	1.235(3)
C61-C62	1.393(3)	O72-C74	1.360(4)
C61-C63	1.371(3)	*Bond angles*	
Pd3-O3	1.9128(15)	O3-Pd3-N3	89.45(7)
Pd3-N3	1.9761(17)	O3-Pd3-O71	87.40(6)
Pd3-O71	1.9983(15)	O71-Pd3-O72	91.85(6)

Table 3.3 Selected bond lengths (Å) and angles (º) for **3.24 B**.

Atoms	**3.24 B**	Atoms	**3.24 B**
Bond lengths		Pd1-O31	1.9844(15)
C1-O1	1.325(2)	Pd1-O32	1.9866(16)
C1-C2	1.390(3)	O31-C32	1.236(3)
C2-C3	1.380(3)	O32-C34	1.235(3)
C3-C4	1.381(3)	*Bond angles*	
Pd1-O1	1.9234(15)	O1-Pd1-N1	88.42(7)
Pd1-N1	1.9628(18)	O31-Pd1-O32	92.47(7)

3.3 Electrochemical Studies of Palladium Complexes

The redox properties of palladium complexes **3.19-3.20** and **3.23-3.25** were studied by cyclic voltammetry in dichloromethane. Each of the palladium complexes possesses two reversible one-electron oxidation processes. As noted in the introduction, redox processes of palladium complexes with redox-active ligands have been shown to be ligand-based where the palladium metal center is redox inert.[141-144] These studies, along with spectroscopic data of the one-electron oxidized forms of **3.19** and **3.20** discussed in Section 3.4, implies that the oxidation processes observed for the palladium complexes **3.19-3.20** and **3.23-3.25** are also ligand based.

The redox processes of the palladium complexes are shifted substantially to more positive potentials in comparison to the redox processes of the corresponding free quinone (Table 3.2). For example, the bispyrazole quinone, **2.31** is oxidized from the hydroquinonate dianion to the semiquinone anion (HQ^{2-}/SQ^{-}) at -1.37 V vs Fc and then

oxidized to quinone (SQ^{-}/Q) at -0.76 V. The Pd(acac) complex of this ligand **3.19** is oxidized at +0.11 V (HQ^{2-}/SQ^{-}) and +0.65 V (SQ^{-}/Q). This is consistent with the palladium metal withdrawing electron density from the ligand, which makes the hydroquinonate dianion harder to oxidize.

The redox potentials can be tuned by varying the ancillary ligand. For example, the palladium hfac complex **3.20** is oxidized at more positive potentials compared to **3.19** which is consistent with the hfac ancillary ligand containing electronegative fluorines which withdraw electron density from the palladium ions increasing the metals Lewis acidity. In addition, oxidation potentials can be modified by changing the bridging hydroquinone ligand. The oxidation potentials of the pyridyl forms of the hydroquinone complexes with Pd(hfac), **3.23** and **3.24** are slightly lower in comparison to **3.20** as was also seen for the free quinones indicating pyridine is more electron donating than pyrazole. The piperidine complex, **3.25**, is oxidized at even lower potentials with respect to the other Pd(hfac) complexes due to the electron donating nature of the methyl-piperidyl substituent. The oxidation potentials for hfac compounds **3.20** and **3.23-3.25** follow the same general trends relative to each other as observed for the corresponding quinones.

Unlike the quinones, there is a fairly large variation in the separation of $E_1^{o'}$ and $E_2^{o'}$ ($\Delta E^{o'}$). The potential separation is a significant parameter because it is an indicator of the potential window in which the semiquinone radical can be accessed. A very small ΔE^{o} indicates that the semiquinone species becomes unstable with respect to disproportionation to the quinone and hydroquinonate species. Direct comparison of the redox potentials of the quinones and corresponding palladium complexes cannot be made

because all of the quinones voltammograms were run in acetonitrile whereas the palladium complexes were run in dichloromethane for solubility reasons. However, qualitative comparisons between the two groups can be made. The quinones showed little change in the peak separation of $E_1^{o'}$ and $E_2^{o'}$ ranging from 0.71-0.76 V (Table 2.4). For the corresponding palladium hfac complexes, **3.20** and **3.23-3.25**, the peak separation is smaller and a larger range between 0.34-0.49 V is observed for $\Delta E^{o'}$. The separation between the two oxidation processes decreases for complexes oxidized at high positive potentials with the smallest separation for **3.20**. This analysis indicates that if a larger difference in peak separation was desired for a metal complex of a *p*-hydroquinone, by making the complex more electron rich the peak separation should increase.

Table 3.4. Redox potentials (V vs Fc) for palladium hydroquinone complexes.

Compound	$E_1^{o'}$	$E_2^{o'}$	$\Delta E^{o'}$
	HQ^{2-}/SQ^{-}	SQ^{-}/Q	
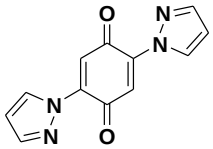 **2.31**	**-1.37**	**-0.76**	**0.61**
	E_{1pa} = *-1.30*	E_{2pa} = *-0.68*	
	E_{1pc} = *-1.44*	E_{2pc} = *-0.80*	
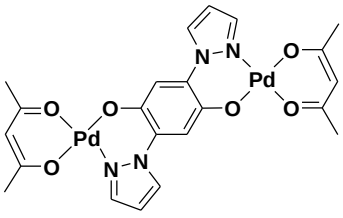 **3.19**	**+0.11**	**+0.65***	**0.54**
	E_{1pa} = *+0.15*	E_{2pa} = *+0.70*	
	E_{1pc} = *+0.07*	E_{2pc} = *+0.60*	

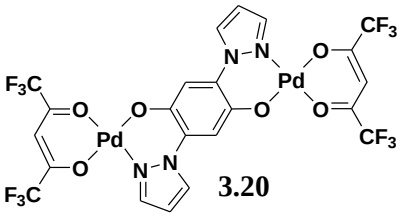 **3.20**	**+0.46** E_{1pa} = +0.49 E_{1pc} = +0.42	**+0.80*** E_{2pa} = +0.86 E_{2pc} = +0.74	**0.34**
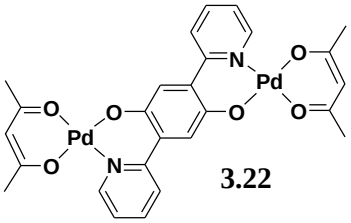 **3.22**	**+0.07** E_{1pa} = +0.11 E_{1pc} = +0.03	**+0.65*** E_{2pa} = +0.70 E_{2pc} = +0.61	**0.58**
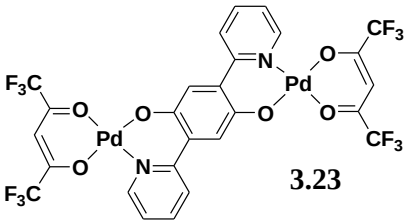 **3.23**	**+0.40** E_{1pa} = +0.44 E_{1pc} = +0.36	**+0.82*** E_{2pa} = +0.87 E_{2pc} = +0.77	**0.42**
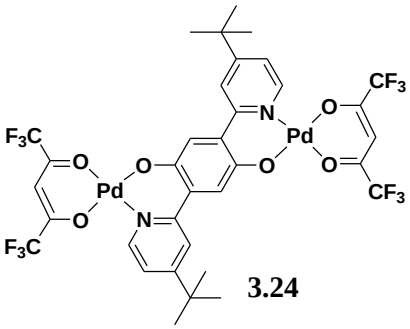 **3.24**	**+0.38** E_{1pa} = +0.42 E_{1pc} = +0.34	**+0.81*** E_{2pa} = +0.85 E_{2pc} = +0.76	**0.43**
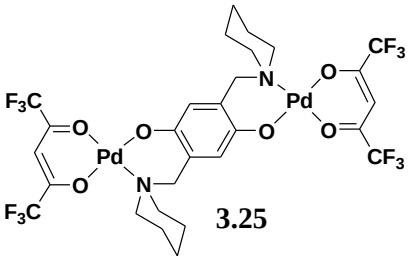 **3.25**	**+0.12** E_{1pa} = +0.16 E_{1pc} = +0.09	**+0.61*** E_{2pa} = +0.66 E_{2pc} = +0.57	**0.49**

(~1mM analyte in dichloromethane with 0.1M Bu_4NBF_4 electrolyte), * denotes quasi-reversible peaks

All cyclic voltammograms and their scan rates can be found in Appendix 1: Figure A-61 to A-66.

The reversibility of the first oxidation process in complexes **3.19-3.20** and **3.23-3.25** was established as being reversible based on: (i). the anodic and cathodic peak currents

being equal in magnitude and (ii). separated by ~0.6V. On the other hand the second oxidation process was determined to be quasi-reversible because it did not meet these criteria. The lower reversibility of the second redox process may be due to the nature of the oxidized product, in which the ligand is in its neutral quinone form, thus coordinating more weakly to the palladium. It is possible that some of the complex decomposes (decomplexation) due to metal and quinone fragmentation resulting from the quinone ligand binding less strongly to the metal in comparison to the semiquinone anion and hydroquinonate dianion.

3.4 *In situ* Chemical Oxidations of Palladium Complexes

In order to gain information with respect to the electronic structure of the oxidized palladium complexes, chemical oxidations and characterization of complexes **3.19** and **3.20** were investigated. Spectroscopic studies of the oxidized complexes with comparisons to related compounds such as the free ligand allows for the oxidation state of the quinone ligand to be identified. Therefore, the reduction and characterization of the free quinone **2.31** was also of importance.

Reduction of **2.31** with one equivalent of cobaltacene (E^o = -1.33 V in DCM vs Fc)[23] as depicted in Scheme 3.8 causes in the initially colourless solution to turn a dark red. The reduced product is very reactive, so much so that characterization must be done *in situ* and immediately after oxidation.

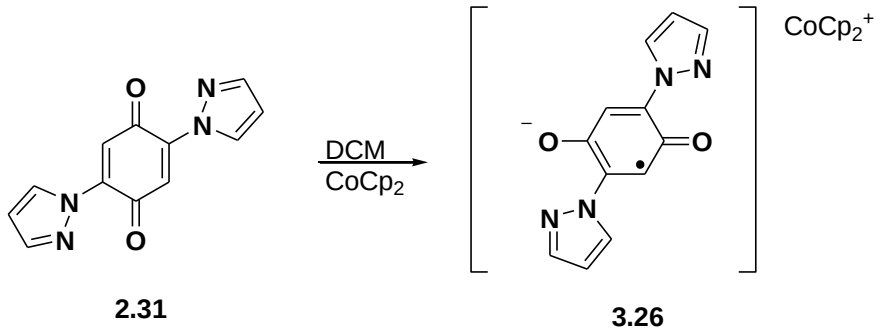

2.31 **3.26**

Scheme 3.8. Chemical reduction of quinone **2.31** to give the corresponding semiquinone radical **3.26.**

Unfortunately, the oxidized cobaltocenium by-product has a weak absorption at 425 nm so no clear isosbestic points were observed when the reduction was carried out in small increments and monitored by UV-Vis. For this reason only the initial spectrum of the quinone **2.31** and the semiquinone radical **3.26** have been shown in Figure 3.3 where the shoulder peak at 425 nm is due to the cobaltacenium cation.

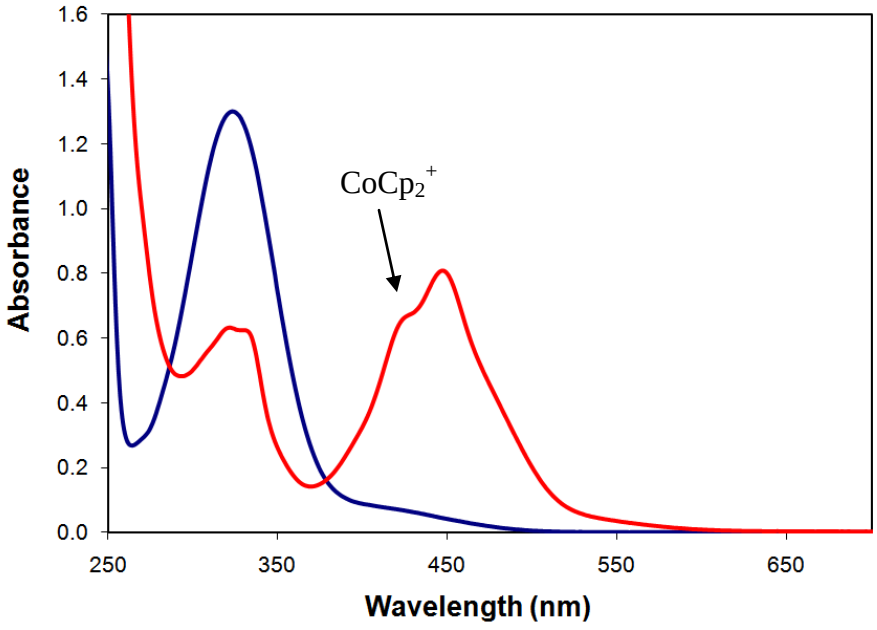

Figure 3.3. UV-Vis of **2.31** (blue) and **3.26** (red) in DCM ($4.5 * 10^{-5}$ M).

Upon reduction a broad absorption emerges at 447 nm. The broad, longer wavelength absorption at 447 nm is typical of both *ortho* and *para*-semiquinones and their complexes which are expected to have π -π^* absorptions red shifted compared to the corresponding quinones.[145-148]

By examining the cyclic voltammograms of **3.19** and **3.20**, an oxidizing agent of appropriate strength was chosen to oxidize the metal complexes to the corresponding semiquinone complexes, **3.27** and **3.28**. $AgPF_6$ has a formal potential of +0.65V vs Fc in DCM[23] and proved to be a good choice for the oxidant as it was strong enough to oxidize both **3.19** and **3.20** to their semiquinone redox couples (Scheme 3.9). Thus a solution of $AgPF_6$ was titrated into a solution of **3.19** in DCM while the progress of the oxidation was monitored by UV-vis spectrometry (Figure 3.4).

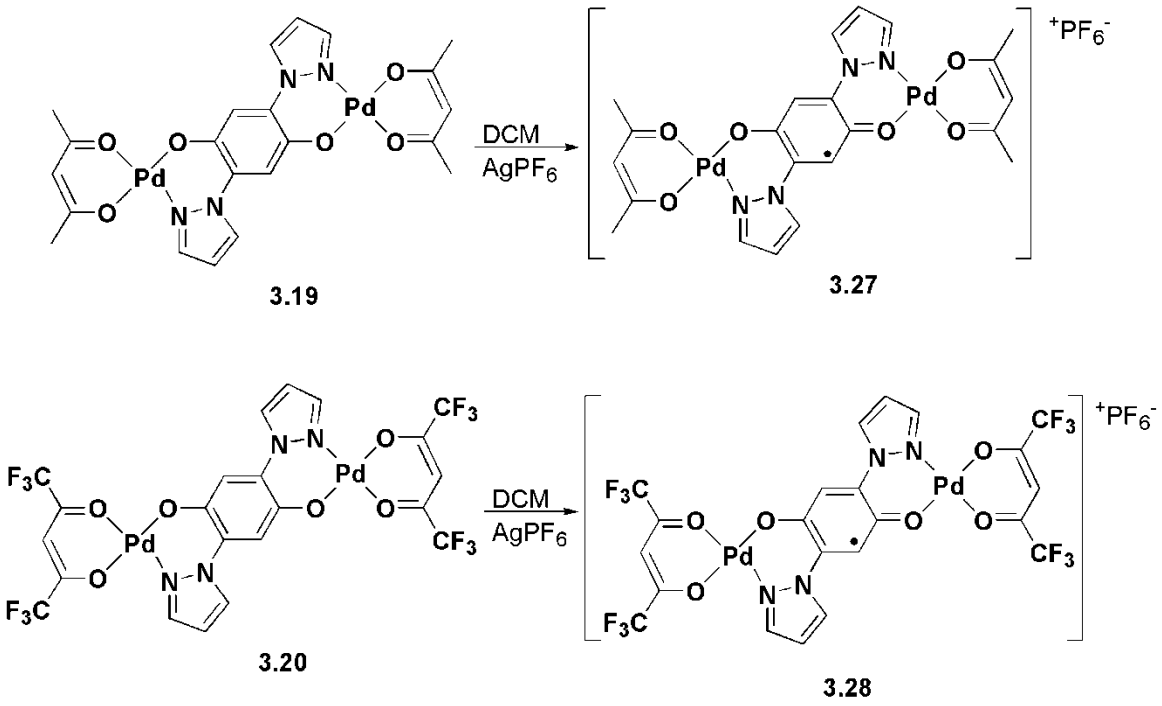

Scheme 3.9. Chemical oxidations of **3.19** and **3.20** to give the corresponding semiquinone complexes **3.27** and **3.28**.

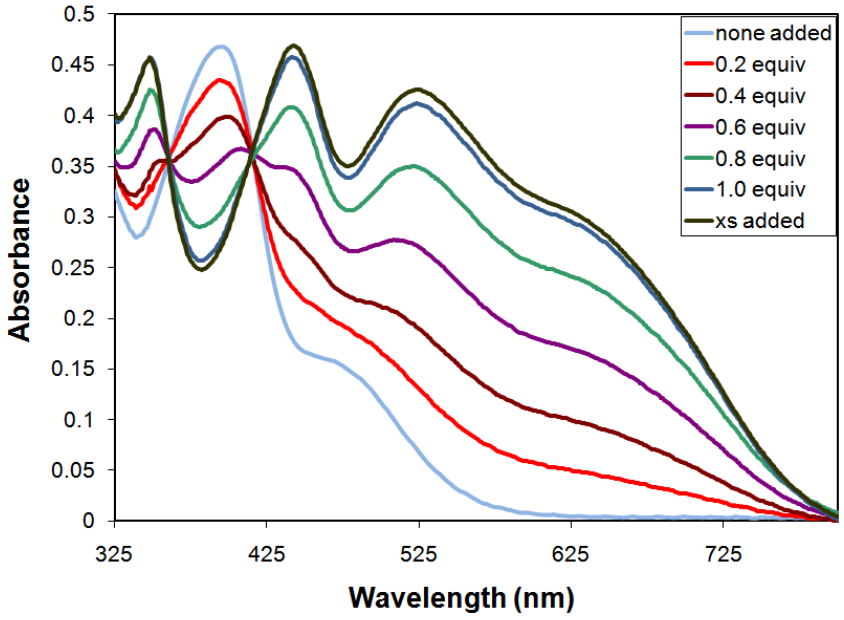

Figure 3.4. UV-vis of **3.19** ($3.0 * 10^{-5}$ M in DCM) with $AgPF_6$ added to generate **3.27**.

As oxidant is added and **3.27** is produced, peaks at 349 nm, 442 nm and 525 nm emerge while the peak at 394 nm recedes. The two isosbestic points at wavelengths of 361 and 415 nm indicates that the oxidation proceeds without any side reactions taking place. In the oxidation of **3.19**, just over 1 equivalent of $AgPF_6$ is required to completely oxidize **3.19** to **3.27**. As was the case for the free bis-pyrazole semiquinone radical, **3.26**, the broad absorption for **3.27** at 525 nm is typical of a semiquinone ligand π-π^* transition. The other absorptions at 349 nm and 442 nm are attributed to π-π^* transitions or charge transfers since d-d transitions would be expected to be much weaker.

The oxidation of **3.20** with $AgPF_6$ results in a similar electronic absorption profile (Figure 3.5). In this case **3.20** already has a very weak and broad absorption at longer wavelength (523 nm) as well as a peak 372 nm. The peak at 372 nm wanes upon oxidation and the peak at 523 nm becomes much stronger and shifts slightly to 535 nm; as well as a shoulder peak growing in at 595 nm. As noted previously, broad absorption peaks at higher wavelengths are typical of semiquinones and attributed to π-π^* transitions. Two isosbestic points are observed at wavelengths of 353 and 413 nm indicating no decomposition or side reactions are taking place in this oxidation. For **3.20**, over two equivalents of the oxidant are required before no changes in the electronic absorption are observed. This is due to **3.20** being oxidized at higher potentials than **3.19** and in this case $AgPF_6$ is not a strong enough oxidant to completely oxidize **3.20** after adding one equivalent.

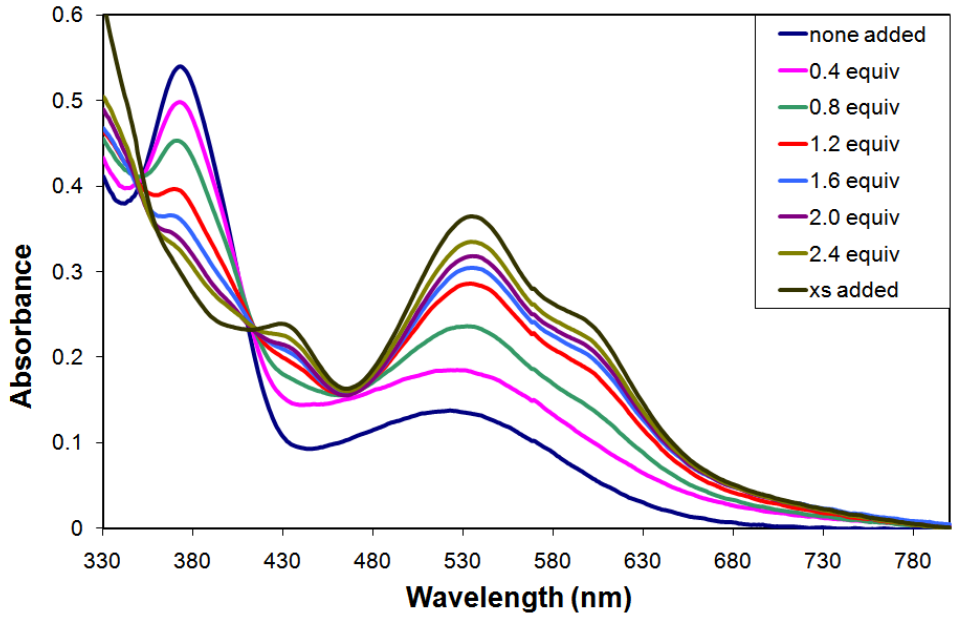

Figure 3.5. **3.20** (3.0 * 10^{-5} M in DCM) titrated with $AgPF_6$ to generate **3.28**.

The EPR spectra of the uncomplexed semiquinone radical **3.26** and the two palladium complexes where the ligand is in the semiquinone oxidation state, **3.27** and **3.28**, were obtained in degassed dichloromethane at room temperature. The simulated and experimental spectra are shown in Figure 3.6. The g-factors of the two palladium complexes **3.27** and **3.28** are very close to that of the free bispyrazole semiquinone ligand. This is a good indication that the radical species has most of its spin density localized to the hydroquinone ligand. The spectra of **3.26**-**3.28** are dominated by a distorted triplet with intensities of approximately 1:2:1, which suggests that the unpaired electron is coupled to two equivalent S = ½ nuclei or most likely the two hydrogens located on the central benzene ring. Coupling to the two nitrogens is not observed as nitrogen has S = 1 so a pentet would be expected if coupling between the radical electron and nitrogen did occur. This suggests that the unpaired electron is not delocalized to the pyrazole rings.

The hyperfine coupling constant for the semiquinone hydrogens is estimated to be 2.0 G for **3.26**. Once complexed the hyperfine coupling constant lowers to 1.9 G for **3.27** and to 1.8 G for **3.28**. The palladium semiquinone complexes slightly smaller hyperfine coupling constants are expected since the palladium systems remove electron density from the semiquinone ligands as is evident from the cyclic voltammograms. In the case of the EPR spectrum of **3.27**, on the outer sides of the peaks (3495 G and 3505 G) there appears to be additional coupling to the palladium (S = 5/2 for ^{105}Pd). However, these peaks are not resolved most likely due to the lower natural abundance of palladium (22.2% for ^{105}Pd) and since this coupling is expected to be of lower intensity.

Table 3.5. EPR hyperfine coupling constants and g-factors.

Compound	α_H (G)	g-factor
3.26	2.0	2.0053
3.27	1.9	2.0066
3.28	1.8	2.0045

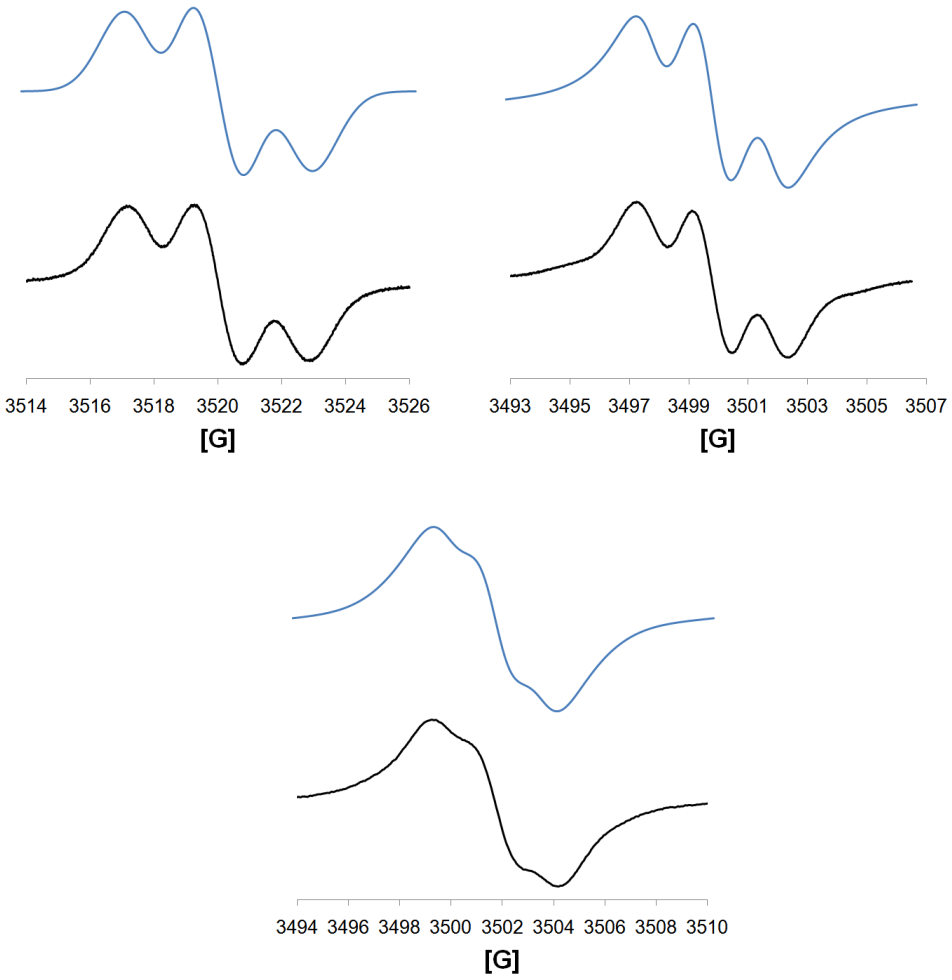

Figure 3.6. Simulated (blue) and experimental (black) EPR spectra of **3.26** (top left), **3.27** (top Right) and **3.28** (bottom) in DCM at RT.

3.5 Summary

Dinuclear square planar palladium complexes of derivatized hydroquinones were prepared successfully. The reversible redox chemistry of the bridging hydroquinone is preserved in the palladium complexes but the redox couples are shifted to much higher potentials. For example, the first oxidation potential (HQ^{2-}/SQ^{-}) is shifted by nearly +1.5

V for the the palladium acac complex **3.19** in comparison to the free quinone **2.31**. In comparison to the *ortho*-semiquinone complex of palladium introduced in Chapter 1, **1.33**, the *para*-hydroquinone palladium complexes are fully reduced at much more positive potentials. For example, **3.19** is fully reduced at a potential below +0.11 V whereas **1.33** is fully reduced below a potential of -0.865 V.[53] This difference in redox behaviour is mainly attributed to the disparity in structural makeup with the *p*-quinones bridging two metal ions and the *o*-semiquinone complex containing two ligands bridged by one metal ion.

The redox potential of the palladium complexes can be tuned by changing the *p*-hydroquinone or ancillary ligand. By making the complex more electron rich, the oxidation potentials are shifted to lower potentials and a larger peak separation is obtained which is significant particularly if the semiquinone redox state is to be accessed. The oxidation potentials for the palladium hfac compounds **3.20** and **3.23-3.25** follow the same trends relative to each other as was established for the analogous quinones in Chapter 2.

The palladium complexes **3.19** and **3.20** have been chemically oxidized to the semiquinone complexes **3.27** and **3.28**. The UV-vis spectra of **3.27** and **3.28** compared with the spectra for the free bis-pyrazolyl semiquinone **3.26** indicates that the oxidation is ligand-based. EPR spectroscopy for **3.27** and **3.28** also indicates the radical is localized to the semiquinone ligand. Therefore **3.27** and **3.28** have a similar, charge localized, electronic structure as *ortho*-semiquinone complexes of palladium.[53] Redox processes are ligand based and the radical is not delocalized significantly on to the palladium ions.

Although complexes of other metal systems were attempted with ligands **2.1** and **2.2**, little success was achieved due in part to the insolubilities of the products isolated. This may be due to **2.1** and **2.2** forming polymeric metal complexes. On the other hand these two ligands formed the least soluble palladium complex so the insolubility of other products may be due to the nature of the ligand. For this reason subsequent complexation attempts with other metal systems should be made with **2.15** as this ligand and its complexes have proved to be much more soluble and more readily form X-ray quality crystals.

These results in conjunction with previous examples of coordinated *p*-hydroquinones indicate *p*-hydroquinones behave similarly to *ortho*-quinones when complexed to a transition metal. Despite stumbling blocks such as poor solubility and the tendency to form oligomeric complexes, the potential for some derivatized *p*-hydroquinones to make paramagnetic complexes or valence tautomeric complexes remains high and relatively untapped.

3.6 Experimental

General experimental aspects can be found in Chapter 2, Section 2.11.

3.6.1 Synthesis

μ-(2,5-Bis(pyrazol-1-yl)-1,4-hydroquinonato)-bis(acetylacetonato palladium) (3.19). In anhydrous deaerated chlorobenzene (50 mL) 2,5-bis(pyrazol-1-yl)-1,4-hydroquinone (40 mg, 0.17 mmol) and NaH were added (8 mg, 0.38 mmol) resulting in a yellow

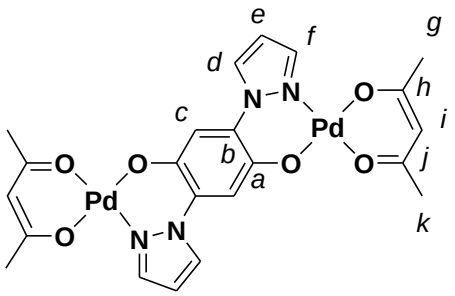

solution. This was lightly heated then added dropwise to a solution of $Pd(acac)_2$ (200 mg, 0.66 mmol) in chlorobenzene (50 mL) under argon. The yellow solution immediately turned red/brown and was then allowed to stir ~2 h resulting in a red precipitate. This was filtered off to give a crystalline red solid that was insoluble in dichloromethane so was discarded. Solvent was pumped off the filtrate to give **3.20** as an orange powder. This was recrystallized from chlorobenzene to give an orange powder 68 mg (63% yield). ^{1}H NMR ($CDCl_3$): δ 8.01 (d, 2H, *J* = 2.6 Hz, H-*d*), 7.78 (d, 2H, *J* = 2.2 Hz, H-*f*), 7.13 (s, 2H, H-*c*), 6.57 (t, 2H, *J* = 2.5 Hz, H-*e*), 5.41 (s, 2H, H-*i*), 2.10 (s, 6H, H-*g*), 2.01 (s, 6H*k*) ppm. ^{13}C NMR (125 MHz, $CDCl_3$): δ 187.6 (C-*j*), 186.1 (C-*h*), 147.6 (C-*f*), 139.8 (C-*a*), 129.2 (C-*d*), 128.0 (C-*b*), 112.2 (C-*e*), 108.4 (C-*c*), 101.4 (C-*i*), 25.9 (C-*k*), 25.7 (C-*g*) ppm. FT-IR (KBr pellet) 3147 (w), 3128 (w), 3052 (w), 3009 (w), 2963 (w), 2923 (w), 1573 (m), 1510 (s), 1496 (s), 1411 (m), 1377 (s), 1331 (m), 1271 (m), 1223 (m), 1200 (m), 1081 (m), 1024 (w), 939 (w), 839 (m), 748 (m) cm^{-1}. UV-Vis (CH_2Cl_2): λ_{max} 236 (56000), 262 (62000), 296 (15000), 465 (5000) nm ($M^{-1}cm^{-1}$). Anal. Calcld. for $C_{22}H_{22}N_4O_6Pd_2$: C, 40.57; H, 3.40; N, 8.60. Found: C, 40.30; H, 3.26; N, 8.37. MS-FAB, *m/z* (%): 651.9 (100) [M^+].

μ-(2,5-Bis(pyrazol-1-yl)-1,4-hydroquinonato)-bis(1,1,1,5,5,5-hexafluoroacetylacetonato palladium) (3.20).

A solution of 2,5-bis(pyrazol-1-yl)-1,4-hydroquinone (52 mg, 0.21 mmol) in anhydrous toluene (50 mL) was added dropwise to a solution of $Pd(hfac)_2$ (225 mg, 0.432 mmol) in

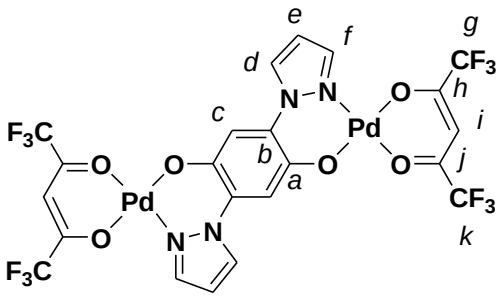

anhydrous toluene (50 mL) under argon. The yellow solution was stirred and darkened immediately upon mixing. The reaction mixture was stirred for ~1 h, then solvent is reduced to ~10 mL and then cooled to 0 ^{o}C. A metallic purple precipitate is then filtered off from the solution with hexane washes to give 172 mg of **3.21** (92% yield). ^{1}H NMR ($CDCl_3$): δ 8.11 (d, 2H*d*, *J* = 2.7 Hz), 7.70 (d, 2H*f*, *J* = 2.4 Hz), 7.21 (s, 2H*c*) 6.69 (t, 2H*e*, *J* = 2.6 Hz), 6.25 (s, 2H*i*) ppm. ^{13}C NMR (125 MHz, $CDCl_3$): δ 147.5 (C-*f*), 139.9 (C-*a*), 129.9 (C-*d*), 128.8 (C-*b*), 112.3 (C-*e*), 109.6 (C-*c*), 92.8 (C-*i*) ppm (not all C signals observed due to the insolubility of this compound). ^{19}F NMR (339MHz, $CDCl_3$) -73.9, -74.4 ppm. FT-IR (KBr pellet): 3156 (w), 1618(m),1499(m), 1459(m), 1419(m), 1328(w), 1260(s), 1212(s), 1149(s), 1109(w), 1089(w), 856(w), 782(w), 751(w) cm^{-1}. UV-Vis (CH_2Cl_2): λ_{max} 261 (49000), 372 (15000), 522 (4000) nm (M^{-1}cm^{-1}). Calcd for $C_{22}H_{10}F_{12}N_4O_6Pd_2$: C, 30.47; H, 1.16; N, 6.46. Found: C, 30.60; H, 1.07; N, 6.42. MS-FAB; *m/z* (%) 867.8 (100) [M^{+}].

μ-(2,5-Bis(pyrid-2-yl)-1,4-hydroquinonato)-bis(acetylacetonato palladium) (3.22).

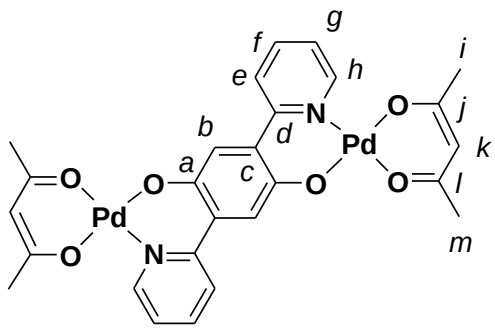

In anhydrous deaerated chlorobenzene (50 mL) 2,5-bis(pyrid-2-yl)-1,4-hydroquinone (35 mg, 0.13 mmol) and NaH were added (6 mg, 0.26 mmol) resulting in a yellow solution. This was immediately added dropwise to a solution of $Pd(acac)_2$ (160 mg, 0.52 mmol) in chlorobenzene (50 mL) under

argon. The yellow solution turns orange and then was refluxed for 2 h turning a dark red. The solution was allowed to cool and then filtered to remove the red precipitate which proved to be insoluble in most organic solvents so was discarded. Solvent was pumped off the filtrate to give **3.22a** as a reddish orange powder. This was recrystallized from chlorobenzene although not all impurities were removed after three attempts. The yield of the reddish orange powder was 32 mg (36% yield). ^{1}H NMR ($CDCl_3$): δ 8.51 (d, 2H, *J* = 5.9 Hz, H-*h*), 7.79 (m, 6H, H-*e,f,g*), 7.35 (s, 2H, H-*b*), 5.37 (s, 2H, H-*k*) ppm 2.10 (s, 6H, H-*g*), 1.98 (s, 6H*k*) ppm. ^{13}C NMR spectra run in $CDCl_3$ gave no discernible signal. FT-IR (thin film on NaCl plate): 2961 (w), 2923 (w), 2866 (w), 1636 (w), 1563 (s), 1520 (s), 1481 (s), 1396 (s), 1273 (m), 1262 (m), 1193 (m), 1115 (s), 1084 (s), 1028 (m), 787 (w) cm^{-1}. No elemental analysis was performed on this sample due to impurities being present.

μ-(2,5-Bis(pyrid-2-yl)-1,4-hydroquinonato)-bis(1,1,1,5,5,5-hexafluoroacetylacetonato palladium) (3.23).

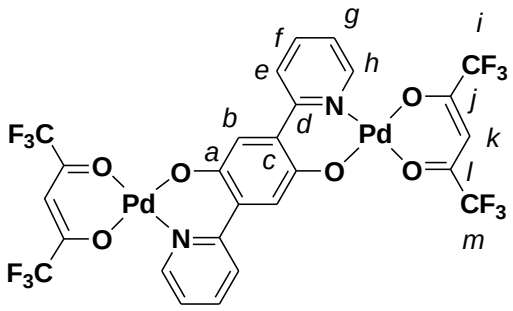

2,5-Bis(pyrid-2-yl)-1,4-hydroquinone (13 mg, 0.048 mmol) and $Pd(hfac)_2$ (50 mg, 0.095 mmol) were dissolved in anhydrous toluene (30 mL). This solution was then refluxed gently for 2 hours turning dark purple. Solvent was reduced to ~10mL and then the solution was allowed to cool to 0 ^{o}C in an ice bath. The purple solid that precipitated was filtered to give 39 mg of **3.22** (90% yield). The compound was recrystallized from toluene yielding needle crystals of X-ray quality. ^{1}H

NMR ($CDCl_3$): δ 8.34 (d, 2H, *J* = 5.8 Hz, H-*h*), 7.99-7.90 (m, 4H, H-*e,f*), 7.42 (s, 2H, H-*b*) 7.39 (ddd, 2H, *J* = 6.7, 6.1, 2.1 Hz, H-*g*), 6.24 (s, 2H, H-*k*) ppm. ^{13}C NMR (125 MHz, $CDCl_3$): δ 176.4 (q, $^2J_{C\text{-}F}$ = 35.7 Hz, C-*l*), 175.3 (q, $^2J_{C\text{-}F}$ = 35.5 Hz, C-*j*), 154.7 (C-*a*), 153.1 (C-*d*), 150.1 (C-*h*), 140.1 (C-*f*), 133.5 (C-*c*), 124.2 (C-*e*), 123.7 (C-*g*), 119.8 (C-*b*), 116.8 (q, $J_{C\text{-}F}$ = 283.8 Hz, C-*m*), 116.8 (q, $J_{C\text{-}F}$ = 284.7 Hz, C-*i*), 92.8 (C-*k*) ppm. ^{19}F NMR (283 MHz, $CDCl_3$) -74.5, -74.9 ppm. FT-IR (thin film on NaCl plate): 3053 (w), 2974 (w), 1625 (m), 1605 (m), 1597 (m), 1552 (m), 1485 (m), 1462 (s), 1429 (m), 1401(m), 1261 (s), 1225 (m), 1202 (m), 1146 (s), 1102 (m), 864 (w), 800 (m), 774 (m), 749 (m), 623 (m), 665 (m) cm^{-1}. UV-Vis (CH_2Cl_2): λ_{max} 245 (31000), 313 (41000), 486 (11000) nm ($M^{-1}cm^{-1}$). Anal. Calcld. for $C_{26}H_{12}F_{12}N_2O_6Pd_2$: C, 35.12; H, 1.35; N, 3.15. Found (Product recrystallized from toluene): C, 37.02; H, 2.01; N, 3.03. Found (Product recrystallized from DCM): C, 34.23; H, 1.62; N, 3.09. The impurity in each case correlates to a small amount of the solvent used in the recrystallization.

μ-(2,5-Bis(4-tert-butylpyrid-2-yl)-1,4-hydroquinonato)-bis(1,1,1,5,5,5-hexafluoroacetylacetonato palladium) (3.24). 2,5-Bis(4-*tert*-butylpyrid-2-yl)-1,4-hydroquinone (72 mg, 0.19 mmol) and $Pd(hfac)_2$ (200 mg, 0.384 mmol) were dissolved in anhydrous toluene (100 mL). This solution was stirred for 1 hour at room temperature then solvent was removed under reduced pressure. A purple powder was obtained which was dissolved in hot hexanes,

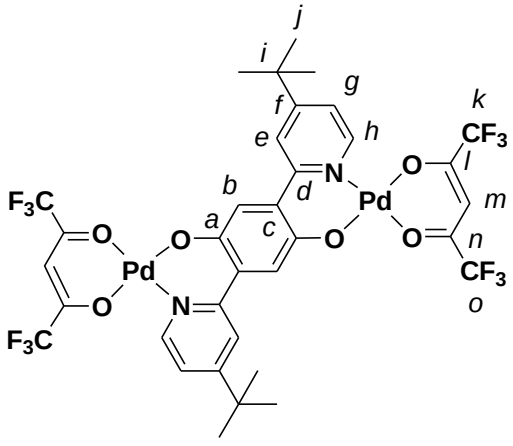

filtered and then cooled. The precipitate was collected yielding 180 mg (94%) of the target complex. X-ray quality crystals were obtained from a solution of toluene allowed to slowly evaporate. ^{1}H NMR ($CDCl_3$): δ 8.20 (d, 2H, J = 6.4 Hz, H-*h*), 7.83 (d, 2H, J = 2.1 Hz, H-*e*), 7.45 (s, 2H, H-*b*) 7.38 (dd, 2H, J = 6.4, 2.2 Hz, H-*g*), 6.21 (s, 2H, H-*m*), 1.39 (s, 18H, H-*j*) ppm. ^{13}C NMR (125 MHz, $CDCl_3$): δ 176.1 (q, $^{2}J_{C\text{-}F}$ = 35.9 Hz, C-*n*), 174.8 (q, $^{2}J_{C\text{-}F}$ = 35.5 Hz, C-*l*), 164.6 (C-*f*), 154.4 (C-*d*), 154.4 (C-*a*), 149.1 (C-*h*), 133.7 (C-*c*), 120.9 (C-*e*), 120.8 (C-*g*), 119.7 (C-*b*), 116.3 (q, $J_{C\text{-}F}$ = 283.8 Hz, C-*o*), 116.2 (q, $J_{C\text{-}F}$ = 284.8 Hz, C-*k*), 92.4 (C-*m*), 35.5 (C-*i*), 30.6 (C-*j*) ppm. ^{19}F NMR (283 MHz, $CDCl_3$) -73.8, -74.5 ppm. FT-IR (thin film on NaCl plate) 2967 (m), 2873 (m), 1624 (s), 1541 (m), 1467 (m), 1401 (m), 1347 (w), 1259 (s), 1209 (s), 1149 (s), 1102 (w), 875 (w), 798 (m), 694 (w), 666 (m) cm^{-1}. UV-Vis (CH_2Cl_2): λ_{max} 236 (31000), 310 (34000), 465 (8700) nm ($M^{-1}cm^{-1}$). Anal. Calcld. for $C_{34}H_{28}F_{12}N_2O_6Pd_2$: C, 40.78; H, 2.82; N, 2.80. Found: C, 41.07; H, 2.94; N, 2.90.

μ-(2,5-Bis(1-piperidylmethyl)-1,4-hydroquinonato)-bis(1,1,1,5,5,5-hexafluoroacetylacetonato palladium) (3.25). 2,5-Bis(1-piperidylmethyl)-1,4-hydroquinone (42 mg, 0.14 mmol) and Pd(hfac)$_2$ (150 mg, 0.288 mmol) were dissolved in anhydrous toluene (50 mL). This solution was stirred for 1 hour then solvent was removed under reduced pressure. A purple powder was obtained which was washed with hexanes. This was recrystallized from toluene yielding 116 mg (91%) of the

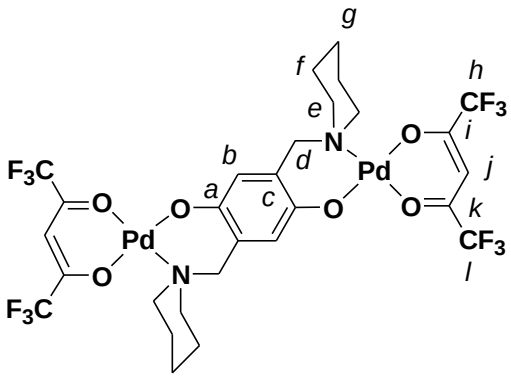

target complex. ^{1}H NMR ($CDCl_3$): δ 6.88 (s, 2H, H-*b*) 6.11 (s, 2H, H-*j*), 3.57 (s, 4H, H-*d*), 3.29-3.10 (m, 8H, H-*e*), 1.96 (m, 4H, H-*f*), 1.76 (m, 2H, H-*f*), 1.50 (m, 6H, H-*f, g*) ppm. ^{13}C NMR (125 MHz, $CDCl_3$): δ 176.1 (q, $^{2}J_{C\text{-}F}$ = 35.7 Hz, C-*k*), 174.0 (q, $^{2}J_{C\text{-}F}$ = 35.2 Hz, C-*i*), 154.5 (C-*a*), 127.9 (C-*c*), 119.3 (C-*b*), 116.5 (q, $J_{C\text{-}F}$ = 283.8 Hz, C-*l*), 116.3 (q, $J_{C\text{-}F}$ = 283.8 Hz, C-*h*), 92.2 (C-*j*), 55.9 (C-*d*), 54.5 (C-*e*), 23.4 (C-*f*), 20.6 (C-*g*) ppm. ^{19}F NMR (283 MHz, $CDCl_3$) -74.1, -74.9 ppm. FT-IR (thin film on NaCl plate): 2920 (m), 2849 (m), 1627 (m), 1607 (w), 1555 (w), 1527 (w), 1457 (m), 1421 (w), 1255 (s), 1207 (m), 1150 (s), 1101 (w), 913 (w), 804 (w), 747 (w), 693 (w), 666 (s) cm^{-1}. UV-Vis (CH_2Cl_2): λ_{max} 233 (22000), 333 (6300), 562 (2700) nm ($M^{-1}cm^{-1}$). Anal. Calcld. for $C_{28}H_{28}F_{12}N_2O_6Pd_2$: C, 36.19; H, 3.04; N, 3.01. Found: C, 36.36; H, 2.94; N, 3.00.

2,5-Bis(pyrazol-1-yl)-1,4-semiquinone cobaltacenium (3.26).

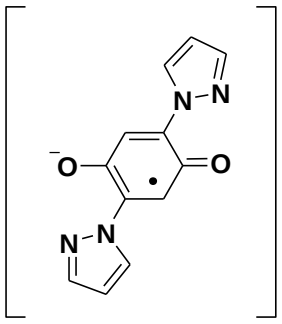

$CoCp_2^+$

2,5-Bis(pyrazol-1-yl)-1,4-quinone (10 mg, 0.042 mmol) was dissolved in DCM (100 mL). This solution was dearated thoroughly for 20 minutes with argon and then cobaltacene (8.2 mg, 0.043 mmol) was added. The solution was stirred for 20 minutes under an argon atmosphere then characterized by UV-vis and EPR. Attempts to isolate the product failed as the compound readily decomposes. UV-Vis (CH_2Cl_2): λ_{max} ~250*, 323 (14000), 447 (18000*) nm ($M^{-1}cm^{-1}$). *Peak at 250 nm also may be caused by cobaltacenium since cobalticenium hexaflourophosphate was shown to absorb strongly in this region. Also cobalticenium hexaflourophosphate has a weak absorbance at ~420 nm so the molar absorptivity of the peak at 447 nm is likely inflated.

μ-(2,5-Bis(pyrazol-1-yl)-1,4-semiquinonato)-bis(acetylacetonate-palladium) hexafluorophosphate (3.27).

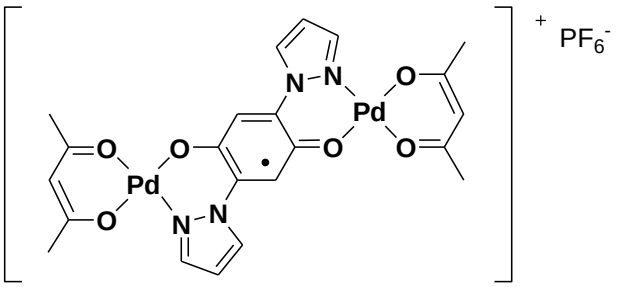

A solution of **3.19** (40 mg, 0.0615 mmol) in DCM (100 mL) was bubbled with argon for twenty minutes. Silver hexafluorophosphate (31 mg, 0.12 mmol) was added and the solution was stirred for 20 minutes under argon. The solution was filtered under argon and then the solvent was removed to give a dark purple solid weighing 45 mg (93%). All subsequent analyses were performed under an inert atmosphere. FT-IR (KBr pellet): 2962 (w), 2923 (m), 2855 (w), 1630 (m), 1576 (m), 1522 (m), 1419 (m), 1308 (s), 1260 (m), 1149 (s), 1084 (m), 1024 (m), 851 (s), 799 (m) cm^{-1}. UV-Vis (CH_2Cl_2): λ_{max} 268 (61000), 310 (18000), 348 (15000), 442 (15000), 524 (13000), 630 (9400) nm ($M^{-1}cm^{-1}$). MS-FAB, *m/z* (%): 651.0 (48) [M^+].

μ-(2,5-Bis(pyrazol-1-yl)-1,4-semiquinonato)-bis(1,1,1,5,5,5-hexafluoroacetylacetonato-palladium) hexafluorophosphate (3.28).

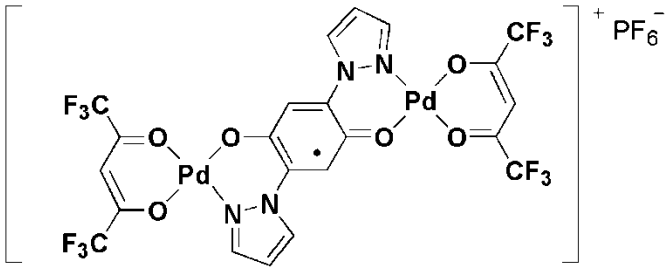

A solution of **3.20** (30 mg, 0.035 mmol) in DCM (100 mL) was bubbled with argon for twenty minutes. Silver hexafluorophosphate (27 mg, 0.11 mmol) was added and the solution was stirred for 20 minutes under argon. The solution was filtered under argon and then the solvent was

removed to give a purple solid weighing 32 mg (90%). All subsequent analyses were performed under an inert atmosphere. FT-IR (KBr pellet): 3170 (w), 2961 (w), 2923 (w), 2851 (w), 1624 (m), 1610 (m), 1516 (m), 1493 (m), 1445 (m), 1422 (m), 1385 (m), 1260 (s), 1232 (s), 1146 (s), 1106 (m), 1091 (m), 670 (m), 838 (s), 814 (m) cm^{-1}. UV-Vis (CH_2Cl_2): λ_{max} 264 (54000), 311 (21000), 430 (6800), 534 (10000), 593 (7100) nm ($M^{-1}cm^{-1}$). MS-FAB, *m/z* (%): 867.9 (100) [M^+].

Chapter 4 Synthesis and Characterization of Boron Complexes of *p*-Hydroquinones and Related Ligands

4.1 Introduction

Research in quinone/hydroquinone coordination chemistry usually focuses on transition metal chemistry. We became interested in the coordination chemistry of a main group element with derivatized *p*-hydroquinones ligands to see how the redox properties of the ligand would be perturbed. Boron was chosen due to the high stability and ease of synthesis often found for organoboron compounds. The electrochemical properties of the boron complexes synthesized were examined along with their optical properties as these compounds turned out to be highly fluorescent.

4.2 Boron Coordination Compounds of Chelating Ligands

There are many examples of conjugated bidentate chelating ligands incorporating one anionic donor and a second neutral donor. Such chelating ligands coordinate with boron and two anionic ancillary ligands to form a neutral four coordinate boron complex as shown by the general example **4.1**. Many of these complexes display fluorescence, driving research in this field.

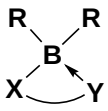

4.1

One of the most studied examples of **4.1** is 4,4-difluoro-4-bora-3a,4a-diaza-*s*-indacene (BODIPY, **4.2**). BODIPY dyes were first discovered by Treibs and Kreuzer in 1968.[149]

However BODIPY received little attention until the late 1980s when its potential for biological labelling was reported.[150] Since then interest in BODIPY has grown, driven by the multitude of derivatives by substitution of the *α*, *β* or *meso* positions of the BODIPY core.[151] There are many other different examples of **4.1** that are luminescent, for instance those based on phenol-pyridine (**4.3**)[152], pyrole-pyridine (**4.4**)[153] and pyrazolyl-anilines (**4.5**)[154] to name a few. Luminescent boron complexes and complexes of other group 13 elements are potentially useful for a variety of applications. For example, these compounds are used in optical devices such as organic-light emitting diodes (OLEDs),[155-157] as fluorescent dyes and sensors,[151,158-160] for nonlinear optics[161] and more recently in light harvesting materials.[162]

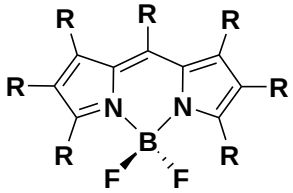

4.2

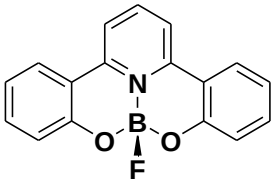

4.3

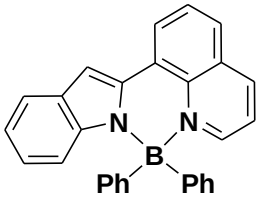

4.4

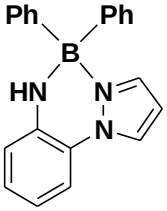

4.5

Despite the large library of BODIPY compounds and other luminescent boron complexes, there are very few examples of dimeric or oligiomeric boron complexes.[163,164] These ladder-type systems have been said to be advantageous because they are often rigid and flat, resulting in good alignment of their π-systems, while binding to two or more elements which can lead to strong luminescence and other desirable electronic properties.[165-168] Kruger *et al.* have prepared bisBODIPY compounds such as **4.6** which had high fluorescent quantum yields but reduced fluorescent lifetimes. Yamaguchi and coworkers have synthesized a dinuclear boron complex bridged by a di(heteroaryl)vinylene based on pyridyl (**4.7**) or thiazolyl groups. These dinuclear boron

compounds have been shown to exhibit strong fluorescence with quantum yields much higher than their mononuclear analogues (Φ = 0.85 for **4.7** vs 0.22 for the mononuclear analogue).[164] Yamashita *et al.* has shown a BF_2 complex which contains an octafluorotetracene moiety (**4.8**) to exhibit *n*-type semiconducting behaviour.[169]

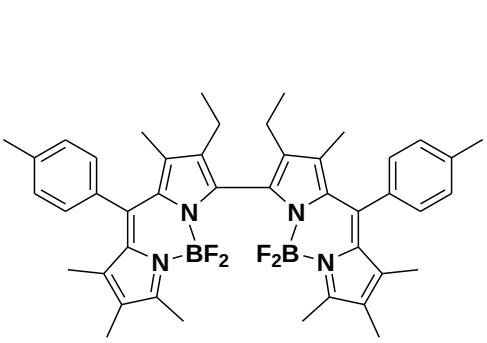

4.6

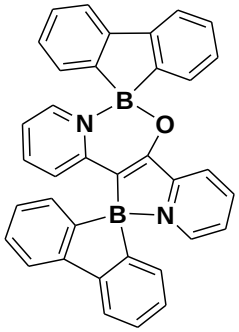

4.7

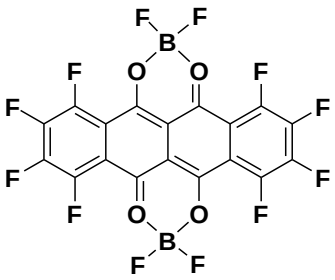

4.8

During the course of our work Zhang and coworkers complexed ligand **2.2** and a similar methylated derivative with boron to give 4 different diboron ladder-type compounds, **4.9-4.12**. These dinuclear boron complexes were shown to be fluorescent and redox active which are reported to be promising candidates as emitters as well as charge-transporting compounds in electroluminescent devices.[110] A mononuclear complex of 2-(pyrid-2-yl)phenol complexed to BPh_2 was also studied (**4.13**). The ligands used in this work were similar to some of those employed in this chapter, but complexes differentiated by the specific substituents on the boron.

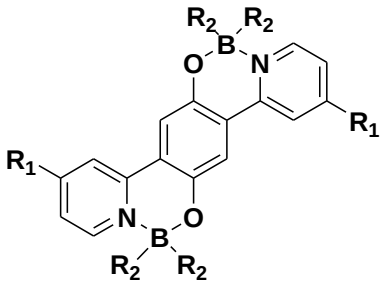

4.9 (R_1 = H, R_2 = Et)
4.10 (R_1 = CH_3, R_2 = Et)
4.11 (R_1 = H, R_2 = Ph)
4.12 (R_1 = CH_3, R_2 = Ph)

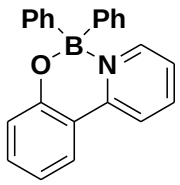

4.13

Among the huge library of boron chelate complexes, the ancillary ligands on boron are most often fluorine and to a lesser extent phenyl. This is mainly the result of the availability of starting materials (ie. BF_3·OEt) and due to the ease of synthesis of complexes containing these ancillary ligands. Although these two popular choices are generally sufficient for many boron complexes, having more options for the ancillary ligand that allow for tailoring of the complexes properties such as solubility, optical and electronic properties is desirable. For example, Ziessel *et al*. have shown that the replacement of the two fluorine atoms in BODIPY with functionalized acetylenic groups opens the doors to a new class of highly luminescent and redox active BODIPY dyes.[170] In this chapter a simple synthesis of luminescent boron complexes of bridging ligands **2.2** and **2.15** utilizing acetate as the ancillary ligand is described. In addition, the luminescence of cross conjugated ladder-type compounds has not been explored. With this in mind the diboron complex of **2.48** was prepared and its physical properties are also reported in this chapter with comparisons to the *para*-hydroquinone diboron complexes that are not cross conjugated and a monoboron diacetate analogue based on 2-(pyrid-2-yl) phenol.

4.3 Synthesis and Characterization of Boron Complexes

4.3.1 Synthesis

There have been very few published examples where boron products containing acetate have been incorporated into the final product. Cotton and Ilsley published the crystal structure of bis(acetato)(acetylacetonato)boron (**4.14**) which was discovered accidently in a reaction containing no acac.[171] Previous work in the Hicks group made use of $B(OAc)_3$ which was generated and used *in situ* to react with formazans to give boratatetrazines (**4.15**).[172] These compounds were stable and could be reduced by cobaltocenium to give the corresponding borataverdazyl radical anions.

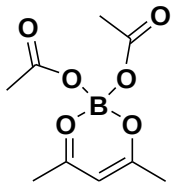

4.14

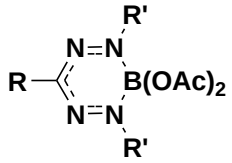

4.15

Using the synthesis of **4.15** as a guide, complexes of boron with *p*-hydroquinones and related ligands were synthesized from $B(OAc)_3$. There has been some controversy with respect to "boron triacetate" in the literature. Initial reports on what was thought to be $B(OAc)_3$ indicated a structure incorporating one boron and three acetates, **4.16**.[173] The isolated compound was later contested to actually be a "pyro" borate structure, **4.17**.[174,175] It is generally now accepted that $B(OAc)_3$ is generated *in situ* and can be isolated as **4.16**, having a reported mp of 120°C which rapidly decomposes to a different compound, **4.17** which has a melting point of 147-148°C.[176]

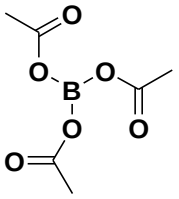

4.16

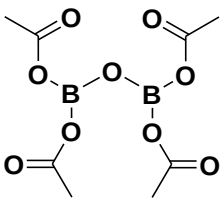

4.17

As a reagent, **4.16** has been used a couple of times successfully as a Lewis acid. For example, in the synthesis of a "dehydrodigalloyl linker unit of agrimoniin-type ellagitannins", boron acetate is used as a Lewis acid in a Diels-Alder reaction[177] and similarly in the synthesis of (±)-6-deoxybrasiliquinone B.[178]

Boron complexes were synthesized by first heating boric acid with acetic acid and acetic anhydride generating an excess of **4.16**. Hydroquinone **2.2** was then dissolved in a mixture of acetic acid/acetic anhydride and added dropwise to the initial mixture of boron acetate with heating for 3 hours (Scheme 4.1). Almost immediately the reaction mixture turned neon yellow with precipitate. The bright yellow product could be isolated by filtration of the precipitate and extraction of the reaction mixture with dichloromethane resulting in a yield of 55%. The product fluoresces yellow/green in solution.

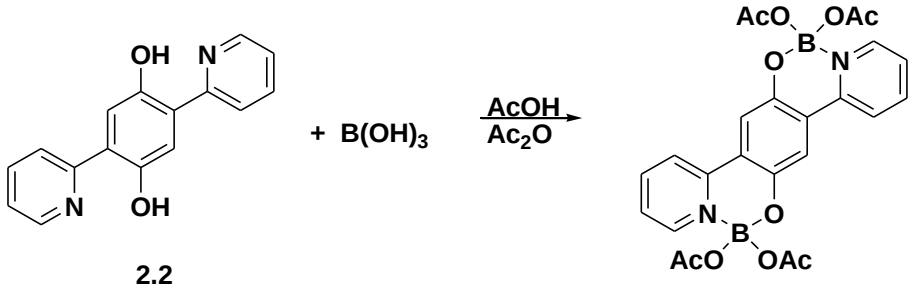

2.2 + $B(OH)_3$ → (AcOH, Ac_2O) → **4.18**

Scheme 4.1 Synthesis of boron acetato complex **4.18**.

The *p*-hydroquinone **2.15** and resorcinol derivative **2.48** were also used in a similar manner to give **4.19** and **4.20** respectively. The mononuclear complex **4.21** was synthesized from 2-(pyrid-2-yl)phenol[179] and studied as a model complex for the diboron complexes.

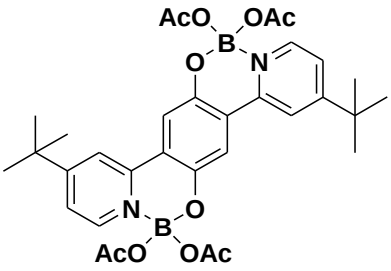

4.19

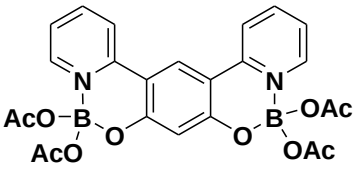

4.20

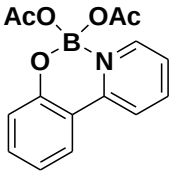

4.21

A second model complex **4.22** was also synthesized in which the acetate ancillary ligands were replaced by fluorines. This fluorinated monoboron compound, **4.22**, has been reported before but incompletely characterized.[180] The reaction of 2-(pyrid-2-yl)phenol (**4.23**) with BF_3•OEt_2 in the presence of triethylamine in DCM resulted in **4.22** (Scheme 4.2). Other BF_2 compounds were targeted such as using hydroquinone **2.15**, however the resulting complex was difficult to purify and characterize due to its poor solubility. This highlights one of the advantages of using acetate as an ancillary ligand, as complexes incorporating acetate have increased solubility in comparison to their fluorinated analogues.

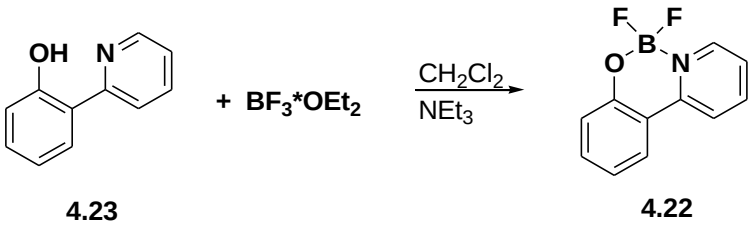

4.23 **4.22**

Scheme 4.2 Synthesis of **4.22**.

The characterization data for complexes **4.18-4.22** is consistent with their proposed structures. All boron acetato compounds **4.18-4.21** are characterized by their ^{11}B NMR spectra, with singlets at ~0.9-1.2 ppm typical of four coordinate boron complexes.[181] The fluorinated analogue **4.20** ^{11}B NMR spectrum consists of a triplet at 0.82 ppm which is comparable to the boron acetato compounds shift but coupled to the two fluorines. The carbonyl of the acetate groups are observed in the complexes ^{13}C NMR spectra at ~172 ppm and in their infrared spectra as a strong absorption in the range of 1700-1720 cm^{-1}. The purity of mononuclear boron acetato complex **4.21** and diboron complex **4.19** was confirmed by HPLC. The purity of **4.21** was particularly important since this compound was used as a standard in the determination of the quantum yields of the other boron complexes. Unfortunately HPLC results for the other boron compounds showed multiple peaks assumed initially to be impurities. However the HPLC data conflicts with the EA and NMR data for these compounds, which suggests they are pure. A more likely explanation for the extra peaks in the HPLC spectra is that these compounds decompose on the HPLC column or in the presence of water which is present in the mobile phase mixture.

4.3.2 X-Ray Structures

X-Ray quality crystals of **4.18** were obtained from dichloromethane layered with hexanes and the structure is displayed in Figure 4.1. The structure of the hydroquinonate ligand of **4.18** is planar, with the boron atom deviating only by 0.025 Å from the ligand plane. The bond distances within the hydroquinone moiety are typical of an aromatic ring while the C1-O1 bond distance is typical of a single bond as summarized in Table 4.1. The dative N1-B1 bond is longer than the covalent boron-oxygen bonds and are consistent with the analogous bond distances in boratatetrazine **4.15**.[172] The boron atoms coordination is a distorted tetrahedral geometry and the acetate groups are orientated in the same direction above and below the plane of the hydroquinone ligand in a similar fashion as **4.15**.

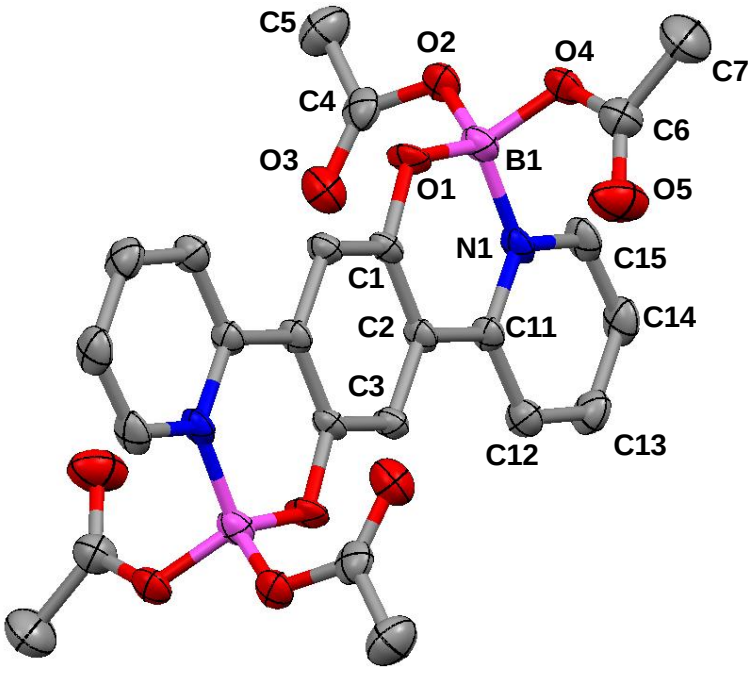

Figure 4.1. Molecular structure of **4.18** with thermal ellipsoids shown at 50% probability level. H atoms have been omitted for clarity.

Table 4.1. Selected bond lengths (Å) and angles (º) for **4.18.**

Atoms	**4.18**	Atoms	**4.18**
Bond lengths		O4-B1	1.466(3)
C1-O1	1.345(2)	*Bond Angles*	
C1-C2	1.387(3)	O1-B1-O2	111.7(2)
C2-C3	1.388(3)	O1-B1-N1	112.00(18)
C1-C3*	1.375(3)	O2-B1-O4	101.91(17)
N1-B1	1.576(3)	O4-B1-N1	109.6(2)
O1-B1	1.427(3)	O1-B1-N1-C15	-177.88(19)
O2-B1	1.451(3)	C12-C11-N1-B1	-179.4(2)

The *tert*-butyl derivative, **4.19**, is much more soluble than any of the other boron compounds. As a result, **4.19** does not precipitate from acetic acid during the synthesis and must be extracted from the reaction mixture. When solvent is removed from a solution of **4.19** a thin film is formed unlike the other boron acetate compounds which all readily form powders. However, recrystallization of **4.19** from DCM/hexane mixtures also resulted in X-ray quality crystals (Figure 4.2). Selected bond distances are summarized in Table 4.2 and are comparable to **4.18**. The structure of **4.19** is not planar; the planes of the pyridine rings are twisted by 11.64^{o} with respect to the plane of the central benzene ring. The boron atom of **4.19** deviates from the plane of the central benzene ring by 0.559 Å, instead being found nearly in the plane of the pyridine ring. The carbonyls of the acetate groups are pointed towards each other in a different orientation than the other boron acetato structures. Unfortunately the *meta* derivative

4.20 has the poorest solubility and despite numerous attempts X-ray quality crystals could not be obtained.

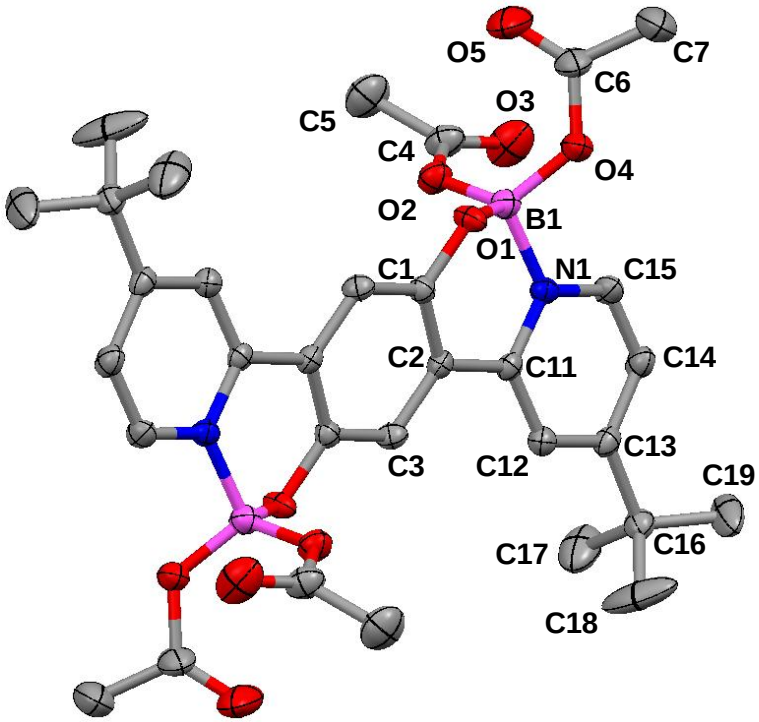

Figure 4.2. Molecular structure of **4.19** with thermal ellipsoids shown at 50% probability level. H atoms have been omitted for clarity.

Table 4.2. Selected bond lengths (Å) and angles (º) for **4.19.**

Atoms	**4.19**	Atoms	**4.19**
Bond lengths		O4-B1	1.455(4)
C1-O1	1.366(3)	*Bond Angles*	
C1-C2	1.402(4)	O1-B1-N1	109.2(2)
C2-C3	1.396(4)	O1-B1-O2	107.0(2)
N1-B1	1.607(4)	O2-B1-O4	117.5(2)
O1-B1	1.430(4)	O1-B1-N1-C15	-152.8(2)
O2-B1	1.469(4)	C12-C11-N1-B1	177.2(2)

X-Ray quality crystals of the monoboron acetato complex **4.21** were obtained from dichloromethane and the structure is shown in Figure 4.3. Bond distances and angles for **4.21** are similar to **4.18** as summarized in Table 4.3. The compound is planar and the boron atom is also in a distorted tetrahedral geometry. The orientation of the acetate groups is also analogous to **4.18**.

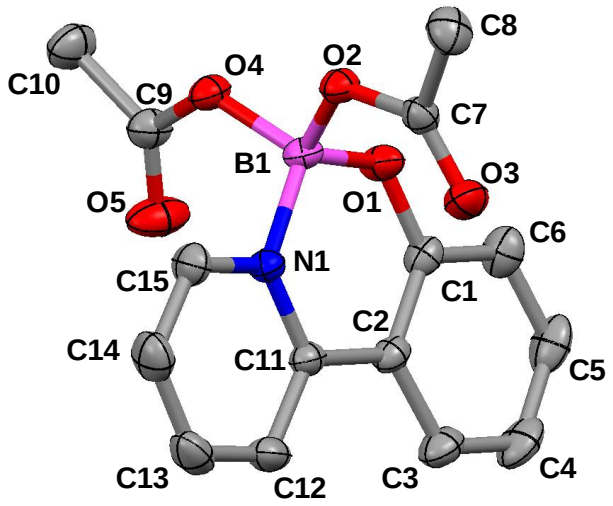

Figure 4.3 Molecular structure of **4.21** with thermal ellipsoids shown at 50% probability level. H atoms have been omitted for clarity.

Table 4.3 Selected bond lengths (Å) and angles (°) for **4.21**

Atoms	**4.21**	Atoms	**4.21**
Bond lengths		O4-B1	1.4688(14)
C1-O1	1.3424(13)	*Bond Angles*	
C1-C2	1.3952(16)	O1-B1-N1	112.03(8)
C2-C3	1.4034(15)	O1-B1-O2	112.23(9)
N1-B1	1.5758(15)	O2-B1-O4	100.95(8)
O1-B1	1.4230(14)	O1-B1-N1-C15	-179.40(10)
O2-B1	1.4719(14)	C12-C11-N1-B1	-178.83(10)

X-ray quality crystals of **4.22** were grown from dichloromethane (Figure 4.4). As was the case with **4.19**, the plane of the pyridyl ring is twisted by 11.61° with respect to the plane of the phenolate ring and the boron is found nearly in the plane of the pyridyl ring. The boron atom is in a distorted tetrahedral geometry and selected bond distances are given in Table 4.4.

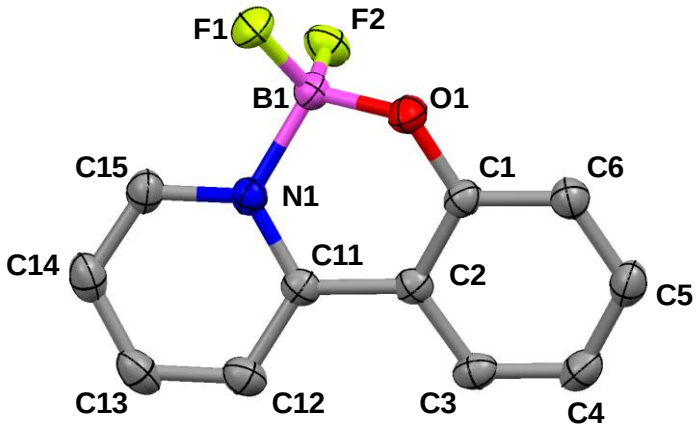

Figure 4.4. Molecular structure of **4.22** with thermal ellipsoids shown at 50% probability level. H atoms have been omitted for clarity.

Table 4.4. Selected bond lengths (Å) and angles (°) for **4.22**

Atoms	**4.22**	Atoms	**4.22**
Bond lengths		F2-B1	1.3864(14)
C1-O1	1.3495(13)	*Bond Angles*	
C1-C2	1.4001(15)	O1-B1-N1	109.44(9)
C2-C3	1.4027(15)	F1-B1-F2	110.59(9)
N1-B1	1.5938(15)	O1-B1-F2	111.99(9)
F1-B1	1.3764(14)	O1-B1-N1-C15	156.34(9)
O1-B1	1.4329(14)	C12-C11-N1-B1	-176.20(10)

4.4 Electrochemistry of Boron Complexes

Cyclic voltammograms of boron complexes **4.18**-**4.22** were obtained. Quasi-reversible oxidation waves are observed for the two *para*-hydroquinone dinuclear boron complexes, **4.18** and **4.19**, at potentials of +1.00 V and +0.95 V respectively (Table 4.5). As expected, the electron donating *tert*-butyl group causes the oxidation of **4.19** to be slightly more facile than **4.18**. The oxidation potentials of **4.18** and **4.19** compared with the redox potentials for the analogous free quinones **2.32** and **2.33** are all shifted to substantially more positive potentials due to the electron withdrawing nature of boron. In comparison to Zhang's diboron phenyl compound **4.11**, the analogous diboron acetato complex **4.18** is oxidized at a higher potential because the phenyl ancillary ligand donates electron density to the boron center resulting in it being less electron withdrawing.[110] It should be noted that Zhang performed their electrochemistry in a different solvent (DCM) but shifts in the redox potentials resulting from changing the solvent medium from CH_3CN to DCM are small enough for this comparison.

For the other boron complexes, **4.20**-**4.22**, no oxidation process is observed within the solvent redox window (CH_3CN, DCM and DMF). Due to the decrease in conjugation for the cross conjugated compound **4.20** and pyridyl-phenolate complexes **4.21**-**4.22**, the oxidized products are expected to be destabilized and found at higher potentials in comparison to **4.18**-**4.19**. Also, Zhang's monoboron compound, **4.13**, is shifted positive by 0.45 V compared to the analogous diboron compound, **4.11**. Therefore, given Zhang's results it is reasonable that the oxidation potentials of complexes **4.20**-**4.22** are not observed given that the more easily oxidized diboron complexes, **4.18**-**4.19**, are oxidized at positive potentials just inside the available solvent window. This result is also an

indication of the cross conjugation of the *meta* complex **4.20** as it behaves more similar to the mononuclear complexes.

Table 4.5 Oxidation potentials (V vs Fc) for boron complexes **4.18** and **4.19**.

Compound		$E_1^{o'}$
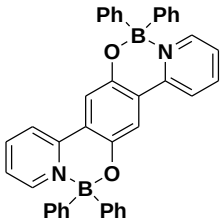	**4.11 (DCM)**[110]	**+0.75**
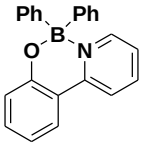	**4.13 (DCM)**[110]	**+1.20**
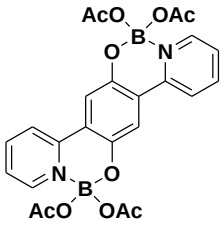	**4.18**	**+1.00*** (E_{1pa} = +1.03, E_{1pc} = +0.97)
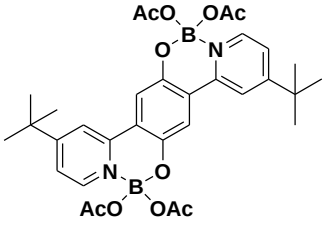	**4.19**	**+0.95*** (E_{1pa} = +1.01, E_{1pc} = +0.90)

~1mM analyte in acetonitrile with 0.1M Bu_4NBF_4 electrolyte.

* quasi-reversible peak

All cyclic voltammograms and their scan rates can be found in Appendix 1: Figure A-67 and Figure A-69.

Reduction processes are also observed for the boron complexes **4.18**-**4.22** and potentials are summarized in Table 4.6. For the *para* dinuclear boron complexes, **4.18**-**4.19**, two reduction waves are observed. The reductions are quasi-reversible and reversibility can be improved above scan rates of 1000 mV/s. The reduction potentials for **4.16**-**4.17** occur at more positive potentials in comparison to that of the free hydroquinone ligands by about 0.6 V. This substantial shift is due to the ligand donating electron density to the boron therefore making it much easier to reduce.

Both of the mononuclear boron complexes, **4.21** and **4.22**, possess one irreversible reduction process. Comparing the redox potentials of the disubstituted complexes **4.18**-**4.19** to the monosubstituted pyridine analogue, **4.21**, the reduction potentials occur at substantially more positive redox values. In this case, the reductions for **4.18**-**4.19** are at more positive potentials and more reversible than for the reduction of **4.21** because of the increase in conjugation for these complexes which helps stabilize the radical anions that result from reduction. In the case of the BF_2 complex, **4.22**, on the return scan an irreversible oxidation wave is also observed. This is not seen for **4.21** although the reason for this difference is unclear.

The poor solubility of **4.20** hampered its electrochemical characterization in acetonitrile. Despite this challenge, one faint irreversible reduction wave is observed at a redox potential very similar to **4.21**. The faint irreversible redox wave for **4.20** has also been confirmed in dichloromethane (-2.09 V vs Fc in DCM), in which the compound has improved solubility. The similar redox potentials for the reduction of the mononuclear boron complex **4.21** and the dinuclear *meta* complex **4.20** is a clear indication of the cross conjugation of the *meta* ligand.

To compare **4.18** electrochemically with Zhang's BPh_2 analogue **4.11** the cyclic voltammogram for **4.18** was also obtained in DMF. The first reduction wave for **4.18** is shifted more positive by 0.12 V in comparison to **4.11**. This is an indication of how the ancillary ligand affects the electron withdrawing ability of the boron center as the more electron donating phenyl ligand makes **4.11** harder to reduce than **4.18**.

Table 4.6. Reduction potentials (V vs Fc) for boron complexes.

Compound	$E_1^{o'}$	$E_2^{o'}$	$\Delta E^{o'}$
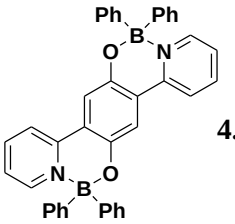 **4.11 (DMF)**[110]	**-1.81**	**~ -2.15**	**~0.34**
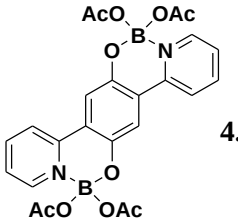 **4.18 (DMF)**	**-1.69** E_{1pa} = *-1.65* E_{1pc} = *-1.73*	**-1.95** E_{2pa} = *-1.91* E_{2pc} = *-1.99*	**0.26**
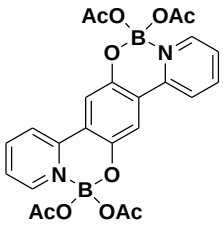 **4.18**	**-1.71** E_{1pa} = *-1.68* E_{1pc} = *-1.75*	**-1.97** E_{2pa} = -1.94 E_{2pc} = -2.01	**0.26**
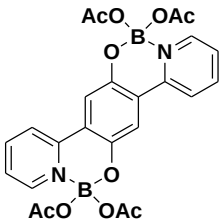 **4.18 (DCM)**	**-1.73** E_{1pa} = *-1.70* E_{1pc} = *-1.77*	**-2.01** E_{2pa} = *-1.97* E_{2pc} = *-2.05*	**0.28**

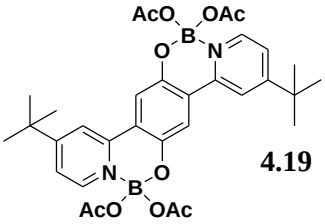	**4.19**	**-1.76** E_{1pa} = *-1.70* E_{1pc} = *-1.81*	**-2.02** E_{2pa} = *-1.95* E_{2pc} = *-2.08*	**0.26**
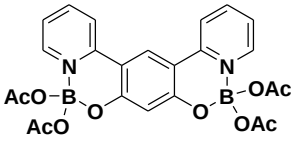	**4.20**	E_{1pc} = *-2.16**	-	-
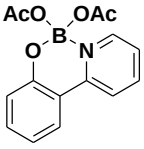	**4.21**	E_{1pc} = *-2.28**	-	-
	**4.22**	E_{1pa} = *-0.89** E_{1pc} = *-2.05**	-	-

~1mM analyte in acetonitrile with 0.1M Bu_4NBF_4 electrolyte, * irreversible peak

All cyclic voltammograms and their scan rates can be found in Appendix 1: Figure A-68 and Figure A-70 to A-74.

4.5 Fluorescence Spectroscopy

4.5.1 Absorbance and emission spectra

The boron complexes all fluoresce in ambient light, so the absorbance and emission spectra of these compounds were obtained. The absorption spectra for **4.18-4.22** are presented in Figure 4.5. The lowest energy band in the absorption spectra of the boron complexes is red-shifted in comparison to the analogous band of the analogous hydroquinone. For example, the lowest energy band for **4.19** is red shifted by 32 nm in comparison to the analogous band for hydroquinone **2.15**. Absorption bands are also red-

shifted for 2-pyrazolyl-anilines complexed to a 4-coordinate boron.[154] Calculations have shown that this red-shift is due to the HOMO being destabilized for the boron complexes.

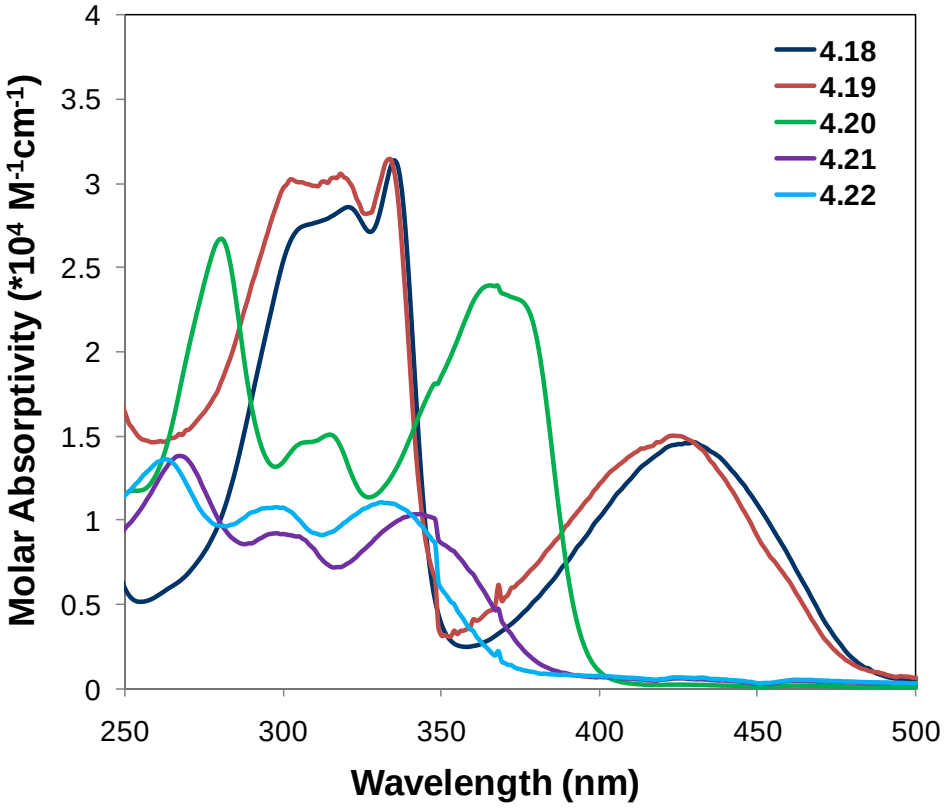

Figure 4.5. Absorption spectra of **4.18**-**4.22** in acetonitrile.

The molar absorptivities of the dinuclear boron complexes are much higher than those of the absorption peaks of the mononuclear boron complexes. The *meta* diboron complex **4.20** and monoboron complexes **4.21**-**4.22** have absorbance and emission bands significantly blue-shifted compared to the two dinuclear *para* complexes **4.18**-**4.19**. The shifting of the bands is consistent with the increased conjugation of **4.18**-**4.19** which results in smaller HOMO-LUMO energy gaps.

The emission spectra of boron complexes **4.18**-**4.22** are shown in Figure 4.6. The electron donating *tert*-butyl groups causes a minimal blue shift of 11 nm when **4.19** is

compared to **4.18**. However, the extended conjugation of **4.18** results in a red-shift of 77 nm in comparison to the monoboron acetato compound **4.21**. On the other hand, the *meta* complex **4.20** is blue-shifted 13 nm in comparison to **4.21,** despite the increase in conjugation for **4.20**. This is consistent with **4.20** being cross conjugated as the small blue-shift of **4.20** is within the range expected from substitution. For example, reports on derivatives of the 8-hydroxyquinoline ligand of *tris*(8-hydroxyquinolinato)aluminum are abundant and generally substitution effects are small for the emission spectra of the complex with a change of ~10 nm regardless of position substituted and extreme shifts up to 35 nm reported only in a few cases.[182] Changing the acetate ancillary ligand to fluorines only has a minimal effect on the absorbance and emission bands. The acetate complex **4.21** has bands slightly red-shifted in comparison to the fluorinated analogue **4.22**.

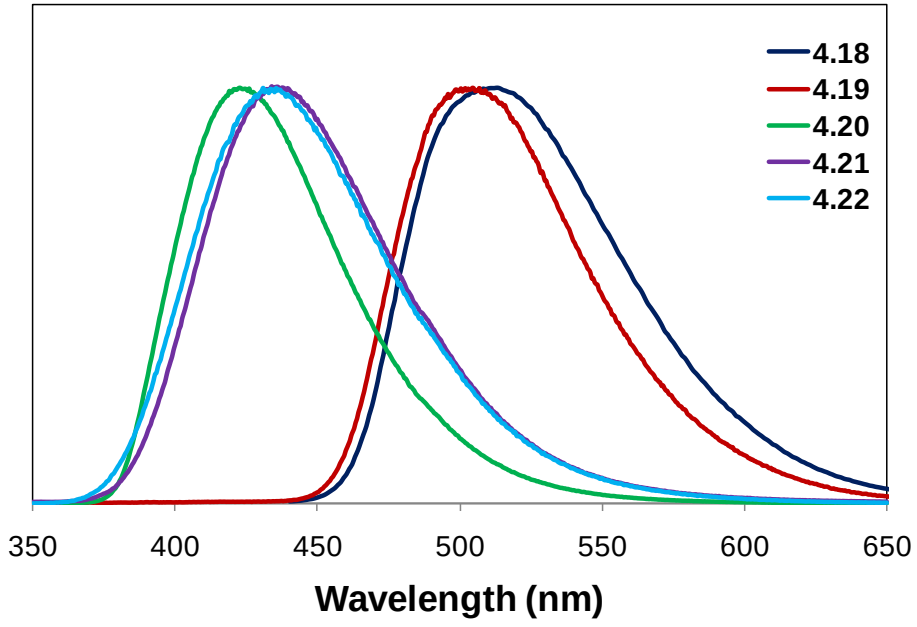

Figure 4.6. Normalized emission spectra of **4.18**-**4.22** in acetonitrile.

Table 4.7. Absorbance λ maxima, emission λ maxima, fluorescence quantum yield (Φ) and singlet state lifetime (τ_s) measurements in acetonitrile.

Compound	Absorbance λ (nm) [ε ($M^{-1}cm^{-1}$)]	Emission λ (nm)	Φ	τ_s (ns)
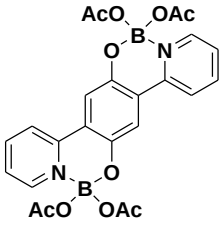 **4.18**	320 [29000], 335 [31000], 430 [15000]	513	0.38 (±0.02)	11.65 (± 0.03)
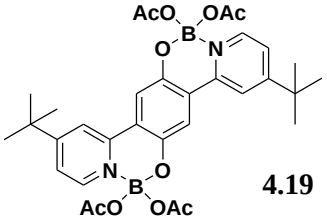 **4.19**	318 [30000], 334 [31000], 422 [15000]	502	0.44 (± 0.01)	10.91 (± 0.02)
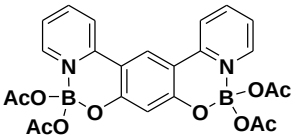 **4.20**	280 [27000], 315 [15000], 368 [24000]	423	0.43 (± 0.01)	2.63 (± 0.01)
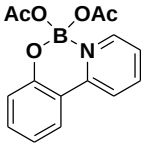 **4.21**	267 [14000], 298 [9000], 343 [10000]	436	0.52 (± 0.01)	9.68 (± 0.02)
 **4.22**	262 [14000], 298 [11000], 330 [11000]	434	0.36 (± 0.02)	6.88 (± 0.01)

4.5.2 Fluorescence quantum yield and lifetime measurements

The quantum yield and lifetime for each boron complex was obtained and this data is summarized in Table 4.7. Quantum yields measured in acetonitrile in the absence of oxygen were found to be between 0.36-0.52 for boron compounds **4.18-4.22**. No clear trends can be associated with the quantum yields of these compounds since many different factors can affect the quantum yield. The monoboron compound **4.21** was found to have the highest quantum yield of 0.52 while the fluorinated analogue, **4.22**, had the lowest quantum yield of 0.36. The difference in the quantum yields of **4.21** and **4.22** is somewhat surprising given that the boron ancillary ligand is not expected to have such a large effect on the quantum yield.

It has been reported that dinuclear boron compounds have higher quantum efficiencies than their mononuclear analogues.[164] However in comparison to **4.21**, all of the dinuclear compounds **4.18-4.22** have slightly lower quantum yields. This follows the same trend reported for Zhang's analogous boron compounds, **4.11-4.13**. Since their measurements were done in a different solvent and it is unclear whether they deoxygenated their samples, direct comparisons with the compounds reported in this thesis cannot be made.

One of the factors that can affect the quantum yield is the alignment of the *p*-orbitals in the π system of the complexes. The twisting of the pyridyl group with respect to the central benzene ring for complexes **4.19** and **4.22** would result in poor alignment of their *p*-orbitals resulting in a lower quantum yield. However, in the case of **4.19** the *tert*-butyl group is electron donating which is known to enhance quantum yields.[183,184] As a result the quantum yield of **4.19** is higher than the quantum yield for **4.18**. These two *para* dinuclear boron compounds were found to have the longest lifetime measurements. On

the other hand, the *meta* analogue, **4.18**, has a similar quantum yield but a much lower fluorescence lifetime.

4.6 Summary

Hydroquinones and related ligands were coordinated to boron diacetato substituents. The extended structure of the two *para* dinuclear boron complexes **4.18** and **4.19** results in these compounds being more easily oxidized or reduced than the mono-substituted boron acetate analogue **4.21**. The *meta* complex, **4.20**, behaves more similar to the mono-substituted boron analogues **4.21** and **4.22**. The oxidation of compounds **4.20-4.22** is not observed and reduction is irreversible occurring at very negative potentials.

The extended delocalization of *para* complexes **4.18** and **4.19** are thought to cause a large red-shift in the absorption and emission spectra although no enhancement is observed in the quantum yields of these dinuclear complexes in comparison to the monoboron compound **4.21**. Despite also having increased conjugation, the *meta* analogue **4.20** behaves more similar to the mono-substituted boron analogue **4.21** spectroscopically. This is likely due to the *meta* complex being cross conjugated. The quantum yields of the boron complexes were in the range between 0.36-0.52, highest for **4.21**. Singlet state lifetime measurements for the complexes were in the range of 2.63-11.65 ns, longest for the *para* compound **4.18** and shortest for the *meta* compound **4.20**.

The acetate ancillary ligand is found to be beneficial for the solubilities of the boron complexes and also advantageous when comparing the quantum yield of **4.21** to the fluorinated analogue **4.22** giving support for the use of acetate as an alternative boron

ancillary ligand. Changing the ancillary ligand from acetate to fluorine has little effect on the complexes redox properties or absorption and emission wavelength.

4.7 Experimental

General experimental aspects can be found in Chapter 2, Section 2.11.

4.7.1 Absorbance and Emission Spectroscopy

Steady-state fluorescence measurements were obtained using a Photon Technology International (PTI) QuantaMaster (QM-2) Luminescence spectrofluorimeter at room temperature. For excitation a 75 W Xenon lamp was used and the slits were set resulting in a bandpass of 2.5 nm for all measurements. Felix software was used to collect the spectra where the step size was set at 0.5 nm and integration time 0.25 s. Solutions were prepared in CH_3CN with the final cell concentration having an absorbance of approximately 0.1 at the excitation wavelength in 1.00 cm x 1.00 cm quartz fluorescence cells. The excitation wavelengths used for all boron compounds studied were between 335-355 nm. The emission scans were recorded between 350 and 650 nm for **4.20**-**4.22**. The two *para*-disubstituted hydroquinone compounds, **4.18** and **4.19** were recorded between 350-750 nm as their emission peaks are red shifted. In each case Raman artifacts from the solvent and baseline were corrected for.

4.7.2 Quantum Yield and Lifetime Measurements

Fluorescence quantum yields were calculated using anthracene as a primary standard for **4.21** and **4.22**. **4.21** was then used as the standard for the other dinuclear boron

compounds and as a secondary standard for **4.22**. Final cell solutions for the quantum yield measurements were prepared to give a matched absorbance (+/- 0.02) of ~0.1 in CH_3CN dearated for 20 min with N_2. The anthracene standard was prepared similarly except in ethanol. Two serial dilutions using the appropriate dearated solvent were made and each set of measurements was completed a second time with a freshly made solution diluted at least once such that a minimum of five data points was obtained which was averaged to give the reported quantum yields.

The following equation (4.1) was used to calculate the quantum yields[185]:

$$\Phi_f = \Phi_s A_s F_u \eta_u^2 / A_u F_s \eta_s^2 \qquad (4.1)$$

Where Φ_x = fluorescence quantum yield of the standard (*s*) or unknown (*u*), A = absorbance at the excitation wavelength, F = area of the emission and η = refractive index of the solvent used.

In ethanol anthracene has a reported quantum yield of $\Phi_f = 0.27$.[186] This was used to calculate a quantum yield of Φ_u =0.52 (+/- 0.01) for **4.21**. Anthracene was picked for the standard as it absorbs in a similar region as **4.21** and its quantum yield allows for both compounds to be measured using the same instrumental parameters (ie. constant slit widths). Using anthracence as the standard for **4.22** the calculated quantum yield was found to be Φ_u =0.34 (+/- 0.01) which compared well to that when **4.21** was used as the secondary standard with Φ_u =0.37 (+/- 0.01). Thus the average value calculated from the two standards for **4.22** was Φ_u = 0.36 (+/- 0.02). **4.21** was then used as the standard for the other 3 dinuclear boron compounds as its absorbance and emission match better than

anthracence. A quantum yield of $\emptyset_u$ = 0.43 (+/- 0.01) was calculated for **4.20**. For **4.18** the quantum yield was found to be $\emptyset_u$ = 0.38 (+/- 0.02). **4.19** had the highest quantum yield of the dinuclear boron compounds with $\emptyset_u$ = 0.44 (+/- 0.01).

Lifetime measurements were performed by Effie Li of Dr. Bohne's group at the University of Victoria using a PTI LS-1 single photon counter with a hydrogen-filled nanosecond-flash lamp. Cell solutions analyzed were prepared in the same way and of the same concentration as those used for the quantum yield measurements.

4.7.3 Synthesis

µ-(2,5-Bis(pyrid-2-yl)-1,4-hydroquinonato)-bis(1,1-diacetato-boron) (4.18).

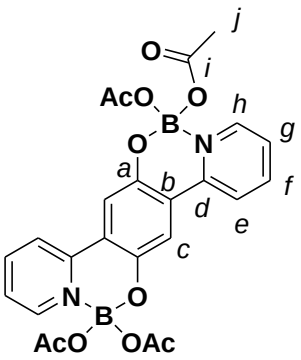

Boric acid (0.50 g, 8.1 mmol) was added to a mixture of acetic acid (2 mL) and acetic anhydride (2 mL) and heated lightly with stirring until all boric acid had dissolved. In a separate Erlenmeyer flask 2,5-bis(pyrid-2-yl)-1,4-hydroquinone (132 mg, 0.50 mmol) was slurried in acetic acid (1 mL) and acetic anhydride (3.8 mL). This solution was then added to the initial solution of boric acid and heated with stirring at ~80^{o}C for 3 hours. After the first 30 min the solution turned bright green and a yellow precipitate was observed. Once the solution had cooled to room temperature the bright yellow precipitate was filtered. The filtrate was extracted with diethyl ether (3 * 30 mL) and then the combined organic extracts were washed with a saturated solution of $Na_2CO_{3\ (aq)}$. The organic layer was dried with $MgSO_4$, filtered and then solvent removed to give more product. The product was purified by column chromatography on alumina using diethyl ether as the eluent. Total yield of pure product

was 144 mg (55% yield). X-Ray quality crystals were obtained by recrystallization from a solution of dichloromethane and hexanes. ^{1}H NMR ($CDCl_3$): δ 8.81 (d, 2H, *J* = 5.7Hz, H-*h*), 8.21-8.11 (m, 4H, H-*e*, *f*), 7.62 (s, 2H, H-*c*), 7.60 (ddd, 2H, *J* = 6.3, 5.7, 1.7Hz, H-*g*), 2.04 (s, 12H, H-*j*) ppm. ^{13}C NMR (125 MHz, $CDCl_3$): δ 172.2 (C-*i*), 149.4 (C-*d*), 148.7 (C-*h*), 143.0 (C-*f*), 142.3 (C-*a*), 123.4 (C-*e*), 121.0 (C-*g*), 120.9 (C-*b*), 115.4 (C-*c*), 23.1 (C-*j*) ppm. ^{11}B NMR (160 MHz, $CDCl_3$): δ 1.14 ppm. FT-IR: (Thin film, NaCl plate) 3083 (w), 2915 (w), 2847 (w), 1705 (s), 1623 (m), 1573 (m), 1512 (s), 1495 (s), 1430 (m), 1373 (m), 1290 (s), 1214 (m), 1171 (m), 1097 (s), 1076 (m), 1059 (s), 1040 (s), 928 (m), 851 (w), 665 (vs) cm^{-1}. Calcld for $C_{24}H_{22}B_2N_2O_{10}$: C, 55.43; H, 4.26; N, 5.39. Found: C, 56.60; H, 4.49; N, 5.24.

μ-(2,5-Bis(4-*tert*-butyl-pyrid-2-yl)-1,4-hydroquinonato)-bis(1,1-diacetato-boron)

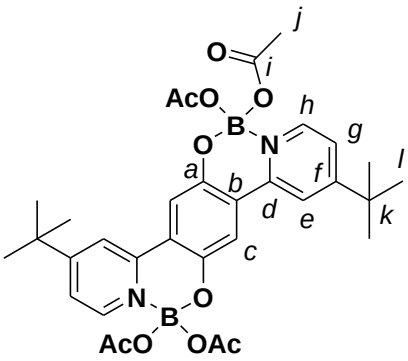

(4.19). Boric acid (0.25 g, 4.0 mmol) was added to a mixture of acetic acid (1 mL) and acetic anhydride (1 mL) and heated lightly with stirring until all boric acid had dissolved. In a separate Erlenmeyer flask 2,5-bis(4-*tert*-butyl-pyrid-2-yl)-1,4-hydroquinone (91 mg, 0.24 mmol) was slurried in acetic acid (0.5 mL) and acetic anhydride (1.9 mL). This solution was then added to the initial solution of boric acid and heated with stirring at ~80 ^{o}C for ~1 hour. After the first 15 min of heating the solution turned bright greenish yellow. After cooling, the solution was extracted with diethyl ether (3 * 30 mL) and then the combined organic extracts were washed with a saturated solution of $Na_2CO_{3\ (aq)}$. The organic layer was dried with $MgSO_4$, filtered and

then the solvent was removed to give a bright yellow powder. The product was purified by column chromatography on alumina using diethyl ether as the eluent. Total yield of pure product was 104 mg (68% yield). X-Ray quality crystals were obtained by recrystallization from a solution of dichloromethane and hexanes. ^{1}H NMR ($CDCl_3$): δ 8.70 (d, 2H, *J* = 6.5Hz, H-*h*), 8.11 (d, 2H, *J* = 1.8Hz, H-*e*), 7.68 (s, 2H, H-*c*), 7.56 (dd, 2H, *J* = 6.5, 1.9Hz, H-*g*), 2.04 (s, 12H, H-*l*), 1.43 (s, 18H, H-*j*) ppm. ^{13}C NMR (125 MHz, $CDCl_3$): δ 172.1 (C-*i*), 167.6 (C-*f*), 148.6 (C-*h*), 148.6 (C-*d*), 142.4 (C-*a*), 121.0 (C-*e*), 120.9 (C-*b*), 117.6 (C-*g*), 115.2 (C-*c*), 36.1(C-*k*), 30.1 (C-*l*), 23.1 (C-*j*) ppm. ^{11}B NMR (160 MHz, $CDCl_3$): δ 1.06 ppm. FT-IR (Thin film, NaCl plate): 3061 (w), 2966 (m), 2873 (w), 1717 (s), 1631 (s), 1550 (s), 1510 (s), 1415 (s), 1371 (s), 1267 (s), 1216 (s), 1142 (s), 1073 (s), 1034 (s), 924 (m), 893 (m), 835 (m), 775 (s), 732 (w), 665 (w) cm^{-1}. Calcld for $C_{32}H_{38}B_2N_2O_{10}$: C, 60.79; H, 6.06; N, 4.43. Found: C, 60.48; H, 6.03; N, 4.59**.**

μ-(4,6-Bis(pyrid-2-yl)-resorcinolato)-bis(1,1-diacetato-boron) (4.20). Boric acid

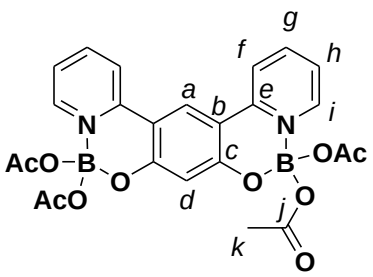

(0.25 g, 4.0 mmol) was added to a mixture of acetic acid (1 mL) and acetic anhydride (1 mL) and heated lightly with stirring until all boric acid had dissolved. In a separate Erlenmeyer flask 4,6-bis(pyrid-2-yl)-benzene-1,3-diol (70 mg, 0.26 mmol) was slurried in acetic acid (0.5 mL) and acetic anhydride (1.9 mL). This solution was then added to the initial solution of boric acid and heated with stirring at ~80 ^{o}C for ~1 hour. After allowing the reaction mixture to cool to room temperature a white precipitate was observed and filtered. The filtrate was extracted with

diethyl ether (3 * 30 mL) and then the combined organic extracts were washed with a saturated solution of $Na_2CO_{3\ (aq)}$. The organic layer was dried with $MgSO_4$, filtered and then solvent removed to give more product. The product was purified by recrystallization from dichloromethane and hexanes. Total yield of pure product was 59 mg (43% yield). ^{1}H NMR ($CDCl_3$): δ 8.56 (d, 2H, *J* = 5.8Hz, H-*i*), 8.35 (s, 1H, H-*a*), 8.2-8.0 (m, 4H, H-*f*, *g*), 7.43 (ddd, 2H, *J* = 7.2, 5.8, 1.5Hz, H-*h*), 6.69 (s, 1H, H-*d*) 2.04 (s, 12H, H-*k*) ppm. ^{13}C NMR (125 MHz, $CDCl_3$): δ 172.2 (C-*j*), 161.5 (C-*e*), 150.5 (C-*c*), 141.6 (C-*i*), 141.6 (C-*g*), 124.0 (C-*a*), 121.8 (C-*f*), 119.2 (C-*h*), 110.0 (C-*b*), 108.3 (C-*d*), 23.2 (C-*k*) ppm. ^{11}B NMR (160 MHz, $CDCl_3$): δ 0.95 ppm. FT-IR (Thin film, NaCl plate): 3084 (w), 3039 (w), 2920 (w), 2845 (w), 1720 (m), 1663 (s), 1618 (s), 1566 (m), 1486 (m), 1435 (w), 1369 (m), 1302 (m), 1289 (s), 1275 (s), 1257 (s), 1202 (s), 1098 (m), 1064 (s), 1030 (s), 902 (w), 876 (w), 851 (w), 785(m), 665 (vs) cm^{-1}. Calcld for $C_{24}H_{22}\ B_2N_2O_{10}$: C, 55.43; H, 4.26; N, 5.39. Found: C, 54.27; H, 4.13; N, 5.25**.**

Bis(1,1-diacetato)-(2-(pyrid-2-yl)-phenolato)-boron (**4.21**). Boric acid (1.0 g, 16 mmol) was added to a mixture of acetic acid (3 mL) and acetic anhydride (3 mL) and heated lightly with stirring. In a separate Erlenmeyer flask, 2-pyrid-2-yl-phenol (180 mg, 1.1 mmol) was slurried in acetic acid (2 mL) and acetic anhydride (7.6 mL). This solution was then added to the initial solution of boric acid and heated with stirring at ~80 ^{o}C for ~1 hour. After allowing the solution to cool to room temperature a white precipitate was observed and filtered. The filtrate was extracted with diethyl ether (3 * 30 mL) and then the combined organic extracts were washed with a saturated solution of

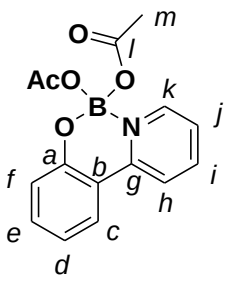

$Na_2CO_{3\ (aq)}$. The organic layer was dried with $MgSO_4$, filtered and then the solvent was removed to give more product. X-Ray quality crystals were obtained by recrystallization from dichloromethane and hexanes. Total yield of pure product was 223 mg (71% yield). ^{1}H NMR ($CDCl_3$): δ 8.64 (d, 1H, *J* = 5.9Hz, H-*k*), 8.16-8.04 (m, 2H, H-*c*, *i*), 7.85 (dd, 1H, *J* = 8.1, 1.6Hz, H-*h*), 7.51-7.41 (m, 2H, H-*d*, *e*), 7.09 (dd, 1H, *J* = 8.4, 1.0Hz, H-*f*), 7.01 (ddd, 1H, *J* = 7.3, 7.1, 1.2Hz, H-*j*) 2.03 (s, 6H, H-*m*) ppm. ^{13}C NMR (125 MHz, $CDCl_3$): δ 172.2 (C-*l*), 156.0 (C-*g*), 151.1 (C-*a*), 141.9 (C-*k*), 141.8 (C-*i*), 134.7 (C-*c*), 125.0 (C-*e*), 122.3 (C-*b*), 120.1 (C-*h*), 119.8 (C-*d*), 119.8 (C-*j*), 115.2 (C-*f*), 23.1 (C-*m*) ppm. ^{11}B NMR (160 MHz, $CDCl_3$): δ 1.16 ppm. FT-IR (Thin film, NaCl plate): 3142 (w), 3109 (w), 3079 (w), 3039 (w), 2976 (w), 2974 (w), 1721 (s), 1702 (s), 1625 (s), 1608 (m), 1587 (m), 1558 (m), 1504 (s), 1485 (m), 1458 (m), 1429 (m), 1374 (m), 1333 (m), 1292 (m), 1275 (s), 1249 (m), 1173 (m), 1157 (w), 1135 (w), 1115 (m), 1096 (m), 1073 (m), 1048 (s), 1042 (s), 945 (m), 925 (s), 852 (m), 769 (m), 754 (m), 666 (m), 632 (m) cm^{-1}. Calcld for $C_{15}H_{14}BNO_5$: C, 60.24; H, 4.72; N, 4.68. Found: C, 60.26; H, 4.67; N, 4.68**.**

Difluoro-(2-(pyrid-2-yl)-phenolato)-boron (**4.22**). 2-Pyrid-2-yl-phenol (500 mg, 2.9 mmol) was added to as solution of anhydrous dichloromethane and deaerated with argon. Triethylamine (1 mL, 7 mmol) was then added causing the clear solution to turn reddish pink. A solution of BF_3*OEt_2 in diethyl ether (46%, 5 mL, 18 mmol) was added by syringe resulting in an orange solution that was stirred for ~10 hours at room temperature. Water was then added and the organic layer was extracted with

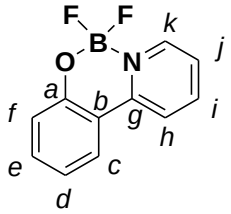

dichloromethane (3 * 30 mL). The organic layer was dried with $MgSO_4$, filtered and then solvent removed to give an orange oil that solidified upon cooling. The solid was recrystallized from dichloromethane to give X-ray quality crystals that were translucent. Total yield of purified product was 166 mg (26% yield). ^{1}H NMR ($CDCl_3$): δ 8.71 (d, 1H, *J* = 5.8Hz, H-*k*), 8.22-8.11 (m, 2H, H-*c*, *i*), 7.83 (dd, 1H, *J* = 8.0, 1.5Hz, H-*h*), 7.58 (ddd, 1H, *J* = 7.3, 6.0, 1.5Hz, H-*d*), 7.50 (ddd, 1H, *J* = 8.6, 7.3, 1.6Hz, H-*e*), 7.19 (dd, 1H, *J* = 8.4, 1.1Hz, H-*f*), 7.05 (ddd, 1H, *J* = 8.2, 7.3, 1.2Hz, H-*j*) ppm. ^{13}C NMR (125 MHz, $CDCl_3$): δ 156.0 (C-*g*), 150.4 (C-*a*), 142.2 (C-*k*), 141.2 (C-*i*), 134.8 (C-*c*), 125.2 (*e*), 122.9 (C-*b*), 120.8 (C-*h*), 120.7 (C-*d*), 120.4 (C-*j*), 115.9 (C-*f*) ppm. ^{11}B NMR (160 MHz, $CDCl_3$): δ 0.82 (t, *J* = 14.8Hz) ppm. FT-IR (Thin film, NaCl plate) 3110 (w), 3045 (w), 2915 (w), 2840(w), 1623 (s), 1605 (s), 1583 (m), 1561 (m), 1503 (s), 1486 (s), 1458 (m), 1433 (s), 1324 (m), 1294 (m), 1261 (m), 1176 (s), 1147 (s), 1117 (vs), 1072 (vs), 932 (s), 760 (vs), 745 (s), 720 (m), 663 (vs) cm^{-1}. Calcld for $C_{11}H_8BF_2NO$: C, 60.33; H, 3.68; N, 6.40. Found: C, 60.26; H, 3.70; N, 6.36**.**

Chapter 5 Conclusions and Future Work

A collection of *para*-hydroquinones and redox related *para*-benzoquinones with bis-bidentate coordination pockets were prepared. The *p*-hydroquinones were substituted in the 2,5-positions with pyrazole, derivatives of pyridine and tertiary amines such as 1-methylpiperidine. Most of these *p*-hydroquinones contained intramolecular hydrogen bonds and can be oxidized reversibly to give stable quinoidal dications, redox behaviour which is distinct from that of non-hydrogen bonded *p*-hydroquinones or *p*-benzoquinones. The coordination chemistry of *p*-hydroquinones and related derivatives with a transition metal, palladium, was examined. The rich redox chemistry of the bridging hydroquinone was preserved and the ligand behaves similarly to *o*-quinones. The coordination chemistry with a main group element, boron, was also examined with these ligands. The boron complexes were very fluorescent and possessed redox properties different from the metal complexes. This work expanded on the library of bis-bidentate *p*-hydroquinones while examining how coordination can perturb the electrochemistry of the ligand.

Initially, the focus of my research was to further expand on the coordination chemistry of *p*-hydroquinones and to this end the syntheses of two literature *p*-hydroquinones **2.1** and **2.2** were optimized. These *p*-hydroquinones contain chelating groups adjacent to the hydroxyl moieties resulting in strong binding to metals. Three new *p*-hydroquinones, **2.15**, **2.19** and **2.29** were also prepared through derivatization of the pyridine groups of **2.2**. Crystal structures of these new hydroquinones indicated the hydroxyl OH groups were intramolecularly hydrogen bound to the adjacent pyridyl groups. By incorporating

an amine non-conjugated with the central benzene ring, a second set of literature hydroquinones **2.27, 2.28** and **2.29** were also prepared. An intramolecular hydrogen bond between the hydroxyl groups and adjacent amine was shown to exist in solution for all *p*-hydroquinones, with the exception of **2.29**. The ^{1}H-NMR of the conjugated hydroquinones, excluding **2.1**, possess chemical shifts in the range of 13-15 ppm for the hydroxyl protons indicating that they have strong intramolecular hydrogen bonds. The OH chemical shifts of the non-conjugated hydroquinones **2.27** and **2.28** are shifted upfield indicating their intramolecular hydrogen bonds are weaker due to the lack of conjugation between the hydrogen bond accepting amines and hydroxyl groups of the hydroquinone. In contrast, there is no intramolecular hydrogen bond in **2.29**, possibly due to the increased degree of conformational flexibility of the bis(cyanoethyl)amine pendant base or the lower basicity of the bis(cyanoethyl)amine. Preparation of the quinone forms of some of these hydroquinones was also performed. The reductions of the derivatized *p*-quinones were similar to *p*-benzoquinone (**1.2),** reduced in two one-electron processes separated by 0.71-0.76 V.

The electrochemistry of the derivatized *p*-hydroquinones proved to be very different in comparison to *p*-hydroquinone (**1.16**) and the derivatized *p*-quinones. With the exception of **2.1** and **2.29**, cyclic voltamemetry showed that all derivatized *p*-hydroquinones can be reversibly oxidized in two overlapping one-electron processes. The oxidation process is thought to be via a CPET process, analogous to the work done by Saveant[48] and Mayer[114]. Hydroquinones with the most basic amines undergo oxidation more easily than those with less basic amines; thus the oxidation potential of the hydroquinone correlates qualitatively with the basicity of the amine hydrogen acceptor. The

irreversibility of the oxidation for **2.1** is thought to be due to the low basicity of the pyrazole group. In the case of **2.29**, irreversibility may be due to it lacking an intramolecular hydrogen bond. Future studies may include the synthesis of new *p*-hydroquinones with different pendant bases to further probe the apparent correlation between the basicity of the hydrogen acceptor and oxidation potential. For example, by adding methyl substituents to the pyrazole groups of **2.1** to give **5.1**, the basicity of the pyrazole would be increased and the oxidation may become reversible. A second example could be the synthesis of *p*-hydroquinone with dimethylbenzylamine in the 2,5-positions (**5.1**) which would have a similar structure to **2.29** with a large degree of conformational flexibility with respect to the pendant base but with a more basic amine than **2.29**. This could help to probe why the intramolecular hydrogen bond is absent in **2.29**.

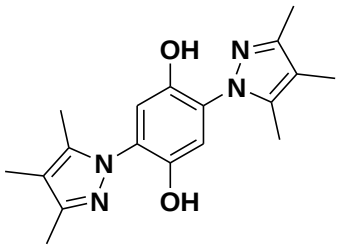

5.1

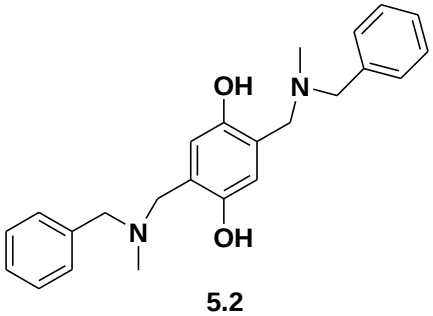

5.2

The reversible oxidations of the derivatized *p*-hydroquinones prompted us to examine the oxidations chemically. For the first time, a new class of *p*-benzoquinone dications were isolated and characterized by chemical oxidation with $NOBF_4$. These *p*-benzoquinone dications resulted from the intramolecular proton transfer of the hydroxyl proton to the adjacent pendant base and possess distinct redox chemistry from normal quinones. Characterization data of the *p*-benzoquinone dications indicate they are also a distinct redox species from the analogous *p*-benzoquinones or *p*-hydroquinones but redox

related to the analogous *p*-hydroquinone as they possess the same electrochemical behaviour. Analysis of solution data for the *p*-benzoquinone dications indicated that the intramolecular hydrogen bond observed in the *p*-hydroquinone was no longer present. The model compound, **2.43**, was also prepared as a methylated bis-piperidinyl quinone dication. Examination of the electrochemical behaviour of **2.43** suggests that the corresponding hydroquinone **2.27** undergoes oxidation at much higher potentials than its quinone form **2.34** because of the positive charges along with the intramolecular proton transfer that occurs upon oxidation. Future work could include studying the kinetics of the chemical oxidation of the *p*-hydroquinones which results in the *p*-quinone dications since these have been shown to be stable. This work would also be beneficial to conclusively prove the proton transfer is by means of a CPET mechanism.

The *meta* analogues to **2.2**, resorcinol derivatives **2.48** and **2.52** were synthesized and characterized. X-ray structures and solution data showed that **2.48** and **2.52** contain intramolecular hydrogen bonds. In contrast to their *para* counterparts, the cyclic voltammetries of **2.48** and **2.52** showed that at high positive potentials they underwent irreversible oxidation. If other coordination complexes of **2.48** are desired, their solubilities could be improved by installing *tert*-butyl groups in the 4-postion to give **5.3** similar to **2.15**.

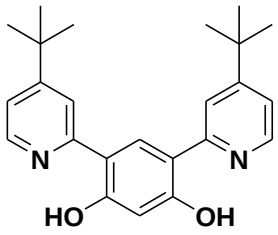

5.3

The chelating *p*-hydroquinones were successfully coordinated to palladium to give dinuclear complexes. Crystal structures obtained along with spectroscopy indicate the bridging ligand is in the hydroquinonate redox state. The reversible redox chemistry of the hydroquinone ligand was preserved but the redox couples were shifted to much higher potentials in comparison to the free ligand. The large shift to higher potentials indicates the palladium ions accepts electron density from the ligand. Changes in the *p*-hydroquinone or ancillary ligand can be used to tune the redox potential of the palladium complexes. More electron rich complexes are oxidized at lower potentials and possess a larger separation between the oxidation processes.

Chemical oxidation of the palladium complexes **3.20** and **3.21** with $AgPF_6$ gives the semiquinone complexes **3.26** and **3.27**. This oxidation is ligand based as indicated by comparisons of the UV-vis spectra for the free bis-pyrazolyl semiquinone **3.25** with those of **3.26** and **3.27**. Additionally, the radical is localized to the semiquinone ligand as indicated by EPR spectroscopy. Thus, the charge-localized electronic structure of **3.26** and **3.27** is similar to the *ortho*-semiquinone complexes of palladium.[53]

The redox state of *o*-quinones in transition metal complexes can be readily assigned from its X-ray crystal structure since the structural features of the different oxidation states are known to differ.[64] Although the same correlation between oxidation state and structural features is expected for *p*-quinones, no X-ray structures of complexes containing *p*-semiquinones or *p*-benzoquinones are known so no correlation can be made. Future work could be the chemical oxidation of complexes **3.22-3.24** to give the semiquinone complexes and see if X-ray quality crystals could be obtained. In particular,

3.23 readily crystallizes and the oxidation product may give the best chance of obtaining X-ray quality crystals of a complex containing the *p*-semiquinone.

Other future work may include the pursuit of dinuclear complexes of paramagnetic metal ions such as cobalt(II). This may result in a complex which displays magnetic phenomena such as valence tautomerism analogous to *ortho*-quinone complexes of cobalt. The *p*-hydroquinone **2.15** has proven to be the best ligand for coordination chemistry as the *tert*-butyl groups increase solubility properties and ease of crystallization for complexes studied. As is such, future work with other metal ions should focus on the coordination chemistry with this ligand. The coordination chemistry of the resorcinol derivatives **2.48** and **2.52** with transition metals has also not been examined. These ligands are expected to coordinate in a similar fashion as **2.2** and dinuclear palladium complexes could be synthesized. The irreversible oxidations of the ligands may become reversible when coordinated with palladium, as was the case for hydroquinone **2.1**.

The coordination chemistry of some of the ligands was all examined with a main group element, boron. The two dinuclear complexes **4.18** and **4.19** containing *p*-hydroquinones were oxidized at high potentials. In comparison the oxidation of the *meta* analogue **4.20** and mononuclear pyridyl-phenolate complexes **4.21** and **4.22** are not observed. The dinuclear complexes **4.18** and **4.19** are also reduced easier than **4.20**-**4.22**, thought to be due to the extended delocalization in the *para* complexes.

The boron complexes were all very fluorescent. The extended delocalization in the *para* complexes **4.18** and **4.19** results in a large red-shift in their excitation and emission spectra. The quantum yields of the boron complexes were high in the range between 0.36-0.52 and the quantum yields of the dinuclear complexes were not enhanced in

comparison to the mononuclear compounds. The acetate ligand in **4.21** was also found to result in a higher quantum yield in comparison to the fluorinated analogue **4.22**. The improved solubility of the complexes containing acetate in conjunction with their quantum yields supports the use of acetate as an alternative boron ancillary ligand.

The electrochemical and spectroscopic data of the *meta* complex **4.20** are a good indication of its cross conjugation as it behaves more similarly to the mononuclear complex **4.21**. By synthesizing **5.3** and subsequently the boron acetate complex, the solubility of the complex could be improved and X-ray quality crystals may be obtained. Other future work could include the coordination chemistry of *p*-hydroquinones with other main group elements like aluminum or even elements such as the lanthanides which could prove to be interesting and to date there are no examples of such complexes found in literature.

References

(1) Patai, S. *The chemistry of the quinonoid compounds* John Wiley and Sons: Interscience: London 1974; Vol. 1.

(2) Patai, S. *The chemistry of the quinonoid compounds*; John Wiley and Sons: Interscience: London, 1974; Vol. 2.

(3) Thomson, R. H. *Pharmacy World & Science*, **1991**, *13*, 70-73.

(4) Cape, J. L.; Bowman, M. K.; Kramer, D. M. *J. Am. Chem. Soc.* **2005**, *127*, 4208-4215.

(5) Brandt, U. *Annu. Rev. Biochem.* **2006**, *75*, 69-92.

(6) Ernster, L.; Dallner, G. *Biochim. Biophys. Acta, Mol. Basis Dis.* **1995**, *1271*, 195-204.

(7) Amesz, J. *Biochim. Biophys. Acta*, **1973**, *301*, 35-51.

(8) Aguilar-Martinez, M.; Macias-Ruvalcaba, N. A.; Bautista-Martinez, J. A.; Gomez, M.; Gonzalez, F. J.; Gonzalez, I. *Curr. Org. Chem.* **2004**, *8*, 1721-1738.

(9) Graige, M. S.; Paddock, M. L.; Bruce, J. M.; Feher, G.; Okamura, M. Y. *J. Am. Chem. Soc.* **1996**, *118*, 9005-9016.

(10) Itoh, S.; Kawakami, H.; Fukuzumi, S. *J. Am. Chem. Soc.* **1998**, *120*, 7271-7277.

(11) Klinman, J. P.; Mu, D. *Annu. Rev. Biochem* **1994**, *63*, 299-344.

(12) Kobori, Y.; Norris, J. R. *J. Am. Chem. Soc.* **2006**, *128*, 4-5.

(13) Lavergen, J.; Matthews, C.; Ginet, N. *Biochemistry* **1999**, *38*, 4542-4552.

(14) Mure, M. *Acc. Chem. Res.* **2004**, *37*, 131-139.

(15) Mure, M.; Wang, S. X.; Klinman, J. P. *J. Am. Chem. Soc.* **2003**, *125*, 6113-6125.

(16) Okamura, M. Y.; Paddock, M. L.; Graige, M. S.; Feher, G. *Biochim. Biophys. Acta, Bioenerg.* **2000**, *1458*, 148-163.

(17) Rao, G. M.; Lown, J. W.; Plambeck, J. A. *J. Electrochem. Soc.* **1978**, *125*, 534-539.

(18) Rich, P. R. *Biochim. Biophys. Acta, Bioenerg.* **2004**, *1658*, 165-171.

(19) Yap, L. L.; Samoilova, R. I.; Gennis, R. B.; Dikanov, S. A. *J. Biol. Chem.* **2006**, *281*, 16879-16887.

(20) Zhang, H. B.; Chobot, S. E.; Osyczka, A.; Wraight, C. A.; Dutton, P. L.; Moser, C. C. *J. Bioenerg. Biomembr.* **2008**, *40*, 493-499.

(21) Zhu, Z. Y.; Gunner, M. R. *Biochemistry*, **2005**, *44*, 82-96.

(22) Ege, S. N. *Organic chemistry*; 4th ed.; Heath: Lexington, Mass., 1998.

(23) Connelly, N. G.; Geiger, W. E. *Chem. Rev.* **1996**, *96*, 877-910.

(24) Bose, D. S.; Idrees, M.; Srikanth, B. *Synthesis*, **2007**, 819-823.

(25) Zanello, P.; Corsini, M. *Coord. Chem. Rev.* **2006**, *250*, 2000-2022.

(26) Muller, O. H.; Baumberger, J. P. *Trans. Electrochem. Soc.* **1937**, *71*, 181-194.

(27) Peover, M. E. *J. Chem. Soc.* **1962**, 4540-&.

(28) Gupta, N.; Linschitz, H. *J. Am. Chem. Soc.* **1997**, *119*, 6384-6391.

(29) Given, P. H.; Peover, M. E. *J. Chem. Soc.* **1960**, 385-393.

(30) Lehmann, M. W.; Evans, D. H. *J. Phys. Chem. B* **2001**, *105*, 8877-8884.

(31) Wightman, R. M.; Cockrell, J. R.; Murray, R. W.; Burnett, J. N.; Jones, S. B. *J. Am. Chem. Soc.* **1976**, *98*, 2562-2570.

(32) Garza, J.; Vargas, R.; Gomez, M.; Gonzalez, I.; Gonzalez, F. J. *J. Phys. Chem. A* **2003**, *107*, 11161-11168.

(33) Macias-Ruvalcaba, N. A.; Gonzalez, I.; Aguilar-Martinez, M. *J. Electrochem. Soc.* **2004**, *151*, E110-E118.

(34) Gomez, M.; Gomez-Castro, C. Z.; Padilla-Martinez, I. I.; Martinez-Martinez, F. J.; Gonzalez, F. J. *J. Electroanal. Chem.* **2004**, *567*, 269-276.

(35) Gomez, M.; Gonzalez, F. J.; Gonzalez, I. *J. Electrochem. Soc.* **2003**, *150*, E527-E534.

(36) Ge, Y.; Lilienthal, R. R.; Smith, D. K. *J. Am. Chem. Soc.* **1996**, *118*, 3976-3977.

(37) Ge, Y.; Miller, L.; Ouimet, T.; Smith, D. K. *J. Org. Chem.* **2000**, *65*, 8831-8838.

(38) Greaves, M. D.; Niemz, A.; Rotello, V. M. *J. Am. Chem. Soc.* **1999**, *121*, 266-267.

(39) Yuasa, J.; Yamada, S.; Fukuzumi, S. *Angew. Chem. Int. Ed.* **2007**, *46*, 3553-3555.

(40) Bailey, S. I.; Ritchie, I. M. *Electrochim. Acta* **1985**, *30*, 3-12.

(41) Quan, M.; Sanchez, D.; Wasylkiw, M. F.; Smith, D. K. *J. Am. Chem. Soc.* **2007**, *129*, 12847-12856.

(42) Bautista-Martinez, J. A.; Gonzalez, I.; Aguilar-Martinez, M. *J. Electroanal. Chem.* **2004**, *573*, 289-298.

(43) Feldman, K. S.; Hester, D. K.; Golbeck, J. H. *Bioorg. Med. Chem. Lett.* **2007**, *17*, 4891-4894.

(44) Aguilar-Martinez, M.; Bautista-Martinez, J. A.; Macias-Ruvalcaba, N.; Gonzalez, I.; Tovar, E.; del Alizal, T. M.; Collera, O.; Cuevas, G. *J. Org. Chem.* **2001**, *66*, 8349-8363.

(45) Sieiro, C.; Sanchez, A.; Crouigneau, P.; Lamy, C. *J. Chem. Soc., Perkin Trans. 2*, **1982**, 1069-1073.

(46) Astudillo, P. D.; Tiburcio, J.; Gonzalez, F. J. *J. Electroanal. Chem.* **2007**, *604*, 57-64.

(47) Amorati, R.; Franchi, P.; Pedulli, G. F. *Angew. Chem. Int. Ed.* **2007**, *46*, 6336-6338.

(48) Costentin, C.; Robert, M.; Saveant, J. M. *J. Am. Chem. Soc.* **2006**, *128*, 8726-8727.

(49) Costentin, C. *Chem. Rev.* **2008**, *108*, 2145-2179.

(50) Avdeef, A.; Sofen, S. R.; Bregante, T. L.; Raymond, K. N. *J. Am. Chem. Soc.* **1978**, *100*, 5362-5370.

(51) Pierpont, C. G.; Buchanan, R. M. *Coord. Chem. Rev.* **1981**, *38*, 45-87.

(52) Bhattacharya, S.; Boone, S. R.; Fox, G. A.; Pierpont, C. G. *J. Am. Chem. Soc.* **1990**, *112*, 1088-1096.

(53) Fox, G. A.; Pierpont, C. G. *Inorg. Chem.* **1992**, *31*, 3718-3723.

(54) Kharisov, B. I.; Mendez-Rojas, M. A.; Garnovskii, A. D.; Ivakhnenko, E. P.; Ortiz-Mendez, U. *J. Coord. Chem.* **2002**, *55*, 745-770.

(55) Raymond, K. N.; Carrano, C. J. *Acc. Chem. Res.* **1979**, *12*, 183-190.

(56) Holt, B. T. O.; Vance, M. A.; Mirica, L. M.; Heppner, D. E.; Stack, T. D. P.; Solomon, E. I. *J. Am. Chem. Soc.* **2009**, *131*, 6421-6438.

(57) Feigl;, F.; Furth, M. *Montash,* **1927**, *48*, 445.

(58) McCleverty, J. A. *Prog. Inorg. Chem.* **1968**, *10*, 49-221.

(59) Schrauze.Gn *Acc. Chem. Res.* **1969**, *2*, 72-&.

(60) Stiefel, E. I.; Waters, J. H.; Billig, E.; Gray, H. B. *J. Am. Chem. Soc.* **1965**, *87*, 3016-&.

(61) Balch, A. L.; Holm, R. H. *J. Am. Chem. Soc.* **1966**, *88*, 5201-&.

(62) Buchanan, R. M.; Wilsonblumenberg, C.; Trapp, C.; Larsen, S. K.; Greene, D. L.; Pierpont, C. G. *Inorg. Chem.* **1986**, *25*, 3070-3076.

(63) Jorgensen, C. K. *Oxidation Numbers and Oxidation States*; Springer: Heidelberg, Germany, 1969.

(64) Carugo, O.; Castellani, C. B.; Djinovic, K.; Rizzi, M. *J. Chem. Soc., Dalton Trans.* **1992**, 837-841.

(65) Shultz, D. A. *Comments Inorg. Chem.* **2002**, *23*, 1-21.

(66) Kahn, O.; Prins, R.; Reedijk, J.; Thompson, J. S. *Inorg. Chem.* **1987**, *26*, 3557-3561.

(67) Dei, A.; Gatteschi, D.; Sangregorio, C.; Sorace, L. *Acc. Chem. Res.* **2004**, *37*, 827-835.

(68) Hendrickson, D. N.; Pierpont, C. G. *Top. Curr. Chem.*, 2004; Vol. 234.

(69) Ruiz, D.; Yoo, J.; Guzei, I. A.; Rheingold, A. L.; Hendrickson, D. N. *Chem. Commun.* **1998**, 2089-2090.

(70) Suenaga, Y.; Pierpont, C. G. *Inorg. Chem.* **2005**, *44*, 6183-6191.

(71) Glick, M. D.; Dahl, L. F. *J. Organomet. Chem.* **1965**, *3*, 200-&.

(72) Drouza, C.; Tolis, V.; Gramlich, V.; Raptopoulou, C.; Terzis, A.; Sigalas, M. P.; Kabanos, T. A.; Keramidas, A. D. *Chem. Commun.* **2002**, 2786-2787.

(73) Thorum, M. S.; Taliaferro, M. L.; Min, K. S.; Miller, J. S. *Polyhedron*, **2007**, *26*, 2247-2251.

(74) Leane, D.; Keyes, T. E. *Inorg. Chim. Acta* **2006**, *359*, 1627-1636.

(75) Dinnebier, R.; Lerner, H. W.; Ding, L.; Shankland, K.; David, W. I. F.; Stephens, P. W.; Wagner, M. *Z. Anorg. Allg. Chem.* **2002**, *628*, 310-314.

(76) Margraf, G.; Kretz, T.; de Biani, F. F.; Laschi, F.; Losi, S.; Zanello, P.; Bats, J. W.; Wolf, B.; Removic-Langer, K.; Lang, M.; Prokofiev, A.; Assmus, W.; Lerner, H. W.; Wagner, M. *Inorg. Chem.* **2006**, *45*, 1277-1288.

(77) Kitagawa, S.; Kawata, S. *Coord. Chem. Rev.* **2002**, *224*, 11-34.

(78) Min, K. S.; Rheingold, A. L.; Miller, J. S. *J. Am. Chem. Soc.* **2006**, *128*, 1770-1770.

(79) Min, K. S.; Rheingold, A. L.; DiPasquale, A.; Miller, J. S. *Inorg. Chem.* **2006**, *45*, 6135-6137.

(80) Min, K. S.; DiPasquale, A. G.; Golen, J. A.; Rheingold, A. L.; Miller, J. S. *J. Am. Chem. Soc.* **2007**, *129*, 2360-2368.

(81) Carbonera, C.; Dei, A.; Letard, J. F.; Sangregorio, C.; Sorace, L. *Angew. Chem. Int. Ed.* **2004**, *43*, 3136-3138.

(82) Tao, J.; Maruyama, H.; Sato, O. *J. Am. Chem. Soc.* **2006**, *128*, 1790-1791.

(83) Kawata, S.; Kitagawa, S.; Kondo, M.; Furuchi, I.; Munakata, M. *Angew. Chem. Int. Ed.* **1994**, *33*, 1759-1761.

(84) Manriquez, J. M.; Yee, G. T.; Mclean, R. S.; Epstein, A. J.; Miller, J. S. *Science*, **1991**, *252*, 1415-1417.

(85) Jain, R.; Kabir, K.; Gilroy, J. B.; Mitchell, K. A. R.; Wong, K. C.; Hicks, R. G. *Nature*, **2007**, *445*, 291-294.

(86) Catalan, J.; Fabero, F.; Guijarro, M. S.; Claramunt, R. M.; Maria, M. D. S.; Focesfoces, M. D.; Cano, F. H.; Elguero, J.; Sastre, R. *J. Am. Chem. Soc.* **1990**, *112*, 747-759.

(87) Shu, W. M.; Valiyaveettil, S. *Chem. Commun.* **2002**, 1350-1351.

(88) Baltzly, R.; Lorz, E. *J. Am. Chem. Soc.* **1948**, *70*, 861.

(89) Desiraju., G. R.; Steiner, T. *The weak hydrogen bond in structural chemistry and biology*; Oxford University Press/International Union of Crystallography: Oxford, 1999; Vol. 9.

(90) Lopez-Alvarado, P.; Avendano, C.; Menendez, J. C. *Synth. Commun.* **2002**, *32*, 3233-3239.

(91) Monkman, A. P.; Palsson, L. O.; Higgins, R. W. T.; Wang, C. S.; Bryce, M. R.; Batsanov, A. S.; Howard, J. A. K. *J. Am. Chem. Soc.* **2002**, *124*, 6049-6055.

(92) Barolo, C.; Nazeeruddin, M. K.; Fantacci, S.; Di Censo, D.; Comte, P.; Liska, P.; Viscardi, G.; Quagliotto, P.; De Angelis, F.; Ito, S.; Gratzel, M. *Inorg. Chem.* **2006**, *45*, 4642-4653.

(93) Cuperly, D.; Gros, P.; Fort, Y. *J. Org. Chem.* **2002**, *67*, 238-241.

(94) Saa, J. M.; Martorell, G.; Garciaraso, A. *J. Org. Chem.* **1992**, *57*, 678-685.

(95) Segelstein, B. E.; Butler, T. W.; Chenard, B. L. *J. Org. Chem.* **1995**, *60*, 12-13.

(96) Kelly, T. R.; Cavero, M. *Org. Lett.* **2002**, *4*, 2653-2656.

(97) Markey, M. D.; Kelly, T. R. *Tetrahedron*, **2008**, *64*, 8381-8388.

(98) Zhang, G.; Zong, R.; Tseng, H. W.; Thummel, R. P. *Inorg. Chem.* **2008**, *47*, 990-998.

(99) Shin, D. W.; Switzer, C. *Chem. Commun.* **2007**, 4401-4403.

(100) Rhile, I. J.; Markle, T. F.; Nagao, H.; DiPasquale, A. G.; Lam, O. P.; Lockwood, M. A.; Rotter, K.; Mayer, J. M. *J. Am. Chem. Soc.* **2006**, *128*, 6075-6088.

(101) Yuan, D. Y.; Zhang, M. J.; Pan, Z. H.; Ma, P. G. *Acta Crystallogr., Sect. E: Struct. Rep. Online*, **2004**, *60*, O1321-O1322.

(102) Fields, D. L.; Reynolds, D. D.; Miller, J. B. *J. Org. Chem.* **1964**, *29*, 2640-&.

(103) Burke, W. J.; Brown, J. E.; Weatherbee, C.; Curtis, D. H. *J. Med. Chem.* **1964**, *7*, 670-&.

(104) Ma, P. G.; Zhang, M. H.; Yang, Q. C.; Yu, J. G. *Chin. J. Struct. Chem.* **2005**, *24*, 311-314.

(105) Gilli, P.; Bertolasi, V.; Ferretti, V.; Gilli, G. *J. Am. Chem. Soc.* **2000**, *122*, 10405-10417.

(106) Lerner, H. W.; Margraf, G.; Kretz, T.; Schiemann, O.; Bats, J. W.; Durner, G.; de Biani, F. F.; Zanello, P.; Bolte, M.; Wagner, M. *Z. Naturforsch., B: Chem. Sci.* **2006**, *61*, 252-264.

(107) Kuboyama, A.; Yamazaki, R.; Yabe, S.; Uehara, Y. *Bull. Chem. Soc. Jpn.* **1969**, *42*, 10-&.

(108) Wilford, J. H.; Archer, M. D. *J. Electroanal. Chem.* **1985**, *190*, 271-277.

(109) Swain, C. G.; Swain, M. S.; Powell, A. L.; Alunni, S. *J. Am. Chem. Soc.* **1983**, *105*, 502-513.

(110) Zhang, Z. L.; Bi, H.; Zhang, Y.; Yao, D. D.; Gao, H. Z.; Fan, Y.; Zhang, H. Y.; Wang, Y.; Wang, Y. P.; Chen, Z. Y.; Ma, D. G. *Inorg. Chem.* **2009**, *48*, 7230-7236.

(111) Maki, T.; Araki, Y.; Ishida, Y.; Onomura, O.; Matsumura, Y. *J. Am. Chem. Soc.* **2001**, *123*, 3371-3372.

(112) Kanamori, D.; Furukawa, A.; Okamura, T.; Yamamoto, H.; Ueyama, N. *Org. Biomol. Chem.* **2005**, *3*, 1453-1459.

(113) Thomas, F.; Jarjayes, O.; Jamet, M.; Hamman, S.; Saint-Aman, E.; Duboc, C.; Pierre, J. L. *Angew. Chem. Int. Ed.* **2004**, *43*, 594-597.

(114) Rhile, I. J.; Mayer, J. M. *J. Am. Chem. Soc.* **2004**, *227*, U1545-U1545.

(115) Costentin, C.; Robert, M.; Saveant, J. M. *J. Am. Chem. Soc.* **2007**, *129*, 9953-9963.

(116) Kalanara.V; Rao, C. N. R.; George, M. V. *J. Chem. Soc. B* **1971**, 2406-&.

(117) Randles, J. E. B. *Trans. Faraday Soc.* **1948**, *44*, 327-38.

(118) Sevcik, A. *Collect. Czech. Chem. Commun.* **1948**, *13*, 349-77.

(119) Zia-ur-Rehman; Shah, A.; Muhammad, N.; Ali, S.; Qureshi, R.; Butler, I. S. *J. Organomet. Chem.* **2009**, *694*, 1998-2004.

(120) Gosting, L. J.; Harned, H. S. *J. Am. Chem. Soc.* **1951**, *73*, 159-61.

(121) Ikeuchi, H.; Naganuma, K.; Ichikawa, M.; Ozawa, H.; Ino, T.; Sato, M.; Yonezawa, H.; Mukaida, S.; Yamamoto, A.; Hashimoto, T. *J. Solution Chem.* **2007**, *36*, 1243-1259.

(122) Gill, N. S.; Nuttall, R. H.; Scaife, D. E.; Sharp, D. W. A. *J. Inorg. Nucl. Chem.* **1961**, *18*, 79-87.

(123) Del Bene, J. E.; Perera, S. A.; Bartlett, R. J. *J. Phys. Chem. A* **1999**, *103*, 8121-8124.

(124) Delpuech, J. J.; Mn., D. *Tetrahedron*, **1970**, *26*, 2723-&.

(125) Markle, T. F.; Mayer, J. M. *Angew. Chem. Int. Ed.* **2008**, *47*, 738-740.

(126) Catalan, J.; Elguero, J. *J. Chem. Soc., Perkin Trans. 2*, **1983**, 1869-1874.

(127) Brown, H. C.; Mihm, X. R. *J. Am. Chem. Soc.* **1955**, *77*, 1723-1726.

(128) Joris, L.; Mitsky, J.; Taft, R. W. *J. Am. Chem. Soc.* **1972**, *94*, 3438-&.

(129) Hall, H. K. *J. Am. Chem. Soc.* **1957**, *79*, 5441-5444.

(130) Stevenson, G. W.; Williamson, D. *J. Am. Chem. Soc.* **1958**, *80*, 5943-5947.

(131) Rhile, I. J.; Mayer, J. M. *Angew. Chem. Int. Ed.* **2005**, *44*, 1598-1599.

(132) Phelan, N. F.; Orchin, M. *J. Chem. Educ.* **1968**, *45*, 633-&.

(133) Nierengarten, H.; Rojo, J.; Leize, E.; Lehn, J. M.; Van Dorsselaer, A. *Eur. J. Inorg. Chem.* **2002**, 573-579.

(134) Kiehlmann, E.; Lauener, R. W. *Can. J. Chem.* **1989**, *67*, 335-344.

(135) Becht, J. M.; Gissot, A.; Wagner, A.; Mioskowski, C. *Chem.- Eur. J.* **2003**, *9*, 3209-3215.

(136) Keyes, T. E.; Jayaweera, P. M.; McGarvey, J. J.; Vos, J. G. *J. Chem. Soc., Dalton Trans.* **1997**, 1627-1632.

(137) Keyes, T. E.; Forster, R. J.; Jayaweera, P. M.; Coates, C. G.; McGarvey, J. J.; Vos, J. G. *Inorg. Chem.* **1998**, *37*, 5925-5932.

(138) Swodenk, W.; Scharfe, G.; (Bayer A.-G.). Application: US US, 1974, p 2 pp.

(139) Siedle, A. R. *Inorg. Synth.* **1990**, *27*, 317-21.

(140) Krisyuk, V. V.; Turgambaeva, A. E.; Rhee, S. W. *Polyhedron*, **2004**, *23*, 809-813.

(141) Senftleber, F. C.; Geiger, W. E. *Inorg. Chem.* **1978**, *17*, 3615-3622.

(142) Chaudhuri, P.; Verani, C. N.; Bill, E.; Bothe, E.; Weyhermuller, T.; Wieghardt, K. *J. Am. Chem. Soc.* **2001**, *123*, 2213-2223.

(143) Herebian, D.; Bothe, E.; Neese, F.; Weyhermuller, T.; Wieghardt, K. *J. Am. Chem. Soc.* **2003**, *125*, 9116-9128.

(144) Kokatam, S. L.; Chaudhuri, P.; Weyhermuller, T.; Wieghardt, K. *Dalton Trans.* **2007**, 373-378.

(145) Miller, J. S.; Krusic, P. J.; Dixon, D. A.; Reiff, W. M.; Zhang, J. H.; Anderson, E. C.; Epstein, A. J. *J. Am. Chem. Soc.* **1986**, *108*, 4459-4466.

(146) Vazquez, C.; Calabrese, J. C.; Dixon, D. A.; Miller, J. S. *J. Org. Chem.* **1993**, *58*, 65-81.

(147) Hartl, F.; Vlcek, A. *Inorg. Chem.* **1996**, *35*, 1257-1265.

(148) Benelli, C.; Dei, A.; Gatteschi, D.; Pardi, L. *Inorg. Chem.* **1989**, *28*, 1476-1480.

(149) Treibs, A.; Kreuzer, F. H. *Annalen Der Chemie-Justus Liebig*, **1968**, *718*, 208-&.

(150) Ulrich, G.; Ziessel, R.; Harriman, A. *Angew. Chem. Int. Ed.* **2008**, *47*, 1184-1201.

(151) Loudet, A.; Burgess, K. *Chem. Rev.* **2007**, *107*, 4891-4932.

(152) Li, Y. Q.; Liu, Y.; Bu, W. M.; Guo, J. H.; Wang, Y. *Chem. Commun.* **2000**, 1551-1552.

(153) Liu, Q. D.; Mudadu, M. S.; Thummel, R.; Tao, Y.; Wang, S. N. *Adv. Funct. Mater.* **2005**, *15*, 143-154.

(154) Liddle, B. J.; Silva, R. M.; Morin, T. J.; Macedo, F. P.; Shukla, R.; Lindeman, S. V.; Gardinier, J. R. *J. Org. Chem.* **2007**, *72*, 5637-5646.

(155) Liu, S.-F.; Wu, Q.; Schmider, H. L.; Aziz, H.; Hu, N.-X.; Popovic, Z.; Wang, S. *J. Am. Chem. Soc.* **2000**, *122*, 3671-3678.

(156) Liu, Y.; Guo, J. H.; Zhang, H. D.; Wang, Y. *Angew. Chem. Int. Ed.* **2002**, *41*, 182-184.

(157) Jia, W. L.; Moran, M. J.; Yuan, Y.-Y.; Lu, Z. H.; Wang, S. *J. Mater. Chem.* **2005**, *15*, 3326-3333.

(158) Ziessel, R.; Ulrich, G.; Harriman, A. *New J. Chem.* **2007**, *31*, 496-501.

(159) Yamaguchi, S.; Akiyama, S.; Tamao, K. *J. Am. Chem. Soc.* **2001**, *123*, 11372-11375.

(160) Kennedy, D. P.; Kormos, C. M.; Burdette, S. C. *J. Am. Chem. Soc.* **2009**, *131*, 8578-8586.

(161) Branger, C.; Lequan, M.; Lequan, R. M.; Barzoukas, M.; Fort, A. *J. Mater. Chem.* **1996**, *6*, 555-558.

(162) Benniston, A. C.; Copley, G. *PCCP* **2009**, *11*, 4124-4131.

(163) Broring, M.; Kruger, R.; Link, S.; Kleeberg, C.; Kohler, S.; Xie, X.; Ventura, B.; Flamigni, L. *Chem.-Eur. J.* **2008**, *14*, 2976-2983.

(164) Zhao, Q.; Zhang, H. Y.; Wakamiya, A.; Yamaguchi, S. *Synthesis*, **2009**, 127-132.

(165) Scherf, U. *J. Mater. Chem.* **1999**, *9*, 1853-1864.

(166) Stampfl, J.; Graupner, W.; Leising, G.; Scherf, U. *J. Lumin.* **1995**, *63*, 117-123.

(167) Yamaguchi, S.; Xu, C. H.; Tamao, K. *J. Am. Chem. Soc.* **2003**, *125*, 13662-13663.

(168) Fukazawa, A.; Yamada, H.; Yamaguchi, S. *Angew. Chem. Int. Ed.* **2008**, *47*, 5582-5585.

(169) Ono, K.; Hashizume, J.; Yamaguchi, H.; Tomura, M.; Nishida, J.; Yamashita, Y. *Org. Lett.* **2009**, *11*, 4326-4329.

(170) Goze, C.; Ulrich, G.; Ziessel, R. *J. Org. Chem.* **2007**, *72*, 313-322.

(171) Cotton, F. A.; Ilsley, W. H. *Inorg. Chem.* **1982**, *21*, 300-302.

(172) Gilroy, J. B.; Ferguson, M. J.; McDonald, R.; Patrick, B. O.; Hicks, R. G. *Chem. Commun.* **2007**, 126-128.

(173) Pictet, A.; Karl, G. *Bull. Soc. Chim. France* **1908**, *3*, 1114.

(174) Gerrard, W.; Wheelans, M. A. *Chem. Ind. (London, U. K.)* **1954**, 758-9.

(175) Hayter, R. G.; Laubengayer, A. W.; Thompson, P. G. *J. Am. Chem. Soc.* **1957**, *79*, 4243-4244.

(176) Lalancet.Jm; Bessette, F.; Cliche, J. M. *Can. J. Chem.* **1966**, *44*, 1577-&.

(177) Feldman, K. S.; Quideau, S.; Appel, H. M. *J. Org. Chem.* **1996**, *61*, 6656-6665.

(178) Krohn, K.; Micheel, J.; Zukowski, M. *Tetrahedron*, **2000**, *56*, 4753-4758.

(179) Maeyama, K.; Kobayashi, M.; Yonezawa, N. *Synth. Commun.* **2001**, *31*, 869-875.

(180) Ye, K.-q. *Jilin Daxue Xuebao, Lixueban*, **2005**, *43*, 219.

(181) Qian, B. X.; Baek, S. W.; Smith, M. R. *Polyhedron*, **1999**, *18*, 2405-2414.

(182) Chen, C. H.; Shi, J. M. *Coord. Chem. Rev.* **1998**, *171*, 161-174.

(183) Han, M. R.; Hirayama, Y.; Hara, M. *Chem. Mater.* **2006**, *18*, 2784-2786.

(184) Gao, B.; Liu, Y.; Geng, Y.; Cheng, Y.; Wang, L.; Jing, X.; Wang, F. *Tetrahedron Lett.* **2009**, *50*, 1649-1652.

(185) *Handbook of Organic Photochemistry*; Eaton, D. F., Ed.; CRC Press: : Boca Ralton
1989; Vol. 1.

(186) Wright, F. J. *J. Phys. Chem.* **1961**, *65*, 381-&.

Appendix

Appendix I - Cyclic Voltammograms

~1mM analyte in acetonitrile with 0.1M Bu_4NBF_4 electrolyte unless noted otherwise.

Peaks resulting from ferrocene standard or ferrocene derivative denoted with * (octamethylferrocene = -0.41 V vs Fc and decamethylferrocene = -0.50V vs Fc).

Appendix II - Crystallographic Data

Appendix III: Complete listings of bond lengths and angles

List of Figures - Appendix

List of Tables - Appendix

Appendix I: Cyclic Voltammograms

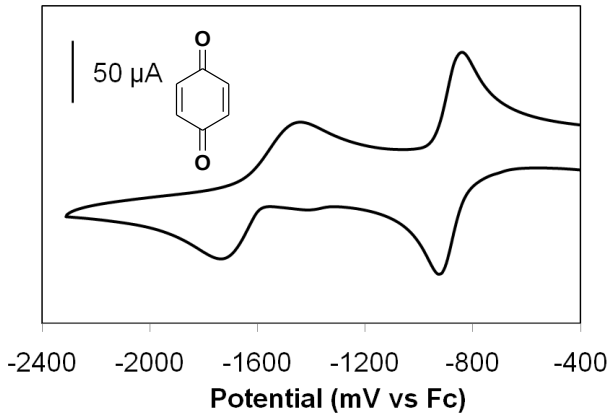

Figure A-1. 1.2 (2mM), 250 mV/s.

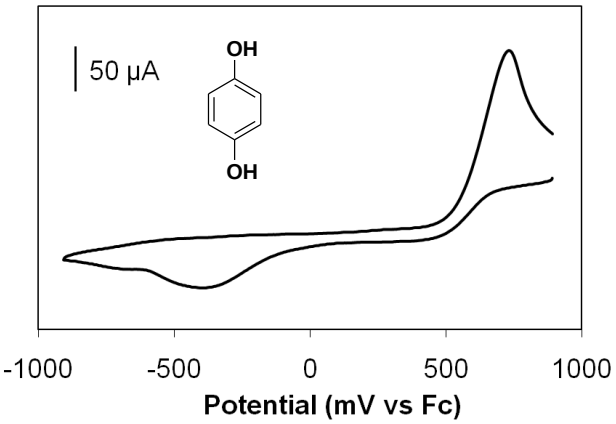

Figure A-2. 1.16 (2mM), 300 mV/s.

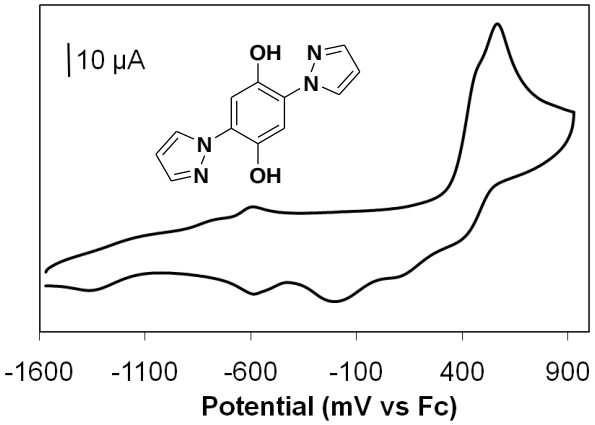

Figure A-3. 2.1, 200 mV/s.

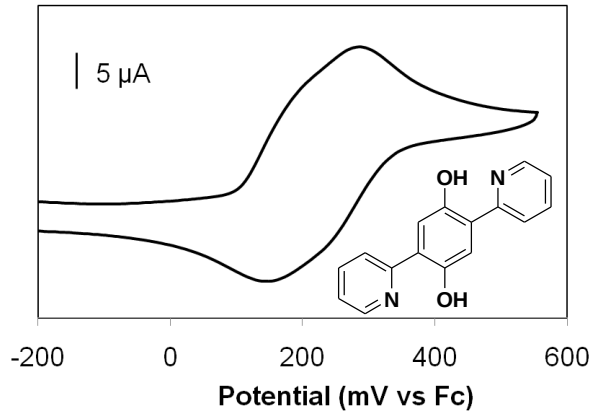

Figure A-4. 2.2, 50 mV/s.

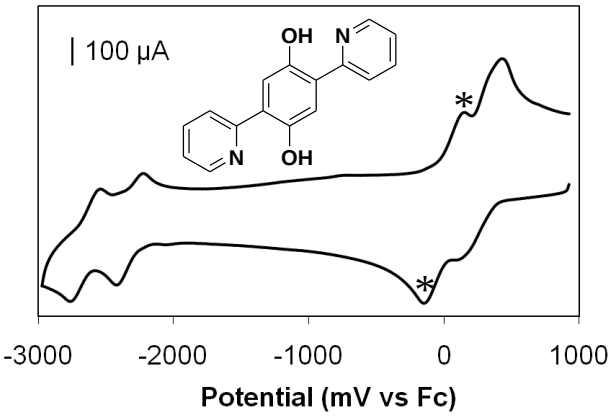

Figure A-5. 2.2, 5000 mV/s.

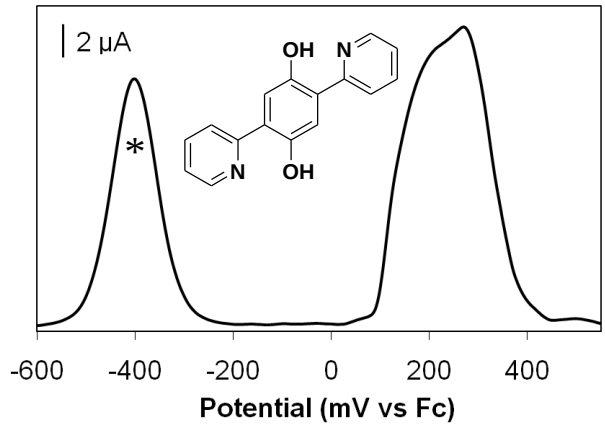

Figure A-6. 2.2, OSWV.

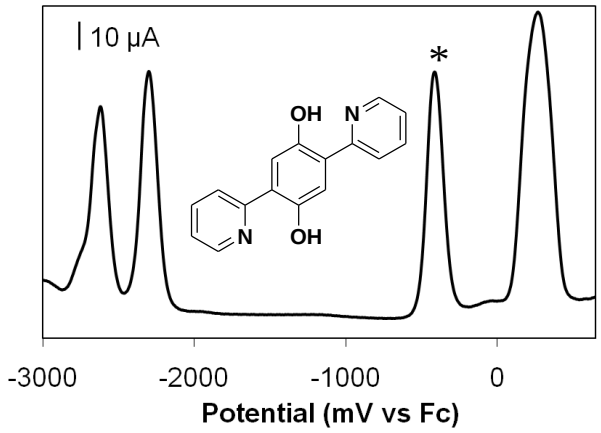

Figure A-7. 2.2, OSWV.

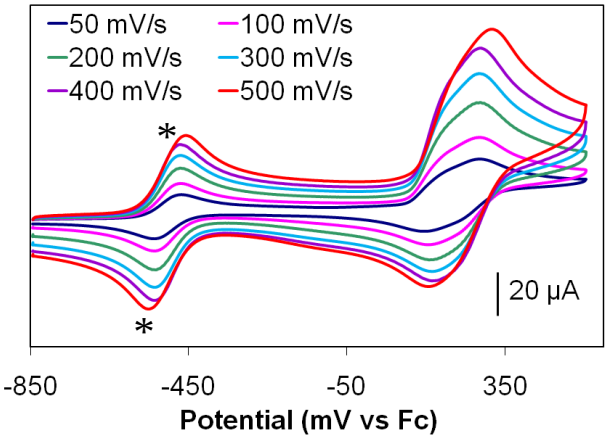

Figure A-8. 2.2, scan rate dependence.

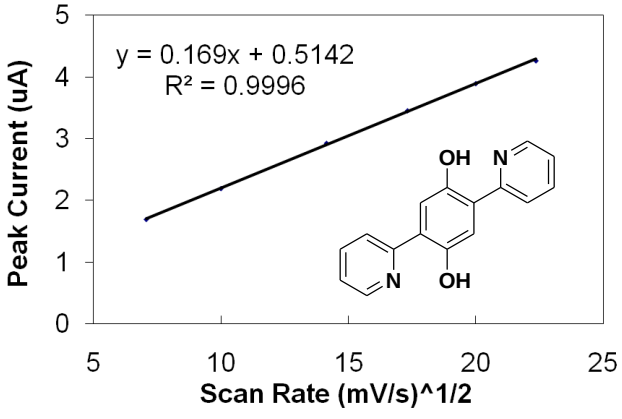

Figure A-9. 2.2, Scan rate$^{1/2}$ vs peak current for anodic peak (310mV vs Fc).

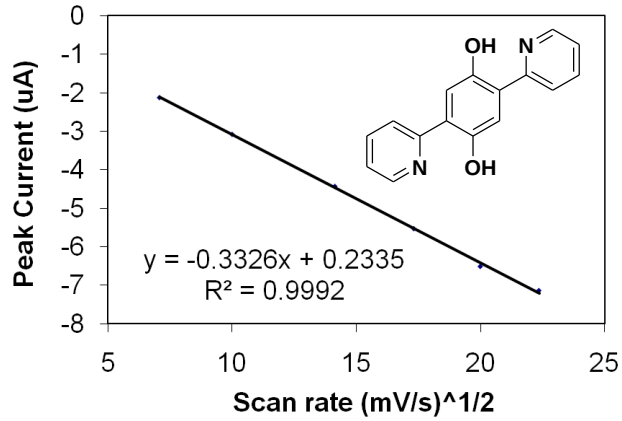

Figure A-10. 2.2, Scan rate$^{1/2}$ vs peak current for cathodic peak (180mV vs Fc).

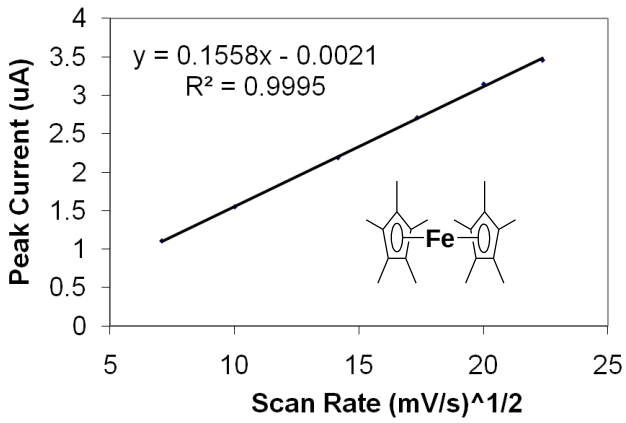

Figure A -11. Decamethylferrocene, Scan rate$^{1/2}$ vs peak current for anodic peak (-540mV vs Fc).

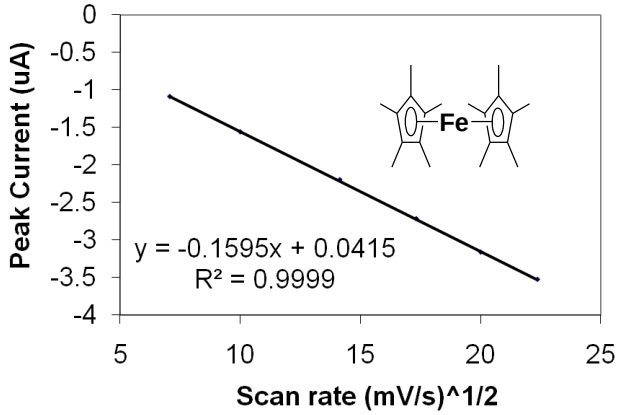

Figure A-12. Decamethylferrocene, Scan rate$^{1/2}$ vs peak current for cathodic peak (-470mV vs Fc).

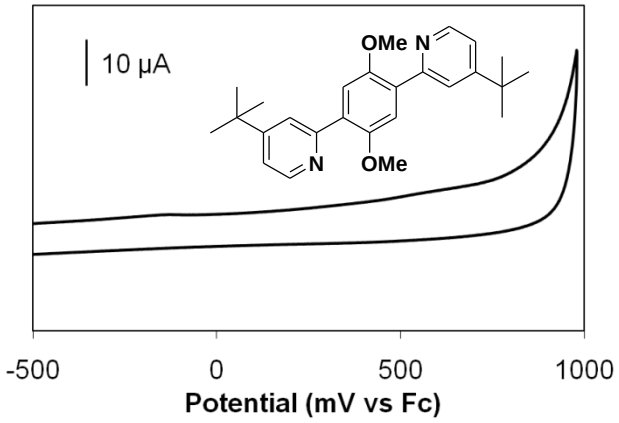

Figure A-13. 2.14, 250 mV/s.

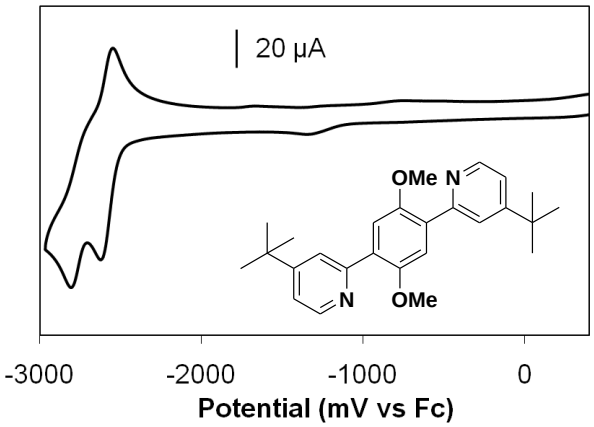

Figure A-14. 2.14, 250 mV/s.

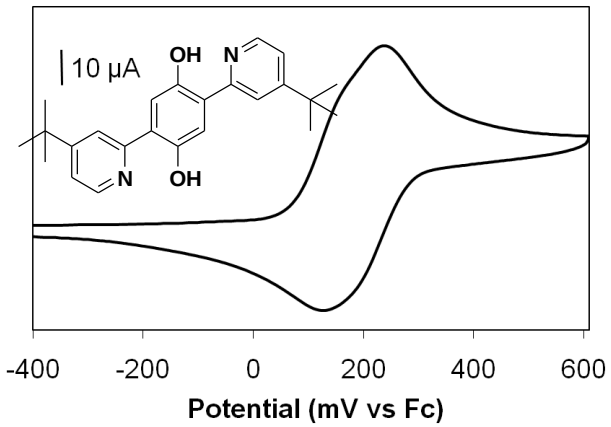

Figure A-15. 2.15, 50 mV/s.

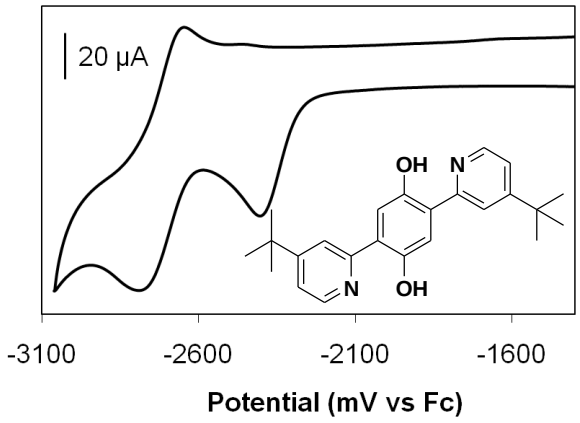

Figure A-16. 2.15, 500 mV/s.

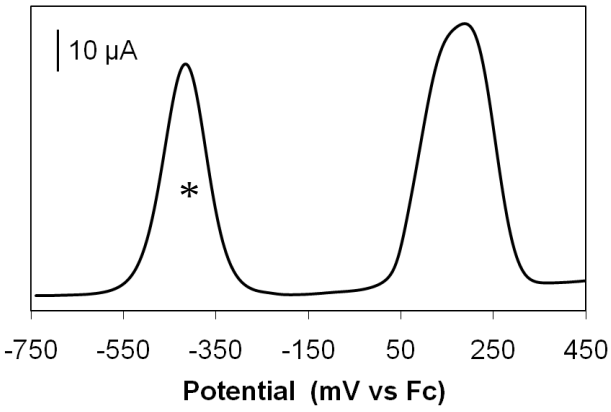

Figure A-17. 2.15, OSWV.

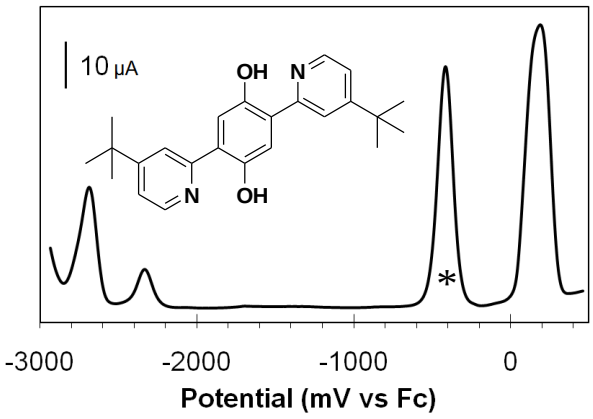

Figure A-18. 2.15, OSWV.

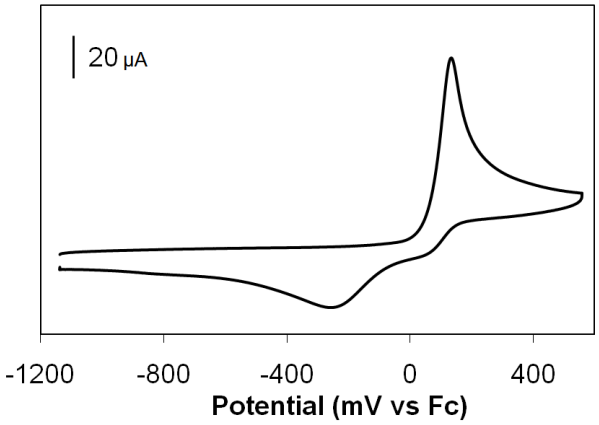

Figure A-19. 2.15 with 1mL pyridine added, 250 mV/s.

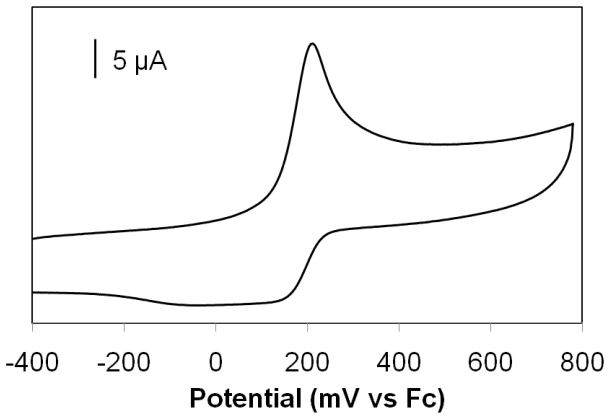

Figure A-20. 2.15 with 1mL DMF added, 250 mV/s.

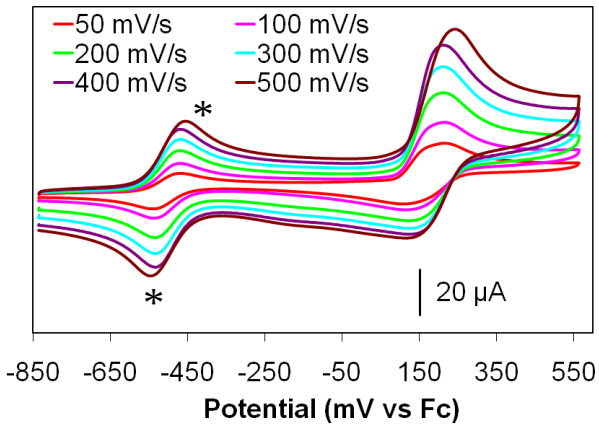

Figure A-21. 2.15, scan rate dependence.

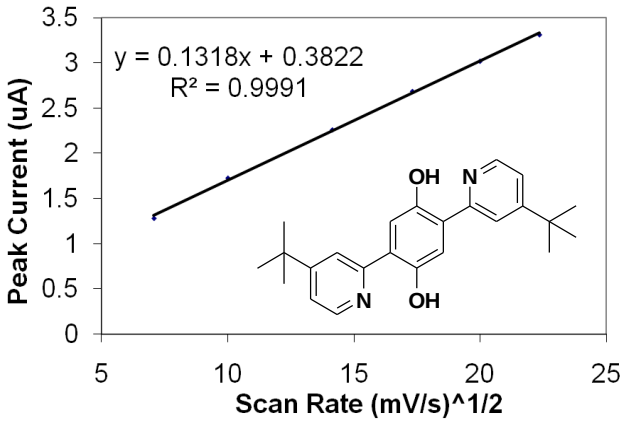

Figure A-22. 2.15, Scan rate$^{1/2}$ vs peak current for anodic peak (130mV vs Fc).

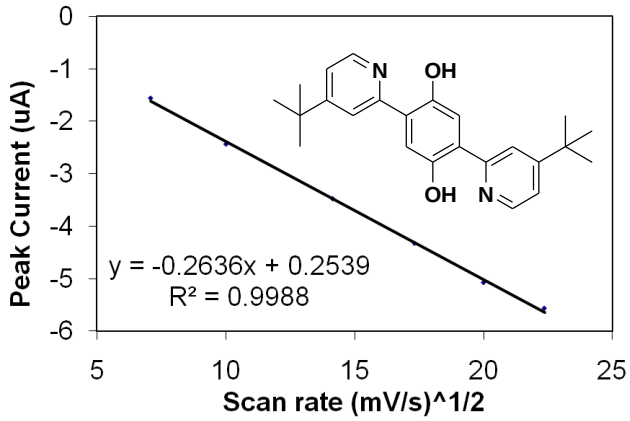

Figure A-23. 2.15, Scan rate$^{1/2}$ vs peak current for cathodic peak (240mV vs Fc).

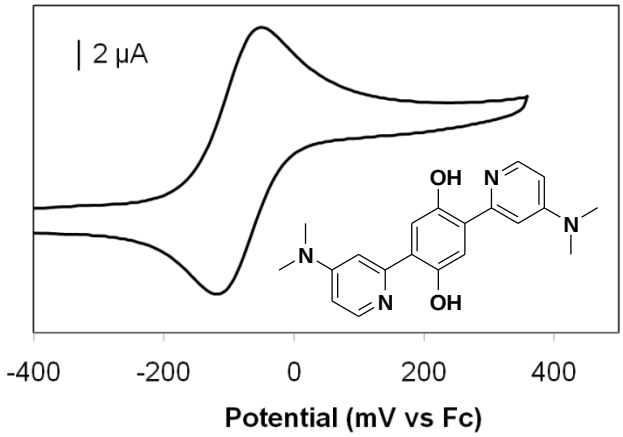

Figure A-24. 2.19, 50 mV/s.

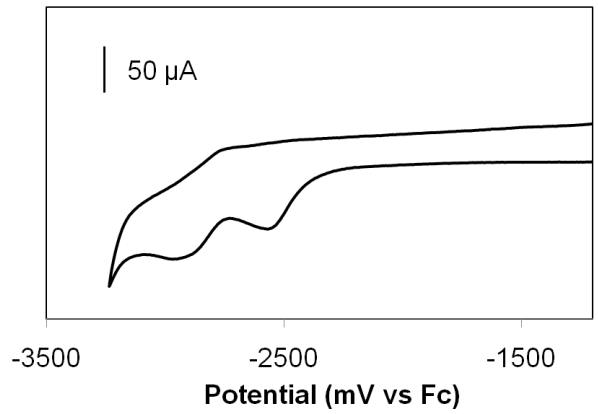

Figure A-25. 2.19, 1000 mV/s.

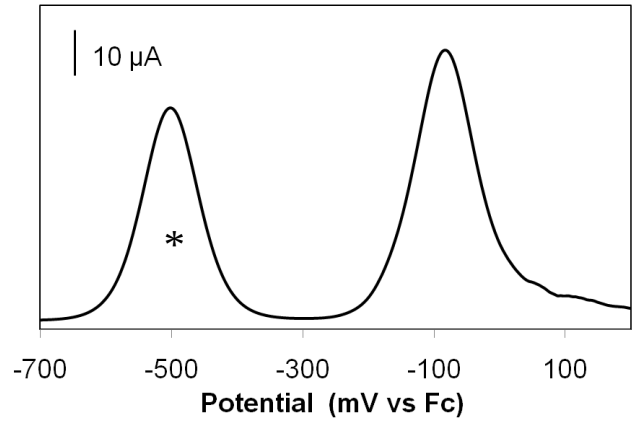

Figure A-26. 2.19, OSWV.

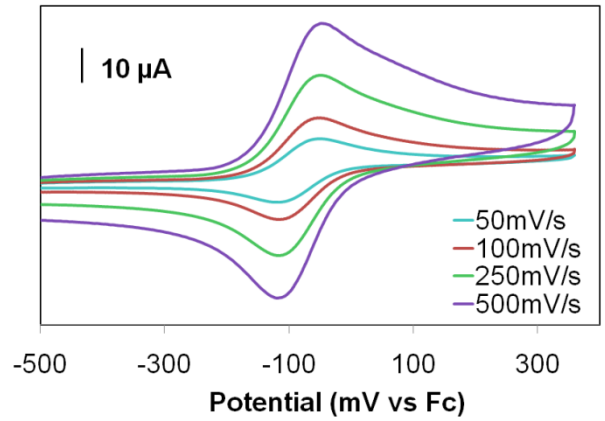

Figure A-27. 2.19, scan rate dependence.

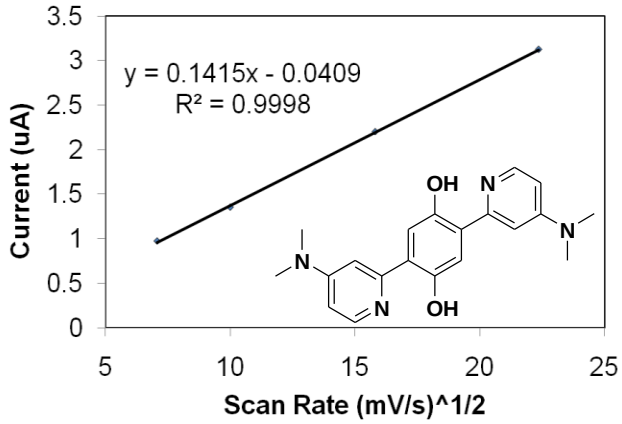

Figure A-28. 2.19, Scan rate$^{1/2}$ vs peak current for anodic peak (-120mV vs Fc).

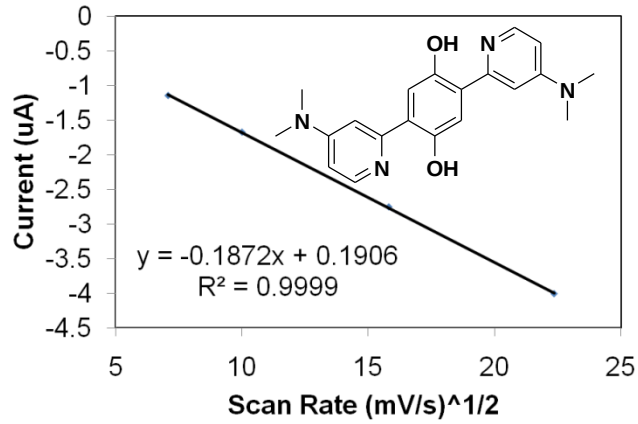

Figure A-29. 2.19, Scan rate$^{1/2}$ vs peak current for cathodic peak (-40mV vs Fc).

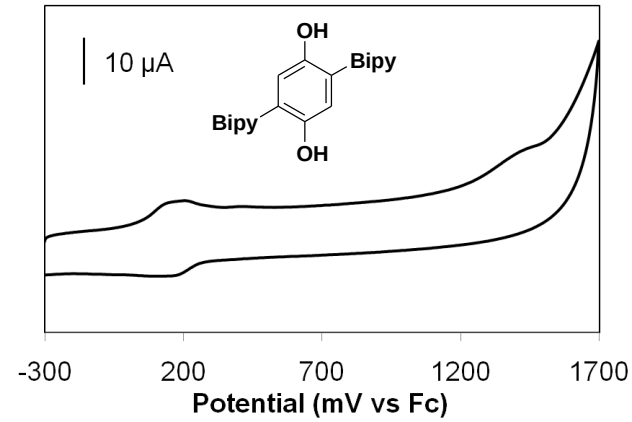

Figure A-30. 2.23, 250 mV/s.

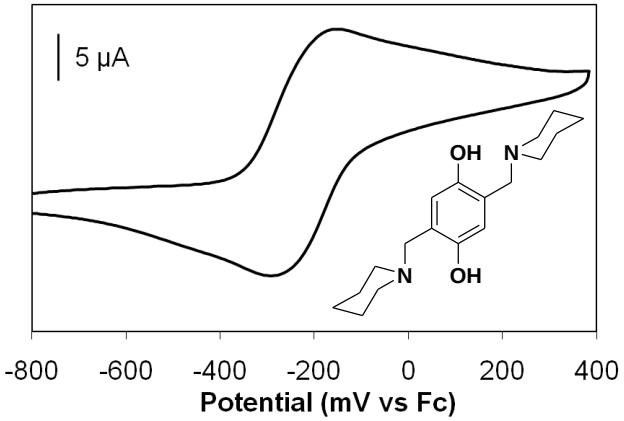

Figure A-31. 2.27, 50 mV/s.

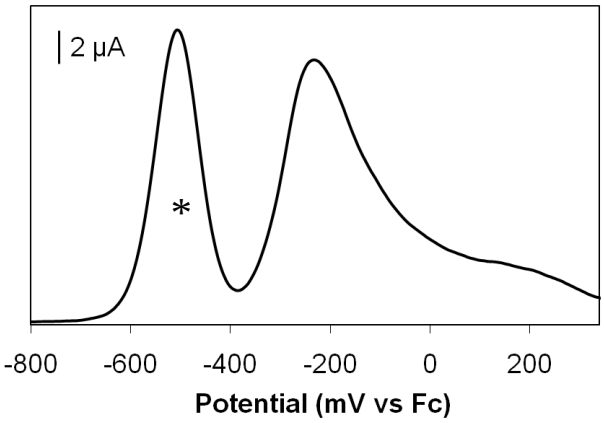

Figure A-32. 2.27, OSWV.

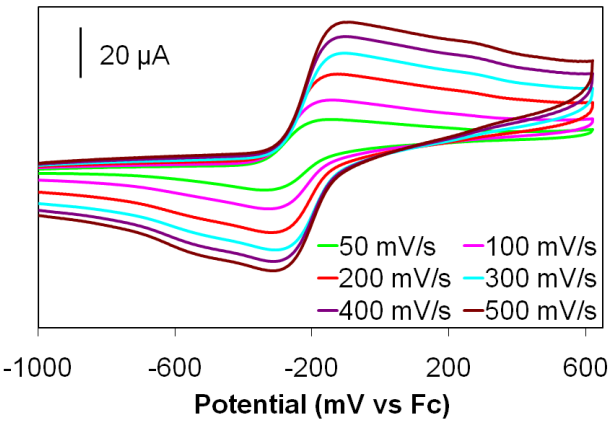

Figure A-33. 2.27, scan rate dependence.

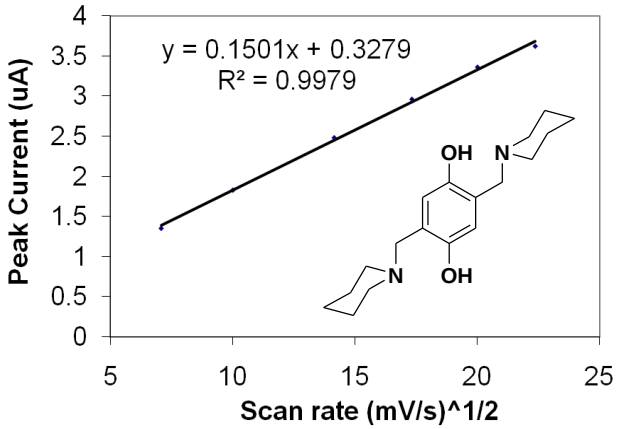

Figure A-34. 2.27, Scan rate$^{1/2}$ vs peak current for anodic peak (-290mV vs Fc).

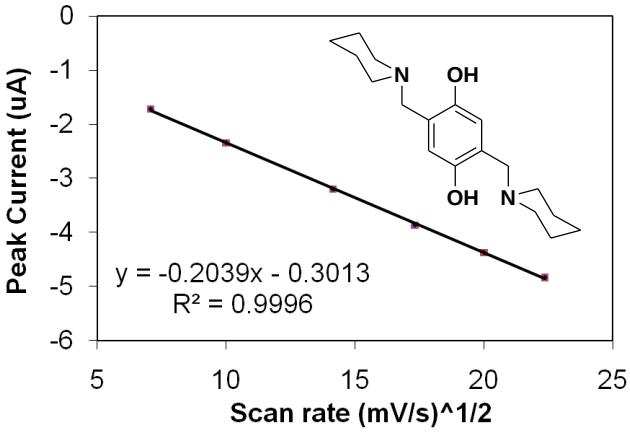

Figure A-35. 2.27, Scan rate$^{1/2}$ vs peak current for cathodic peak (-150mV vs Fc).

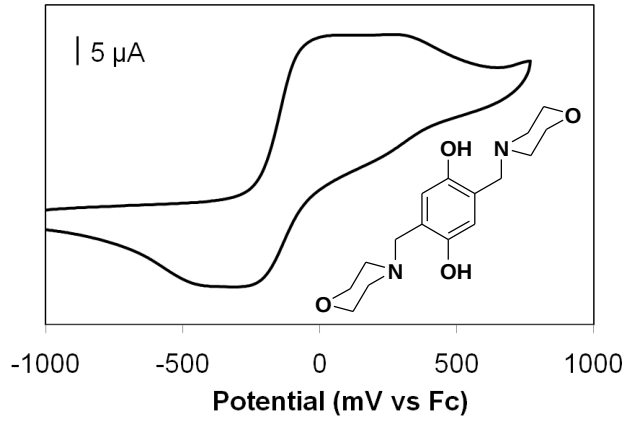

Figure A-36. 2.28, 50 mV/s.

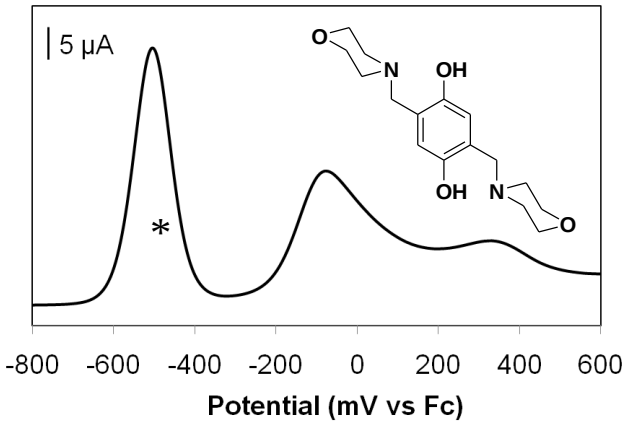

Figure A-37. 2.28, OSWV.

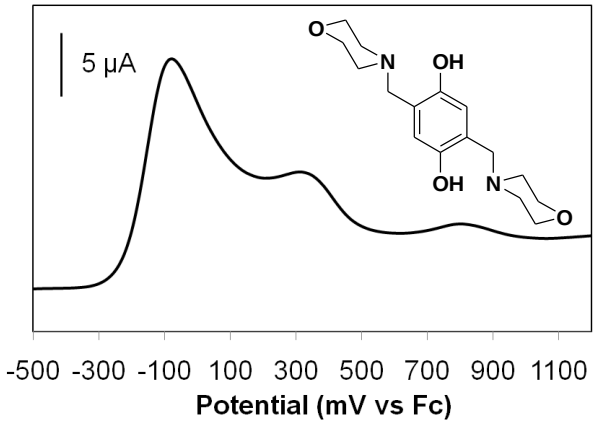

Figure A-38. 2.28, OSWV.

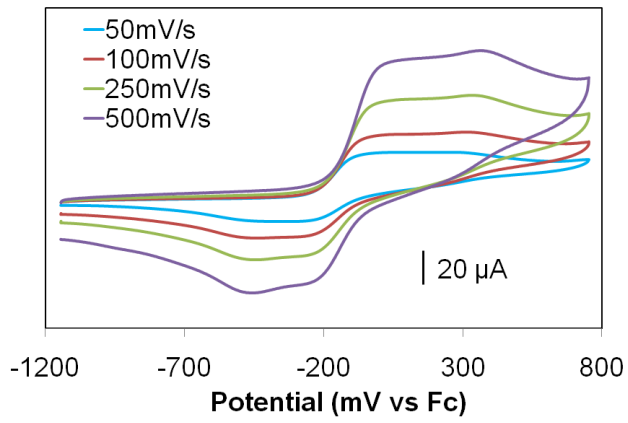

Figure A-39. 2.28, scan rate dependence.

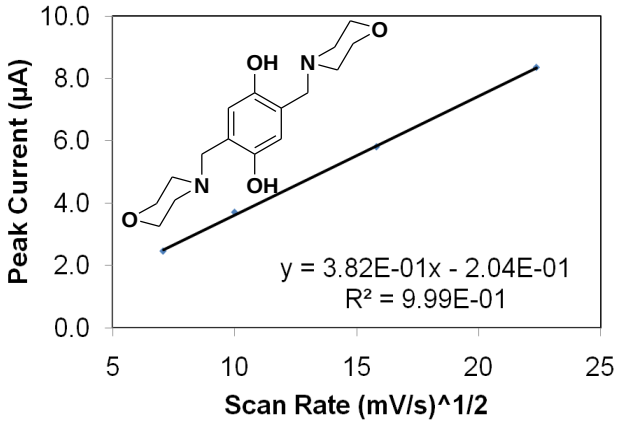

Figure A-40. 2.28, Scan rate$^{1/2}$ vs peak current for anodic peak (40mV vs Fc).

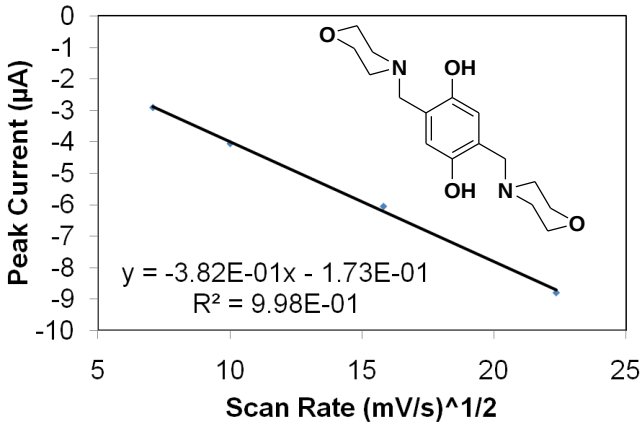

Figure A-41. 2.28, Scan rate$^{1/2}$ vs peak current for cathodic peak (-280mV vs Fc).

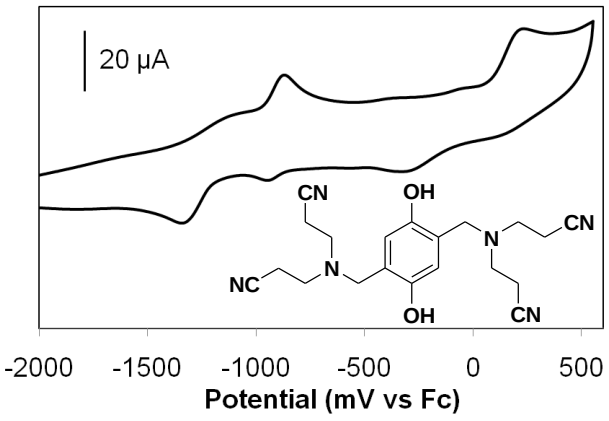

Figure A-42. 2.29, 250 mV/s.

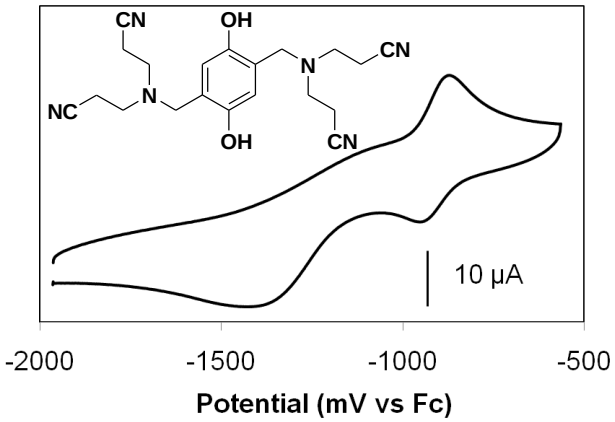

Figure A-43. 2.29, 250 mV/s.

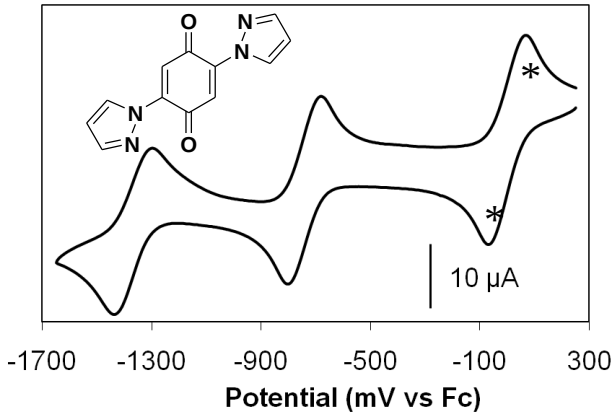

Figure A-44. 2.31, DCM, 100 mV/s.

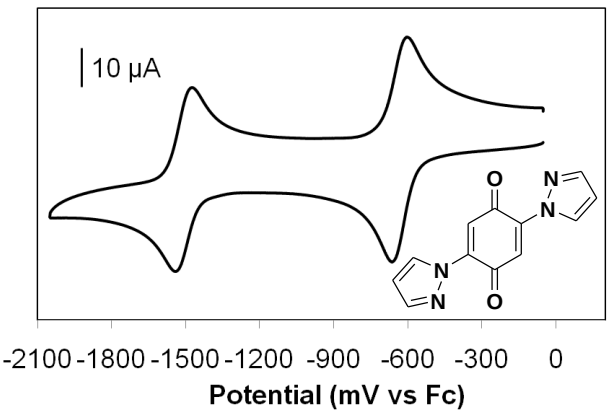

Figure A-45. 2.31, DMF, 250 mV/s.

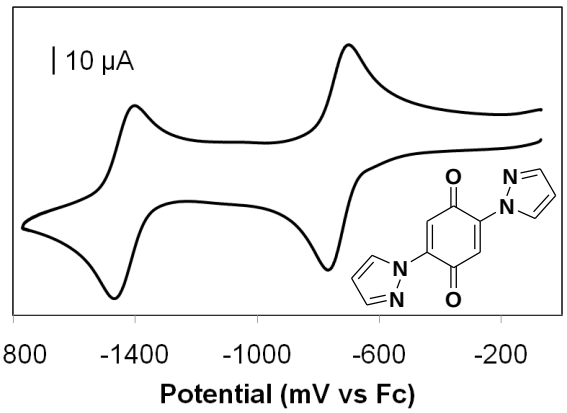

Figure A-46. 2.31, ACN, 250 mV/s.

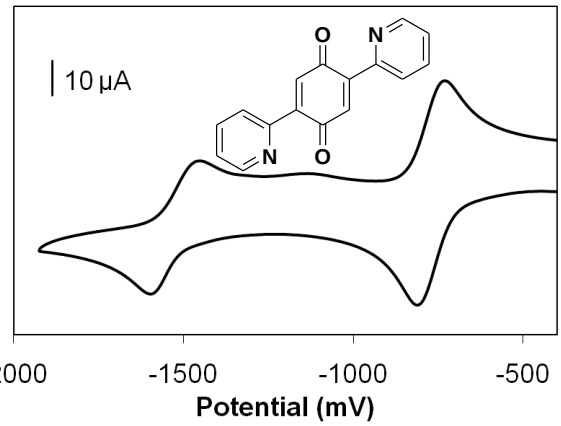

Figure A-47. 2.32, 100 mV/s.

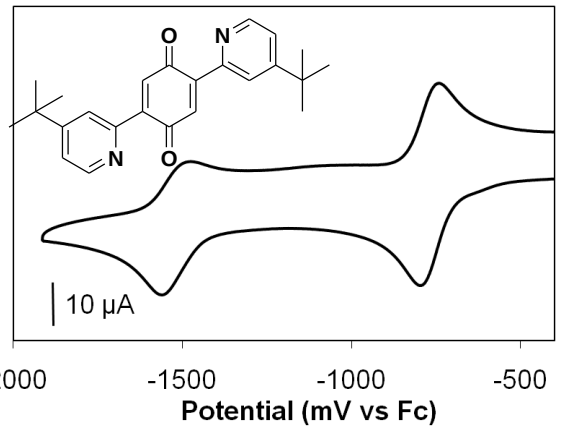

Figure A-48. 2.33, 250 mV/s.

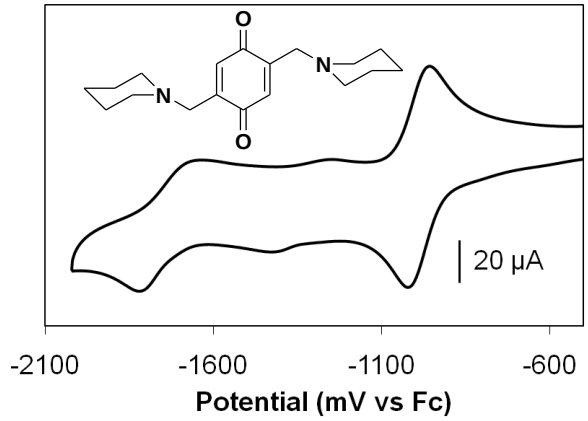

Figure A-49. 2.34, 250 mV/s.

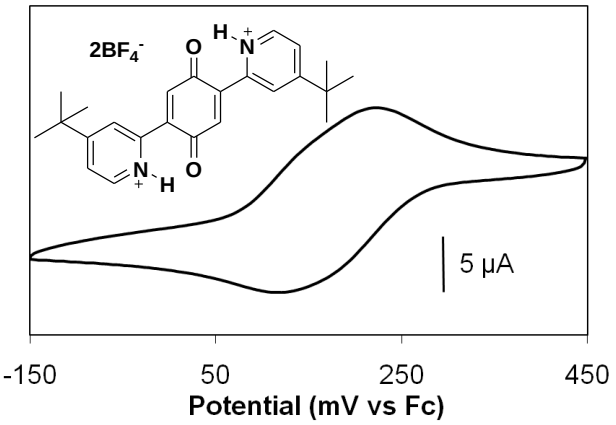

Figure A-50. 2.37, 50 mV/s.

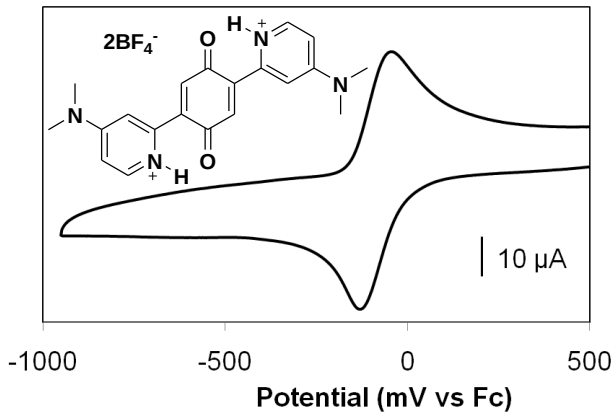

Figure A-51. 2.38, 250 mV/s.

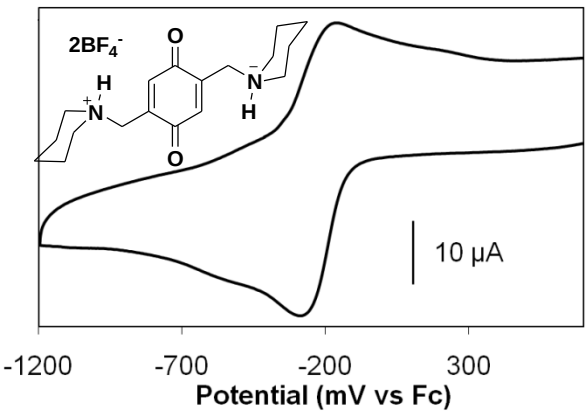

Figure A-52. 2.39, 250 mV/s.

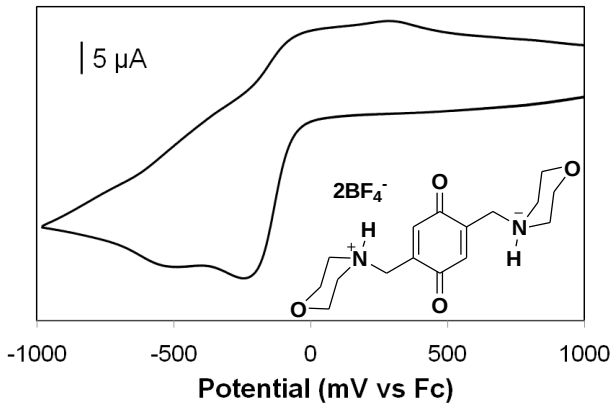

Figure A-53. 2.40, 100 mV/s.

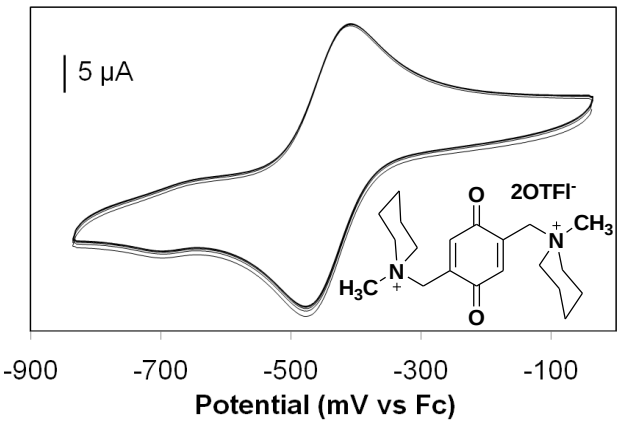

Figure A-54. 2.43, 250 mV/s.

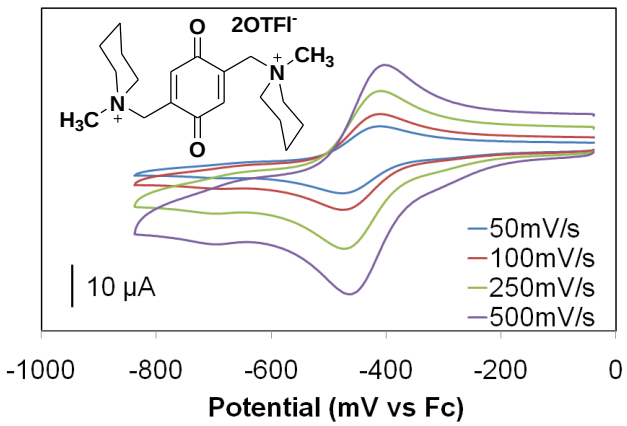

Figure A-55. 2.43, scan rate dependence.

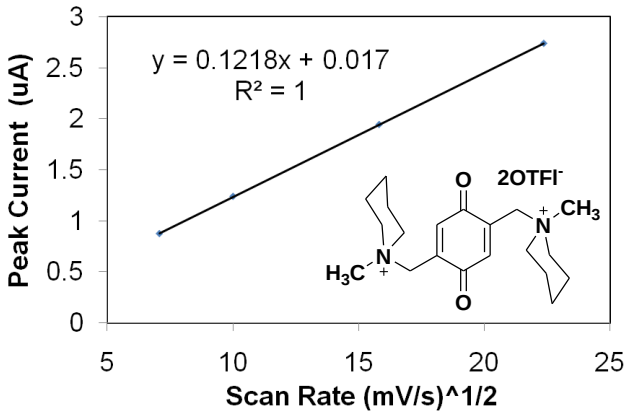

Figure A-56. 2.43, Scan rate$^{1/2}$ vs peak current for anodic peak (-410mV vs Fc).

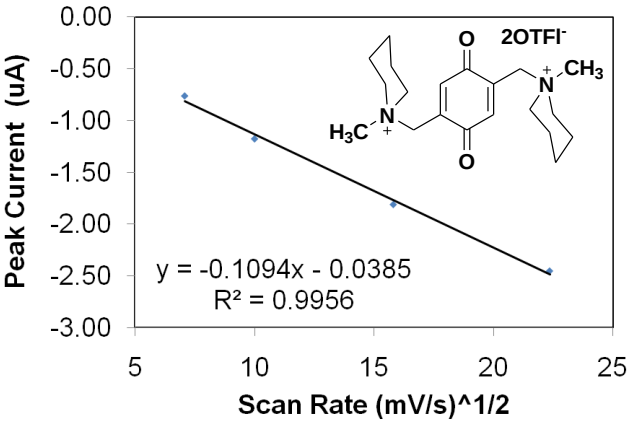

Figure A-57. 2.43, Scan rate$^{1/2}$ vs peak current for cathodic peak (-480mV vs Fc).

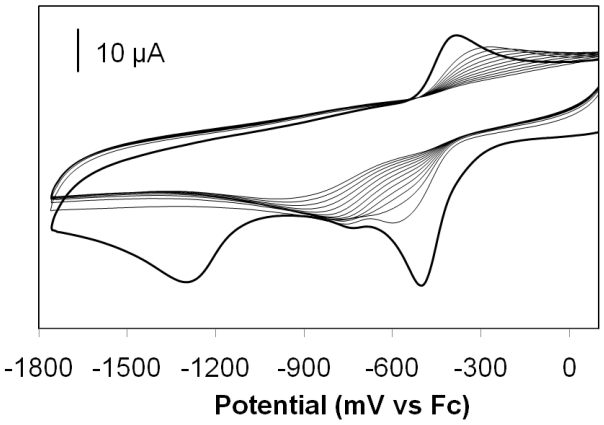

Figure A-58. 2.43, 500 mV/s.

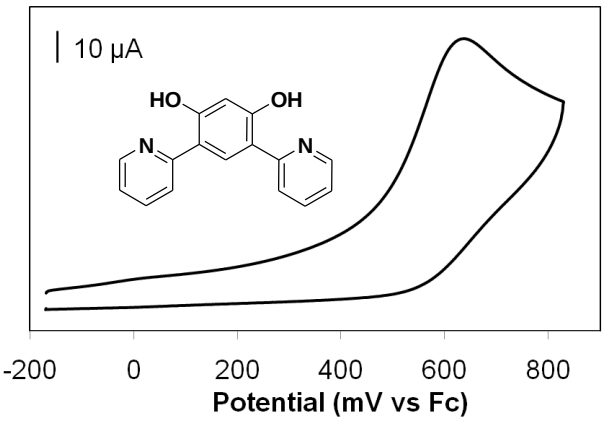

Figure A-59. 2.48, 250 mV/s.

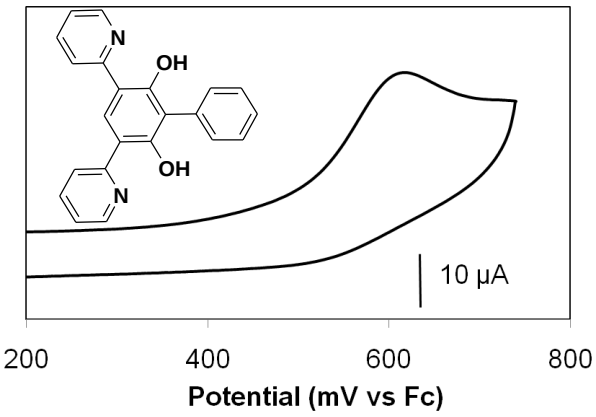

Figure A-60. 2.52, 250 mV/s.

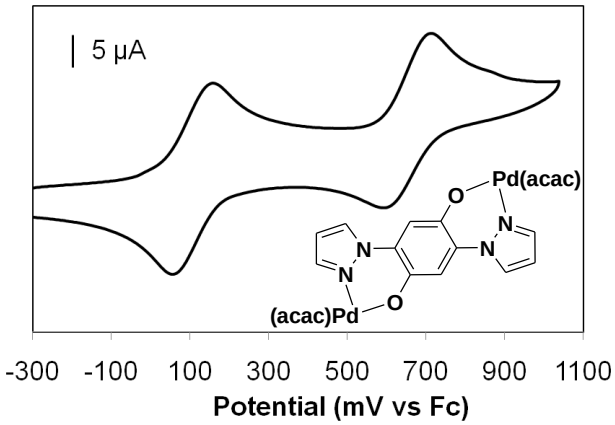

Figure A-61. 3.19, DCM, 100mv/s.

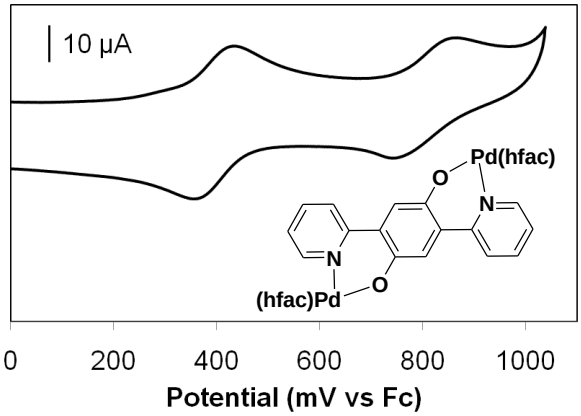

Figure A-64. 3.23, DCM, 250 mV/s.

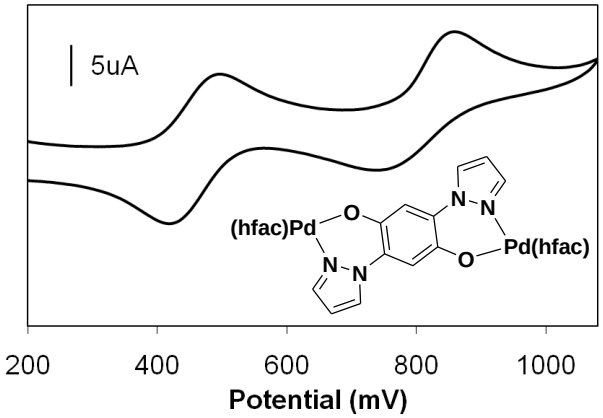

Figure A 62. 3.20, DCM, 60 mV/s.

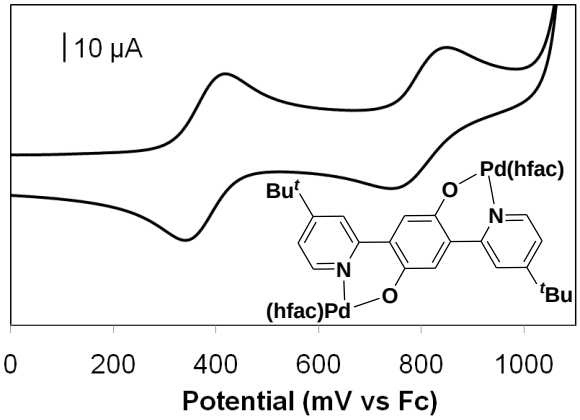

Figure A-65. 3.24, DCM, 250 mV/s.

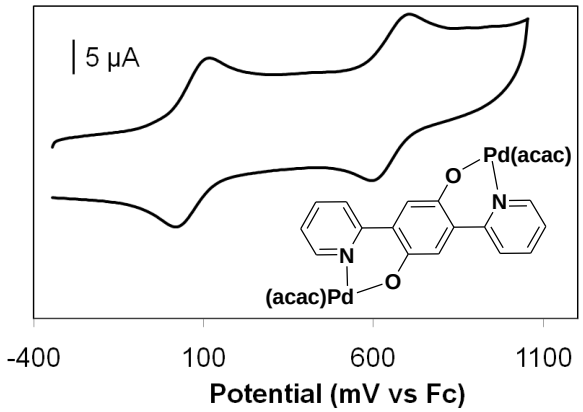

Figure A-63. 3.22, DCM, 300 mV/s.

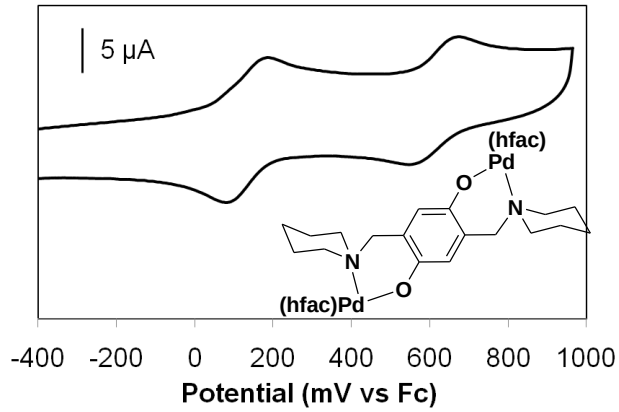

Figure A-66. 3.25, DCM, 250 mV/s.

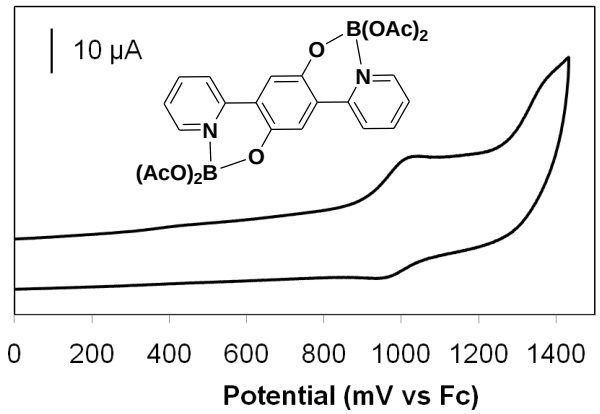

Figure A-67. 4.18, 250 mV/s.

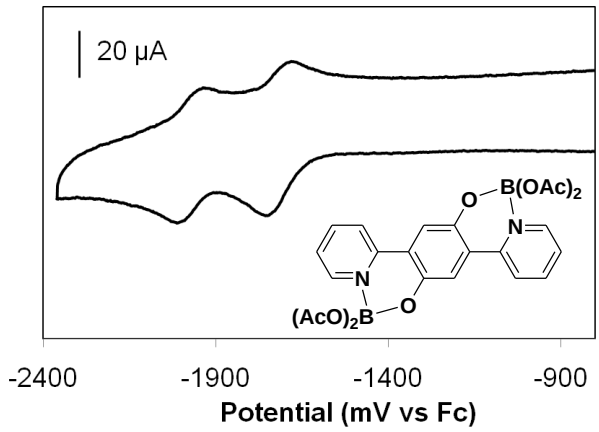

Figure A-68. 4.18, 1000 mV/s.

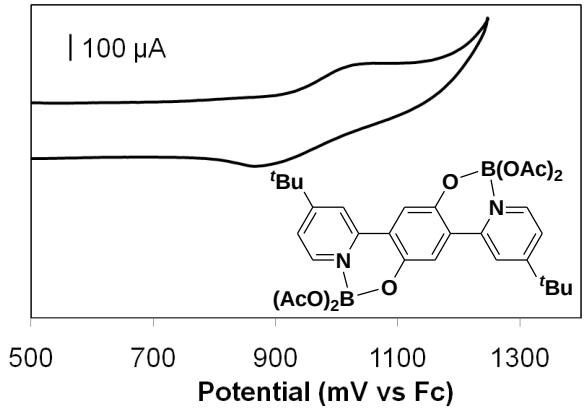

Figure A-69. 4.19, 5120 mV/s.

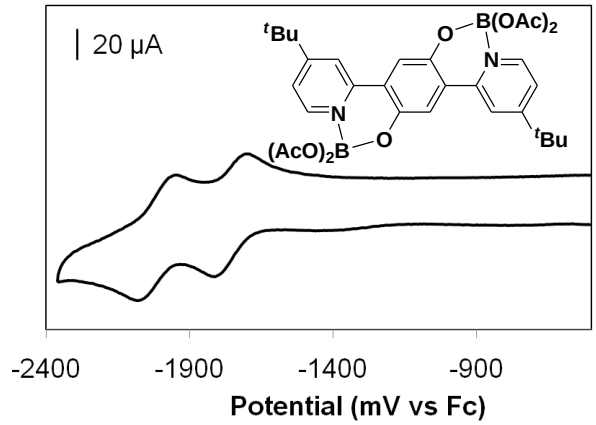

Figure A-70. 4.19, 1000 mV/s.

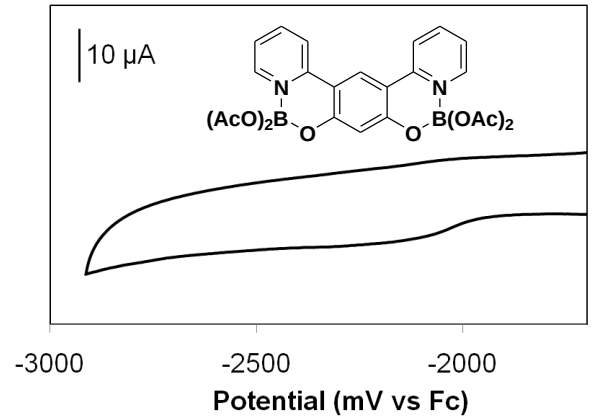

Figure A-71. 4.20, 250 mV/s.

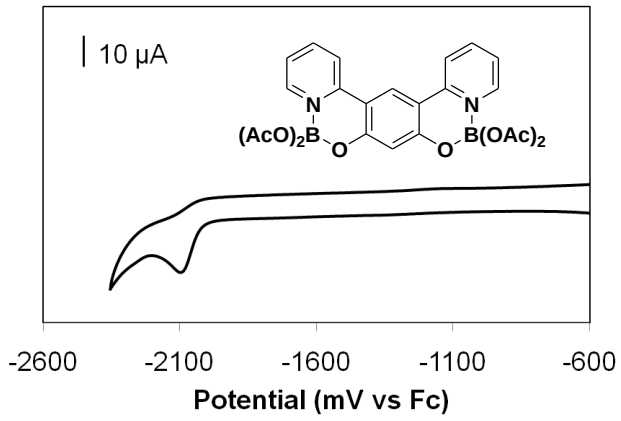

Figure A-72. . 4.20, DCM, 250 mV/s.

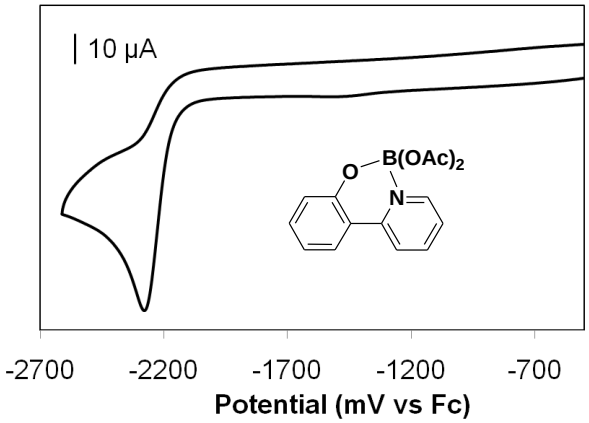

Figure A-73. 4.21, 250 mV/s.

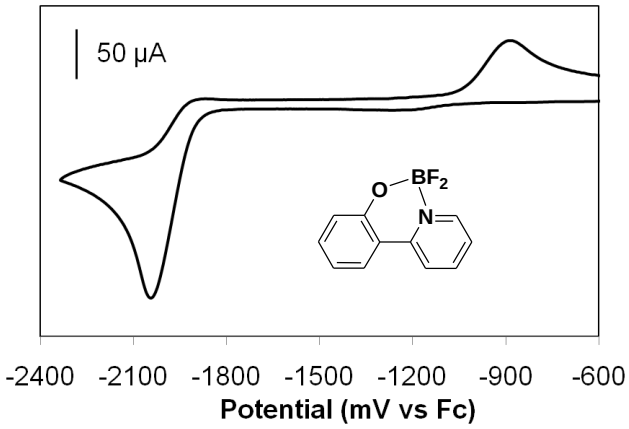

Figure A-74. 4.22, 250 mV/s

Appendix II: Crystallographic Data

Table A-1. Crystallographic parameters.

	2.15	**2.19**	**2.23**	**2.39**
formula	$C_{24}H_{28}N_2O_2$	$C_{21}H_{24}N_4O_2Cl_2$	$C_{26}H_{18}N_4O_2$	$C_{18}H_{28}N_2OB_2F_8$
FW	376.48	435.34	418.44	478.04
crystal dim. (mm)	0.10x0.35x0.35	0.10x0.40x0.45	0.05x0.12x0.40	0.02x0.10x0.46
a (Å)	6.8537(7)	16.7935(7)	11.5919(11)	6.0244(8)
b (Å)	8.3676(8)	7.6274(3)	6.7183(7)	7.2870(7)
c (Å)	8.7224(9)	17.0632(8)	24.903(3)	12.5745(16)
α (deg)	82.096(6)	90.0	90.0	94.711(4)
β (deg)	83.128(5)	111.414(2)	96.561(5)	93.618(4)
γ (deg)	87.998(5)	90.0	90.0	103.777(4)
volume ($Å^3$)	5220.68(5)	2034.8(8)	1926.7(3)	532.37(11)
p_{calc} (g/cm^3)	1.271	1.421	1.443	1.491
system	triclinic	monoclinic	monoclinic	triclinic
space group	*P* -1 (#2)	*P* 2/*n* (#13)	*P* $2_1/c$ (#14)	*P* -1 (#2)
Z	1	4	4	1
μ (cm^{-1})	0.81	3.45	0.94	1.42
T (K)	173	173	173	173
$2\theta_{max}$ (deg)	56.3	56.1	55.9	51.5
total reflections	9934	23989	18744	4987
unique reflections; (R_{int})	2374; (0.024)	4910; (0.028)	4620; (0.043)	1963; (0.026)
no. of parameters	134	285	297	150
R_1[a]; wR_2[b]	0.051; 0.117	0.061; 0.121	0.106; 0.126	0.060; 0.110

[a] $R_1 = \Sigma(|F_0| - |F_c|)/\Sigma|F_0|$ [b] $wR_2 = [\Sigma(w(F_0^2 - F_c^2)^2/\Sigma w(F_0^2)^2]^{1/2}$

Table A-2. Crystallographic parameters.

	2.40	**2.48**	**2.52**
formula	$C_{16}H_{24}N_2O_4B_2F_8$	$C_{16}H_{12}N_2O_2$	$C_{22}H_{16}N_2O_2$
FW	481.99	264.28	340.37
crystal dim. (mm)	0.03x0.10x0.52	0.05x0.10x0.45	0.10x0.22x0.50
a (Å)	7.1471(3)	13.071(3)	11.466(2)
b (Å)	12.3017(7)	23.884(6)	6.7448(13)
c (Å)	12.2378(7)	3.7601(9)	21.311(4)
α (deg)	90.0	90.0	90.0
β (deg)	105.341(2)	90.0	90.424(11)
γ □(deg)	90.0	90.0	90.0
volume ($Å^3$)	1037.63(9)	1173.9(5)	1648.0(5)
p_{calc} (g/cm^3)	1.543	1.495	1.372
system	monoclinic	orthorhombic	monoclinic
space group	*P* -1 (#2)	*P na*2_1 (#33)	*P* $2_1/c$ (#14)
Z	2	4	4
μ (cm^{-1})	1.287	1.01	0.89
T (K)	193	173	173
$2\theta_{max}$ (deg)	52.80	56.3	56.3
total reflections	11957	7695	15860
unique reflections; (R_{int})	6271; (0.0458)	2734; (0.048)	3977; (0.039)
no. of parameters	447	189	244
R_1[a]; wR_2[b]	0.0541; 0.1467	0.080; 0.106	0.090; 0.131

[a] $R_1 = \Sigma(|F_0| - |F_c|)/\Sigma|F_0|$ [b] $wR_2 = [\Sigma(w(F_0^2 - F_c^2)^2/\Sigma w(F_0^2)^2]^{1/2}$

Table A-3. Crystallographic parameters.

	3.23	**3.24**	**4.18**
formula	$C_{29.50}H_{16}F_{12}N_2O_6Pd_2$	$C_{65}H_{58}N_3O_9F_{18}Pd_3$	$C_{25}H_{24}B_2N_2O_2Cl_2$
FW	935.24	1686.34	604.98
crystal dim. (mm)	0.53x0.08x0.03	0.12x0.35x0.50	0.03x0.40x0.50
a (Å)	8.4631 (12)	13.543(3)	7.5251(15)
b (Å)	10.9762 (16)	15.193(3)	8.6588(15)
c (Å)	17.935 (3)	16.623(4)	10.666(2)
α (deg)	74.243 (2)	84.411(8)	81.613(9)
β (deg)	82.624 (2)	75.996(9)	82.685(9)
γ □(deg)	74.447 (2)	75.114(8)	87.034(9)
volume ($Å^3$)	1542.0 (4)	3205(1)	681.5(2)
p_{calc} (g/cm^3)	2.014	1.747	1.474
system	triclinic	triclinic	triclinic
space group	*P* $2_1/c$ (#14)	*P* -1 (#2)	*P* -1 (#2)
Z	2	2	1
μ (cm^{-1})	1.53	9.45	2.99
T (K)	193	173	173
$2\theta_{max}$ (deg)	56.0	56.0	52.7
total reflections	11114	67764	9732
unique reflections; (R_{int})	2459; (0.029)	15894; (0.025)	2681; (0.045)
no. of parameters	149	900	174
R_1[a]; wR_2[b]	0.075; 0.113	0.034; 0.072	0.088; 0.152

[a] $R_1 = \Sigma(|F_0| - |F_c|)/\Sigma|F_0|$ [b] $wR_2 = [\Sigma(w(F_0^2 - F_c^2)^2/\Sigma w(F_0^2)^2]^{1/2}$

Table A-4. Crystallographic parameters.

	4.19	**4.21**	**4.22**
formula	$C_{32}H_{38}N_2O_{10}B_2$	$C_{15}H_{14}BNO_5$	$C_{11}H_8NOBF_2$
FW	632.26	299.08	218.99
crystal dim. (mm)	0.02x0.10x0.50	0.22x0.45x0.48	0.24x0.30x0.45
a (Å)	6.1199(14)	10.1738(13)	8.2074(4)
b (Å)	11.104(3)	7.6121(10)	11.2099(5)
c (Å)	12.337(3)	18.383(3)	10.3948(4)
α (deg)	96.092(10)	90.0	90.0
β (deg)	100.294(11)	91.469(5)	96.568(2)
γ □(deg)	102.834(10)	90.0	90.0
volume (Å^3)	794.9(3)	1423.2(3)	950.09(7)
p_{calc} (g/cm^3)	1.321	1.396	1.531
system	triclinic	monoclinic	monoclinic
space group	*P* -1 (#2)	*P* 21/*c* (#14)	*P* 2_1/*c* (#14)
Z	1	4	4
μ (cm^{-1})	0.97	1.04	1.23
T (K)	173	173	173
$2\theta_{max}$ (deg)	48.6	56.2	56.2
total reflections	10812	16843	10995
unique reflections; (R_{int})	2490; (0.043)	3454; (0.026)	2292; (0.022)
no. of parameters	213	201	145
R_1[a]; wR_2[b]	0. 092; 0.146	0.047; 0.105	0.041; 0.094

[a] $R_1 = \Sigma(|F_0| - |F_c|)/\Sigma|F_0|$ [b] $wR_2 = [\Sigma(w(F_0^2 - F_c^2)^2/\Sigma w(F_0^2)^2]^{1/2}$

Appendix III: Complete listings of bond lengths and angles

Table A-5. Bond lengths [Å] and angles [deg] for **2.15**.

Bond lengths	
C(1)-O(1)	1.3567(14)
C(1)-C(3)	1.3813(14)
C(1)-C(2)	1.4034(16)
C(2)-C(3)#1	1.3856(16)
C(2)-C(11)	1.4755(14)
C(3)-C(2)#1	1.3856(16)
C(3)-H(3)	0.9500
C(11)-N(1)	1.3457(15)
C(11)-C(12)	1.3851(15)
C(12)-C(13)	1.3878(14)
C(12)-H(12)	0.9500
C(13)-C(14)	1.3840(16)
C(13)-C(16)	1.5230(15)
C(14)-C(15)	1.3756(17)
C(14)-H(14)	0.9500
C(15)-N(1)	1.3316(14)
C(15)-H(15)	0.9500
C(16)-C(17)	1.5251(17)
C(16)-C(18)	1.5253(18)
C(16)-C(19)	1.5258(15)
C(17)-H(17A)	0.9800
C(17)-H(17B)	0.9800
C(17)-H(17C)	0.9800
C(18)-H(18A)	0.9800
C(18)-H(18B)	0.9800
C(18)-H(18C)	0.9800
C(19)-H(19A)	0.9800
C(19)-H(19B)	0.9800
C(19)-H(19C)	0.9800
O(1)-H(1)	0.90(2)
Bond Angles	
O(1)-C(1)-C(3)	117.60(10)
O(1)-C(1)-C(2)	122.82(10)
C(3)-C(1)-C(2)	119.58(10)
C(3)#1-C(2)-C(1)	117.93(10)
C(3)#1-C(2)-C(11)	120.65(10)
C(1)-C(2)-C(11)	121.38(10)
C(1)-C(3)-C(2)#1	122.47(10)
C(1)-C(3)-H(3)	118.8
C(2)#1-C(3)-H(3)	118.8
N(1)-C(11)-C(12)	121.48(10)
N(1)-C(11)-C(2)	116.68(10)
C(12)-C(11)-C(2)	121.80(10)
C(11)-C(12)-C(13)	121.06(10)

C(11)-C(12)-H(12)	119.5
C(13)-C(12)-H(12)	119.5
C(14)-C(13)-C(12)	116.39(10)
C(14)-C(13)-C(16)	123.28(10)
C(12)-C(13)-C(16)	120.27(10)
C(15)-C(14)-C(13)	119.79(10)
C(15)-C(14)-H(14)	120.1
C(13)-C(14)-H(14	120.1
N(1)-C(15)-C(14)	123.73(11)
N(1)-C(15)-H(15)	118.1
C(14)-C(15)-H(15)	118.1
C(13)-C(16)-C(17)	108.29(10)
C(13)-C(16)-C(18)	110.35(9)
C(17)-C(16)-C(18)	109.49(11)
C(13)-C(16)-C(19)	111.84(10)
C(17)-C(16)-C(19)	108.85(10)
C(18)-C(16)-C(19)	108.00(10)
C(16)-C(17)-H(17A)	109.5
C(16)-C(17)-H(17B)	109.5
H(17A)-C(17)-H(17B)	109.5
C(16)-C(17)-H(17C)	109.5
H(17A)-C(17)-H(17C)	109.5
H(17B)-C(17)-H(17C)	109.5
C(16)-C(18)-H(18A)	109.5
C(16)-C(18)-H(18B)	109.5
H(18A)-C(18)-H(18B)	109.5
C(16)-C(18)-H(18C)	109.5
H(18A)-C(18)-H(18C)	109.5
H(18B)-C(18)-H(18C)	109.5
C(16)-C(19)-H(19A)	109.5
C(16)-C(19)-H(19B)	109.5
H(19A)-C(19)-H(19B)	109.5
C(16)-C(19)-H(19C)	109.5
H(19A)-C(19)-H(19C)	109.5
H(19B)-C(19)-H(19C)	109.5
C(15)-N(1)-C(11)	117.54(10)
C(1)-O(1)-H(1)	105.0(12)

Table A-6. Bond lengths [Å] and angles [deg] for **2.19**.

Bond lengths	
C(1)-O(1)	1.3669(17)
C(1)-C(6)	1.393(2)
C(1)-C(2)	1.4175(19)
C(2)-C(3)	1.394(2)
C(2)-C(11)	1.4907(19)
C(3)-C(4)	1.388(2)

C(3)-H(3)	0.95
C(4)-O(2)	1.3627(18)
C(4)-C(5)	1.4180(19)
C(5)-C(6)	1.394(2)
C(5)-C(21)	1.4888(19)
C(6)-H(6)	0.95
C(11)-N(1)	1.359(2)
C(11)-C(12)	1.396(2)
C(12)-C(13)	1.415(2)
C(12)-H(12)	0.95
C(13)-N(2)	1.362(2)
C(13)-C(14)	1.414(2)
C(14)-C(15)	1.373(2)
C(14)-H(14)	0.95
C(15)-N(1)	1.344(2)
C(15)-H(15)	0.95
C(16)-N(2)	1.449(2)
C(16)-H(16A)	0.98
C(16)-H(16B)	0.98
C(16)-H(16C)	0.98
C(17)-N(2)	1.457(2)
C(17)-H(17A)	0.98
C(17)-H(17B)	0.98
C(17)-H(17C)	0.98
C(21)-N(3)	1.3548(19)
C(21)-C(22)	1.3897(19)
C(22)-C(23)	1.417(2)
C(22)-H(22)	0.95
C(23)-N(4)	1.3600(19)
C(23)-C(24)	1.413(2)
C(24)-C(25)	1.372(2)
C(24)-H(24)	0.95
C(25)-N(3)	1.346(2)
C(25)-H(25)	0.95
C(26)-N(4)	1.450(2)
C(26)-H(26A)	0.98
C(26)-H(26B)	0.98
C(26)-H(26C)	0.98
C(27)-N(4)	1.4577(19)
C(27)-H(27A)	0.98
C(27)-H(27B)	0.98
C(27)-H(27C)	0.98
C(28)-Cl(1)#1	1.7650(16)
C(28)-Cl(1)	1.7650(16)
C(28)-H(28A)	0.99
C(28)-H(28B)	0.99
C(29)-Cl(2)	1.800(6)
C(29)-Cl(2)#2	1.800(6)
C(29)-H(29A)	0.99
C(29)-H(29B)	0.99

O(1)-H(1O)	0.88(2)
O(2)-H(2O)	0.94(3)
Bond Angles	
O(1)-C(1)-C(6)	117.60(10)
O(1)-C(1)-C(2)	122.82(10)
C(6)-C(1)-C(2)	119.58(10)
C(3)-C(2)-C(1)	117.93(10)
C(3)-C(2)-C(11)	120.65(10)
C(1)-C(2)-C(11)	121.38(10)
C(4)-C(3)-C(2)	122.47(10)
C(4)-C(3)-H(3)	118.8
C(2)-C(3)-H(3)	118.8
O(2)-C(4)-C(3)	121.48(10)
O(2)-C(4)-C(5)	116.68(10)
C(3)-C(4)-C(5)	121.80(10)
C(6)-C(5)-C(4)	121.06(10)
C(6)-C(5)-C(21)	119.5
C(4)-C(5)-C(21)	119.5
C(1)-C(6)-C(5)	116.39(10)
C(1)-C(6)-H(6)	123.28(10)
C(5)-C(6)-H(6)	120.27(10)
N(1)-C(11)-C(12)	119.79(10)
N(1)-C(11)-C(2)	120.1
C(12)-C(11)-C(2)	120.1
C(11)-C(12)-C(13)	123.73(11)
C(11)-C(12)-H(12)	118.1
C(13)-C(12)-H(12)	118.1
N(2)-C(13)-C(14)	108.29(10)
N(2)-C(13)-C(12)	110.35(9)
C(14)-C(13)-C(12)	109.49(11)
C(15)-C(14)-C(13)	111.84(10)
C(15)-C(14)-H(14)	108.85(10)
C(13)-C(14)-H(14)	108.00(10)
N(1)-C(15)-C(14)	116.94(13)
N(1)-C(15)-H(15)	122.80(13)
C(14)-C(15)-H(15)	120.25(13)
N(2)-C(16)-H(16A)	117.00(13)
N(2)-C(16)-H(16B)	121.24(13)
H(16A)-C(16)-H(16B)	121.75(13)
N(2)-C(16)-H(16C)	122.85(13)
H(16A)-C(16)-H(16C)	118.6
H(16B)-C(16)-H(16C)	118.6
N(2)-C(17)-H(17A)	117.48(13)
N(2)-C(17)-H(17B)	122.36(13)
H(17A)-C(17)-H(17B)	120.16(13)
N(2)-C(17)-H(17C)	117.18(13)
H(17A)-C(17)-H(17C)	121.64(13)
H(17B)-C(17)-H(17C)	121.17(13)
N(3)-C(21)-C(22)	122.55(13)
N(3)-C(21)-C(5)	118.7

C(22)-C(21)-C(5)	118.7
C(21)-C(22)-C(23)	121.82(13)
C(21)-C(22)-H(22)	115.95(13)
C(23)-C(22)-H(22)	122.23(13)
N(4)-C(23)-C(24)	120.57(14)
N(4)-C(23)-C(22)	119.7
C(24)-C(23)-C(22)	119.7
C(25)-C(24)-C(23)	121.99(14)
C(25)-C(24)-H(24)	121.71(15)
C(23)-C(24)-H(24)	116.29(14)
N(3)-C(25)-C(24)	119.16(14)
N(3)-C(25)-H(25)	120.4
C(24)-C(25)-H(25)	120.4
N(4)-C(26)-H(26A)	124.82(15)
N(4)-C(26)-H(26B)	117.6
H(26A)-C(26)-H(26B)	117.6
N(4)-C(26)-H(26C)	109.5
H(26A)-C(26)-H(26C)	109.5
H(26B)-C(26)-H(26C)	109.5
N(4)-C(27)-H(27A)	109.5
N(4)-C(27)-H(27B)	109.5
H(27A)-C(27)-H(27B)	109.5
N(4)-C(27)-H(27C)	109.5
H(27A)-C(27)-H(27C)	109.5
H(27B)-C(27)-H(27C)	109.5
Cl(1)#1-C(28)-Cl(1)	109.5
Cl(1)#1-C(28)-H(28A)	109.5
Cl(1)-C(28)-H(28A)	109.5
Cl(1)#1-C(28)-H(28B)	122.07(13)
Cl(1)-C(28)-H(28B)	115.78(12)
H(28A)-C(28)-H(28B)	122.14(13)
Cl(2)-C(29)-Cl(2)#2	120.25(14)
Cl(2)-C(29)-H(29A)	119.9
Cl(2)#2-C(29)-H(29A)	119.9
Cl(2)-C(29)-H(29B)	121.92(13)
Cl(2)#2-C(29)-H(29B)	121.51(14)
H(29A)-C(29)-H(29B)	116.57(13)
C(15)-N(1)-C(11)	119.07(14)
C(13)-N(2)-C(16)	120.5
C(13)-N(2)-C(17)	120.5
C(16)-N(2)-C(17)	124.56(14)
C(25)-N(3)-C(21)	117.7
C(23)-N(4)-C(26)	117.7
C(23)-N(4)-C(27)	109.5
C(26)-N(4)-C(27)	109.5
C(1)-O(1)-H(1O)	109.5
C(4)-O(2)-H(2O)	109.5

Table A-7. Bond lengths [Å] and angles [deg] for **2.23**.

Bond lengths	
C(1)-O(1)	1.360(2)
C(1)-C(6)	1.373(2)
C(1)-C(2)	1.411(3)
C(2)-C(3)	1.394(2)
C(2)-C(7)	1.478(2)
C(3)-C(4)	1.378(2)
C(3)-H(3)	0.95
C(4)-O(2)	1.363(2)
C(4)-C(5)	1.411(2)
C(5)-C(6)	1.393(2)
C(5)-C(17)	1.471(2)
C(6)-H(6)	0.95
C(7)-N(1)	1.346(2)
C(7)-C(8)	1.397(2)
C(8)-C(9)	1.371(2)
C(8)-H(8)	0.95
C(9)-C(10)	1.377(3)
C(9)-H(9)	0.95
C(10)-C(11)	1.383(3)
C(10)-H(10)	0.95
C(11)-N(1)	1.341(2)
C(11)-C(12)	1.486(2)
C(12)-N(2)	1.343(2)
C(12)-C(13)	1.390(3)
C(13)-C(14)	1.380(2)
C(13)-H(13)	0.95
C(14)-C(15)	1.374(2)
C(14)-H(14)	0.95
C(15)-C(16)	1.378(3)
C(15)-H(15)	0.95
C(16)-N(2)	1.335(2)
C(16)-H(16)	0.95
C(17)-N(3)	1.349(2)
C(17)-C(18)	1.402(2)
C(18)-C(19)	1.372(2)
C(18)-H(18)	0.95
C(19)-C(20)	1.381(3)
C(19)-H(19)	0.95
C(20)-C(21)	1.385(3)
C(20)-H(20)	0.95
C(21)-N(3)	1.345(2)
C(21)-C(22)	1.483(2)
C(22)-N(4)	1.345(2)
C(22)-C(23)	1.385(2)
C(23)-C(24)	1.378(2)
C(23)-H(23)	0.95

C(24)-C(25)	1.374(3)
C(24)-H(24)	0.95
C(25)-C(26)	1.380(3)
C(25)-H(25)	0.95
C(26)-N(4)	1.334(2)
C(26)-H(26)	0.95
O(1)-H(1O)	0.98(3)
O(2)-H(2O)	0.99(3)
Bond Angles	
O(1)-C(1)-C(6)	117.17(16)
O(1)-C(1)-C(2)	122.49(16)
C(6)-C(1)-C(2)	120.35(16)
C(3)-C(2)-C(1)	116.83(16)
C(3)-C(2)-C(7)	121.11(16)
C(1)-C(2)-C(7)	122.05(16)
C(4)-C(3)-C(2)	122.80(17)
C(4)-C(3)-H(3)	118.6
C(2)-C(3)-H(3)	118.6
O(2)-C(4)-C(3)	117.07(16)
O(2)-C(4)-C(5)	122.69(16)
C(3)-C(4)-C(5)	120.24(16)
C(6)-C(5)-C(4)	116.86(16)
C(6)-C(5)-C(17)	120.69(16)
C(4)-C(5)-C(17)	122.45(16)
C(1)-C(6)-C(5)	122.93(17)
C(1)-C(6)-H(6)	118.5
C(5)-C(6)-H(6)	118.5
N(1)-C(7)-C(8)	120.45(16)
N(1)-C(7)-C(2)	116.54(16)
C(8)-C(7)-C(2)	123.00(16)
C(9)-C(8)-C(7)	119.19(17)
C(9)-C(8)-H(8)	120.4
C(7)-C(8)-H(8)	120.4
C(8)-C(9)-C(10)	119.90(18)
C(8)-C(9)-H(9)	120
C(10)-C(9)-H(9)	120
C(9)-C(10)-C(11)	118.86(18)
C(9)-C(10)-H(10)	120.6
C(11)-C(10)-H(10)	120.6
N(1)-C(11)-C(10)	121.43(17)
N(1)-C(11)-C(12)	117.03(16)
C(10)-C(11)-C(12)	121.54(16)
N(2)-C(12)-C(13)	122.13(17)
N(2)-C(12)-C(11)	115.91(16)
C(13)-C(12)-C(11)	121.96(16)
C(14)-C(13)-C(12)	119.25(17)
C(14)-C(13)-H(13)	120.4
C(12)-C(13)-H(13)	120.4
C(15)-C(14)-C(13)	119.10(18)
C(15)-C(14)-H(14)	120.4

C(13)-C(14)-H(14)	120.5
C(14)-C(15)-C(16)	117.99(18)
C(14)-C(15)-H(15)	121
C(16)-C(15)-H(15)	121
N(2)-C(16)-C(15)	124.37(18)
N(2)-C(16)-H(16)	117.8
C(15)-C(16)-H(16)	117.8
N(3)-C(17)-C(18)	120.02(16)
N(3)-C(17)-C(5)	116.89(15)
C(18)-C(17)-C(5)	123.09(16)
C(19)-C(18)-C(17)	119.52(17)
C(19)-C(18)-H(18)	120.2
C(17)-C(18)-H(18)	120.2
C(18)-C(19)-C(20)	120.07(17)
C(18)-C(19)-H(19)	120
C(20)-C(19)-H(19)	120
C(19)-C(20)-C(21)	118.30(17)
C(19)-C(20)-H(20)	120.8
C(21)-C(20)-H(20)	120.8
N(3)-C(21)-C(20)	121.98(16)
N(3)-C(21)-C(22)	116.56(16)
C(20)-C(21)-C(22)	121.44(16)
N(4)-C(22)-C(23)	122.91(17)
N(4)-C(22)-C(21)	116.10(16)
C(23)-C(22)-C(21)	120.97(16)
C(24)-C(23)-C(22)	118.92(17)
C(24)-C(23)-H(23)	120.5
C(22)-C(23)-H(23)	120.5
C(25)-C(24)-C(23)	118.89(18)
C(25)-C(24)-H(24)	120.6
C(23)-C(24)-H(24)	120.6
C(24)-C(25)-C(26)	118.47(18)
C(24)-C(25)-H(25)	120.8
C(26)-C(25)-H(25)	120.8
N(4)-C(26)-C(25)	123.99(18)
N(4)-C(26)-H(26)	118
C(25)-C(26)-H(26)	118
C(11)-N(1)-C(7)	120.13(16)
C(16)-N(2)-C(12)	117.16(17)
C(21)-N(3)-C(17)	120.08(15)
C(26)-N(4)-C(22)	116.78(16)
C(1)-O(1)-H(1O)	106.1(15)
C(4)-O(2)-H(2O)	106.6(15)

Table A-8. Bond lengths [Å] and angles [deg] for **2.39**.

Bond lengths

C(1)-O(1)	1.2245(18)
C(1)-C(3)#1	1.472(2)
C(1)-C(2)	1.4848(19)
C(2)-C(3)	1.334(2)
C(2)-C(4)	1.505(2)
C(3)-C(1)#1	1.472(2)
C(3)-H(3)	0.95
C(4)-N(1)	1.4998(19)
C(4)-H(4A)	0.99
C(4)-H(4B)	0.99
C(5)-N(1)	1.503(2)
C(5)-C(6)	1.518(2)
C(5)-H(5A)	0.99
C(5)-H(5B)	0.99
C(6)-C(7)	1.519(2)
C(6)-H(6A)	0.99
C(6)-H(6B)	0.99
C(8)-C(7)	1.516(2)
C(8)-C(9)	1.517(2)
C(8)-H(8A)	0.99
C(8)-H(8B)	0.99
C(9)-N(1)	1.509(2)
C(9)-H(9A)	0.99
C(9)-H(9B)	0.99
C(7)-H(7A)	0.99
C(7)-H(7B)	0.99
B(1)-F(1)	1.367(2)
B(1)-F(2)	1.373(2)
B(1)-F(3)	1.386(2)
B(1)-F(4)	1.401(2)
N(1)-H(1N)	0.914(19)
Bond Angles	
O(1)-C(1)-C(3)#1	119.92(14)
O(1)-C(1)-C(2)	121.12(14)
C(3)#1-C(1)-C(2)	118.94(13)
C(3)-C(2)-C(1)	118.53(13)
C(3)-C(2)-C(4)	124.17(14)
C(1)-C(2)-C(4)	117.26(14)
C(2)-C(3)-C(1)#1	122.44(13)
C(2)-C(3)-H(3)	118.8
C(1)#1-C(3)-H(3)	118.8
N(1)-C(4)-C(2)	113.88(12)
N(1)-C(4)-H(4A)	108.8
C(2)-C(4)-H(4A)	108.8
N(1)-C(4)-H(4B)	108.8
C(2)-C(4)-H(4B)	108.8
H(4A)-C(4)-H(4B)	107.7
N(1)-C(5)-C(6)	110.83(13)
N(1)-C(5)-H(5A)	109.5
C(6)-C(5)-H(5A)	109.5

N(1)-C(5)-H(5B)	109.5
C(6)-C(5)-H(5B)	109.5
H(5A)-C(5)-H(5B)	108.1
C(5)-C(6)-C(7)	111.50(14)
C(5)-C(6)-H(6A)	109.3
C(7)-C(6)-H(6A)	109.3
C(5)-C(6)-H(6B)	109.3
C(7)-C(6)-H(6B)	109.3
H(6A)-C(6)-H(6B)	108
C(7)-C(8)-C(9)	111.28(13)
C(7)-C(8)-H(8A)	109.4
C(9)-C(8)-H(8A)	109.4
C(7)-C(8)-H(8B)	109.4
C(9)-C(8)-H(8B)	109.4
H(8A)-C(8)-H(8B)	108
N(1)-C(9)-C(8)	109.81(13)
N(1)-C(9)-H(9A)	109.7
C(8)-C(9)-H(9A)	109.7
N(1)-C(9)-H(9B)	109.7
C(8)-C(9)-H(9B)	109.7
H(9A)-C(9)-H(9B)	108.2
C(8)-C(7)-C(6)	109.91(15)
C(8)-C(7)-H(7A)	109.7
C(6)-C(7)-H(7A)	109.7
C(8)-C(7)-H(7B)	109.7
C(6)-C(7)-H(7B)	109.7
H(7A)-C(7)-H(7B)	108.2
F(1)-B(1)-F(2)	111.56(15)
F(1)-B(1)-F(3)	110.93(16)
F(2)-B(1)-F(3)	110.32(16)
F(1)-B(1)-F(4)	109.74(15)
F(2)-B(1)-F(4)	108.16(16)
F(3)-B(1)-F(4)	105.94(14)
C(4)-N(1)-C(5)	111.69(11)
C(4)-N(1)-C(9)	109.78(12)
C(5)-N(1)-C(9)	110.92(13)
C(4)-N(1)-H(1N)	107.4(12)
C(5)-N(1)-H(1N)	111.2(11)
C(9)-N(1)-H(1N)	105.7(11)

Table A-9. Bond lengths [Å] and angles [deg] for **2.40**.

Bond lengths	
C(1)-O(1)	1.224(2)
C(1)-C(3)	1.471(3)
C(1)-C(2)	1.483(3)
C(2)-C(3)#1	1.333(2)

C(2)-C(4)	1.499(2)
C(3)-C(2)#1	1.333(2)
C(3)-H(3)	0.95
C(4)-N(1)	1.504(2)
C(4)-H(4A)	0.99
C(4)-H(4B)	0.99
C(5)-N(1)	1.496(2)
C(5)-C(6)	1.515(3)
C(5)-H(5A)	0.99
C(5)-H(5B)	0.99
C(6)-O(2)	1.418(3)
C(6)-H(6A)	0.99
C(6)-H(6B)	0.99
C(7)-O(2)	1.416(3)
C(7)-C(8)	1.512(3)
C(7)-H(7A)	0.99
C(7)-H(7B)	0.99
C(8)-N(1)	1.505(2)
C(8)-H(8A)	0.99
C(8)-H(8B)	0.99
B(1)-F(2)	1.363(3)
B(1)-F(1)	1.370(3)
B(1)-F(4)	1.385(3)
B(1)-F(3)	1.390(3)
N(1)-H(1N)	0.876(19)
Bond Angles	
O(1)-C(1)-C(3)	121.17(16)
O(1)-C(1)-C(2)	120.01(17)
C(3)-C(1)-C(2)	118.81(14)
C(3)#1-C(2)-C(1)	120.06(16)
C(3)#1-C(2)-C(4)	122.23(16)
C(1)-C(2)-C(4)	117.57(14)
C(2)#1-C(3)-C(1)	121.11(16)
C(2)#1-C(3)-H(3)	119.4
C(1)-C(3)-H(3)	119.4
C(2)-C(4)-N(1)	113.54(15)
C(2)-C(4)-H(4A)	108.9
N(1)-C(4)-H(4A)	108.9
C(2)-C(4)-H(4B)	108.9
N(1)-C(4)-H(4B)	108.9
H(4A)-C(4)-H(4B)	107.7
N(1)-C(5)-C(6)	110.04(15)
N(1)-C(5)-H(5A)	109.7
C(6)-C(5)-H(5A)	109.7
N(1)-C(5)-H(5B)	109.7
C(6)-C(5)-H(5B)	109.7
H(5A)-C(5)-H(5B)	108.2
O(2)-C(6)-C(5)	111.24(18)
O(2)-C(6)-H(6A)	109.4
C(5)-C(6)-H(6A)	109.4

O(2)-C(6)-H(6B)	109.4
C(5)-C(6)-H(6B)	109.4
H(6A)-C(6)-H(6B)	108
O(2)-C(7)-C(8)	111.08(16)
O(2)-C(7)-H(7A)	109.4
C(8)-C(7)-H(7A)	109.4
O(2)-C(7)-H(7B)	109.4
C(8)-C(7)-H(7B)	109.4
H(7A)-C(7)-H(7B)	108
N(1)-C(8)-C(7)	110.17(16)
N(1)-C(8)-H(8A)	109.6
C(7)-C(8)-H(8A)	109.6
N(1)-C(8)-H(8B)	109.6
C(7)-C(8)-H(8B)	109.6
H(8A)-C(8)-H(8B)	108.1
F(2)-B(1)-F(1)	112.0(2)
F(2)-B(1)-F(4)	108.74(19)
F(1)-B(1)-F(4)	107.45(18)
F(2)-B(1)-F(3)	109.29(19)
F(1)-B(1)-F(3)	109.06(18)
F(4)-B(1)-F(3)	110.29(19)
C(5)-N(1)-C(4)	112.69(13)
C(5)-N(1)-C(8)	109.99(15)
C(4)-N(1)-C(8)	109.55(14)
C(5)-N(1)-H(1N)	107.3(12)
C(4)-N(1)-H(1N)	108.2(12)
C(8)-N(1)-H(1N)	109.0(12)
C(7)-O(2)-C(6)	109.53(15)

Table A-10. Bond lengths [Å] and angles [deg] for **2.48**.

Bond lengths	
C(1)-O(1)	1.339(3)
C(1)-C(2)	1.371(3)
C(1)-C(6)	1.413(3)
C(2)-C(3)	1.369(3)
C(2)-H(2)	0.95
C(3)-O(2)	1.342(3)
C(3)-C(4)	1.412(3)
C(4)-C(5)	1.384(3)
C(4)-C(21)	1.465(3)
C(5)-C(6)	1.386(3)
C(5)-H(5)	0.95
C(6)-C(11)	1.459(3)
C(11)-N(1)	1.344(3)
C(11)-C(12)	1.388(3)
C(12)-C(13)	1.369(3)

C(12)-H(12)	0.95
C(13)-C(14)	1.374(3)
C(13)-H(13)	0.95
C(14)-C(15)	1.363(3)
C(14)-H(14)	0.95
C(15)-N(1)	1.328(3)
C(15)-H(15)	0.95
C(21)-N(2)	1.344(3)
C(21)-C(22)	1.385(3)
C(22)-C(23)	1.371(3)
C(22)-H(22)	0.95
C(23)-C(24)	1.378(3)
C(23)-H(23)	0.95
C(24)-C(25)	1.362(3)
C(24)-H(24)	0.95
C(25)-N(2)	1.328(3)
C(25)-H(25)	0.95
O(1)-H(1)	0.97(3)
O(2)-H(2O)	0.92(3)
Bond Angles	
O(1)-C(1)-C(2)	117.4(2)
O(1)-C(1)-C(6)	122.5(2)
C(2)-C(1)-C(6)	120.1(2)
C(3)-C(2)-C(1)	122.0(2)
C(3)-C(2)-H(2)	119
C(1)-C(2)-H(2)	119
O(2)-C(3)-C(2)	117.92(19)
O(2)-C(3)-C(4)	122.0(2)
C(2)-C(3)-C(4)	120.0(2)
C(5)-C(4)-C(3)	116.7(2)
C(5)-C(4)-C(21)	121.40(19)
C(3)-C(4)-C(21)	121.89(19)
C(4)-C(5)-C(6)	124.6(2)
C(4)-C(5)-H(5)	117.7
C(6)-C(5)-H(5)	117.7
C(5)-C(6)-C(1)	116.5(2)
C(5)-C(6)-C(11)	121.7(2)
C(1)-C(6)-C(11)	121.8(2)
N(1)-C(11)-C(12)	119.7(2)
N(1)-C(11)-C(6)	117.2(2)
C(12)-C(11)-C(6)	123.1(2)
C(13)-C(12)-C(11)	120.7(2)
C(13)-C(12)-H(12)	119.6
C(11)-C(12)-H(12)	119.6
C(12)-C(13)-C(14)	118.7(2)
C(12)-C(13)-H(13)	120.7
C(14)-C(13)-H(13)	120.7
C(15)-C(14)-C(13)	118.1(2)
C(15)-C(14)-H(14)	120.9
C(13)-C(14)-H(14)	120.9

N(1)-C(15)-C(14)	123.9(2)
N(1)-C(15)-H(15)	118.1
C(14)-C(15)-H(15)	118.1
N(2)-C(21)-C(22)	120.2(2)
N(2)-C(21)-C(4)	115.96(19)
C(22)-C(21)-C(4)	123.8(2)
C(23)-C(22)-C(21)	119.5(2)
C(23)-C(22)-H(22)	120.3
C(21)-C(22)-H(22)	120.3
C(22)-C(23)-C(24)	119.5(2)
C(22)-C(23)-H(23)	120.2
C(24)-C(23)-H(23)	120.2
C(25)-C(24)-C(23)	118.2(2)
C(25)-C(24)-H(24)	120.9
C(23)-C(24)-H(24)	120.9
N(2)-C(25)-C(24)	123.0(2)
N(2)-C(25)-H(25)	118.5
C(24)-C(25)-H(25)	118.5
C(15)-N(1)-C(11)	118.9(2)
C(25)-N(2)-C(21)	119.6(2)
C(1)-O(1)-H(1)	107.9(19)
C(3)-O(2)-H(2O)	103.4(18)

Table A-11. Bond lengths [Å] and angles [deg] for **2.52**.

Bond lengths	
C(1)-O(1)	1.3460(18)
C(1)-C(2)	1.398(2)
C(1)-C(6)	1.414(2)
C(2)-C(3)	1.395(2)
C(2)-C(31)	1.4872(19)
C(3)-O(2)	1.3444(17)
C(3)-C(4)	1.418(2)
C(4)-C(5)	1.383(2)
C(4)-C(21)	1.468(2)
C(5)-C(6)	1.381(2)
C(5)-H(5)	0.95
C(6)-C(11)	1.477(2)
C(11)-N(1)	1.343(2)
C(11)-C(12)	1.395(2)
C(12)-C(13)	1.377(2)
C(12)-H(12)	0.95
C(13)-C(14)	1.375(3)
C(13)-H(13)	0.95
C(14)-C(15)	1.370(2)
C(14)-H(14)	0.95
C(15)-N(1)	1.3356(19)

C(15)-H(15)	0.95
C(21)-N(2)	1.344(2)
C(21)-C(22)	1.386(2)
C(22)-C(23)	1.369(3)
C(22)-H(22)	0.95
C(23)-C(24)	1.370(3)
C(23)-H(23)	0.95
C(24)-C(25)	1.369(2)
C(24)-H(24)	0.95
C(25)-N(2)	1.340(2)
C(25)-H(25)	0.95
C(31)-C(32)	1.386(2)
C(31)-C(36)	1.388(2)
C(32)-C(33)	1.387(2)
C(32)-H(32)	0.95
C(33)-C(34)	1.378(2)
C(33)-H(33)	0.95
C(34)-C(35)	1.374(3)
C(34)-H(34)	0.95
C(35)-C(36)	1.384(2)
C(35)-H(35)	0.95
C(36)-H(36)	0.95
O(1)-H(1)	0.95(2)
O(2)-H(2)	1.00(2)
Bond Angles	
O(1)-C(1)-C(2)	117.72(13)
O(1)-C(1)-C(6)	121.55(13)
C(2)-C(1)-C(6)	120.73(14)
C(3)-C(2)-C(1)	119.39(13)
C(3)-C(2)-C(31)	120.44(13)
C(1)-C(2)-C(31)	120.15(13)
O(2)-C(3)-C(2)	117.31(13)
O(2)-C(3)-C(4)	121.48(13)
C(2)-C(3)-C(4)	121.20(13)
C(5)-C(4)-C(3)	116.87(14)
C(5)-C(4)-C(21)	121.30(13)
C(3)-C(4)-C(21)	121.83(13)
C(6)-C(5)-C(4)	124.28(14)
C(6)-C(5)-H(5)	117.9
C(4)-C(5)-H(5)	117.9
C(5)-C(6)-C(1)	117.53(13)
C(5)-C(6)-C(11)	121.19(13)
C(1)-C(6)-C(11)	121.27(14)
N(1)-C(11)-C(12)	119.96(14)
N(1)-C(11)-C(6)	116.69(13)
C(12)-C(11)-C(6)	123.34(15)
C(13)-C(12)-C(11)	119.48(16)
C(13)-C(12)-H(12)	120.3
C(11)-C(12)-H(12)	120.3
C(14)-C(13)-C(12)	119.93(15)

C(14)-C(13)-H(13)	120
C(12)-C(13)-H(13)	120
C(15)-C(14)-C(13)	117.78(15)
C(15)-C(14)-H(14)	121.1
C(13)-C(14)-H(14)	121.1
N(1)-C(15)-C(14)	123.21(17)
N(1)-C(15)-H(15)	118.4
C(14)-C(15)-H(15)	118.4
N(2)-C(21)-C(22)	119.36(15)
N(2)-C(21)-C(4)	116.89(13)
C(22)-C(21)-C(4)	123.75(14)
C(23)-C(22)-C(21)	120.52(17)
C(23)-C(22)-H(22)	119.7
C(21)-C(22)-H(22)	119.7
C(22)-C(23)-C(24)	119.67(17)
C(22)-C(23)-H(23)	120.2
C(24)-C(23)-H(23)	120.2
C(25)-C(24)-C(23)	117.72(17)
C(25)-C(24)-H(24)	121.1
C(23)-C(24)-H(24)	121.1
N(2)-C(25)-C(24)	123.18(16)
N(2)-C(25)-H(25)	118.4
C(24)-C(25)-H(25)	118.4
C(32)-C(31)-C(36)	118.24(14)
C(32)-C(31)-C(2)	120.23(13)
C(36)-C(31)-C(2)	121.51(14)
C(31)-C(32)-C(33)	121.35(15)
C(31)-C(32)-H(32)	119.3
C(33)-C(32)-H(32)	119.3
C(34)-C(33)-C(32)	119.20(16)
C(34)-C(33)-H(33)	120.4
C(32)-C(33)-H(33)	120.4
C(35)-C(34)-C(33)	120.48(15)
C(35)-C(34)-H(34)	119.8
C(33)-C(34)-H(34)	119.8
C(34)-C(35)-C(36)	120.00(16)
C(34)-C(35)-H(35)	120
C(36)-C(35)-H(35)	120
C(35)-C(36)-C(31)	120.72(16)
C(35)-C(36)-H(36)	119.6
C(31)-C(36)-H(36)	119.6
C(15)-N(1)-C(11)	119.62(14)
C(25)-N(2)-C(21)	119.54(14)
C(1)-O(1)-H(1)	103.2(14)
C(3)-O(2)-H(2)	105.2(12)

Table A-12. Bond lengths [Å] and angles [deg] for **3.23**.

Bond lengths	
Pd(1)-O(1)	1.950(4)
Pd(1)-O(31)	2.027(4)
Pd(1)-O(32)	2.028(4)
Pd(1)-N(1)	2.001(6)
Pd(2)-O(2)	1.945(4)
Pd(2)-O(41)	2.031(4)
Pd(2)-O(42)	2.027(4)
Pd(2)-N(2)	2.014(5)
F(31A)-C(31)	1.319(2)[a]
F(32A)-C(31)	1.316(2)[a]
F(33A)-C(31)	1.325(2)[a]
F(31B)-C(31)	1.320(2)[a]
F(32B)-C(31)	1.324(2)[a]
F(33B)-C(31)	1.318(2)[a]
F(34)-C(35)	1.301(9)
F(35)-C(35)	1.290(8)
F(36)-C(35)	1.342(8)
F(41)-C(41)	1.329(9)
F(42)-C(41)	1.327(8)
F(43)-C(41)	1.315(8)
F(44)-C(45)	1.328(10)
F(45)-C(45)	1.299(9)
F(46)-C(45)	1.289(9)
O(1)-C(1)	1.340(7)
O(2)-C(4)	1.332(7)
O(31)-C(32)	1.256(8)
O(32)-C(34)	1.258(8)
O(41)-C(42)	1.254(7)
O(42)-C(44)	1.262(8)
N(1)-C(11)	1.357(8)
N(1)-C(15)	1.347(8)
N(2)-C(21)	1.364(8)
N(2)-C(25)	1.355(8)
C(1)-C(2)	1.431(9)
C(1)-C(6)	1.388(9)
C(2)-C(3)	1.396(9)
C(2)-C(11)	1.472(9)
C(3)-C(4)	1.387(9)
C(4)-C(5)	1.434(9)
C(5)-C(6)	1.382(9)
C(5)-C(21)	1.476(9)
C(11)-C(12)	1.394(9)
C(12)-C(13)	1.381(10)
C(13)-C(14)	1.388(10)
C(14)-C(15)	1.372(10)
C(21)-C(22)	1.397(9)
C(22)-C(23)	1.381(9)
C(23)-C(24)	1.377(9)

C(24)-C(25)	1.362(9)
C(31)-C(32)	1.537(8)
C(32)-C(33)	1.371(10)
C(33)-C(34)	1.390(10)
C(34)-C(35)	1.533(10)
C(41)-C(42)	1.523(10)
C(42)-C(43)	1.381(9)
C(43)-C(44)	1.380(10)
C(44)-C(45)	1.522(10)
Bond Angles	
O(1)-Pd(1)-O(31)	178.24(18)
O(1)-Pd(1)-O(32)	88.73(19)
O(1)-Pd(1)-N(1)	88.9(2)
O(31)-Pd(1)-O(32)	92.24(19)
O(31)-Pd(1)-N(1)	90.2(2)
O(32)-Pd(1)-N(1)	176.2(2)
O(2)-Pd(2)-O(41)	177.50(18)
O(2)-Pd(2)-O(42)	86.71(19)
O(2)-Pd(2)N-(2)	89.75(19)
O(41)-Pd(2)-O(42)	92.10(18)
O(41)-Pd(2)-N(2)	91.33(19)
O(42)-Pd(2)-N(2)	175.5(2)
Pd(1)-O(1)-C(1)	112.0(4)
Pd(2)-O(2)-C(4)	115.3(4)
Pd(1)-O(31)-C(32)	122.4(5)
Pd(1)-O(32)-C(34)	122.5(4)
Pd(2)-O(41)-C(42)	122.5(4)
Pd(2)-O(42)-C(44)	123.1(4)
Pd(1)-N(1)-C(11)	121.7(4)
Pd(1)-N(1)-C(15)	119.0(4)
C(11)-N(1)-C(15)	119.0(6)
Pd(2)-N(2)-C(21)	122.7(4)
Pd(2)-N(2)-C(25)	117.6(4)
C(21)-N(2)-C(25)	119.3(5)
O(1)-C(1)-C(2)	122.3(6)
O(1)-C(1)-C(6)	120.1(6)
C(2)-C(1)-C(6)	117.6(6)
C(1)-C(2)-C(3)	119.1(6)
C(1)-C(2)-C(11)	120.7(6)
C(3)-C(2)-C(11)	120.2(6)
C(2)-C(3)-C(4)	123.1(6)
O(2)-C(4)-C(3)	119.1(6)
O(2)-C(4)-C(5)	123.4(6)
C(3)-C(4)-C(5)	117.4(6)
C(4)-C(5)-C(6)	119.5(6)
C(4)-C(5)-C(21)	120.7(6)
C(6)-C(5)-C(21)	119.6(6)
C(1)-C(6)-C(5)	123.2(6)
N(1)-C(11)-C(2)	119.8(6)
N(1)-C(11)-C(12)	120.0(6)

C(2)-C(11)-C(12)	120.2(6)
C(11)-C(12)-C(13)	120.2(7)
C(12)-C(13)-C(14)	119.3(6)
C(13)-C(14)-C(15)	117.9(7)
N(1)-C(15)-C(14)	123.5(7)
N(2)-C(21)-C(5)	120.6(6)
N(2)-C(21)-C(22)	119.0(6)
C(5)-C(21)-C(22)	120.4(6)
C(21)-C(22)-C(23)	121.2(6)
C(22)-C(23)-C(24)	118.2(6)
C(23)-C(24)-C(25)	119.6(7)
N(2)-C(25)-C(24)	122.6(6)
F(31A)-C(31)-(F32A)	107.2(3)[a]
F(31A)-C(31)-F(33A)	106.1(3)[a]
F(31A)-C(31)-C(32)	112.6(5)
F(32A)-C(31)-F(33A)	105.7(3)[a]
F(32A)-C(31)-C(32)	116.7(6)
F(33A)-C(31)-C(32)	107.8(6)
F(31B)-C(31)-F(32B)	105.9(3)[a]
F(31B)-C(31)-F(33B)	106.7(3)[a]
F(31B)-C(31)-C(32)	117.6(6)
F(32B)-C(31)-F(33B)	105.6(3)[a]
F(32B)-C(31)-C(32)	102.3(7)
F(33B)-C(31)-C(32)	117.4(7)
O(31)-C(32)-C(31)	111.6(6)
O(31)-C(32)-C(33)	129.9(7)
C(31)-C(32)-C(33)	118.5(6)
C(32)-C(33)-C(34)	123.2(6)
O(32)-C(34)-C(33)	129.5(6)
O(32)-C(34)-C(35)	111.9(6)
C(33)-C(34)-C(35)	118.5(6)
F(34)-C(35)-F(35)	108.4(7)
F(34)-C(35)-F(36)	104.8(7)
F(34)-C(35)-C(34)	112.7(6)
F(35)-C(35)-F(36)	106.2(6)
F(35)-C(35)-C(34)	111.6(6)
F(36)-C(35)-C(34)	112.6(6)
F(41)-C(41)-F(42)	105.6(6)
F(41)-C(41)-F(43)	107.0(7)
F(41)-C(41)-C(42)	112.8(6)
F(42)-C(41)-F(43)	105.9(7)
F(42)-C(41)-C(42)	111.8(6)
F(43)-C(41)-C(42)	113.3(6)
O(41)-C(42)-C(41)	113.8(6)
O(41)-C(42)-C(43)	129.7(7)
C(41)-C(42)-C(43)	116.4(6)
C(42)-C(43)-C(44)	123.7(7)
O(42)-C(44)-C(43)	128.8(6)
O(42)-C(44)-C(45)	112.4(6)
C(43)-C(44)-C(45)	118.8(6)

F(44)-C(45)-F(45)	104.2(7)
F(44)-C(45)-F(46)	104.2(8)
F(44)-C(45)-C(44)	111.2(7)
F(45)-C(45)-F(46)	110.1(8)
F(45)-C(45)-C(44)	112.6(7)
F(46)-C(45)-C(44)	113.8(7)

[a] Bond distance or angle restrained during refinement.

Table A-13. Bond lengths [Å] and angles [deg] for **3.24**.

Bond lengths	
C(1)-O(1)	1.325(2)
C(1)-C(6)	1.373(3)
C(1)-C(2)	1.390(3)
C(2)-C(3)	1.380(3)
C(2)-C(11)	1.454(3)
C(3)-C(4)	1.381(3)
C(3)-H(3)	0.95
C(4)-O(2)	1.314(2)
C(4)-C(5)	1.389(3)
C(5)-C(6)	1.382(3)
C(5)-C(21)	1.457(3)
C(6)-H(6)	0.95
C(10)-C(16)	1.493(4)
C(10)-H(10A)	0.98
C(10)-H(10B)	0.98
C(10)-H(10C)	0.98
C(11)-N(1)	1.343(3)
C(11)-C(12)	1.369(3)
C(12)-C(13)	1.377(3)
C(12)-H(12)	0.95
C(13)-C(14)	1.375(3)
C(13)-C(16)	1.500(3)
C(14)-C(15)	1.345(3)
C(14)-H(14)	0.95
C(15)-N(1)	1.333(3)
C(15)-H(15)	0.95
C(16)-C(18)	1.491(4)
C(16)-C(17)	1.513(4)
C(17)-H(17A)	0.98
C(17)-H(17B)	0.98
C(17)-H(17C)	0.98
C(18)-H(18A)	0.98
C(18)-H(18B)	0.98
C(18)-H(18C)	0.98
C(21)-N(2)	1.342(3)

C(21)-C(22)	1.367(3)
C(22)-C(23)	1.373(3)
C(22)-H(22)	0.95
C(23)-C(24)	1.370(3)
C(23)-C(26)	1.500(3)
C(24)-C(25)	1.345(3)
C(24)-H(24)	0.95
C(25)-N(2)	1.328(3)
C(25)-H(25)	0.95
C(26)-C(27)	1.500(3)
C(26)-C(28)	1.509(3)
C(26)-C(29)	1.520(3)
C(27)-H(27A)	0.98
C(27)-H(27B)	0.98
C(27)-H(27C)	0.98
C(28)-H(28A)	0.98
C(28)-H(28B)	0.98
C(28)-H(28C)	0.98
C(29)-H(29A)	0.98
C(29)-H(29B)	0.98
C(29)-H(29C)	0.98
C(31)-F(33)	1.281(3)
C(31)-F(32)	1.303(4)
C(31)-F(31)	1.306(4)
C(31)-C(32)	1.507(3)
C(32)-O(31)	1.236(3)
C(32)-C(33)	1.357(3)
C(33)-C(34)	1.375(3)
C(33)-H(33)	0.95
C(34)-O(32)	1.235(3)
C(34)-C(35)	1.509(3)
C(35)-F(36)	1.215(7)
C(35)-F(34B)	1.249(7)
C(35)-F(35B)	1.269(8)
C(35)-F(34)	1.277(7)
C(35)-F(35)	1.289(8)
C(35)-F(36B)	1.292(8)
C(41)-F(43)	1.297(3)
C(41)-F(42)	1.297(3)
C(41)-F(41)	1.308(4)
C(41)-C(42)	1.503(4)
C(42)-O(41)	1.244(3)
C(42)-C(43)	1.362(3)
C(43)-C(44)	1.364(4)
C(43)-H(43)	0.95
C(44)-O(42)	1.245(3)
C(44)-C(45)	1.504(3)
C(45)-F(44)	1.287(3)
C(45)-F(45)	1.293(3)
C(45)-F(46)	1.294(3)

N(1)-Pd(1)	1.9628(18)
N(2)-Pd(2)	1.9702(17)
O(1)-Pd(1)	1.9234(15)
O(2)-Pd(2)	1.9106(15)
O(31)-Pd(1)	1.9844(15)
O(32)-Pd(1)	1.9866(16)
O(41)-Pd(2)	1.9890(16)
O(42)-Pd(2)	1.9853(16)
C(51)-N(3)	1.335(2)
C(51)-C(52)	1.380(3)
C(51)-C(61)	1.451(3)
C(52)-C(53)	1.367(3)
C(52)-H(52)	0.95
C(53)-C(54)	1.364(3)
C(53)-C(56)	1.510(3)
C(54)-C(55)	1.356(3)
C(54)-H(54)	0.95
C(55)-N(3)	1.325(3)
C(55)-H(55)	0.95
C(56)-C(59)	1.498(3)
C(56)-C(57)	1.505(3)
C(56)-C(58)	1.508(3)
C(57)-H(57A)	0.98
C(57)-H(57B)	0.98
C(57)-H(57C)	0.98
C(58)-H(58A)	0.98
C(58)-H(58B)	0.98
C(58)-H(58C)	0.98
C(59)-H(59A)	0.98
C(59)-H(59B)	0.98
C(59)-H(59C)	0.98
C(61)-C(63)	1.371(3)
C(61)-C(62)	1.393(3)
C(62)-O(3)	1.312(2)
C(62)-C(63)#1	1.372(3)
C(63)-C(62)#1	1.372(3)
C(63)-H(63)	0.95
C(71)-F(72B)	1.207(9)
C(71)-F(72)	1.253(6)
C(71)-F(73B)	1.261(9)
C(71)-F(71)	1.270(8)
C(71)-F(73)	1.315(9)
C(71)-F(71B)	1.341(6)
C(71)-C(72)	1.523(3)
C(72)-O(71)	1.235(3)
C(72)-C(73)	1.360(4)
C(73)-C(74)	1.362(3)
C(73)-H(73)	0.95
C(74)-O(72)	1.245(3)
C(74)-C(75)	1.496(3)

C(75)-F(76)	1.274(3)
C(75)-F(75)	1.300(3)
C(75)-F(74)	1.302(3)
N(3)-Pd(3)	1.9761(17)
O(3)-Pd(3)	1.9128(15)
O(71)-Pd(3)	1.9983(15)
O(72)-Pd(3)	1.9878(15)
C(80)-C(81)	1.364(4)
C(80)-C(85)	1.374(4)
C(80)-C(86)	1.474(5)
C(81)-C(82)	1.337(5)
C(81)-H(81)	0.95
C(82)-C(83)	1.349(5)
C(82)-H(82)	0.95
C(83)-C(84)	1.340(5)
C(83)-H(83)	0.95
C(84)-C(85)	1.357(5)
C(84)-H(84)	0.95
C(85)-H(85)	0.95
C(86)-H(86A)	0.98
C(86)-H(86B)	0.98
C(86)-H(86C)	0.98
C(90)-C(96)	1.364(12)
C(90)-C(91)	1.39
C(90)-C(95)	1.39
C(91)-C(92)	1.39
C(91)-H(91)	0.95
C(92)-C(93)	1.39
C(92)-H(92)	0.95
C(93)-C(94)	1.39
C(93)-H(93)	0.95
C(94)-C(95)	1.39
C(94)-H(94)	0.95
C(95)-H(95)	0.95
C(96)-H(96A)	0.98
C(96)-H(96B)	0.98
C(96)-H(96C)	0.98
Bond Angles	
O(1)-C(1)-C(6)	119.12(19)
O(1)-C(1)-C(2)	123.01(19)
C(6)-C(1)-C(2)	117.83(19)
C(3)-C(2)-C(1)	119.15(19)
C(3)-C(2)-C(11)	119.95(19)
C(1)-C(2)-C(11)	120.90(19)
C(2)-C(3)-C(4)	123.01(19)
C(2)-C(3)-H(3)	118.5
C(4)-C(3)-H(3)	118.5
O(2)-C(4)-C(3)	117.83(18)
O(2)-C(4)-C(5)	124.53(19)
C(3)-C(4)-C(5)	117.60(19)

C(6)-C(5)-C(4)	119.17(19)
C(6)-C(5)-C(21)	118.82(18)
C(4)-C(5)-C(21)	122.01(18)
C(1)-C(6)-C(5)	123.14(19)
C(1)-C(6)-H(6)	118.4
C(5)-C(6)-H(6)	118.4
C(16)-C(10)-H(10A)	109.5
C(16)-C(10)-H(10B)	109.5
H(10A)-C(10)-H(10B)	109.5
C(16)-C(10)-H(10C)	109.5
H(10A)-C(10)-H(10C)	109.5
H(10B)-C(10)-H(10C)	109.5
N(1)-C(11)-C(12)	119.93(19)
N(1)-C(11)-C(2)	119.57(19)
C(12)-C(11)-C(2)	120.5(2)
C(11)-C(12)-C(13)	121.5(2)
C(11)-C(12)-H(12)	119.3
C(13)-C(12)-H(12)	119.3
C(14)-C(13)-C(12)	116.6(2)
C(14)-C(13)-C(16)	123.0(2)
C(12)-C(13)-C(16)	120.4(2)
C(15)-C(14)-C(13)	120.5(2)
C(15)-C(14)-H(14)	119.8
C(13)-C(14)-H(14)	119.8
N(1)-C(15)-C(14)	122.4(2)
N(1)-C(15)-H(15)	118.8
C(14)-C(15)-H(15)	118.8
C(18)-C(16)-C(10)	109.9(3)
C(18)-C(16)-C(13)	111.4(2)
C(10)-C(16)-C(13)	107.5(2)
C(18)-C(16)-C(17)	109.5(3)
C(10)-C(16)-C(17)	107.9(3)
C(13)-C(16)-C(17)	110.6(2)
C(16)-C(17)-H(17A)	109.5
C(16)-C(17)-H(17B)	109.5
H(17A)-C(17)-H(17B)	109.5
C(16)-C(17)-H(17C)	109.5
H(17A)-C(17)-H(17C)	109.5
H(17B)-C(17)-H(17C)	109.5
C(16)-C(18)-H(18A)	109.5
C(16)-C(18)-H(18B)	109.5
H(18A)-C(18)-H(18B)	109.5
C(16)-C(18)-H(18C)	109.5
H(18A)-C(18)-H(18C)	109.5
H(18B)-C(18)-H(18C)	109.5
N(2)-C(21)-C(22)	119.46(18)
N(2)-C(21)-C(5)	120.43(18)
C(22)-C(21)-C(5)	120.10(18)
C(21)-C(22)-C(23)	122.02(19)
C(21)-C(22)-H(22)	119

C(23)-C(22)-H(22)	119
C(24)-C(23)-C(22)	116.51(19)
C(24)-C(23)-C(26)	123.44(19)
C(22)-C(23)-C(26)	120.02(19)
C(25)-C(24)-C(23)	120.0(2)
C(25)-C(24)-H(24)	120
C(23)-C(24)-H(24)	120
N(2)-C(25)-C(24)	123.0(2)
N(2)-C(25)-H(25)	118.5
C(24)-C(25)-H(25)	118.5
C(23)-C(26)-C(27)	108.21(18)
C(23)-C(26)-C(28)	111.28(19)
C(27)-C(26)-C(28)	109.0(2)
C(23)-C(26)-C(29)	109.50(18)
C(27)-C(26)-C(29)	110.5(2)
C(28)-C(26)-C(29)	108.3(2)
C(26)-C(27)-H(27A)	109.5
C(26)-C(27)-H(27B)	109.5
H(27A)-C(27)-H(27B)	109.5
C(26)-C(27)-H(27C)	109.5
H(27A)-C(27)-H(27C)	109.5
H(27B)-C(27)-H(27C)	109.5
C(26)-C(28)-H(28A)	109.5
C(26)-C(28)-H(28B)	109.5
H(28A)-C(28)-H(28B)	109.5
C(26)-C(28)-H(28C)	109.5
H(28A)-C(28)-H(28C)	109.5
H(28B)-C(28)-H(28C)	109.5
C(26)-C(29)-H(29A)	109.5
C(26)-C(29)-H(29B)	109.5
H(29A)-C(29)-H(29B)	109.5
C(26)-C(29)-H(29C)	109.5
H(29A)-C(29)-H(29C)	109.5
H(29B)-C(29)-H(29C)	109.5
F(33)-C(31)-F(32)	107.4(3)
F(33)-C(31)-F(31)	109.2(3)
F(32)-C(31)-F(31)	105.3(2)
F(33)-C(31)-C(32)	114.3(2)
F(32)-C(31)-C(32)	110.9(2)
F(31)-C(31)-C(32)	109.3(2)
O(31)-C(32)-C(33)	129.4(2)
O(31)-C(32)-C(31)	111.6(2)
C(33)-C(32)-C(31)	119.1(2)
C(32)-C(33)-C(34)	123.1(2)
C(32)-C(33)-H(33)	118.5
C(34)-C(33)-H(33)	118.5
O(32)-C(34)-C(33)	129.3(2)
O(32)-C(34)-C(35)	113.3(2)
C(33)-C(34)-C(35)	117.4(2)
F(36)-C(35)-F(34B)	127.8(6)

F(36)-C(35)-F(35B)	68.7(7)
F(34B)-C(35)-F(35B)	107.8(6)
F(36)-C(35)-F(34)	110.0(8)
F(34B)-C(35)-F(34)	36.1(6)
F(35B)-C(35)-F(34)	135.9(5)
F(36)-C(35)-F(35)	105.9(7)
F(34B)-C(35)-F(35)	68.7(6)
F(35B)-C(35)-F(35)	42.7(5)
F(34)-C(35)-F(35)	103.6(6)
F(36)-C(35)-F(36B)	36.2(7)
F(34B)-C(35)-F(36B)	109.9(7)
F(35B)-C(35)-F(36B)	104.1(6)
F(34)-C(35)-F(36B)	79.5(6)
F(35)-C(35)-F(36B)	133.8(6)
F(36)-C(35)-C(34)	115.1(4)
F(34B)-C(35)-C(34)	115.0(4)
F(35B)-C(35)-C(34)	108.7(5)
F(34)-C(35)-C(34)	110.8(4)
F(35)-C(35)-C(34)	110.8(4)
F(36B)-C(35)-C(34)	110.7(4)
F(43)-C(41)-F(42)	108.2(3)
F(43)-C(41)-F(41)	106.8(2)
F(42)-C(41)-F(41)	105.9(3)
F(43)-C(41)-C(42)	113.9(2)
F(42)-C(41)-C(42)	111.7(2)
F(41)-C(41)-C(42)	109.8(2)
O(41)-C(42)-C(43)	128.9(2)
O(41)-C(42)-C(41)	112.1(2)
C(43)-C(42)-C(41)	119.0(2)
C(42)-C(43)-C(44)	122.6(2)
C(42)-C(43)-H(43)	118.7
C(44)-C(43)-H(43)	118.7
O(42)-C(44)-C(43)	129.8(2)
O(42)-C(44)-C(45)	111.9(2)
C(43)-C(44)-C(45)	118.3(2)
F(44)-C(45)-F(45)	106.6(3)
F(44)-C(45)-F(46)	108.1(2)
F(45)-C(45)-F(46)	106.8(3)
F(44)-C(45)-C(44)	113.6(2)
F(45)-C(45)-C(44)	110.7(2)
F(46)-C(45)-C(44)	110.8(2)
C(15)-N(1)-C(11)	119.07(19)
C(15)-N(1)-Pd(1)	118.93(16)
C(11)-N(1)-Pd(1)	121.84(14)
C(25)-N(2)-C(21)	118.90(18)
C(25)-N(2)-Pd(2)	117.07(14)
C(21)-N(2)-Pd(2)	123.71(14)
C(1)-O(1)-Pd(1)	111.78(12)
C(4)-O(2)-Pd(2)	118.34(13)
C(32)-O(31)-Pd(1)	122.84(15)

C(34)-O(32)-Pd(1)	122.62(15)
C(42)-O(41)-Pd(2)	122.60(16)
C(44)-O(42)-Pd(2)	122.13(15)
O(1)-Pd(1)-N(1)	88.42(7)
O(1)-Pd(1)-O(31)	178.49(6)
N(1)-Pd(1)-O(31)	90.20(7)
O(1)-Pd(1)-O(32)	88.90(7)
N(1)-Pd(1)-O(32)	177.14(7)
O(31)-Pd(1)-O(32)	92.47(7)
O(2)-Pd(2)-N(2)	91.06(7)
O(2)-Pd(2)-O(42)	86.06(7)
N(2)-Pd(2)-O(42)	175.70(7)
O(2)-Pd(2)-O(41)	177.08(6)
N(2)-Pd(2)-O(41)	91.15(7)
O(42)-Pd(2)-O(41)	91.62(7)
N(3)-C(51)-C(52)	119.35(18)
N(3)-C(51)-C(61)	119.98(17)
C(52)-C(51)-C(61)	120.68(18)
C(53)-C(52)-C(51)	122.40(18)
C(53)-C(52)-H(52)	118.8
C(51)-C(52)-H(52)	118.8
C(54)-C(53)-C(52)	116.07(19)
C(54)-C(53)-C(56)	120.74(18)
C(52)-C(53)-C(56)	123.18(18)
C(55)-C(54)-C(53)	120.32(19)
C(55)-C(54)-H(54)	119.8
C(53)-C(54)-H(54)	119.8
N(3)-C(55)-C(54)	122.98(19)
N(3)-C(55)-H(55)	118.5
C(54)-C(55)-H(55)	118.5
C(59)-C(56)-C(57)	108.2(2)
C(59)-C(56)-C(58)	109.1(2)
C(57)-C(56)-C(58)	109.2(2)
C(59)-C(56)-C(53)	112.04(18)
C(57)-C(56)-C(53)	107.79(18)
C(58)-C(56)-C(53)	110.38(19)
C(56)-C(57)-H(57A)	109.5
C(56)-C(57)-H(57B)	109.5
H(57A)-C(57)-H(57B)	109.5
C(56)-C(57)-H(57C)	109.5
H(57A)-C(57)-H(57C)	109.5
H(57B)-C(57)-H(57C)	109.5
C(56)-C(58)-H(58A)	109.5
C(56)-C(58)-H(58B)	109.5
H(58A)-C(58)-H(58B)	109.5
C(56)-C(58)-H(58C)	109.5
H(58A)-C(58)-H(58C)	109.5
H(58B)-C(58)-H(58C)	109.5
C(56)-C(59)-H(59A)	109.5
C(56)-C(59)-H(59B)	109.5

H(59A)-C(59)-H(59B)	109.5
C(56)-C(59)-H(59C)	109.5
H(59A)-C(59)-H(59C)	109.5
H(59B)-C(59)-H(59C)	109.5
C(63)-C(61)-C(62)	118.79(18)
C(63)-C(61)-C(51)	119.49(18)
C(62)-C(61)-C(51)	121.55(18)
O(3)-C(62)-C(63)#1	118.06(18)
O(3)-C(62)-C(61)	123.51(18)
C(63)#1-C(62)-C(61)	118.26(18)
C(61)-C(63)-C(62)#1	122.95(18)
C(61)-C(63)-H(63)	118.5
C(62)#1-C(63)-H(63)	118.5
F(72B)-C(71)-F(72)	69.7(6)
F(72B)-C(71)-F(73B)	112.7(8)
F(72)-C(71)-F(73B)	133.6(5)
F(72B)-C(71)-F(71)	125.3(7)
F(72)-C(71)-F(71)	114.1(6)
F(73B)-C(71)-F(71)	24.6(7)
F(72B)-C(71)-F(73)	35.4(7)
F(72)-C(71)-F(73)	103.2(5)
F(73B)-C(71)-F(73)	81.5(6)
F(71)-C(71)-F(73)	101.3(6)
F(72B)-C(71)-F(71B)	110.5(7)
F(72)-C(71)-F(71B)	44.6(4)
F(73B)-C(71)-F(71B)	100.6(5)
F(71)-C(71)-F(71B)	76.3(6)
F(73)-C(71)-F(71B)	135.5(5)
F(72B)-C(71)-C(72)	113.8(4)
F(72)-C(71)-C(72)	111.5(3)
F(73B)-C(71)-C(72)	109.0(5)
F(71)-C(71)-C(72)	114.1(5)
F(73)-C(71)-C(72)	111.7(4)
F(71B)-C(71)-C(72)	109.5(3)
O(71)-C(72)-C(73)	129.4(2)
O(71)-C(72)-C(71)	113.9(2)
C(73)-C(72)-C(71)	116.7(2)
C(72)-C(73)-C(74)	123.1(2)
C(72)-C(73)-H(73)	118.4
C(74)-C(73)-H(73)	118.4
O(72)-C(74)-C(73)	129.2(2)
O(72)-C(74)-C(75)	112.9(2)
C(73)-C(74)-C(75)	117.9(2)
F(76)-C(75)-F(75)	107.4(3)
F(76)-C(75)-F(74)	107.4(2)
F(75)-C(75)-F(74)	106.5(2)
F(76)-C(75)-C(74)	112.3(2)
F(75)-C(75)-C(74)	109.9(2)
F(74)-C(75)-C(74)	113.0(2)
C(55)-N(3)-C(51)	118.80(17)

C(55)-N(3)-Pd(3)	117.47(14)
C(51)-N(3)-Pd(3)	123.37(13)
C(62)-O(3)-Pd(3)	116.15(13)
C(72)-O(71)-Pd(3)	123.09(15)
C(74)-O(72)-Pd(3)	123.14(15)
O(3)-Pd(3)-N(3)	89.45(7)
O(3)-Pd(3)-O(72)	179.24(6)
N(3)-Pd(3)-O(72)	91.30(6)
O(3)-Pd(3)-O(71)	87.40(6)
N(3)-Pd(3)-O(71)	176.60(7)
O(72)-Pd(3)-O(71)	91.85(6)
C(81)-C(80)-C(85)	118.2(3)
C(81)-C(80)-C(86)	121.4(3)
C(85)-C(80)-C(86)	120.4(3)
C(82)-C(81)-C(80)	121.1(3)
C(82)-C(81)-H(81)	119.5
C(80)-C(81)-H(81)	119.5
C(81)-C(82)-C(83)	120.7(3)
C(81)-C(82)-H(82)	119.7
C(83)-C(82)-H(82)	119.7
C(84)-C(83)-C(82)	119.3(3)
C(84)-C(83)-H(83)	120.3
C(82)-C(83)-H(83)	120.3
C(83)-C(84)-C(85)	121.2(3)
C(83)-C(84)-H(84)	119.4
C(85)-C(84)-H(84)	119.4
C(84)-C(85)-C(80)	119.5(3)
C(84)-C(85)-H(85)	120.3
C(80)-C(85)-H(85)	120.3
C(80)-C(86)-H(86A)	109.5
C(80)-C(86)-H(86B)	109.5
H(86A)-C(86)-H(86B)	109.5
C(80)-C(86)-H(86C)	109.5
H(86A)-C(86)-H(86C)	109.5
H(86B)-C(86)-H(86C)	109.5
C(96)-C(90)-C(91)	116.7(6)
C(96)-C(90)-C(95)	123.3(6)
C(91)-C(90)-C(95)	120
C(90)-C(91)-C(92)	120
C(90)-C(91)-H(91)	120
C(92)-C(91)-H(91)	120
C(93)-C(92)-C(91)	120
C(93)-C(92)-H(92)	120
C(91)-C(92)-H(92)	120
C(92)-C(93)-C(94)	120
C(92)-C(93)-H(93)	120
C(94)-C(93)-H(93)	120
C(95)-C(94)-C(93)	120
C(95)-C(94)-H(94)	120
C(93)-C(94)-H(94)	120

C(94)-C(95)-C(90)	120
C(94)-C(95)-H(95)	120
C(90)-C(95)-H(95)	120
C(90)-C(96)-H(96A)	109.5
C(90)-C(96)-H(96B)	109.5
H(96A)-C(96)-H(96B)	109.5
C(90)-C(96)-H(96C)	109.5
H(96A)-C(96)-H(96C)	109.5
H(96B)-C(96)-H(96C)	109.5

Table A-14. Bond lengths [Å] and angles [deg] for **4.18**.

Bond lengths	
C(6)-O(5)	1.199(3)
C(6)-O(4)	1.328(3)
C(6)-C(7)	1.488(4)
C(7)-H(7A)	0.98
C(7)-H(7B)	0.98
C(7)-H(7C)	0.98
O(4)-B(1)	1.466(3)
C(1)-O(1)	1.345(2)
C(1)-C(3)#1	1.375(3)
C(1)-C(2)	1.387(3)
C(2)-C(3)	1.388(3)
C(2)-C(11)	1.459(3)
C(3)-C(1)#1	1.375(3)
C(3)-H(3)	0.95
C(4)-O(3)	1.208(3)
C(4)-O(2)	1.330(3)
C(4)-C(5)	1.474(4)
C(5)-H(5A)	0.98
C(5)-H(5B)	0.98
C(5)-H(5C)	0.98
C(11)-N(1)	1.350(3)
C(11)-C(12)	1.382(3)
C(12)-C(13)	1.377(3)
C(12)-H(12)	0.95
C(13)-C(14)	1.375(3)
C(13)-H(13)	0.95
C(14)-C(15)	1.357(4)
C(14)-H(14)	0.95
C(15)-N(1)	1.358(3)
C(15)-H(15)	0.95
B(1)-O(1)	1.427(3)
B(1)-O(2)	1.451(3)
B(1)-N(1)	1.576(3)
Bond Angles	

O(5)-C(6)-O(4)	123.5(2)
O(5)-C(6)-C(7)	124.0(2)
O(4)-C(6)-C(7)	112.4(2)
C(6)-C(7)-H(7A)	109.5
C(6)-C(7)-H(7B)	109.5
H(7A)-C(7)-H(7B)	109.5
C(6)-C(7)-H(7C)	109.5
H(7A)-C(7)-H(7C)	109.5
H(7B)-C(7)-H(7C)	109.5
C(6)-O(4)-B(1)	120.90(18)
O(1)-C(1)-C(3)#1	116.78(19)
O(1)-C(1)-C(2)	122.7(2)
C(3)#1-C(1)-C(2)	120.53(19)
C(1)-C(2)-C(3)	117.8(2)
C(1)-C(2)-C(11)	120.29(19)
C(3)-C(2)-C(11)	121.9(2)
C(1)#1-C(3)-C(2)	121.6(2)
C(1)#1-C(3)-H(3)	119.2
C(2)-C(3)-H(3)	119.2
O(3)-C(4)-O(2)	122.9(2)
O(3)-C(4)-C(5)	124.0(3)
O(2)-C(4)-C(5)	113.0(2)
C(4)-C(5)-H(5A)	109.5
C(4)-C(5)-H(5B)	109.5
H(5A)-C(5)-H(5B)	109.5
C(4)-C(5)-H(5C)	109.5
H(5A)-C(5)-H(5C)	109.5
H(5B)-C(5)-H(5C)	109.5
N(1)-C(11)-C(12)	118.7(2)
N(1)-C(11)-C(2)	117.82(19)
C(12)-C(11)-C(2)	123.41(19)
C(13)-C(12)-C(11)	120.9(2)
C(13)-C(12)-H(12)	119.6
C(11)-C(12)-H(12)	119.6
C(14)-C(13)-C(12)	119.4(2)
C(14)-C(13)-H(13)	120.3
C(12)-C(13)-H(13)	120.3
C(15)-C(14)-C(13)	118.4(2)
C(15)-C(14)-H(14)	120.8
C(13)-C(14)-H(14)	120.8
C(14)-C(15)-N(1)	122.3(2)
C(14)-C(15)-H(15)	118.9
N(1)-C(15)-H(15)	118.9
O(1)-B(1)-O(2)	111.7(2)
O(1)-B(1)-O(4)	111.5(2)
O(2)-B(1)-O(4)	101.91(17)
O(1)-B(1)-N(1)	112.00(18)
O(2)-B(1)-N(1)	109.72(19)
O(4)-B(1)-N(1)	109.6(2)
C(11)-N(1)-C(15)	120.2(2)

C(11)-N(1)-B(1)	123.03(19)
C(15)-N(1)-B(1)	116.75(17)
C(1)-O(1)-B(1)	123.68(18)
C(4)-O(2)-B(1)	120.88(18)

Table A-15. Bond lengths [Å] and angles [deg] for **4.19**.

Bond lengths	
C(1)-O(1)	1.366(3)
C(1)-C(3)#1	1.381(4)
C(1)-C(2)	1.402(4)
C(2)-C(3)	1.396(4)
C(2)-C(11)	1.468(4)
C(3)-C(1)#1	1.381(4)
C(3)-H(3)	0.95
C(4)-O(3)	1.207(4)
C(4)-O(2)	1.332(4)
C(4)-C(5)	1.486(5)
C(5)-H(5A)	0.98
C(5)-H(5B)	0.98
C(5)-H(5C)	0.98
C(6)-O(5)	1.202(4)
C(6)-O(4)	1.338(4)
C(6)-C(7)	1.493(5)
C(7)-H(7A)	0.98
C(7)-H(7B)	0.98
C(7)-H(7C)	0.98
C(11)-N(1)	1.369(3)
C(11)-C(12)	1.392(4)
C(12)-C(13)	1.385(4)
C(12)-H(12)	0.95
C(13)-C(14)	1.395(4)
C(13)-C(16)	1.533(4)
C(14)-C(15)	1.374(4)
C(14)-H(14)	0.95
C(15)-N(1)	1.344(4)
C(15)-H(15)	0.95
C(16)-C(19)	1.506(4)
C(16)-C(17)	1.521(5)
C(16)-C(18)	1.535(5)
C(17)-H(17A)	0.98
C(17)-H(17B)	0.98
C(17)-H(17C)	0.98
C(18)-H(18A)	0.98
C(18)-H(18B)	0.98
C(18)-H(18C)	0.98
C(19)-H(19A)	0.98

C(19)-H(19B)	0.98
C(19)-H(19C)	0.98
B(1)-O(1)	1.430(4)
B(1)-O(4)	1.455(4)
B(1)-O(2)	1.469(4)
B(1)-N(1)	1.607(4)
Bond Angles	
O(1)-C(1)-C(3)#1	118.5(2)
O(1)-C(1)-C(2)	121.1(2)
C(3)#1-C(1)-C(2)	120.3(2)
C(3)-C(2)-C(1)	118.1(2)
C(3)-C(2)-C(11)	121.9(2)
C(1)-C(2)-C(11)	120.0(2)
C(1)#1-C(3)-C(2)	121.6(3)
C(1)#1-C(3)-H(3)	119.2
C(2)-C(3)-H(3)	119.2
O(3)-C(4)-O(2)	123.4(3)
O(3)-C(4)-C(5)	124.2(3)
O(2)-C(4)-C(5)	112.4(3)
C(4)-C(5)-H(5A)	109.5
C(4)-C(5)-H(5B)	109.5
H(5A)-C(5)-H(5B)	109.5
C(4)-C(5)-H(5C)	109.5
H(5A)-C(5)-H(5C)	109.5
H(5B)-C(5)-H(5C)	109.5
O(5)-C(6)-O(4)	123.4(3)
O(5)-C(6)-C(7)	124.4(3)
O(4)-C(6)-C(7)	112.1(3)
C(6)-C(7)-H(7A)	109.5
C(6)-C(7)-H(7B)	109.5
H(7A)-C(7)-H(7B)	109.5
C(6)-C(7)-H(7C)	109.5
H(7A)-C(7)-H(7C)	109.5
H(7B)-C(7)-H(7C)	109.5
N(1)-C(11)-C(12)	119.3(2)
N(1)-C(11)-C(2)	117.3(2)
C(12)-C(11)-C(2)	123.5(2)
C(13)-C(12)-C(11)	122.4(3)
C(13)-C(12)-H(12)	118.8
C(11)-C(12)-H(12)	118.8
C(12)-C(13)-C(14)	116.2(3)
C(12)-C(13)-C(16)	121.3(3)
C(14)-C(13)-C(16)	122.5(3)
C(15)-C(14)-C(13)	120.6(3)
C(15)-C(14)-H(14)	119.7
C(13)-C(14)-H(14)	119.7
N(1)-C(15)-C(14)	122.3(3)
N(1)-C(15)-H(15)	118.8
C(14)-C(15)-H(15)	118.8
C(19)-C(16)-C(17)	108.2(3)

C(19)-C(16)-C(13)	112.3(2)
C(17)-C(16)-C(13)	108.6(2)
C(19)-C(16)-C(18)	108.3(3)
C(17)-C(16)-C(18)	108.8(3)
C(13)-C(16)-C(18)	110.6(3)
C(16)-C(17)-H(17A)	109.5
C(16)-C(17)-H(17B)	109.5
H(17A)-C(17)-H(17B)	109.5
C(16)-C(17)-H(17C)	109.5
H(17A)-C(17)-H(17C)	109.5
H(17B)-C(17)-H(17C)	109.5
C(16)-C(18)-H(18A)	109.5
C(16)-C(18)-H(18B)	109.5
H(18A)-C(18)-H(18B)	109.5
C(16)-C(18)-H(18C)	109.5
H(18A)-C(18)-H(18C)	109.5
H(18B)-C(18)-H(18C)	109.5
C(16)-C(19)-H(19A)	109.5
C(16)-C(19)-H(19B)	109.5
H(19A)-C(19)-H(19B)	109.5
C(16)-C(19)-H(19C)	109.5
H(19A)-C(19)-H(19C)	109.5
H(19B)-C(19)-H(19C)	109.5
O(1)-B(1)-O(4)	109.0(3)
O(1)-B(1)-O(2)	107.0(2)
O(4)-B(1)-O(2)	117.5(2)
O(1)-B(1)-N(1)	109.2(2)
O(4)-B(1)-N(1)	104.9(2)
O(2)-B(1)-N(1)	109.1(2)
C(15)-N(1)-C(11)	119.3(2)
C(15)-N(1)-B(1)	120.8(2)
C(11)-N(1)-B(1)	119.9(2)
C(1)-O(1)-B(1)	117.8(2)
C(4)-O(2)-B(1)	124.2(2)
C(6)-O(4)-B(1)	126.3(2)

Table A-16. Bond lengths [Å] and angles [deg] for **4.21**.

Bond lengths	
C(1)-O(1)	1.3424(13)
C(1)-C(6)	1.3936(16)
C(1)-C(2)	1.3952(16)
C(2)-C(3)	1.4034(15)
C(2)-C(11)	1.4541(16)
C(3)-C(4)	1.3742(19)
C(3)-H(3)	0.95
C(4)-C(5)	1.382(2)

C(4)-H(4)	0.95
C(5)-C(6)	1.3770(18)
C(5)-H(5)	0.95
C(6)-H(6)	0.95
C(7)-O(3)	1.2067(14)
C(7)-O(2)	1.3296(14)
C(7)-C(8)	1.4953(16)
C(8)-H(8A)	0.98
C(8)-H(8B)	0.98
C(8)-H(8C)	0.98
C(9)-O(5)	1.2023(14)
C(9)-O(4)	1.3297(14)
C(9)-C(10)	1.4962(17)
C(10)-H(10A)	0.98
C(10)-H(10B)	0.98
C(10)-H(10C)	0.98
C(11)-N(1)	1.3525(13)
C(11)-C(12)	1.3963(16)
C(12)-C(13)	1.3675(19)
C(12)-H(12)	0.95
C(13)-C(14)	1.379(2)
C(13)-H(13)	0.95
C(14)-C(15)	1.3646(18)
C(14)-H(14)	0.95
C(15)-N(1)	1.3479(14)
C(15)-H(15)	0.95
B(1)-O(1)	1.4230(14)
B(1)-O(4)	1.4688(14)
B(1)-O(2)	1.4719(14)
B(1)-N(1)	1.5758(15)
Bond Angles	
O(1)-C(1)-C(6)	117.25(10)
O(1)-C(1)-C(2)	122.44(10)
C(6)-C(1)-C(2)	120.31(11)
C(1)-C(2)-C(3)	118.14(11)
C(1)-C(2)-C(11)	120.28(10)
C(3)-C(2)-C(11)	121.58(11)
C(4)-C(3)-C(2)	121.35(12)
C(4)-C(3)-H(3)	119.3
C(2)-C(3)-H(3)	119.3
C(3)-C(4)-C(5)	119.62(11)
C(3)-C(4)-H(4)	120.2
C(5)-C(4)-H(4)	120.2
C(6)-C(5)-C(4)	120.53(12)
C(6)-C(5)-H(5)	119.7
C(4)-C(5)-H(5)	119.7
C(5)-C(6)-C(1)	120.05(12)
C(5)-C(6)-H(6)	120
C(1)-C(6)-H(6)	120
O(3)-C(7)-O(2)	123.28(11)

O(3)-C(7)-C(8)	124.41(11)
O(2)-C(7)-C(8)	112.30(10)
C(7)-C(8)-H(8A)	109.5
C(7)-C(8)-H(8B)	109.5
H(8A)-C(8)-H(8B)	109.5
C(7)-C(8)-H(8C)	109.5
H(8A)-C(8)-H(8C)	109.5
H(8B)-C(8)-H(8C)	109.5
O(5)-C(9)-O(4)	123.77(11)
O(5)-C(9)-C(10)	123.93(11)
O(4)-C(9)-C(10)	112.30(10)
C(9)-C(10)-H(10A)	109.5
C(9)-C(10)-H(10B)	109.5
H(10A)-C(10)-H(10B)	109.5
C(9)-C(10)-H(10C)	109.5
H(10A)-C(10)-H(10C)	109.5
H(10B)-C(10)-H(10C)	109.5
N(1)-C(11)-C(12)	118.54(10)
N(1)-C(11)-C(2)	117.95(9)
C(12)-C(11)-C(2)	123.50(10)
C(13)-C(12)-C(11)	120.60(11)
C(13)-C(12)-H(12)	119.7
C(11)-C(12)-H(12)	119.7
C(12)-C(13)-C(14)	119.70(11)
C(12)-C(13)-H(13)	120.2
C(14)-C(13)-H(13)	120.2
C(15)-C(14)-C(13)	118.46(12)
C(15)-C(14)-H(14)	120.8
C(13)-C(14)-H(14)	120.8
N(1)-C(15)-C(14)	122.08(11)
N(1)-C(15)-H(15)	119
C(14)-C(15)-H(15)	119
O(1)-B(1)-O(4)	111.50(9)
O(1)-B(1)-O(2)	112.23(9)
O(4)-B(1)-O(2)	100.95(8)
O(1)-B(1)-N(1)	112.03(8)
O(4)-B(1)-N(1)	110.08(9)
O(2)-B(1)-N(1)	109.52(9)
C(15)-N(1)-C(11)	120.61(10)
C(15)-N(1)-B(1)	116.43(9)
C(11)-N(1)-B(1)	122.96(9)
C(1)-O(1)-B(1)	124.24(9)
C(7)-O(2)-B(1)	121.40(9)
C(9)-O(4)-B(1)	120.87(9)

Table A-17. Bond lengths [Å] and angles [deg] for **4.22**.

Bond lengths	
C(1)-O(1)	1.3495(13)
C(1)-C(6)	1.3957(15)
C(1)-C(2)	1.4001(15)
C(2)-C(3)	1.4027(15)
C(2)-C(11)	1.4628(14)
C(3)-C(4)	1.3737(16)
C(3)-H(3)	0.95
C(4)-C(5)	1.3903(18)
C(4)-H(4)	0.95
C(5)-C(6)	1.3783(17)
C(5)-H(5)	0.95
C(6)-H(6)	0.95
C(11)-N(1)	1.3566(14)
C(11)-C(12)	1.3911(15)
C(12)-C(13)	1.3735(17)
C(12)-H(12)	0.95
C(13)-C(14)	1.3827(18)
C(13)-H(13)	0.95
C(14)-C(15)	1.3689(17)
C(14)-H(14)	0.95
C(15)-N(1)	1.3506(14)
C(15)-H(15)	0.95
B(1)-F(1)	1.3764(14)
B(1)-F(2)	1.3864(14)
B(1)-O(1)	1.4329(14)
B(1)-N(1)	1.5938(15)
Bond Angles	
O(1)-C(1)-C(6)	118.44(10)
O(1)-C(1)-C(2)	121.21(9)
C(6)-C(1)-C(2)	120.32(10)
C(1)-C(2)-C(3)	118.32(10)
C(1)-C(2)-C(11)	119.99(10)
C(3)-C(2)-C(11)	121.68(10)
C(4)-C(3)-C(2)	121.22(11)
C(4)-C(3)-H(3)	119.4
C(2)-C(3)-H(3)	119.4
C(3)-C(4)-C(5)	119.73(11)
C(3)-C(4)-H(4)	120.1
C(5)-C(4)-H(4)	120.1
C(6)-C(5)-C(4)	120.47(11)
C(6)-C(5)-H(5)	119.8
C(4)-C(5)-H(5)	119.8
C(5)-C(6)-C(1)	119.92(11)
C(5)-C(6)-H(6)	120
C(1)-C(6)-H(6)	120
N(1)-C(11)-C(12)	118.95(10)
N(1)-C(11)-C(2)	117.53(9)
C(12)-C(11)-C(2)	123.52(10)

C(13)-C(12)-C(11)	120.38(11)
C(13)-C(12)-H(12)	119.8
C(11)-C(12)-H(12)	119.8
C(12)-C(13)-C(14)	119.63(11)
C(12)-C(13)-H(13)	120.2
C(14)-C(13)-H(13)	120.2
C(15)-C(14)-C(13)	118.71(11)
C(15)-C(14)-H(14)	120.6
C(13)-C(14)-H(14)	120.6
N(1)-C(15)-C(14)	121.65(11)
N(1)-C(15)-H(15)	119.2
C(14)-C(15)-H(15)	119.2
F(1)-B(1)-F(2)	110.59(9)
F(1)-B(1)-O(1)	109.73(9)
F(2)-B(1)-O(1)	111.99(9)
F(1)-B(1)-N(1)	108.69(9)
F(2)-B(1)-N(1)	106.29(8)
O(1)-B(1)-N(1)	109.44(9)
C(15)-N(1)-C(11)	120.66(9)
C(15)-N(1)-B(1)	118.71(9)
C(11)-N(1)-B(1)	120.44(8)
C(1)-O(1)-B(1)	119.44(8)